REPORT DOCUMENTATION PAGE

Form Approved OMB NO. 0704-0188

The public reporting burden for this collection of information is estimated to average 1 hour per response, including the time for reviewing instructions, searching existing data sources, gathering and maintaining the data needed, and completing and reviewing the collection of information. Send comments regarding this burden estimate or any other aspect of this collection of information, including suggesstions for reducing this burden, to Washington Headquarters Services, Directorate for Information Operations and Reports, 1215 Jefferson Davis Highway, Suite 1204, Arlington VA, 22202-4302. Respondents should be aware that notwithstanding any other provision of law, no person shall be subject to any oenalty for failing to comply with a collection of information if it does not display a currently valid OMB control number.
PLEASE DO NOT RETURN YOUR FORM TO THE ABOVE ADDRESS.

1. REPORT DATE (DD-MM-YYYY)	2. REPORT TYPE	3. DATES COVERED (From - To)
10-08-2015	MS Thesis	-

4. TITLE AND SUBTITLE

Effect of Fly Ash and Silica Fume on the Mechanical Properties of Cement Paste at Different Stages of Hydration

5a. CONTRACT NUMBER
W911NF-11-2-0043

5b. GRANT NUMBER

5c. PROGRAM ELEMENT NUMBER
611104

6. AUTHORS
Lucas Suarez

5d. PROJECT NUMBER

5e. TASK NUMBER

5f. WORK UNIT NUMBER

7. PERFORMING ORGANIZATION NAMES AND ADDRESSES
North Carolina A&T State University
1601 East Market Street

Greensboro, NC 27411 -0001

8. PERFORMING ORGANIZATION REPORT NUMBER

9. SPONSORING/MONITORING AGENCY NAME(S) AND ADDRESS (ES)

U.S. Army Research Office
P.O. Box 12211
Research Triangle Park, NC 27709-2211

10. SPONSOR/MONITOR'S ACRONYM(S)
ARO

11. SPONSOR/MONITOR'S REPORT NUMBER(S)
59544-MA-PIR.24

12. DISTRIBUTION AVAILIBILITY STATEMENT

Approved for public release; distribution is unlimited.

13. SUPPLEMENTARY NOTES

The views, opinions and/or findings contained in this report are those of the author(s) and should not contrued as an official Department of the Army position, policy or decision, unless so designated by other documentation.

14. ABSTRACT

This thesis investigates the effect of fly ash and silica fume on cement paste hydration. Percentages of each additive will replace the cement by volume to be studied at five ages. These percentages will be compared alongside a controlled cement paste without additives. Testing will be carried out on 350 samples. The testing methods used are a Forney Universal Testing Machine and MTS Landmark Servohydraulic Testing System (MTS) for compressive strength on cylinders and cubes, respectively. Fourier Transfer Infrared Spectroscopy (FTIR) monitored

15. SUBJECT TERMS

Cement Paste, fly ash, silica fume, hydration, mechanical properties

16. SECURITY CLASSIFICATION OF:			17. LIMITATION OF ABSTRACT	15. NUMBER OF PAGES	19a. NAME OF RESPONSIBLE PERSON
a. REPORT	b. ABSTRACT	c. THIS PAGE			Ram Mohan
UU	UU	UU	UU		19b. TELEPHONE NUMBER 336-285-2867

Report Title

Effect of Fly Ash and Silica Fume on the Mechanical Properties of Cement Paste at Different Stages of Hydration

ABSTRACT

This thesis investigates the effect of fly ash and silica fume on cement paste hydration. Percentages of each additive will replace the cement by volume to be studied at five ages. These percentages will be compared alongside a controlled cement paste without additives. Testing will be carried out on 350 samples. The testing methods used are a Forney Universal Testing Machine and MTS Landmark Servohydraulic Testing System (MTS) for compressive strength on cylinders and cubes, respectively. Fourier Transfer Infrared Spectroscopy (FTIR) monitored the hydration with spectra, and Scanning Electron Microscope (SEM) generated images for regional analysis.

Compressive strength testing demonstrated that silica fume replacement had the highest overall stress under water curing. Replacement of fly ash exhibited the highest overall stress under vacuum curing. Fly ash and silica fume both have the best MTS stress-strain curves in later ages.

FTIR and SEM testing showed an increase in the change of CSH area with age. SEM testing revealed the formation of pores, CSH, and CH in images at all ages. The area of CSH grows most in early ages and diminishes over time. It is clear that the method of curing makes a difference in hydration. Further research is needed on the method of vacuum sealing hardened cement paste.

Effect of Fly Ash and Silica Fume on the Mechanical Properties of Cement Paste at Different Stages of Hydration

Lucas Suarez

North Carolina A&T State University

A thesis submitted to the graduate faculty

in partial fulfillment of the requirements for the degree of

MASTER OF SCIENCE

Department: Civil, Architectural, and Environmental Engineering

Major: Civil Engineering

Major Professor: Dr. Taher Abu-Lebdeh

Greensboro, North Carolina

2015

The Graduate School
North Carolina Agricultural and Technical State University

This is to certify that the Master's Thesis of

Lucas Suarez

has met the thesis requirements of
North Carolina Agricultural and Technical State University

Greensboro, North Carolina
2015

Approved by:

Dr. Taher Abu-Lebdeh
Major Professor

Dr. Ram Mohan
Committee Member

Dr. Miguel Picornell
Committee Member

Dr. Sameer Hamoush
Department Chair

Dr. Sanjiv Sarin
Dean, The Graduate School

© Copyright by

Lucas Suarez

2015

Biographical Sketch

Lucas Suarez is a civil engineering graduate student seeking to build lasting personal relationships and acquire critical insight into qualities that will best benefit his personal and professional development. He recognizes the importance of collaboration, best formed understanding the significance of his role in research role and possessing academic responsibilities.

As a student, he has gained valuable lessons in the classroom that will work in conjunction with his professional experience to form a product. Being adaptable and personable were two of the key characteristics of his personality that enabled him to complete this thesis. Under those circumstances, he is devoted to working with a purpose and is committed to evaluate the components of structures within the field of civil engineering.

Mr. Suarez has a strong determination to reach his full potential in all that he does. In addition, he is a very ambitious individual and admires the guidance provided from professionals of all backgrounds. Mr. Suarez looks forward to earning his Master of Science degree in civil engineering. The next step is to take the Professional Engineer and Leadership in Energy and Environmental Design Accredited Professional exam as well, after developing experience in the engineering field. As a researcher and professional, he is very interested in affecting change where it is needed for the better state of society.

Dedication

I would like to express my deepest gratitude to both my immaculate parents, Jose and Dominga Suarez, my brother Emmanuel, my sister Penelope, and my girlfriend Carisse. These extremely extraordinary individuals have believed in me before beginning my career as a civil engineer. That has inspired to me to reach my full potential as a professional and pursue higher education. I am certain I will maintain a mindset of principles as I delve further into my career. My motivation for advancement is derived from the notion of many invaluable contributions and sacrifices made in order to further myself.

Completion of this thesis is an attribute that marks a very special milestone. This a representation of the content of the work I came create and lies in my identity from now on in the field of research. I am confident I will be able to produce with respectable quality from the preparation I have received during the research that was conducted. I owe all of my progress to these loving people. Thank you for a lifetime of positive influence and ultimately never losing faith. Love you very much!

Acknowledgments

I would like to express my sincerest gratification for all of the guidance and support of all that have contributed to completion of graduate studies. I am deeply indebted to my advisor Dr. Taher Abu-Lebdeh who has kindly offered an abundance of support. In the two years of my preparation of research and matriculation throughout my courses, I feel very fortunate to have had such a motivating and persistent individual to reference. The phases of research have all been a very smooth transition into the other due to the determination of an advisor.

I would also like to thank Dr. Miguel Picornell for his constant reassurance and his expertise. In addition, I want to thank Dr. Ram Mohan for serving on my advisory committee, as well for his generous advice. Likewise, I am thankful for the encouragement and knowledge from Dr. Sameer Hamoush. I am confident I will be able to produce with quality from the preparation I have received during the research that was conducted. Many thanks to all the people that have I have had the opportunity to know in North Carolina A&T State University, whose friendship and relationship I will always cherish.

However, as a researcher I have learned lessons that I will be able to apply in leadership and team efforts in my career that follows. I would like to thank my team of fellow researchers and the Cherry crew for their persistence, reinforcement, and active participation. I appreciate the flexibility of these individuals in helping resolve any issues in the path of research. In times of apprehension, I enjoy how easily it seemed to create a solution to be able to continue. Faced with obstacles that conversely affected other facets of the research, my advisory committee was always prepared to work toward overcoming these obstacles. The support in part for this work by U.S. Army Research Office under a cooperative agreement award contract No. W911NF-11-2-0043.

Table of Contents

List of Figures

List of Tables

Abstract

This thesis investigates the effect of fly ash and silica fume on cement paste hydration. Percentages of each additive will replace the cement by volume to be studied at five ages. These percentages will be compared alongside a controlled cement paste without additives. Testing will be carried out on 350 samples. The testing methods used are a Forney Universal Testing Machine and MTS Landmark Servohydraulic Testing System (MTS) for compressive strength on cylinders and cubes, respectively. Fourier Transfer Infrared Spectroscopy (FTIR) monitored the hydration with spectra, and Scanning Electron Microscope (SEM) generated images for regional analysis.

Compressive strength testing demonstrated that silica fume replacement had the highest overall stress under water curing. Replacement of fly ash exhibited the highest overall stress under vacuum curing. Fly ash and silica fume both have the best MTS stress-strain curves in later ages.

FTIR and SEM testing showed an increase in the change of CSH area with age. SEM testing revealed the formation of pores, CSH, and CH in images at all ages. The area of CSH grows most in early ages and diminishes over time. It is clear that the method of curing makes a difference in hydration. Further research is needed on the method of vacuum sealing hardened cement paste.

CHAPTER 1

Introduction

1.1 Portland Cement

Portland cement or Ordinary Portland Cement (OPC) in its simplest form was invented nearly 200 years ago, and the reaction it has with water is termed hydration. To produce Portland cement, lime, clay and other naturally available minerals partially integrate to form clinker nodes upon cooling. Clinker is mostly composed of phases containing calcium oxide, silicon dioxide, aluminum oxide and ferric oxide among other minor chemical components. The clinker is mixed with typically five percent gypsum, also known as calcium sulphate. The hydration comes to play when the solid volume of cement paste increases, and it is converted in a rigid solid. The binding properties of cement are derived from the hydrates, being the reaction products.

1.2 Cement Hydration

1.2.1 Cement background. The process of cement hydration occurs when water is added to dry cement; this reaction is termed 'hydration'. The hydration of cement paste is responsible for the development of essentially every engineering property of cement paste. Some properties include hardening, temperature rise, and shrinkage which can lead to cracking. Similarly, the degradation resistance of cement is a property that is less recognized (Artioli 2013). Cement is manufactured by the crushing, milling, and proper proportioning of lime (CaO), silica (SiO_2), alumina (Al_2O_3), Iron (Fe_2O_3), and gypsum ($CaSO_4 \cdot 2H_2O$).
When cement is in the anhydrous state, or without water, four main types of minerals exists: alite (C_3S), belite (C_2S), tricalcium aluminate (C_3A) and tetracalcium aluminoferrite (C_4AF). Other chemicals that may exist are: sodium oxide (Na_2O), potassium oxide (K_2O) and gypsum (CSH_2).

These chemical compounds are formed within the cement clinker and contribute to the cement properties in several ways.

Alite: Alite is a compound that hydrates and hardens at an accelerated rate. It's largely responsible for the initial setting and early strength of the cement paste.

Belite: This compounds hydrates and hardens at a slow rate. It's largely responsible for the cement paste's strength gained after one week of hardening.

Tricalcium Aluminate: This compound doesn't contribute much to the strength of the cement paste. However, it liberates a lot of the heat during the beginning stages of hydration.

Tetracalcium Aluminoferrite: Is a compound which doesn't affect the cement pastes strength much. It acts as a fluxing agent which reduces the melting temperature of the raw materials within the kiln (Garcia-Mate 2013). The mixing of these chemical compounds is what allows cement manufactures to produce the different types of cement. There are five types of Portland cement designated by ASTM standards.

Type 1: General purpose cement with very high C_3S content for early strength development. Typically used for construction of buildings, bridges, pavements, precast structures, etc.

Type 2: Moderate sulfate resistance cement with low C_3A content below 8%. Usually used for structures exposed to water containing sulfate ions or soil.

Type 3: High early strength cement which is grounded more finely and containing slightly more C_3S.Used for rapid construction and in cold weather.

Type 4: Cement with low heat of hydration and a low content of C_3A and C_3S. Used for massive structures, such as dams, but otherwise rarely used.

Type 5: High sulfate resistance cement with very low C_3A content. Typically used for structures exposed to high levels of sulfate ions.

For this research study, cement Type 1 will be used to conduct all experimental testing. A series of chemical reactions takes place during the hydration process of cement paste. Once water is added to the cement, the tricalcium aluminate reacts with the gypsum to produce ettringite and heat. Next, the tricalcium silicate is hydrated to produce the calcium silicate hydrates, lime and heat. The CSH has a fiber like structure that is visible in imagery. Once the gypsum is gone, the ettringite becomes unstable and begins to react with the remaining tricalcium aluminate to form monosulfate aluminate hydrate crystals.

During a sulfate deficient solution the monosulfate crystals become unstable. The crystals then resort back into ettringite during the presence of sulfates. The increase in the crystal size is what causes the cement cracking when subjected to sulfate attack. The belite hydrates to form calcium silicate hydrates and heat. The calcium silicate hydrates during this phase generates strength within the cement paste. This process has a very slow rate; however, this compound produces the long-term strength of cement concrete. The ferrite goes through two progressive reactions with the gypsum. The first reaction is when the ettringite reacts with the water and gypsum to form ettringite, lime and alumia hydroxides. The second reaction occurs when the ferrite further reacts with the ettringite that was formed during the first reaction.

1.3 Relation of Strength to Hydration

Calcium Silicate Hydrate (CSH) is the main and most important constituent of cement paste. Its hydration forms most of the new solid phases that give hardened cement paste its strength. Hydration phases can be seen in Figure 1.1 as a scanning electron microscope (SEM)

image, the topic will be reiterated into further detail in this thesis. A rising tendency to use cement paste as a structural material at early ages is evident in much of modern engineering.

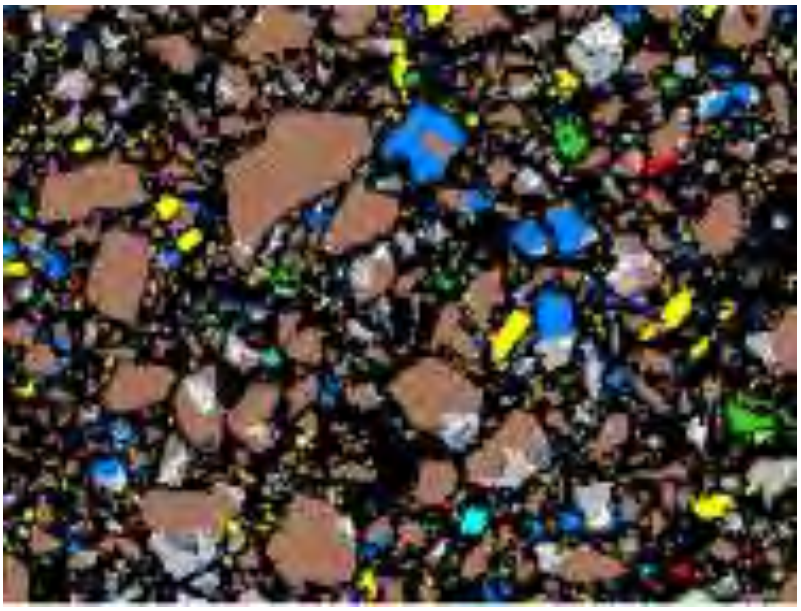

Figure 1.1: SEM image with color coding based on hydration chemical phases (Artioli, 2013)

Natural pozzolans materials that are finely ground and are used in combination with calcium hydroxide and water to exhibit cementitious properties. These materials have also been shown to increase the strength of ordinary Portland cement and promoted a decrease in the porosity. The formation of a finer pore size distribution of the cement paste. The ability to set, harden quickly, and gain greater strength makes various type of cement the main material utilized in modern day construction. The most common types of cement range from Type I to Type V. This research will be using Type I cement as it is the most suitable and is most used for general purposes.

1.3.1 Hydration kinetics. When water is added to the cement, an exothermic reaction occurs; which means the reaction generates heat. Using a technique call conduction calorimetry, the rate at which the heat evolution can be monitored. Three principal reactions occur during this

process which can be broken down into four periods. Prior to the first stage period, almost immediately after adding water, the clinker sulphates and gypsum dissolve to produce an alkaline and sulfate solution. After mixing occurs, period one or the dissolution period takes place when alite reacts with water to form an aluminate gel. This gel reacts with the sulfate within the solution to form small crystals of ettringite. The alite phase only last for a few minutes but is very exothermic. After which period two begins.

Period two is referred to as the dormant stage or induction period due to the relatively low heat generated. This stage last a few hours and causes the cement paste to become stiff and unworkable. At the end of this stage, the alite and belite start to react to formulate calcium silicate hydrate and calcium hydroxide as seen in Figure 1.2. This occurrence takes place in period three or the nucleation period in which the cement paste strengths increases with time. The hydration process continues as the crystals react more with the water during the tricalcium aluminate phase. The tetracalcium aluminoferrite phase starts when water is first added but then slows down due to a layer of iron hydroxide gel coating the aluminoferrite. Lastly, the fourth period or the diffusion period where dissolved cement diffuse out into pores or water diffuses in to cement grains very slowly.

From the hydration process of cement and water, several products are formed from this reaction. From these products, there are four main types which are: calcium silicate hydrate, calcium hydroxide, calcium aluminates and calcium sulfoaluminates.

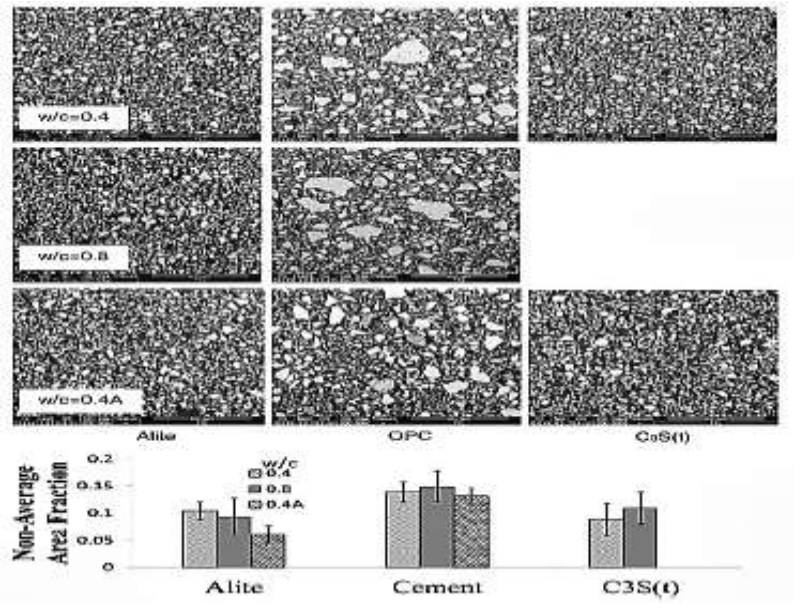

Figure 1.2: Areas of alite and cement in the SEM images at several w/c ratios (Kirby, 2011)

1.4 Additives

1.4.1 Effect of fly ash. The re-use of supplemental cementitious materials like fly ash gives a new value to the product deemed waste. Although this may be true, the addition of this supplemental material is known to have adverse effects on the compressive strength of the cement. The replacement of cement with fly ash by percentage effects the properties, those being both the filler and dilution effects. Fly ash contains pozzolans, a siliceous material possessing cementitious properties, and consumes CH in the pozzolanic reaction. Zhang (2000) found that less CH will decelerate the hydration reaction, best for the overall hydration of the specimen. The higher the fly as replacement percent, inversely the CH content is reduced (Lam et al., 2000), (Zhang, 2000).

Class F fly ash has a good susceptibility to reducing the alkali-silica reaction (ASR). This classification will mitigate this issue better than class C fly ash. ASR forms a gel that swell as it absorbs water from the surrounding cement paste. The reaction if left alleviated will

constitute severe expansion in cement. Thus the permeability of the cement will also increase if there is no modification of the gel properties. (Garcia-Mate et al., 2013).

1.4.2 Effect of silica fume. The silica fume additive contains pozzolans which are siliceous and aluminous material which have no cementitious properties. However it will react with calcium hydroxide once hydrated. A pozzolanic reaction between silica fume and lime formed during cement hydration does not occur during the early stages of hydration. The presence of silica fume slightly increases the rate of cement hydration during the first few hours of hydration. Likewise, this indicates that silica fume affects hydration by the nucleating effect of its surface when it still exists as a chemically inert filler. Either the surface of silica fume increases the number of nuclei, but crystal growth is slower; Or the poisoning effect of adsorbed silicates retard the nucleation and growth of CH. Of major significance is how silica fume affects the total heat of hydration and infers that the same is occurring to the initial hydration reactions. The calorimetric study indicated that the hydration was modified by the presence of silica fume. The silica fume showed high activity in the early stages; and accelerated the hydration rate as compared to that of the reference cement paste. The fine silica fume particles provided nucleation sites for growth of hydrates. After silica fume hydrates grow both strength and the hydration heat increases and the pozzolanic activity takes over. (Kadri & Duval, 2009).

1.5 Hydrated Products

1.5.1 Calcium silicate hydrate. Calcium silicate hydrate (CSH) is the most critical hydration product as it fills the largest amount of space in hydrated cement and holds the microstructure together. The induction or dormant phase of Portland cement hydration allows for the mixing of the cement with additives to continue during transportation elsewhere, along with placement and setting of the mix. In this phase of hydration, the versatility of the cement is

best captured. CSH occupies approximately 50% of the paste volume and responsible to nearly all of the engineering properties of the cement paste. It forms a continuous layer which binds the cement particles into a cohesive solid on a nanometer level (Bullard et al., 2011).

1.5.2 Calcium hydroxide. Calcium hydroxide (CH) occupies approximately 15% of the cement paste by volume. CH forms as crystals within the cement paste, that nucleate in the capillary pores and are large enough to be seen on an optical microscope. Calcium silicate hydrate and calcium hydroxide are both byproducts of the reaction of alite and water. Belite and alite are both minerals that react similarly with hydration (Kirby, 2011).

1.5.3 Calcium aluminates and sulfoaluminate phases. Calcium aluminate phases incorporate the hydration products which form the tricalcium aluminate and tetracalcium aluminoferrite minerals. They occupy approximately 15% to 25% by volume of the cement paste. They do not contribute as much to the engineering properties as of CSH in the cement paste. However, they cause the cement paste to undergo sulfate attacks which hinders the cement paste (Garcia-Mate et al 2013).

Cement paste goes through unavoidable complex interactions with the surrounding environment, captured by chemical and physical changes. Thermal, drying, and autonomous deformations are the primary sources of dimensional changes in cement paste. Early age cracking is often associated to such deformations, especially when cement paste is restrained. A major determinant of hydration kinetics is the particle size which reflects the change in surface area exposed to water (Monteagudo, S.M et al 2014).

1.6 Significance

In an effort to better comprehend the mechanisms underlying cement hydration, the use of new technology is needed to enhance the prediction of properties. The nanoscience field of

study analyzes the measurement and characterization of the nanostructure of cement material to understand how the product affects macro-scale properties. A lack of knowledge on hydration process makes improving, predicting, and controlling the performance of Portland cement difficult. However, with the persistence of research and experimentation such as Infrared Radiation (IR) this deficit can be eliminated.

The chemistry behind cement hydration is commonly studied using spectroscopic methods. This present work investigates the mechanical properties of cement paste as it goes under several stages of hydration, monitored by SEM and FTIR. FTIR can study both the crystalline and amorphous groups within cement paste. IR operates by utilizing groups of atoms on molecules which absorbs various wavelengths of infrared light, depending on the atoms corresponding to that specific molecule, immediate surroundings and its geometry (Ylmén et al., 2009).

Plenty of progress has come towards the understanding and prediction of cement hydration. Modern cement technology requires further development of the Portland cement properties due to increased building demands. The rapidly expanding movement to minimize the physical footprint of the magnitude of cement production leads to technological advancement at the nano-scale. Cement being the most universal material in the world is nanostructured but strongly influences performance on a macro-scale. The evolution of technology and instrumentation is allowing for nanotechnology to become more relevant the civil engineering infrastructure.

1.7 Thesis Objective

The objective of this thesis is to investigate the effect on cement hydration of supplemental fly ash or silica fume on the mechanical properties of cement paste. The

integration of these two additives were studied to analyze their effect in accelerating C_3S. Percentages of each additive will replace the cement by volume at 5% and 10% to be studied at 3, 7, 14, 28, and 56 day ages. Testing will be carried out on 350 samples using a Forney Universal Testing Machine, MTS Landmark Servohydraulic Testing System (MTS), Fourier Transfer Infrared Spectroscopy (FTIR), and Scanning Electron Microscope (SEM). The testing methods will portray the compressive strength, modulus of elasticity, spectra, and images of the samples. This study will provide an understanding and insight towards the roles of fly ash or silica fume in the hydration properties of cement paste at various stages of hydration.

CHAPTER 2

Literature Review

2.1 Heat of Hydration

Heat evolution determinations can stem from various methods of testing that test the reacted cement. Pang et al. (2013) show that hydration of cement is represented by the rate of change of the overall reacted weight of cement. Chemical shrinkage tests is a recent development that also evaluates hydration mechanisms. In addition, in comparison to the chemical shrinkage, isothermal calorimetry is more instituted as a method of determining overall cement hydration. The isothermal calorimetry measures the heat of hydration of a cement paste with a constant temperature. However, the effect of curing temperature on cement hydration needs to be validated with more heat evolution testing (Pang et al., 2013).

2.2 Effect of Additives

Berodier & Scrivener (2012) both discover that acceleration rate increases as the particle fineness is increased due to surface nucleation. They found that more inert the particle is, the more the kinetics of cement is improved (Berodier, E., & Scrivener, K. 2012). Ferron et al. (2013) discuss the effects of applied shear forces on the aggregation of hardened cement paste (Ferron et al., 2013). In relation to chemical constituents, SEM imagery can uncover many physical changes that can serve a platform to build on. Scrivener (2004) shows that CSH with lower carbon to silica ratio is usually darker than a higher ratio in backscattered imagery such as CH. At a relatively high magnification the researcher must view various areas to achieve a full analysis (Scrivener, 2004).

2.3 Constituents

2.3.1 Calcium silicate hydrate (CSH). Calcium Silicate Hydrate is one of the major prevalent cement constituents. This reaction is a byproduct of hydration and grows over time. It is more apparent as it ages, especially with images from SEM. In addition, preparation of epoxy impregnated specimens with a polish provided significantly higher resolution than just polishing. In the case of advanced resolution capabilities, very thorough specimen polishing is required (Diamond & Kjellsen, 2006).

Recalling the fundamental thermal influence, the saturation of cement governs the amount of dissolution and growth of crystals. Bentz (2006) reported that at early hydration is higher that later hydration which allows for more dissolution. Cement paste was prepared showing that hydrating under sealed conditions increases the hydration rate by about 20% (Bentz, 2006).

2.3.2 Tricalcium silicate (C_3S). Tricalcium Silicate is another widespread constituent of cement. Alite is an assigned name that is common in literature for this chemical compound in the cement paste. Kjellsen. & Justnes (2004) found that the tricalcium silicate paste consists of features such as CH that completely fills up some porous areas, cores that are bordered by CSH product, and porous product (Kjellsen & Justnes, 2004).

Trapote-Barreira et al. (2013) reveal that SEM verified that CSH gel particles that precipitated CH from the C_3S hydration reaction. The reaction occurrence comes from the areas of highly concentrated diffused product (Trapote-Barreira, 2013). Thomas (2009) discovered that CSH densifies more slowly over time but acts opposite to heating curing (Thomas 2009).

2.4 Compressive Strength

The present work deals with the measurement of compressive strength which is an important parameter influencing the mechanical properties of cement paste. Lam et al. (2000) highlighted that the strength of cement paste is dependent on the gel to space ratio that is in turn dependent on the degree of hydration of the cement. Paulo de Castro Gomes (1997) highlighted using backscattered imaging to quantitate the relation between the hydration and the age of the cement paste. Hydration phases corresponded to peaks in the histogram that included porosity, other hydrated products, calcium hydroxide, inner product, and unhydrated product peaks, from left to right as a percentage of the total area. In all, these percentages that are acquired by backscattered imaging signify the total amount of pixels in the image file. Another method of porosity phase quantification is required to estimate hydration with higher accuracy (Paulo de Castro Gomes, 1997).

2.5 Supplemental Materials

2.5.1 Fly ash. Fly ash is a residue left from coal combustion and production. Fly ash consists of complex combinations of alumina, silica, unburned carbon, and various metallic oxides. The main chemical components in fly ash is silicon dioxide (SiO_2), aluminum oxide (Al_2O_3), iron oxide (Fe_2O_3), and lime (CaO). There are two commonly used classifications of fly ash used in cement paste supplementation, Classification F and C. Class F fly ash absorbs water from the surrounding cement paste much better than class C fly ash. For these reasons classification F will be used in this research experimental program.

Garcia-Mate et al. (2013) shine light on the possibility of high w/c ratios causing severe expansion that result in poor final strength and that lower initial particle sizes may reduce expansion. Porosity affects the mechanical strength and as it decreases over time by decreasing

water content, increasing strength (Garcia-Mate, et al., 2013). Narmluk & Nawa (2011) show that the higher the temperature the stronger the reaction. The degree of hydration of the cement in fly ash-cement paste was higher than that in pure Portland cement paste. The volume of the gel pores gets reduced as the CSH accumulates to occupy that space. Fly ash contains pozzolans, a siliceous material possessing cementitious properties, and consumes CH in the pozzolanic reaction (Narmluk & Nawa, 2011).

Replacing cement with fly ash is known to lower the early strength. With more fly replacement and higher water to binder ratio the compressive strength reduction is larger. Even a minor increase in water to cement ratio matches a great increase in the degree of hydration. With an increase of water to cement ratio of 0.2 from 0.2 to 0.4, the degree of hydration rises by 40% after 28 days. The hydration of cement in high-volume fly ash cement mix benefited from a water to cement ratio increase (Lam et al., 2000).

Furthermore, it is viewed as appropriate to have fly ash as an adequate replacement material with regards to hydration benefits. Zhang et al. (2000) found that less CH will decelerate the hydration reaction, best for the overall hydration of the specimen. The higher the fly as replacement percent, inversely the CH content is reduced (Zhang, Y.M., 2000).

2.5.2 Silica fume. This supplemental material is a fine white powder byproduct from silicon metal or ferrosilicon alloy production is very reactive in cement. Silicon dioxide makes up a large percentage of what is known as silica fume. A study by Zelic, J et al. (2000) shows that the pozzolanic reaction between silica fume and lime formed during cement hydration does not occur until three days of hydration (Zelic et al., 2000).

Kadri & Duval (2009) investigated the influence of the silica fume content on the heat of hydration of cement paste which gives information about the initial hydration reactions. The

silica fume showed high activity in the early stages; and accelerated the hydration rate as compared to that of the reference cement paste. The fine silica fume particles provided nucleation sites for growth of hydrates. After the growth, both strength and the hydration heat increased and the pozzolanic activity took over. A substitution of Portland cement by 10% silica fume produced greater strength as compared to that of the reference cement paste (Kadri & Duval, 2009).

Kjellsen et al. (1999) disclose that the compressive strength of cement paste is optimal with replacements of silica fume at a range of 10% to 20%. The strengths test were conducted on cement paste with water to cement ratios of 0.25, 0.3, 0.35, and 0.4 but 0.25 had the highest result at 28 days. The strength was above 100 MPa for both 10% and 20% at the 0.25 ratio. Compressive strength is more dependent on the decrease of water to cement ratio than the substitutions of percentages of silica fume (Kjellsen et al., 1999).

CHAPTER 3

Methodology

3.1 Experimental Procedure

This experimental study will investigate the strength and hydration of Portland cement with fly ash or silica fume compared to cement paste without the replacements. Compressive testing was carried out using a Forney and MTS testing machines. FTIR and SEM were used to monitor and portray the chemical transformations of the cement paste. Approximately 210 of tests were conducted using 4 in. by 8 in. cylinders and 2 in. cubes. The followings materials were used for testing.

3.2 Materials

The cementitious materials used during this study were Portland cement, fly ash, and silica fume.

3.2.1 Portland cement. The cement used in this study was of Portland cement Cemex Type 1. This cement complies with ASTM C-150, Type 1 and Federal specifications SS-C-1960/3, Type 1. The cement was obtained from Adams an Oldcastle Company and manufactured by Lafarge Building Materials, INC. Adams Products is located on Sandy Ridge Road in Colfax, North Carolina. Chemical analysis of Portland cement is shown in Table 3.1.

3.2.2 Fly ash. Fly ash is a by-product of coal-fired electric generating plants. It's the finely divided residue resulting from the combustion of ground or powdered coal, which is transported from the firebox through the boiler by flue gases. Fly ash consists of complex combinations of amorphous and crystalline phases. It is a mixture of alumina, silica, unburned carbon, and various metallic oxides. The main chemical components in fly ash is silicon dioxide (SiO_2), aluminum oxide (Al_2O_3), iron oxide (Fe_2O_3), and lime (CaO). There are two commonly

used classifications of fly ash used in cement paste supplementation, Classification F and C. Class F fly ash has a good susceptibility to reducing the alkali-silica reaction (ASR). This classification will mitigate this issue better than class C fly ash. Classification F will be used in this research experimental program.

3.2.3 Silica fume. Silica fume is a very fine noncrystalline silica produced in electric arc furnaces as a byproduct of the production of elemental silicon or alloys containing silicon. Also known as microsilica and is a worthy admixture. Silicon dioxide makes up a large percentage. Table 3.1*:*

Mix Design of the Cement Paste

Chemical	Portland Cement (%)	Fly Ash (%)	Silica Fume (%)
SiO_2	20.2	58.7	94.3
Al_2O_3	4.8	31.4	1.1
CaO	64.3	0.73	0.49
MgO	1.2	0.7	0.87
Fe_2O_3	3.2	3.7	0.7
Na_2O	0.49	0.24	0.42
K_2O	0.31	0.92	1.32
SO_3	2.9	0.2	-
LOI, Loss of Ignition	1.3	3.61	0.8

3.3 Cement Paste Mix Design

For the experimental setup, five (5) mix designs were created. The first mix, M_1, was the control mix with cement and water. The next four mixes, M_2, M_3, M_4, and M_5, consisted of a 5 and 10 percent of cement replacement by volume of fly ash and silica fume respectively. The water to cement (w/c) ratio was 0.40 for all mixes. The composition and cement paste mixes are displayed in Table 3.2.

(a) **(b)**

Figure 3.1: Materials: (a) fly ash and (b) silica fume

Table 3.2*:*

Combination and Properties of Cement Paste

Description	Control	5% F.A.	10% F.A.	5% S.F.	10% S.F.
Mix. No.	**M1**	**M2**	**M3**	**M4**	**M5**
Cement (lbs.)	24	24	24	24	24
Fly Ash (lbs.)	0	0.88	1.76	0	0
Silica Fume (lbs.)	0	0	0	0.84	1.68
Water (lbs.)	9.6	9.952	10.3	9.94	10.27
w/c	0.4	0.4	0.4	0.4	0.4
Yield (Ft^3)	0.277	0.287	0.297	0.289	0.300

For all mixes eight (8) cylinders and six cubes were created for each age (hydration stage). The cylinders used were comprised of plastic molds, 4 inches in diameter and 8 inches in depth, in compliance with ASTM C-470. The cubes used in testing were made of brass molds,

exactly 2 inch cube, and able to form three cubic specimens within each mold; and too in compliance with ASTM standards.

3.4 Mixing Procedure

All materials were placed in a clean, labeled stainless steel mixing bowl and weighed to the nearest ten thousandth of a pound. The cement and fly ash or silica fume were measured and dry mixed together by hand to reduce the loss of fine particles. Next, following ASTM Standard C-305, the water was poured into a rotary mixer bowl. The dry mixture (cement and additive) was then added to the mixer bowl. The Hobart HL 200, 20 quart mixer was used for all mixtures and illustrated in Figure 3.2.

Figure 3.2: Hobart mixer

Once the materials were in the bowl, they were mixed at a low rate (59 agitator rpm) for 30 seconds. After mixing on low speed, the mixing rate was increased to Level 1 (107 agitator rpm) for one minute. After finishing mixing, the mixture was carefully poured into cylinder and cube molds. The cylinders and cubes were then prodded, vibrated and leveled before stored away for curing. One cylinder from each batch mixture was weighed and measured to obtain the unit

weight. See Appendix E for unit weight values of all mixtures. See Figures 3.3 for mixing process.

For this experiment, a total of 150 cubes and 200 cylinders, totaling 350 samples, were made, cured, and tested. Table 3.3 displays the number of samples for both water and vacuum curing; representing the percent of fly ash and silica fume that corresponds to the days set to cure.

3.5 Testing Equipment

Several testing machines were used throughout this experimental study to obtain required data. The cement paste strength data was obtained using the Forney and MTS machines. The Forney machine was used for cylinder breaking and the MTS used for cube breaking. SEM and FTIR were used to analyze cement paste segments taken from each designed mix.

3.5.1 Forney machine. A Forney Universal Testing Machine was used to carry out all cylinders testing for compression. It has a 400 kip load capacity and a loading rate of 12000 lb./in. Figure 3.4 shows the Forney testing machine.

3.5.2 MTS. MTS systems are designed to provide high performance, flexibility and easy operational use. For this experimental study, the MTS Landmark Servohydraulic Testing System was used at a loading rate of 0.01 in/s; as seen in Figure 3.5. These systems include MTS software, FlexTest controls, MTS servohydraulic technology, and a complete selection of accessories.

3.5.3 Fourier transform infrared spectroscopy (FTIR). The functional groups of a compound were examined using Fourier Transform Infrared Spectroscopy (FTIR). The Thermo Scientific Nicolet iS10 FT-IR Spectrometer delivers the highest confidence in the verification and identification of materials. Its many features includes creating standard operating procedures

Figure 3.3: Mixing process of cylinders and cubes

Table 3.3*:*

Number of Cement Paste Samples

	Water Cure									
	Cubes					Cylinders				
	Control	Fly Ash		Silica Fume		Control	Fly Ash		Silica Fume	
Days	0%	5%	10%	5%	10%	0%	5%	10%	5%	10%
3	3	3	3	3	3	4	4	4	4	4
7	3	3	3	3	3	4	4	4	4	4
14	3	3	3	3	3	4	4	4	4	4
28	3	3	3	3	3	4	4	4	4	4
56	3	3	3	3	3	4	4	4	4	4
	Vacuum Cure									
	Cubes					Cylinders				
	Control	Fly Ash		Silica Fume		Control	Fly Ash		Silica Fume	
Days	0%	5%	10%	5%	10%	0%	5%	10%	5%	10%
3	3	3	3	3	3	4	4	4	4	4
7	3	3	3	3	3	4	4	4	4	4
14	3	3	3	3	3	4	4	4	4	4
28	3	3	3	3	3	4	4	4	4	4
56	3	3	3	3	3	4	4	4	4	4
		Total Cubes:		150		Total Cylinders:		200	Total Samples:	350

Figure 3.4: Forney universal testing machine

Figure 3.5: MTS landmark servohydraulic testing system

(SOPs) and suitable tests, verifies the quality of materials, identifies unknowns or mixtures, and can quantify mixture ingredients. The Nicolet iS10 has been specifically created for material

characterization and developing a final report. With the use of OMNIC Specta software, the Nicolet iS10 can manage results and provide accurate and valid answers. The Nicolet iS10 consists of System Performance Verification (SPV) which tests the instrument against ASTM E-1421 method to insure quality performance. SPV is a tool used to ensure the spectrometer is performing as expected, at all times. The Nicolet iS10 consists of an optical system which seals and desiccates the unit to protect the instrument from humidity and solvent vapors. Figure 3.6 displays the FTIR.

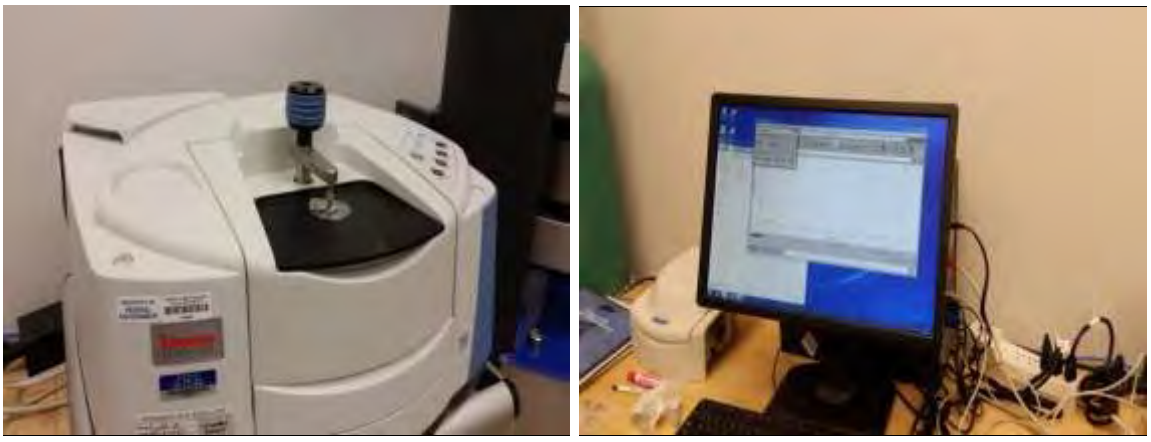

Figure 3.6: Fourier transform infrared spectrometer

For this experimental testing the Nicolet iS10 FTIR Spectrometer was used to identify and compare the unknowns within the cement paste mixtures. The FTIR spectrometer was used to identify the chemical properties during the hydration process.

3.5.4 Scanning electron microscopy (SEM). The high definition SEM EVO LS 10 made by ZEISS, was used for microstructure characterization and analysis of the hardened cement paste specimens. EVO LS 10 has full environmental capabilities to capture nano scale interactions of samples under various pressures, temperatures, and humidities. It includes EVO

HD, which further increases an image resolution and contrast using a high definition beam source technology with low acceleration voltages. During experimentation, the SEM was set into the environmental mode (EP) which allows atmosphere in the chamber since the sample is based on hydration. The scanning speed was set to four, which automatically changed the scanning cycle to 731 ms. The EP target set to 50 Pa, the KV value was set to 10 KV and the beam current to 46.0 µA. Figure 3.7 displays the SEM EVO LS.

Figure 3.7: Scanning electron microscopy EVO LS 10

3.6 Testing Procedures

After mixing, the cylinders and cubes were filled and labeled in accordance to standard specifications. As seen in Figure 3.8, all cylinders and cubes were unmolded after 24 hours and then half were cured in water and the other half vacuum cured for 3, 7, 14, 28, and 56 days until age of testing. After curing, the cylinders and cubes were dried in air for approximately one hour before testing.

Two methods were used for the curing process, water and vacuum sealing. Water curing involved the standard placement of the cement paste specimen into a water tank, completely

submerged in water. For vacuum curing, cement paste specimens were incased in vacuum seal bags and remained completely sealed until age of testing. The vacuum sealer used was a FoodSaver appliance series 2200 and displayed in Figure 3.9**.**

Figure 3.8: Unmolding cubes

Nearly half of the cement paste specimens created from each mix were cured in water and the other half vacuum sealed. For all mixes, the first four cylinders numbered 1, 2, 3, and 4, and the first three cubes numbers 1, 2, and 3, were water cured. The remaining cylinders and cubes, numbers 5, 6, 7, 8 and 4, 5, 6 respectively, were vacuum sealed. See Table 3.4 for labeling of cylinders and cubes for corresponding form of curing.

3.6.1 Testing procedure for Forney. The remaining cylinders and cubes were broken under compression using Forney for cylinder testing and MTS for cube testing. The Forney machine tests were performed with a load rate of approximately 12,000 lbs. /min. Cylinders were capped with either rubber pads or a capping compound in accordance to ASTM C-617. Forney

captured the maximum peak load applied to each cylinder under testing. See Figure 3.10 for Forney cylinder testing.

Figure 3.9: Vacuum sealer

3.6.2 Testing procedure for MTS. The MTS machine was preset to carry-out compressive strength testing for 2 inch cement paste cubes. The load rate for the MTS machine was 0.01 in/s. Once the cubes were ready for testing, each cube was placed in the center of the MTS bottom deck, outlined by circle rings. The cubes were then raised and properly positioned before running the test. After re-clearing the displacement, the test was ready to be performed.

Once each cube was tested till breakage, the data results were stored. Images of MTS tests are displayed in Figure 3.11. Each test run results obtained displayed the displacement in inches, loading in pounds, and the time in seconds. This data was later transferred to Excel to calculate the stress and strain, and further portrayed in the results.

Table 3.4*:*

Curing Labels for Cylinders and Cubes

	Cylinders		Cubes	
Curing Type	**Water**	**Vacuum**	**Water**	**Vacuum**
M1	1	5	1	4
	2	6	2	5
	3	7	3	6
	4	8	-	-
M2	1	5	1	4
	2	6	2	5
	3	7	3	6
	4	8	-	-
M3	1	5	1	4
	2	6	2	5
	3	7	3	6
	4	8	-	-
M4	1	5	1	4
	2	6	2	5
	3	7	3	6
	4	8	-	-

3.6.3 Testing procedure for FTIR. Once a cylinder or cube was crushed under compression, small samples were collected and later analyzed (the same day) with the FTIR machine. Each sample was labeled and stored in plastic bags until further testing was ready to commence. Prior to the sample placement onto the FTIR machine, the Omnic software was open to set-up the Experimental Setup. The program was set to collect and refresh data every 4 scans up to 8 scans. A background collection was collected prior to every sample being tested. The

FTIR transform and subtraction of the background were performed automatically. A sample was then placed on top of the FTIR's diamond and pressed down by a device to prevent space between the sample and diamond.

Figure 3.10: Forney machine in testing

Figure 3.11: MTS machine in testing

Five or more scans were performed for each sample, and the average of the total spectrums was saved. The tests were performed in the same fashion for each sample and data

collected was stored onto the Omnic program window. Later analysis were performed, along with data and results portrayed within the results section.

3.6.4 Testing procedure for SEM. Once the desired testing date was reached, one cylinder from each mix (water and vacuum cured) was cored using a Milwaukee Coring Rig Dymodrill, to extract a sample from the center. See Figure 3.12 for coring drill. Maintain balance on coring drill for safety and a smooth core. Core cement paste at 3, 7, 14, 28, and 56 days. Anchor down with two clinches, hook up hose, hook up extension cord, turn on water and drill, and turn crank slowly to lower. After the entire length of the cement is cored the drill can be raised. The core will either drop into the hole of the specimen or remain in the drill which requires a hammer to release the air pressure. With dried core label six lines for seven sections using a marker to mark a line at every inch. The samples received from the coring drill were later taken to the Joint School of Nanoscience and Nanoengineering (JSNN) laboratories, where they were prep for SEM imaging. Within the JSNN lab, a segment from each sample was cutout from the center of each cored sample using a diamond saw, seen in Figure 3.13. Use the gold soluble solvent to keep the saw cool while cutting. These segments were approximately ¾ inches in diameter and ¾ inches in depth. The segments were properly labeled with the percentage of fly ash or silica fume, curing type, and testing day and an arrow directing to the bottom surface used for imaging.

Once cutout and labeled, the segments were placed into a small container with the arrow on the samples pointing downward. The samples were then epoxied using 33% hardener and 66% resin, seen in Figure 3.14. To cover the samples with an epoxy coating begin with cleaning the blue containers for specimens by hand, and apply the release agent with a q-tip on all surfaces. Right after the epoxy mixture was poured; the samples were placed into a vacuum

pump and set to 27 kPa until bubbles formed at the surface. The samples were left for approximately nine hours until the epoxy mixture harden.

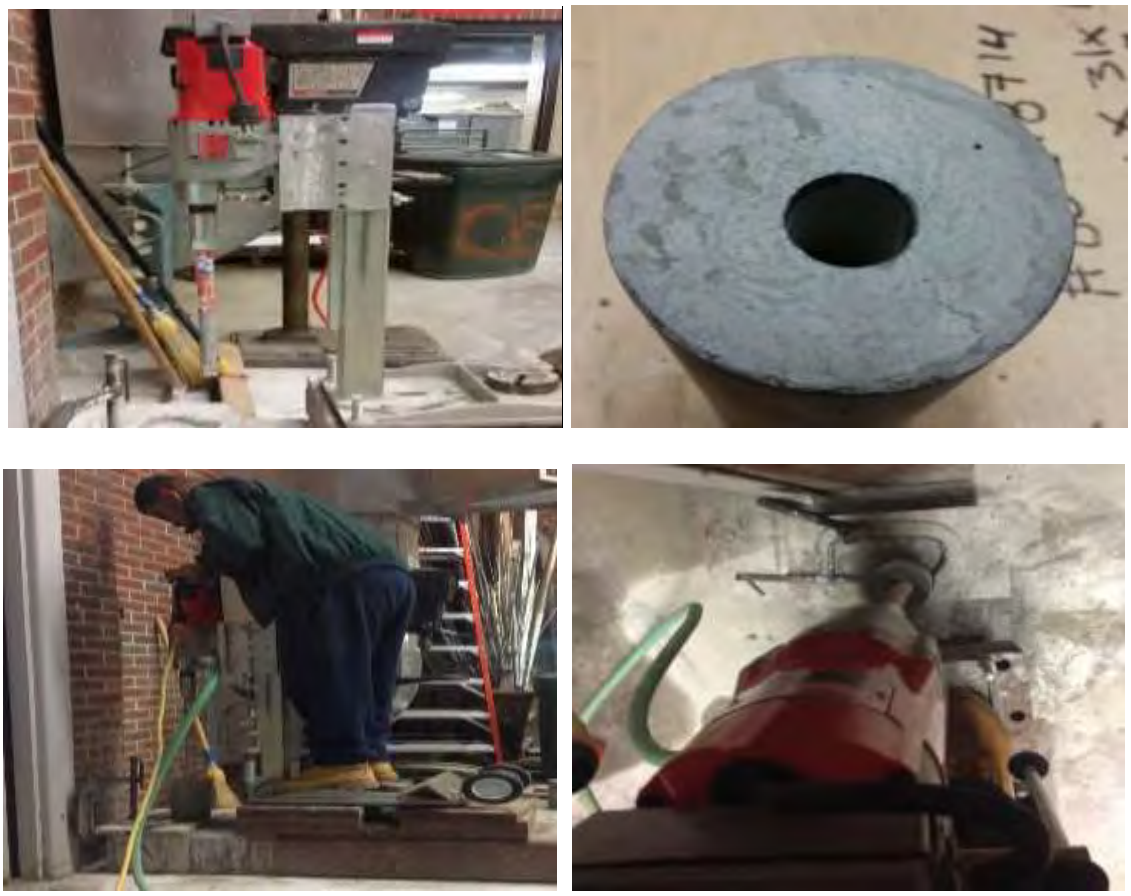

Figure 3.12: Milwaukee coring rig dymodrill

Once the desired time was reached, the segments were sanded and polished using a MetaServ 250 grinder-polisher, seen in Figure 3.15. The polisher was able to polish up to four samples at one time using the multiple sample holder attachment making sure to have the direction of the arrow pointing down. With three pounds of force applied and at a constant 175 revolutions per minute, the samples were placed through five polishing pads. First, a two minute grind with 240 grit paper.

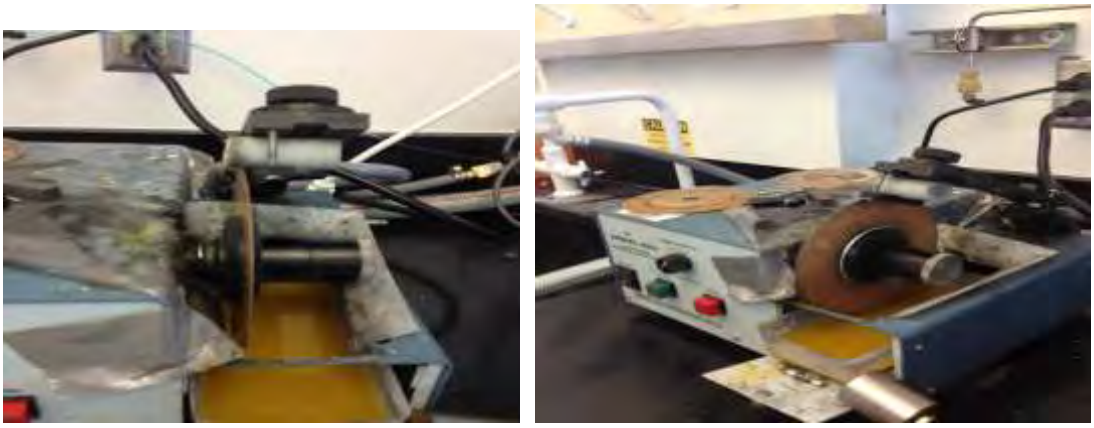

Figure 3.13: Diamond saw

Figure 3.14: Epoxy resin and hardener

Following, a four minute grind with 400 grit paper, an eight minute grind with 600 grit paper, a 12 minute grind with 1200 grit paper and a 15 minute polish of six micrometer grit paper using a six micrometer diamond polishing compound. All grinding also included ethylene glycol for lubrication. Afterwards, the samples were placed into a container filled with ethanol and sonicated for 10 minutes using the sonicator under the fume hood.

Figure 3.15: MetaServ 250 grinder-polisher

The samples were then ready for microscopic examination. Figures 3.16 portrays the SEM sample preparation process. The samples were placed onto a sample holder using black carbon tape, and positioned into the SEM. To access the software, click the SEM icon on the desktop to login.

First, vent the chamber in the vacuum tab. The SEM chamber can be seen in Figure 3.17. Slide in the sample holder holding all the samples with the open channel flat surface on the bottom facing the flat surface on the SEM so it is centered, calibrated, and connects well. Second, go to environmental mode (EP) which allows atmosphere in the chamber since the sample is based on hydration. In the scanning tab, select a speed of four which will automatically change the scanning cycle time to 731 ms. Verify the noise reduction is set to Line lnt which integrates the lines of the image for a clearer scan and the N is seven. In the vacuum tab, hit the pump button to pump the chamber since the samples are prepared to be processed for imagery. While the chamber pumps, hit the camera button on the keyboard to go ahead and get the first sample under the beam.

Figure 3.16: Preparation of SEM samples

In the stage navigation window that can be found in the side docking panel, make sure that the stage is set for carousel eight or nine stub. Raise the z no closer than 7.5mm with left joystick. Do not accelerate the stage up too quickly as it could collide with the beam and damage it. Another option for aligning the sample under the beam is to center it using the real time stage location in the stage navigation window to double click on the exact location that needs to be made the new center. This will place the sample under the cross hairs. Use the same center point technique in the stage navigation window to move the stage around for the processing of the next sample. Make certain that the tilt is on 0.0 degrees, type into the box if necessary. Make sure the stage is calibrated.

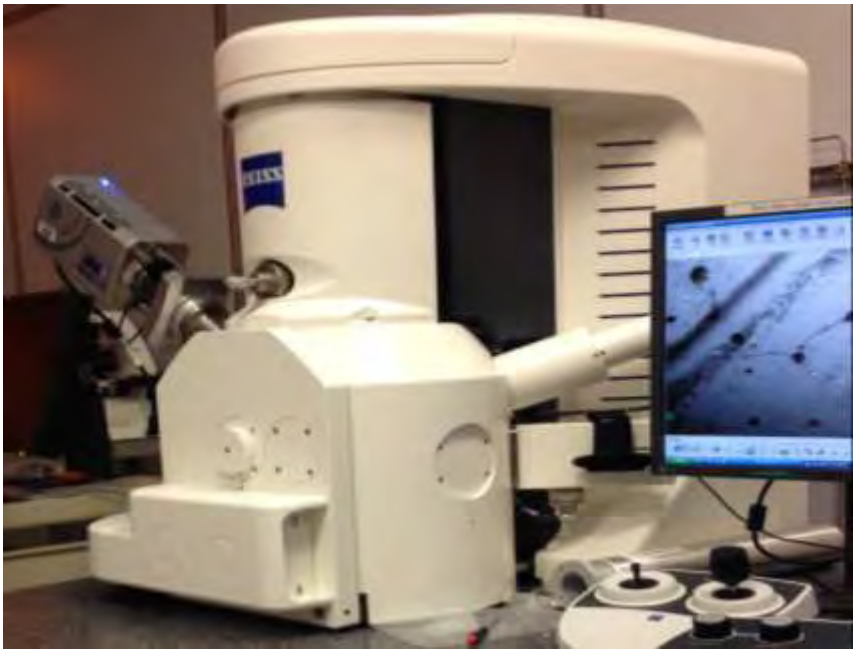

Figure 3.17: SEM beam chamber and gun

Pump the gun in the gun tab, do not ever vent the gun. A voltage of between 10 and 20 kV is appropriate for the gun. The voltage setting can be seen in the EHT target. Do not change the fill target amperage which is 1.876 A. For the best resolution use a spot size greater than or equal to 500 but start at 500 to achieve a signal and progressively get smaller over time. If the spot size is made smaller, some slight refocusing may be necessary. Keep beam current at 46.0 µA. Also in the gun tab, the beam state should not be grayed out anymore meaning the beam is ready then click on drop down menu and find Beam On to turn on the beam. In the detector tab, make sure the Signal A=BSD which is backscatter mode. If backscatter mode is switched on but there is not a good enough image to determine anything, start with Signal A=VPSE G3. This is the default signal for the SEM and can offer a descent alignment to serve a starting point. The SEM has electron fields using aperture to focus light into a beam. There will not be a Collector Bias so zero volts for this is appropriate.

Next, align beam by clicking on the emission button in the apertures tab and positioning the light to the center by using the shift and tilt arrows in the window. The backscatter window can be opened from the side bar with the arrow on the right edge of the image. In the BSD window, for backscatter mode, make sure it's on COM, not TOPO. Note the brightness and contrast when switching over to C2 BSD, backscatter mode in the detectors tab, because it will change. Make sure auto range is unchecked and that all quadrants are on positive detection. Using the BSD Gain at a high level has the clearest image for cement and the best reduction of noise from vibrations.

Now the cycle, each of the setting must be adjusted in the same order for however many repetitions it take to correct the image to its very best. All the settings are adjusted using knobs on the keyboard seen in Figure 3.18. First, use the reduce button to shrink the image to smaller area so that the scanning is faster and the changes made are more easily seen. Next, increase the magnification using the knob as far as any object can be noted. Focus on the object using the focus knob, if can't focus then back off magnification. Use the X and Y stigmator knobs to clear the image up as much as possible, it is a subtle change so focus your vision on defined lines. Without using the stigmator knobs the entire image will rotate when focusing. Lastly, find the maximum gun tilt by getting the image all white then find the middle grounds where it is the brightest, can tell by when it begins to get darker. Do for both X and Y gun tilts. Repeat the cycle until the objects can on the image cannot get anymore clearer due to such a high magnification.

Begin by looking for features like a uniformly gray area, bubbly rocks, calcium hydroxide which is smoother rocks with darker edges, tricalcium silicate is the fiber looking crystals, and other hydrated product is in the gray area. A usual good starting point is setting the

brightness to 50% and the contrast to 25%. If there is not enough gray on the image, the contrast is too high so lower. The repetition is continued until the best balance of contrast and brightness is achieved. To select a new center use Ctrl + Tab to have cross hair appear then select the point with the mouse. In environmental mode charging is reduced which changes the colors in the current window. Consistently check on the aperture light for any changes if so move back to the middle. Also, make sure the box is checked for "move in vent on stage navigation" and "track z" in the stage navigation window.

Figure 3.18: SEM keyboard

Open the histogram using the button on the bottom right after the scanning is complete to see if the adjusts are feasible. The histogram is the best tool to determine the balance after each slight adjustment in either. Scanning is complete when the Line Int = Done appears. Make sure the bottom bar shows fine and not course so adjusting is not an over adjustment. Stay away from dry balls because there is bad hydration there. If the last peak is highest make darker. More darkness brings main peak higher. Darkness via the brightness or the contrast knob brings the

histogram to the left. More brightness makes the little outside peaks higher and shifts peak to right more than contrast does. The lower the contrast, the higher the side peaks on the histogram. Try to get the histogram to show three or four peaks. Double clicking on an open histogram figure window can refresh after any changes in the image have been made.

To save the image, like the one in Figure 3.19, go to file in the toolbar then save in the directory location where all images are. Remember to be consist with the naming convention of the images for future referencing purposes. Save three images for each area. A separate image of each of the following need to saved: the original alone, the original with the data zone bar on the bottom, and the original with the histogram. It is recommended to use a scan speed of three or four to expedite the processing and using a speed of seven or eight when the clearest image is finalized. Be careful on faster scan speeds since they might over correct the contrast. Do not use a scan speed slower than eight because there is no noticeable difference in the quality of the image. Hit the freeze button on the scanning tab. Freeze scan once more at a slower speed to display the image clearer.

The images can grow more out of focus over time since the beam does shift and tilt on its own. Check on the tilt and the shift for this reason. Move the sample directly under beam if the image center has changed. Repeat the imaging and saving for a total of three areas for each sample. In the gun tab, select shutdown in the beam state window. In the vacuum tab, hit the vent button to vent the chamber and access the samples. Go to extended pressure dropdown menu then hit go to HV then hit pump so the vacuum is not damaged from over exertion. Finally, go to file and logoff.

For the Matlab analysis shown in Appendix A, a script is written in the editor to run the code that processes the images from the SEM. There are a total of five outputs from the Matlab

script. The five outputs are figures with their own windows that consist of images, histograms, and area percentages. The first is a figure of the original image of the sample as figure one. The second is a figure of the original image after it is analyzed with pixel color coding. The third is a figure of a histogram of the original image representing the pixel count of the level of gray. The fourth is a figure of a histogram of the original image with color coding divided into three distinct areas. The fifth are percentages of each of the areas compared to the complete histogram. The color coding is used to represent the five major hydration phases that are present in the image. These three phases are, from left to right, porosity, calcium silicate hydrate, and calcium hydroxide.

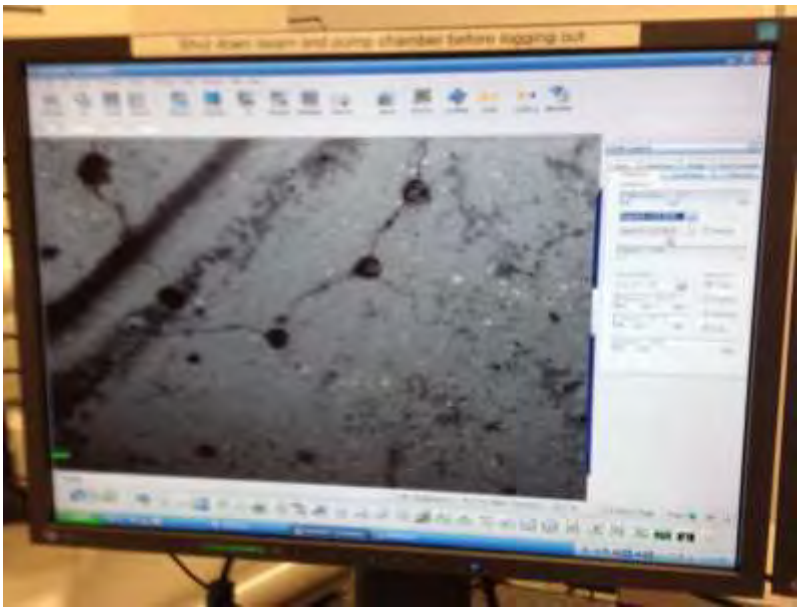

Figure 3.19: SEM monitor with image

In further detail, the script is a collection of commands that are all read once it is run using the correct format. Matlab is a powerful tool and a very precise one as well. One slight punctuation error can cause the entire script to fail to run at all and in the command window error statements in red show what should be corrected. The good thing about the script is that to the

far right of the command line in question will be a box with a certain color depending on the severity of the mistake. A solution appears as the cursor hovers over the box. Once the line is corrected the box is replaced with a green line. Some of functions of the commands in the script call the original image from its location in the hard drive, repeat loops until conditions are satisfied, or calculate a mathematical expression.

In the original image a Gaussian filter was selected for all analysis. In this filter there is a fixed standard deviation (σ) value of 0.4 that represents an optimal grayscale which avoids noise vibrations in the image. Theses settings were selected for all image analysis. The outputs that follow are dependent of the initial filter to the original image. Open Matlab in Citrix and open the Matlab script attached. Set all the images that are going to be analyzed as the current directory in the left window of Matlab. In the Editor window, the script should be open. Change the image name to the one that is going to be analyzed in the uiopen and the imload lines. The name from the first line can be copied to the next. Run the script. Evaluate the bounds or threshold set within the histogram. The threshold is the left and right bounds of each hydration phase in the histogram. They should be placed at the location that is at the tangent point of peaks' slope.

Take a note of the better placed threshold from the visual inspection. For example the porosity might have a threshold of 0 to 60, CSH has one from 61 to 170, and CH has one from 171 to 255. In the script I have assigned a variable for each bound. For example, the porosity has T1 and T2 for its left and right bound, respectfully. The same would be done for both CSH and CH for their bounds (T3, T4, T5, and T6). Adjust the values for the variables to the ones from the inspection. Only have to change T2 and T4 since T3 and T5 depend on them, respectively. Rerun the script for the same image with the new bounds gathered to display the

three images and the two histograms. Using the snipping tool, select the images and the histograms. Open a word document and write the name of the image from step 2 in it. Copy and paste the snips into the word document below the name of the image. There should be total of five. Use the same order as they were displayed. For example the snip from figure 1 would go first then then the snip from figure 2 and so on. Also include the porosity, CSH, and CH areas from the command window after the last histogram.

CHAPTER 4

Results

4.1 Compressive Strength

4.1.1 Forney universal testing machine. The Forney Universal Testing Machine was responsible for determining axial compressive strength for all cylinders. The Forney machine is reliable enough to ensure repeatable results even at high levels of force until failure. Recognition of the Forney machine comes from being able to change to a compressive strength setting, quality results, and minimal frame elongation. By definition the compressive strength of the sample is the maximum load divided by the cross-sectional area. The significance of the compressive strength testing is to validate a mix design for the safety in the duration of the cement paste structure and its user. The results from testing are displayed by column graphs in the following figures. Figure 4.1 shows the average compressive strengths for all water cured testing cylinders. This figure represents the 0%, 5% and 10% of fly ash and silica fume to cement replacements, against the 3, 7, 14, 28 and 56 day tests. As shown in the figure, the 10% of silica fume consistently outperforms the 5% silica fume and the control at all ages except three days. Figure 4.2 show the average compressive strengths for all vacuum cured testing cylinders. Table 4.1 displays the compressive strengths values which corresponds with the plotted data in Figure 4.1. Table 4.2 displays the compressive strengths values which corresponds with the plotted data in Figure 4.2.

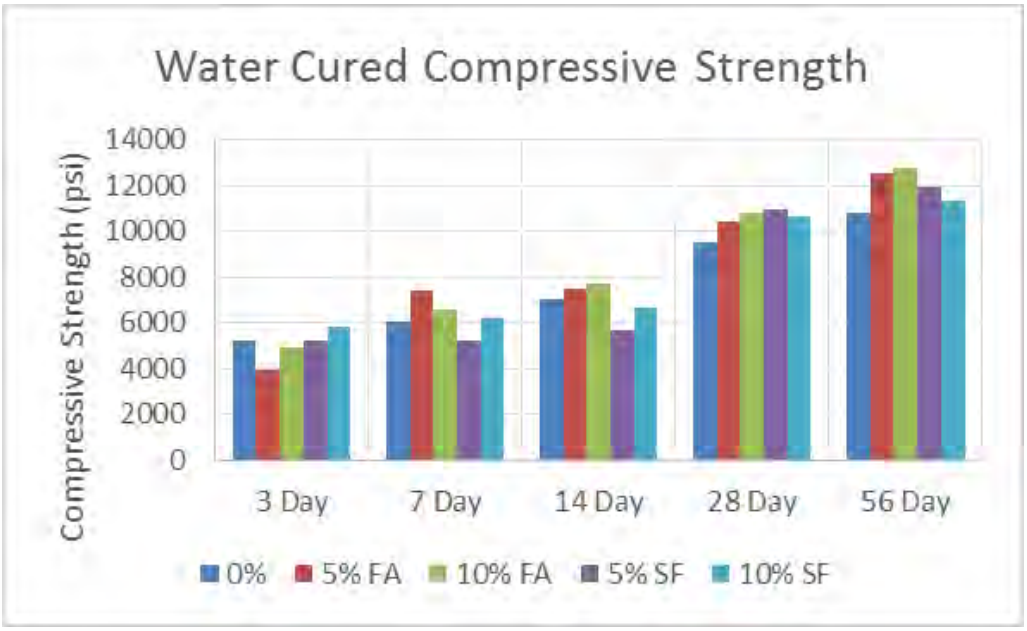

Figure 4.1: Average cylinder compressive strength results for all water cured samples

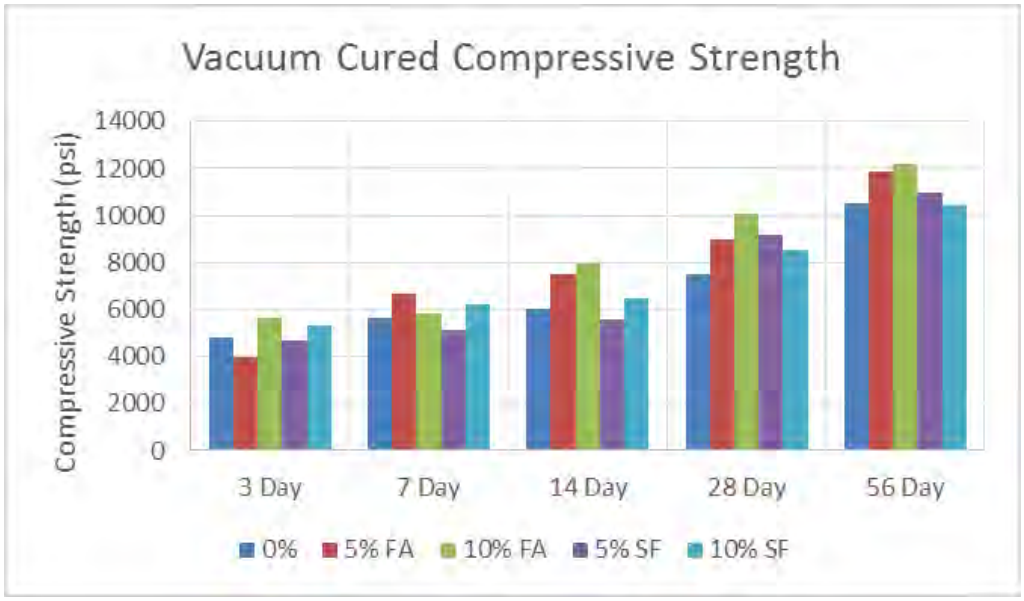

Figure 4.2: Average cylinder compressive strength results for all vacuum cured samples

In both the water and vacuum curing, the compressive strength increased with each age.

Table 4.1:

Cylinder Compressive Strength Values for all Water Cured Samples

Average Compressive Strength Results (psi)					
Replacement (%)	**3 Day**	**7 Day**	**14 Day**	**28 Day**	**56 Day**
0%	5219	6058	7033	9505	10842
5% FA	3973	7396	7462	10440	12511
10% FA	4910	6567	7682	10836	12798
5% SF	5197	5207	5649	10933	11920
10% SF	5822	6231	6628	10619	11329

Table 4.2:

Cylinder Compressive Strength Values for all Vacuum Cured Samples

Average Compressive Strength Results (psi)					
Replacement (%)	**3 Day**	**7 Day**	**14 Day**	**28 Day**	**56 Day**
0%	4838	5616	6056	7503	10508
5% FA	3990	6652	7507	8967	11880
10% FA	5931	5812	7929	10057	12166
5% SF	4651	5124	5582	9180	10998
10% SF	5333	6250	6463	8545	10467

To compare the cylinder compressive strengths of the reference curing methods, a separate column graph was created to represent the comparison. Figure 4.3 displays the average cylinder strength of the 0% controlled samples that were water and vacuum cured at all testing ages. Similarly, Table 4.3 shows the compressive strength values which corresponds to the data plotted in Figure 4.3. This data shows the water curing samples with a higher compressive strength at all testing ages than that of the vacuum cured samples.

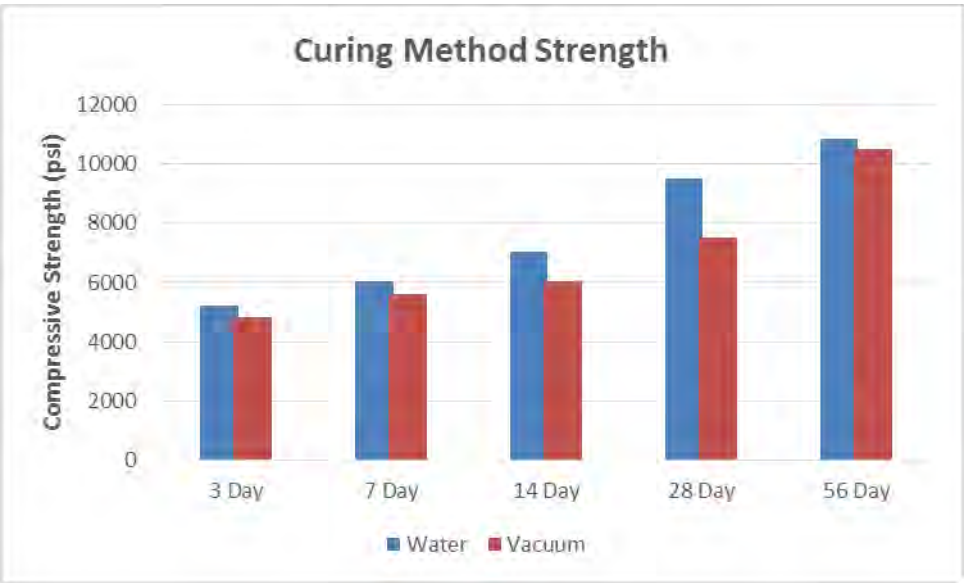

Figure 4.3: Cylinder comressive strengths of water and vacuum cured controlled cment paste

In comparing curing methods, water curing outperformed vacuum curing in compressive strength of cylinders at all ages. Also, there is strong correlation of increasing strength from 3 to 56 days for either curing method.

Table 4.3:

Cylinder Compressive Strength for Both Curing Control Samples

Compressive Strength of Both Curing Methods (psi)					
Reference	**3 Day**	**7 Day**	**14 Day**	**28 Day**	**56 Day**
Water	5219	6058	7033	9505	10842
Vacuum	4838	5616	6056	7503	10508

See Tables 4.4 and 4.5 to compare cube ultimate compressive strength for water and vacuum curing of all replacements, respectively.

Table 4.4:

Cube Ultimate Compressive Strength for Water Curing for All Replacements

Ultimate Compressive Strength (psi)				
Replacement (%)	**3 Day**	**7 Day**	**28 Day**	**56 Day**
0%	6149	8377	11921	12793
5% FA	4465	8157	12002	14219
10% FA	5321	7208	12176	11702
5% SF	4903	5559	13248	12755
10% SF	6262	6693	12068	12606

Table 4.5*:*

Cube Ultimate Compressive Strength for Vacuum Curing for All Replacements

Ultimate Compressive Strength (psi)				
Replacement (%)	**3 Day**	**7 Day**	**28 Day**	**56 Day**
0%	5070	7542	8526	12220
5% FA	4785	7667	9963	13497
10% FA	6055	6502	11275	9812
5% SF	4828	5513	10152	11896
10% SF	5735	6713	9706	11627

4.1.2 MTS stress-strain curves. The stress –strain curves yield the behavior and properties of the cement hydration with each supplemental material by displaying the deformation with applied uniaxial compression stress. The significance of the stress-strain curve is to evaluate the properties of a material including the elastic limit, yield strength, ultimate strength, and to determine the Young's Modulus. Stress-strain curves were developed from each concrete cube tested with the MTS Landmark Servohydraulic testing system. From each test performed, the loading (in pounds), displacement (in inches), and time (in seconds) were extracted and imported into Microsoft Excel to determine the stress and strain. The stress was obtained by dividing the load at each time interval, by the surface area of the specimen. The strain was acquired by dividing the displacement (or change in material length), by the original length of the specimen. As stated in the experimental procedure, each material was casted into three cubes; 0%, 5% and 10% of fly ash and silica fume to cement replacement for water and vacuum curing. The stress-strain curves created from the three cubes were averaged together to obtain a single averaged stress-strain curve for each material tested.

4.1.2.1 Fly ash (FA). Additional figures were created to compare the different curing days against the change in fly ash percentages that can be found in Appendix D. Figure 4.4 shows the seven day stresses for 0%, 5%, and 10% fly ash replacement for both water and vacuum cured samples.

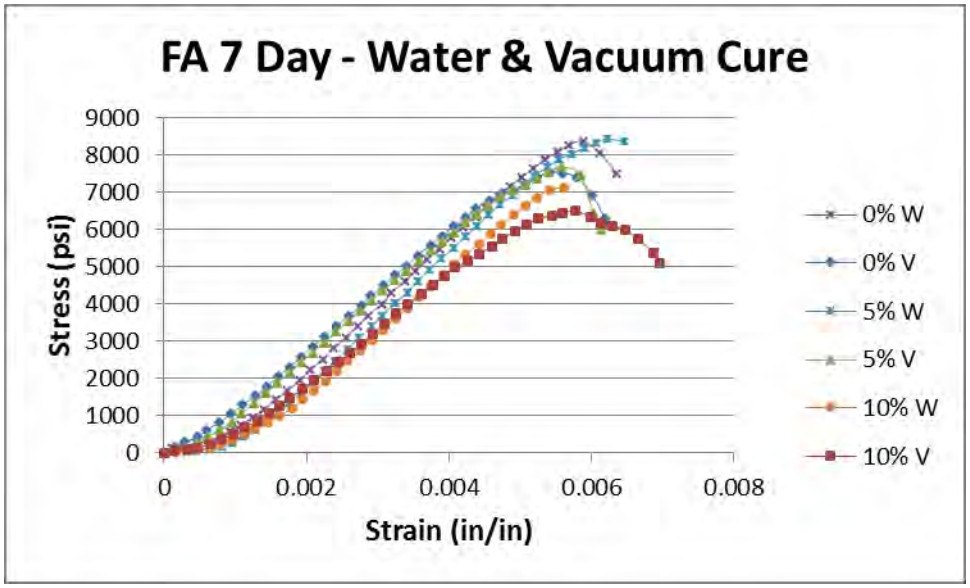

Figure 4.4: 7-day stress-strain curves of controlled cement paste, 5%, and 10% fly ash

4.1.2.2 Silica fume (SF). Figure 4.5 shows the 56 day stresses for 0%, 5%, and 10% fly ash replacement for both water and vacuum cured samples.

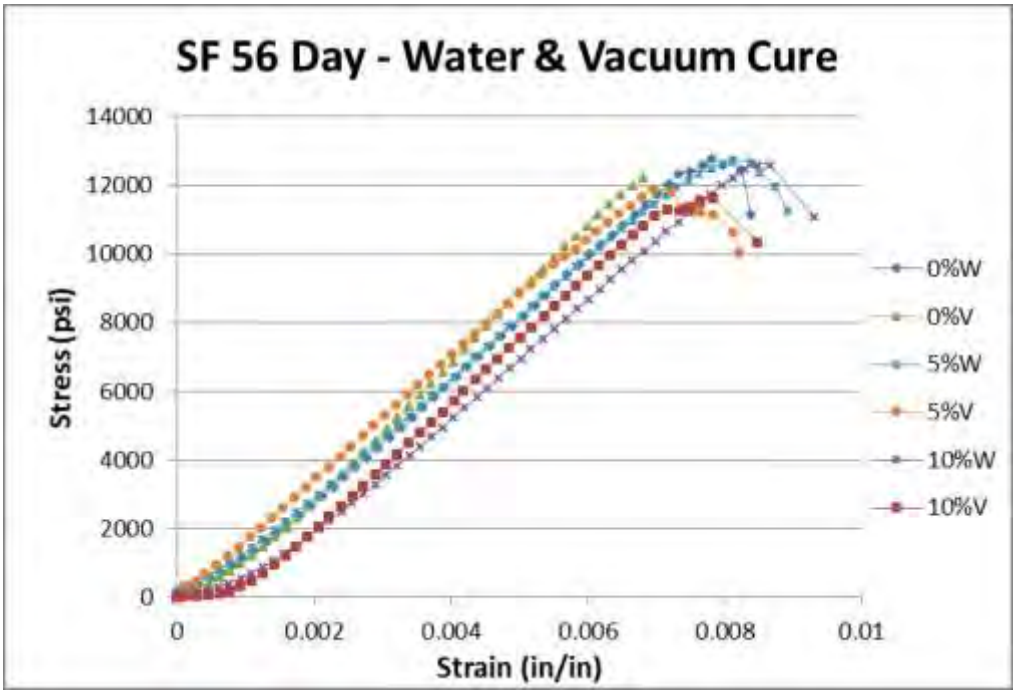

Figure 4.5: 56-day stress-strain curves of controlled cement paste, 5%, and 10% silica fume

4.1.3 Modulus of elasticity. The modulus of elasticity (or elastic modulus or Young's modulus) is a value or number which measures the materials deformation once a force is applied. It describes the materials tensile elasticity or the materials tendency to deform along an axis when the force applied is along the same axis. The modulus tests were performed following ASTM standard C496. The test results are portrayed in the following figure**,** Figure 4.6, by a line graph. Each line signifies a different testing material. As seen in Figure 4.7, the reference 0% water and the 0% vacuum cured samples performed similarly in elasticity. However, with the addition of fly and silica fume, the deformation significantly increases during each age of testing. Table 4.4 portrays the elastic modulus values of the modulus test shown in Figure 4.6 and 4.7. The results indicate the elasticity of the 0%, 5%, and 10% water and vacuum cured samples for all testing ages.

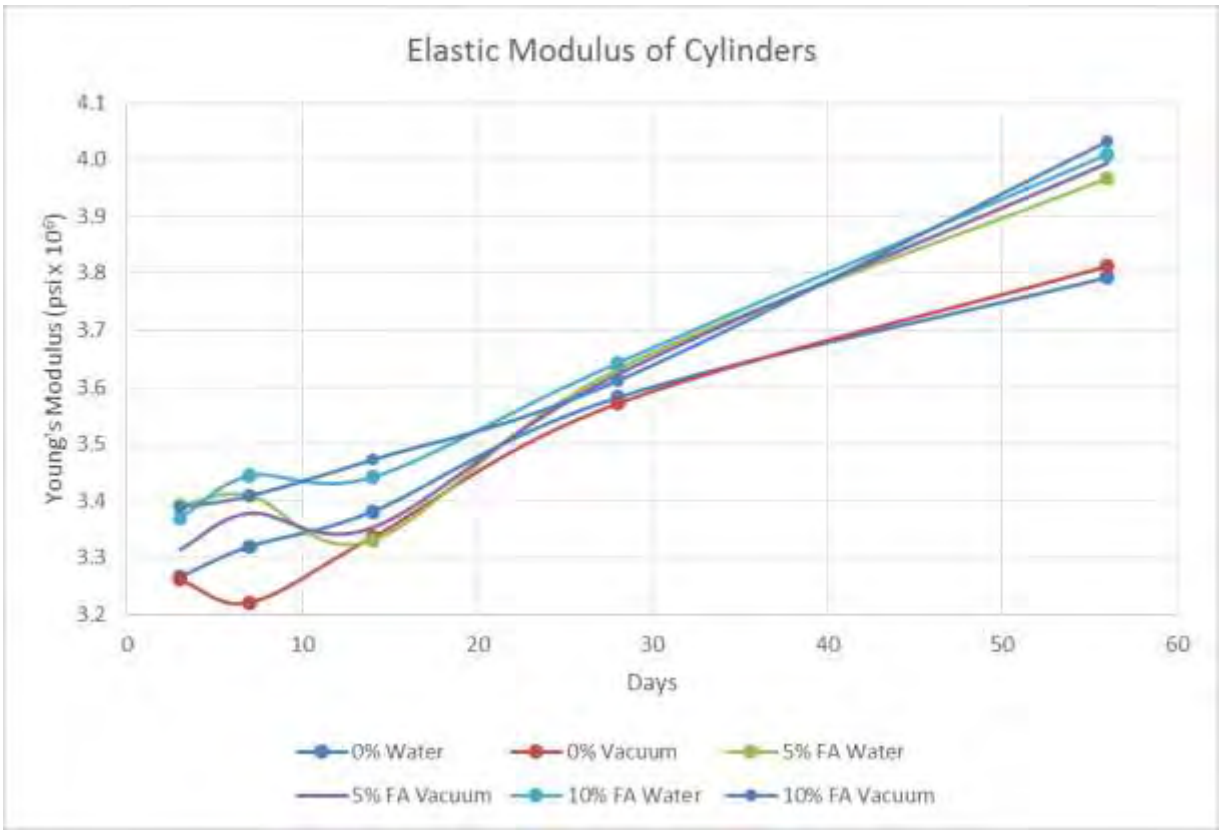

Figure 4.6: Elastic modulus of water and vacuum cured fly ash at all testing ages

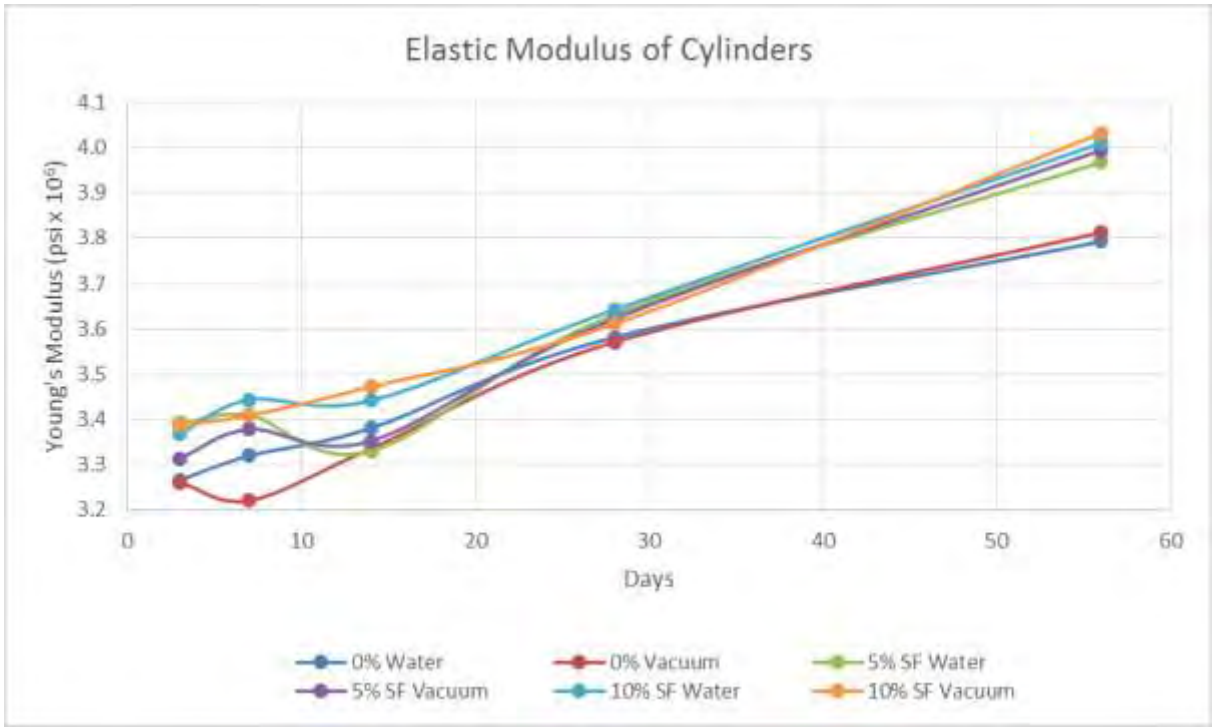

Figure 4.7: Elastic modulus of water and vacuum cured fly ash at all testing ages

Table 4.6:

Elastic Modulus Test Results for all Replacements and Testing Ages

Elastic Modulus Test Results (psi x10^6)					
Replacements	**3 Day**	**7 Day**	**14 Day**	**28 Day**	**56 Day**
0% Water	3.27	3.32	3.38	3.58	3.79
0% Vacuum	3.22	3.26	3.33	3.57	3.81
5% FA Water	3.39	3.41	3.33	3.63	3.97
5% FA Vacuum	3.31	3.38	3.35	3.62	3.99
10% FA Water	3.37	3.44	3.44	3.64	4.01
10% FA Vacuum	3.39	3.41	3.47	3.61	4.03
5% SF Water	3.25	3.34	3.39	4.09	4.17
5% SF Vacuum	3.18	3.38	3.42	4.13	4.21
10% SF Water	3.34	3.38	3.40	4.12	4.20
10% SF Vacuum	3.36	3.37	3.42	4.15	4.24

4.2 FTIR

Fourier Transform Infrared Spectroscopy (FTIR) was used to monitor the hydration process and to approximate the amount of CSH formation within all samples. Infrared or IR, is a type of invisible radiation which falls within the spectrum beyond red light. IR is invisible electromagnetic radiation or radiant energy with longer wavelengths than that of visible light. The IR wavelength or spectrum ranges between 700 nm to 1 mm; corresponding to a frequency range of 430 THz to 300 GHz. Infrared is divided into subdivision, usually consisting of three spectra regions of near, mid and far. The wavelength range for each region varies depending of the technology used in gathering the infrared light. The near infrared region is approximately 12800 to 4000 cm^{-1}; mid infrared is approximately between 4000 to 200 cm^{-1}; and far infrared is

approximately between 1000 to 50 cm^{-1}. However, in spectroscopy the region of study falls within the mid infrared region.

Spectroscopy is a technique used to identify molecules by their analysis of constituent bonds. Infrared absorption spectroscopy is a method to determine structures of molecules with its characteristic absorption of infrared radiation. All chemical bonds vibrate within the IR range with each chemical bond of a molecule vibrating at a frequency characteristic to that bond. A group of atoms in a molecule, such as CSH may have multiple modes of oscillation due to the stretching and bending of the bonded group. When there is a change in dipole in the molecule, then the molecule will absorb a photon that has the same frequency. Molecules absorb radiation of specific wavelengths that cause changes in dipole when the sample is exposed to infrared radiation. When viewing a spectrum, the number of absorption peaks is associated to the number of vibrational freedom of that specific molecule. Likewise, the intensity of absorption peaks is associated to the change of dipole and the transition of energy levels. The spectrum comes from the energy released from the frequency of the bond; the stronger the bond, the higher the number. A spectrum of all the absorption frequencies of that sample are then recorded using light radiation from 4000 to 400 cm^{-1}. Most organic compounds and inorganic ions fall within this region, making it a commonly used region for infrared spectroscopy.

4.2.1 Process of using FTIR.

Step 1:

The first step in using the FTIR is sample preparation. The samples used for this study were fragments obtained from the crushing of the cement paste cylinder and cubes, succeeding the compressive tests. Each sample varied in size but was able to completely cover the diamond

used for testing. Figure 4.8 shows a cement paste sample placed under the FTIR and ready for testing.

Figure 4.8: Cement paste sample under FTIR testing

Step 2:

Before placing the specimen or sample onto the FTIR plate, a background check has to be performed. A background check is performed to remove traces of dissolved gases and solvent molecules that can contribute information to the sample that does not exist within the sample. See Figure 4.9 for illustrated background spectrum. The background spectrum contains information about of the surrounding gasses and solvent molecules. This spectrum can then be subtracted away from the spectrum obtained from the sample tested. This subtraction process is an automatic feather and process that happens whenever a new sample is tested.

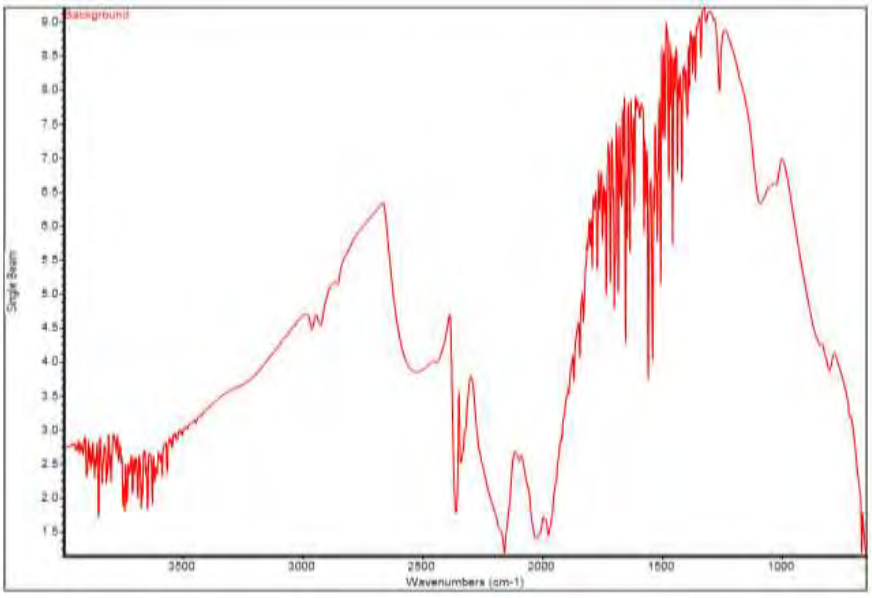

Figure 4.9: Background spectrum collected prior to collection of sample spectrums

Step 3:

After the background has been collected, the first sample can be collected. A single beam spectrum from the sample is then created, containing the absorption bands from that specific sample. For this experimental study, at least 5 spectrums were collected for each sample, and the average of all the spectrums collected was recorded and used for results and discussion. Figure 4.10 shows the average of 5 spectrums or tests collected for 0% cement replacement after 3 days water cured.

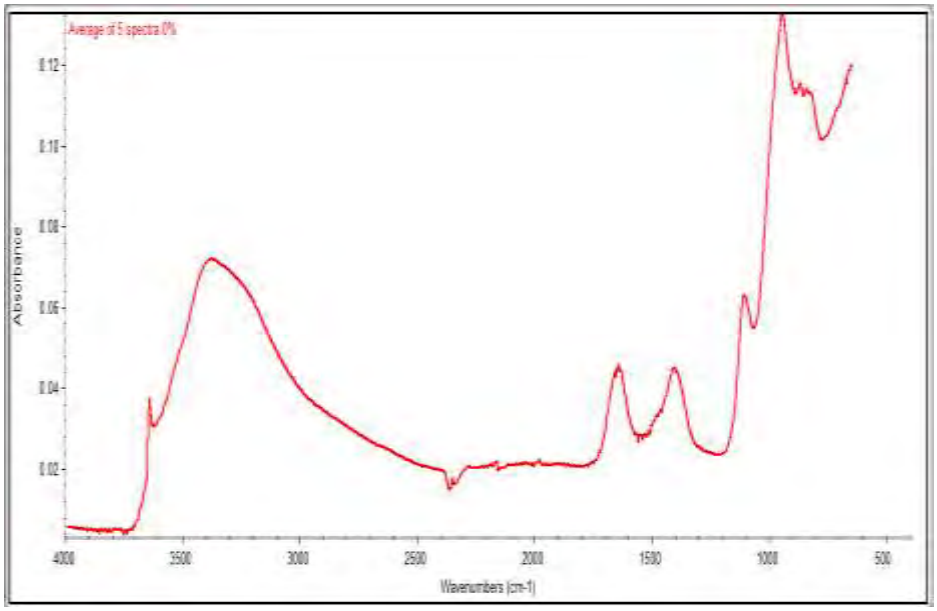

Figure 4.10: Average spectrum of 5 spectrums collects for sample

Step 4:

After each sample spectrum has been obtained, data analysis was carried out and observed using the OMNIC software. For each sample, the absorption frequency bands assigned to each sample spectrum was observed for normal modes of vibrations within the molecules. These spectrums were later analyzed and compared within the discussion.

4.2.2 Hydration of cement paste. In this study, the hydration process was monitored for 3, 7, 14, 28, and 56 days, by acquiring an FTIR spectrum for each sample under water and vacuum curing. While collecting the spectrums for the 14 day test results, samples were collected 5 to 6 days after the 14 day age of testing. This was due to a malfunction with the FTIR machine, which postpone the exact time allotted to collect the 14 day spectrums. Once the 14 day spectrums were collected at a later date, the spectrums shown to be inconsistent and unreliable in comparison to the other days tested. Because of the 14 day spectrums collected on a later day and portraying spectrums irregular to exact 14 day test results; the 14 day spectrums were removed from the results and discussion within this study. Therefore, the results will portray the

remaining days tested at the proposed age of testing, which are the 3, 7, 28, and 56 days for both water and vacuum cured samples.

Figure 4.11 is the reference spectrum for the anhydrate dry cement. As seen in the figure, two major peaks occur around the wavelength numbers of 877 cm^{-1} and 1100 cm^{-1}. From the chemical composition of Portland cement and from past literature for possible assignment for peaks observed on cement spectrum; the peaks can possibly be assigned to the CaO and the SiO_2 for the two peaks respectively (Ylmen, 2009).

The recorded spectra for the hydrated 3, 7, 28, and 56 day water and vacuum cured samples are displayed in Figures 4.12 and 4.13 respectively. A full set of FTIR spectra can be found in Appendix C. The curing days increase from 3 to 56 days, from bottom to top of the spectra. From previous literature, signatures of hydration can be seen within the 900 to 1200 cm^{-1} region. Also notice the large peak in the area of 3400 cm^{-1}, which can be associated with hydrogen bond (O-H) or capillary water within that region. The broad band in this region (approximately 2400 to 3600 cm^{-1}) is caused by the stretching vibrations of the O-H groups of hydroxyls with a range of hydrogen bonds. As the hydration process continues with time, more of the H_2O molecules complement the production of calcium silicate hydrate (CSH) shown within the 900 to 1200 cm^{-1} region (Bjornstrom, 2004).

For comparison purposes, spectra were created using the change in fly ash replacement in respect to the specific day tested, for both water and vacuum cured samples. The remaining spectra for the 5% and 10% fly ash and silica fume replacements for both water and vacuum cured are displayed in Appendix D. Calcium silicate hydrate is a weak bond structure which appears around 1100 cm^{-1} and can be associated with the peak in that region. To enhance these effects in the 900 to 1200 cm^{-1} region, serval difference spectra were created by subtracting the

spectrum of the dry cement from the spectrums of the hydrated test samples. By using the dry cement spectrum as a reference, the spectroscopic features within the 900 to 1200 cm^{-1} region can be seen more clearly and can observe the development of CSH within this region. To enhance the effects of the spectroscopic feathers of each sample, the reference dry cement spectrum was subtracted from each sample spectrum. The purpose of this subtraction technique is to remove the bonds of the reference material away from that of the sample material tested. This is performs by determining the difference in absorbance between the two spectra and plotting the difference against the wavenumber. When doing so, the reference spectrum is automatically multiplied by a subtraction factor so the reference materials bonds subtract out property (Pavia & Lampman, 2008). Figure 4.14 displays the results from the reference dry cement spectrum subtracted from the 0% control sample spectra for all testing days. Figure 4.15 displays the same data from Figure 4.14; however the spectra are offset for clarity.

The remaining difference spectra for all testing samples including fly ash and silica fume content and vacuum cured are portrayed in Appendix D. Knowing that the formation of CSH occurs within the approximate region of 900 to 1100 cm^{-1}, spectra can be zoomed into this area for further analysis. In Figure 4.16, the areas of the 0% control samples that were water cured, were calculated and shaded with the corresponding spectrum for all testing days. Spectra are still offset for clarity purposes. Figure 4.17 represents the same data presented in Figure 4.16; however the spectra are zoomed into a range of 800 to 1600 cm^{-1} and offset so better visualization. Knowing that the polymerization of silica to form CSH occurs within this approximate region, spectra can be zoomed in for further analysis.

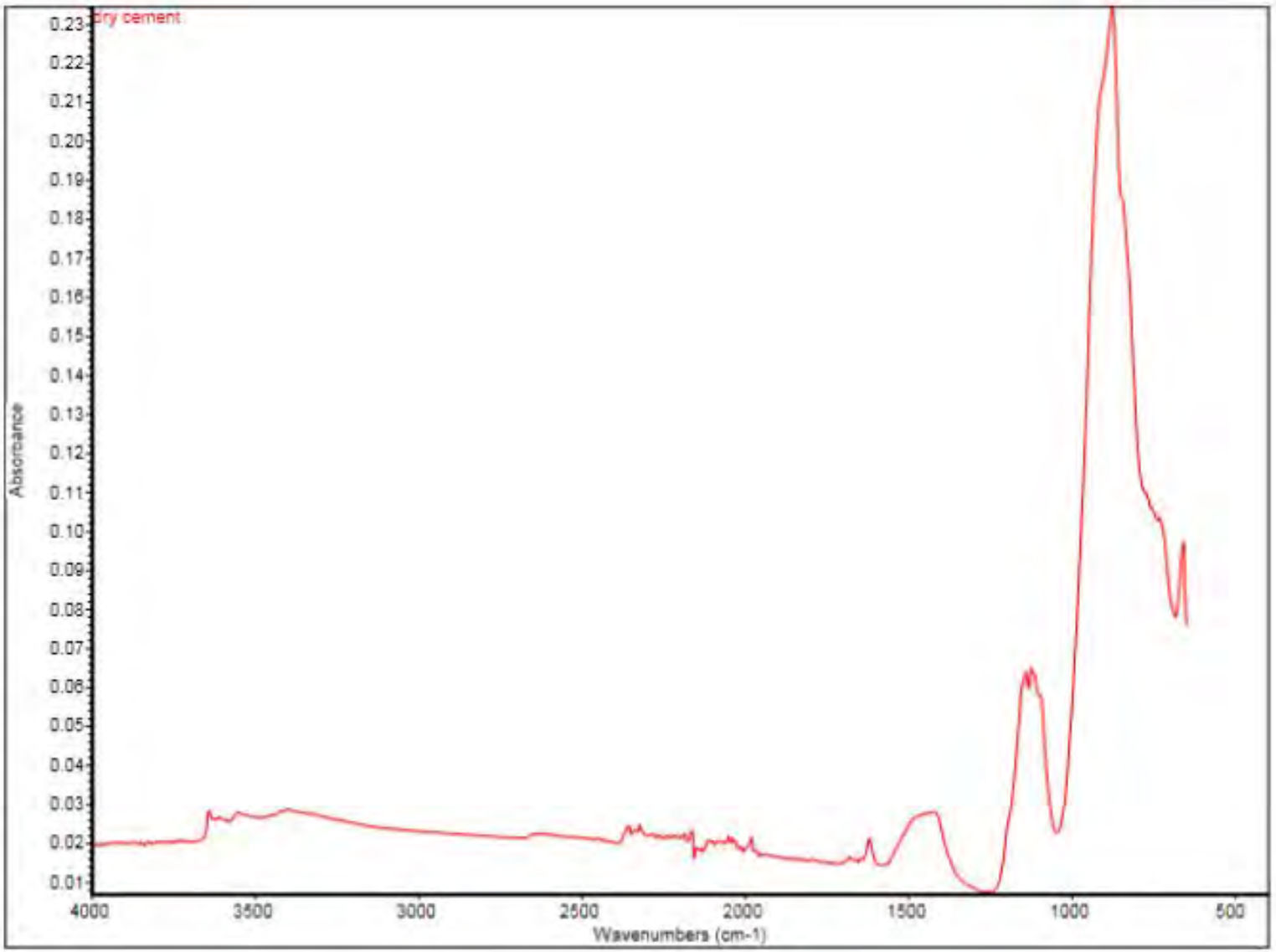

Figure 4.11: Spectrum of anhydrate dry cement

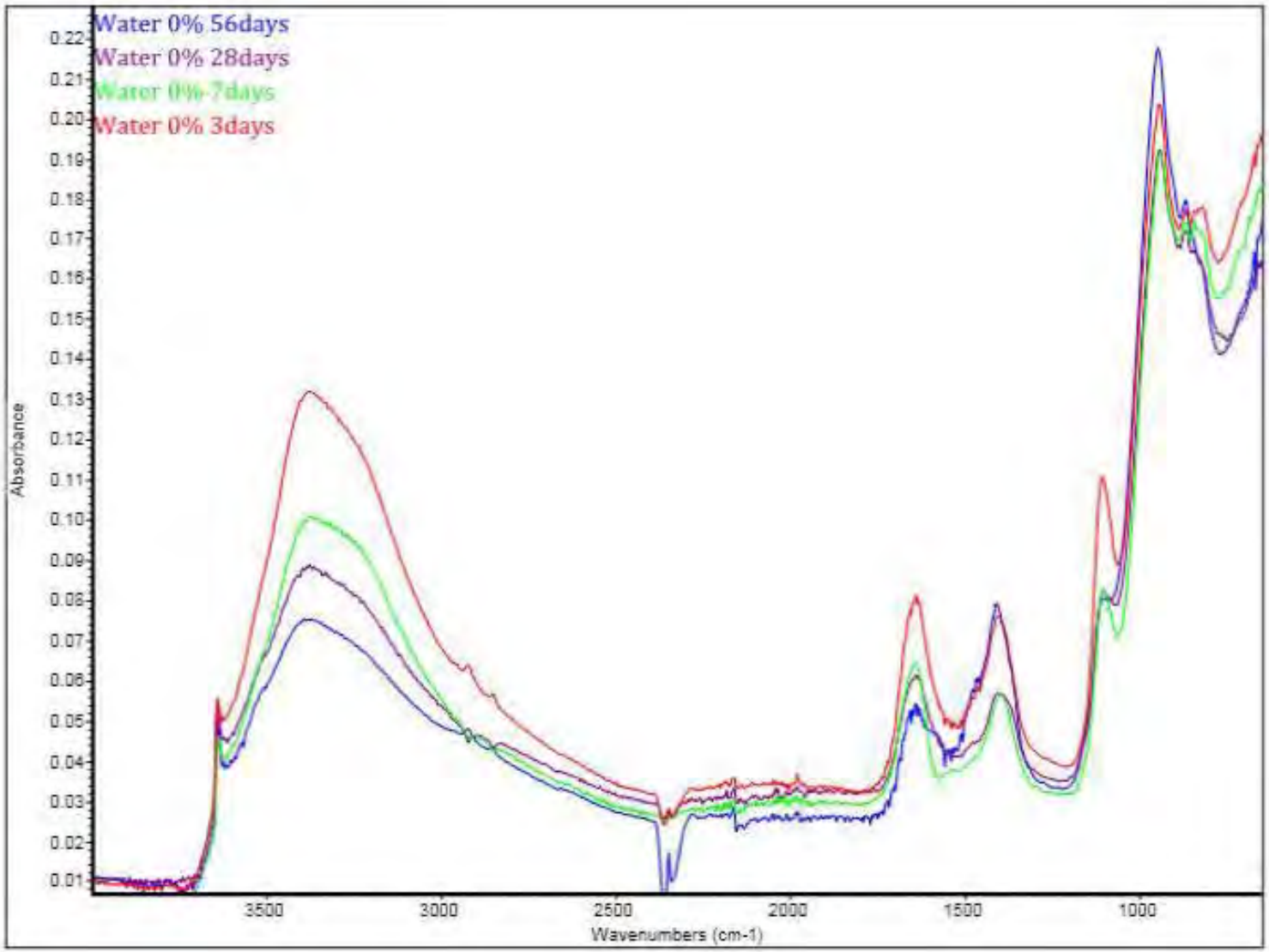

Figure 4.12: Absorbance of 0% reference spectra of water cured samples, 3 to 56 day tests

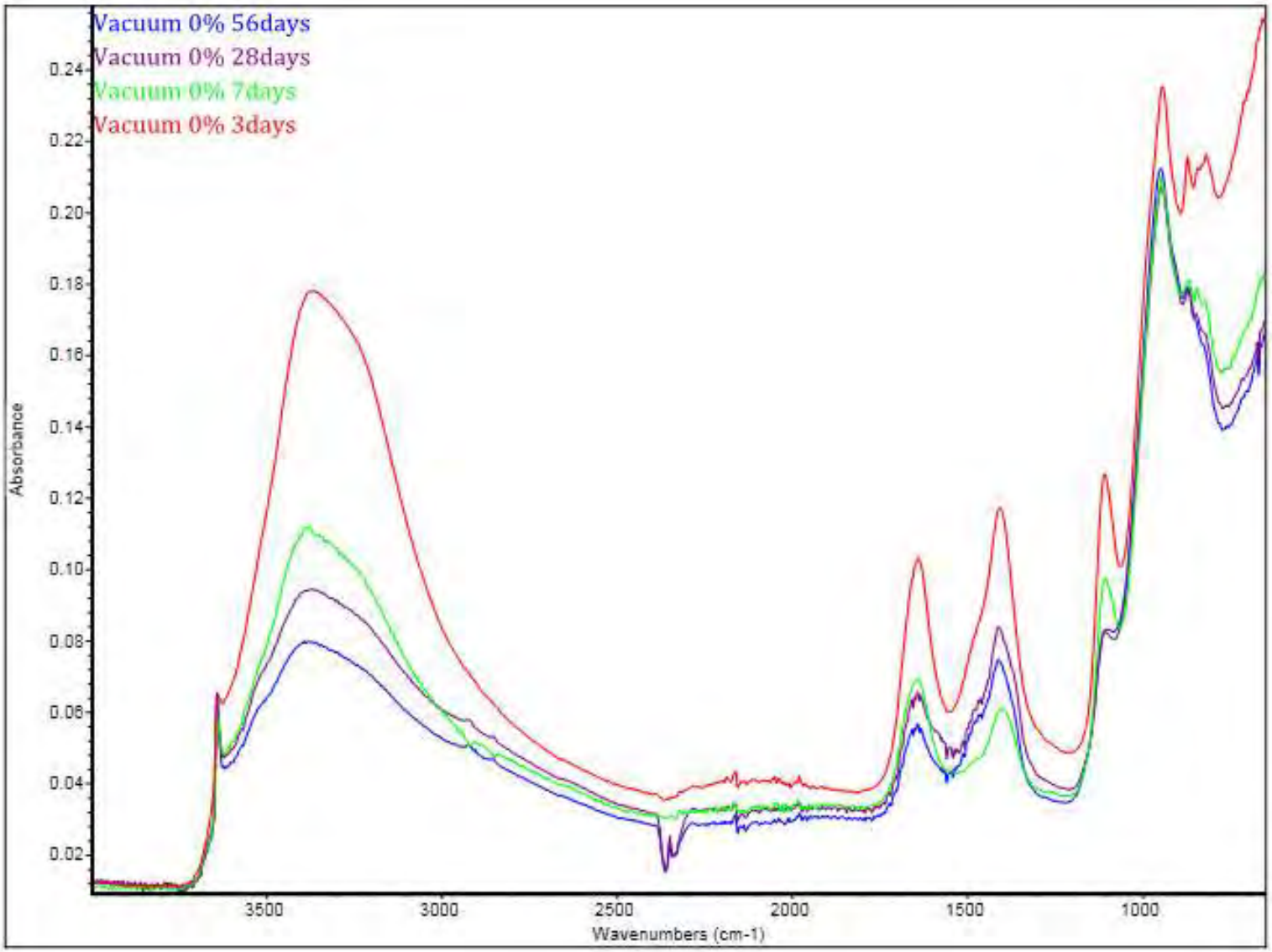

Figure 4.13: Absorbance of 0% reference spectra of vacuum cured samples, 3 to 56 day tests

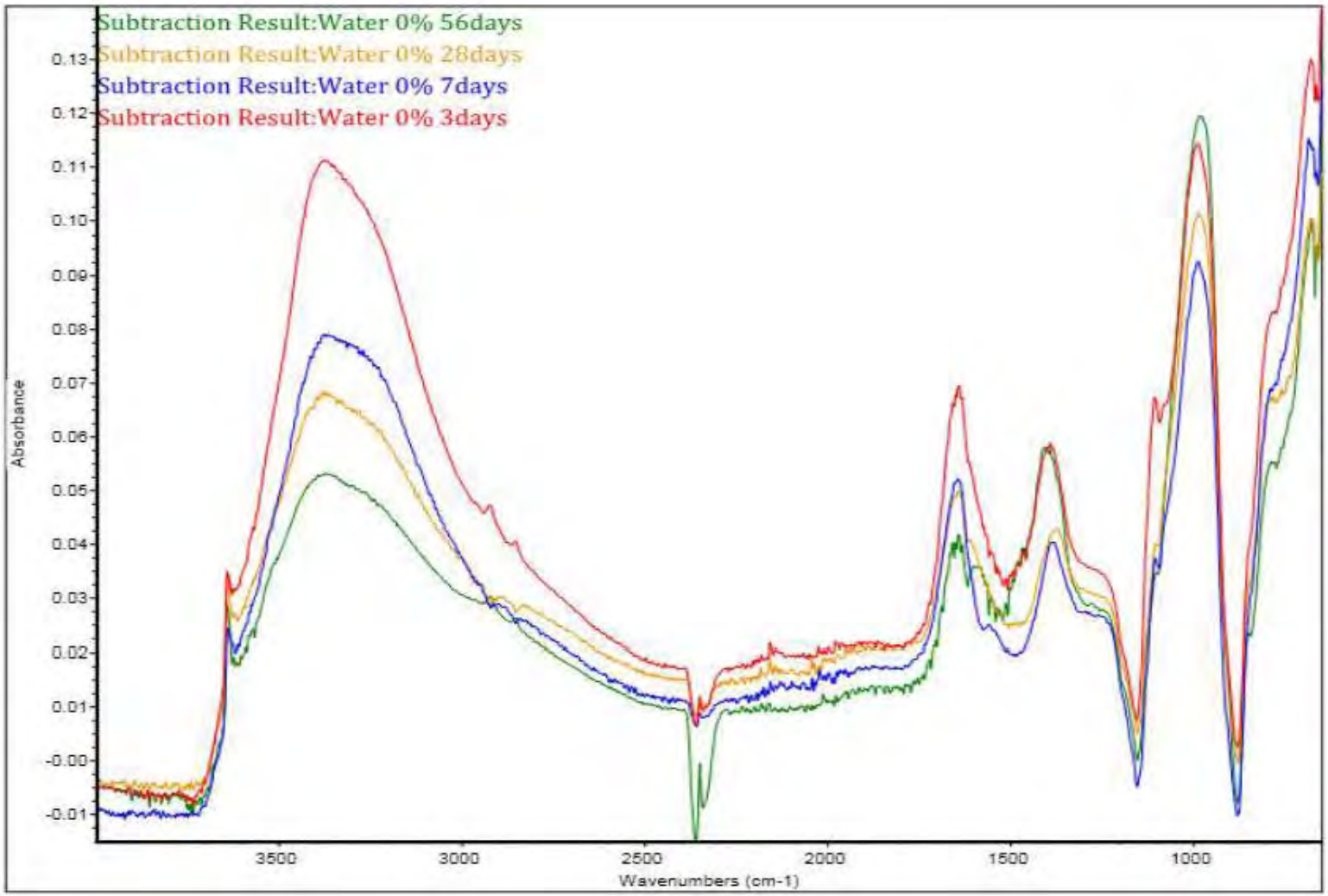

Figure 4.14: Difference spectra of controlled water cured samples for all ages

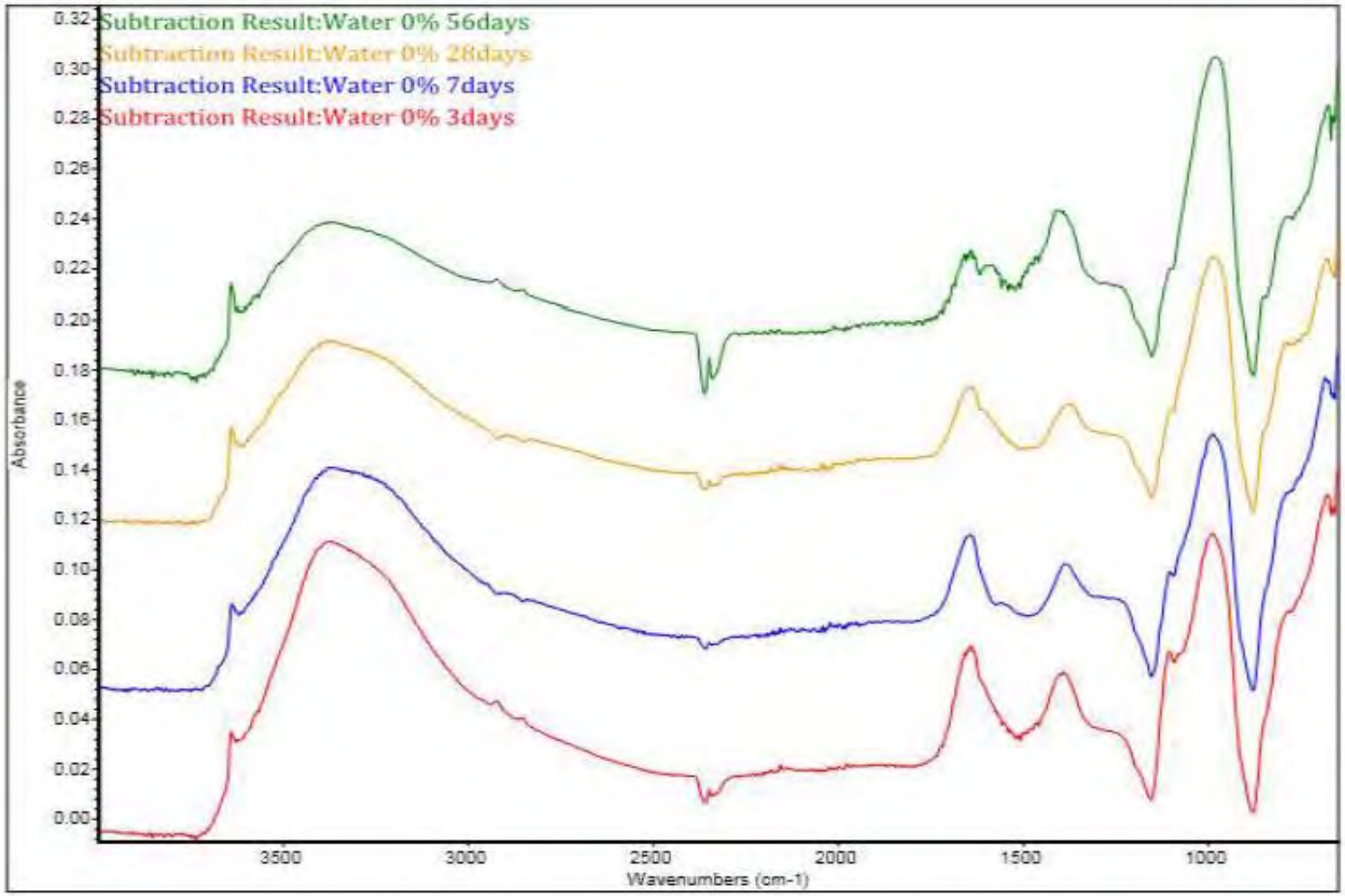

Figure 4.15: Offest dfference spectra of controlled water cured samples for all ages

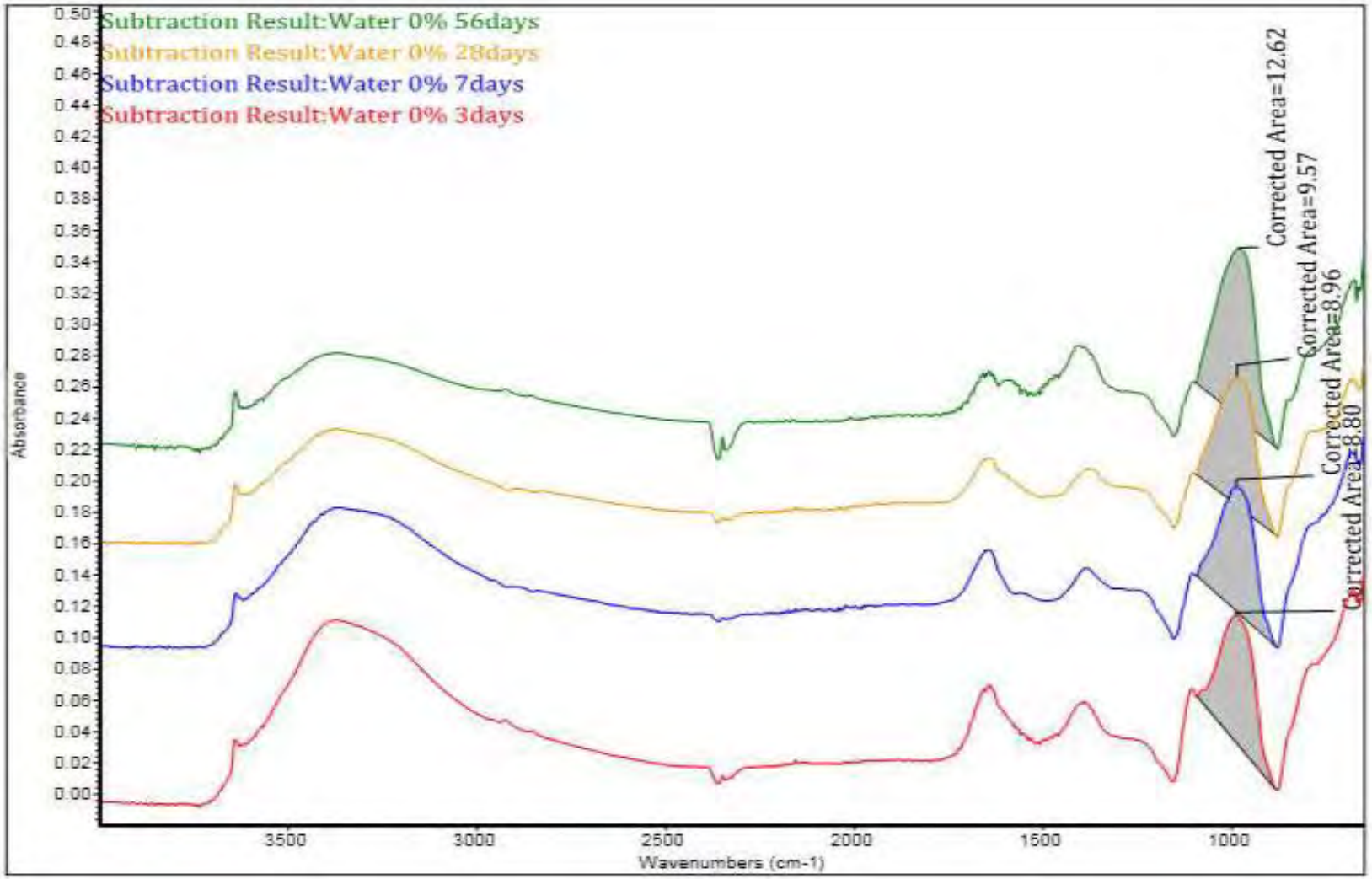

Figure 4.16: Offest spectra of control water cured samples for all ages with CSH area

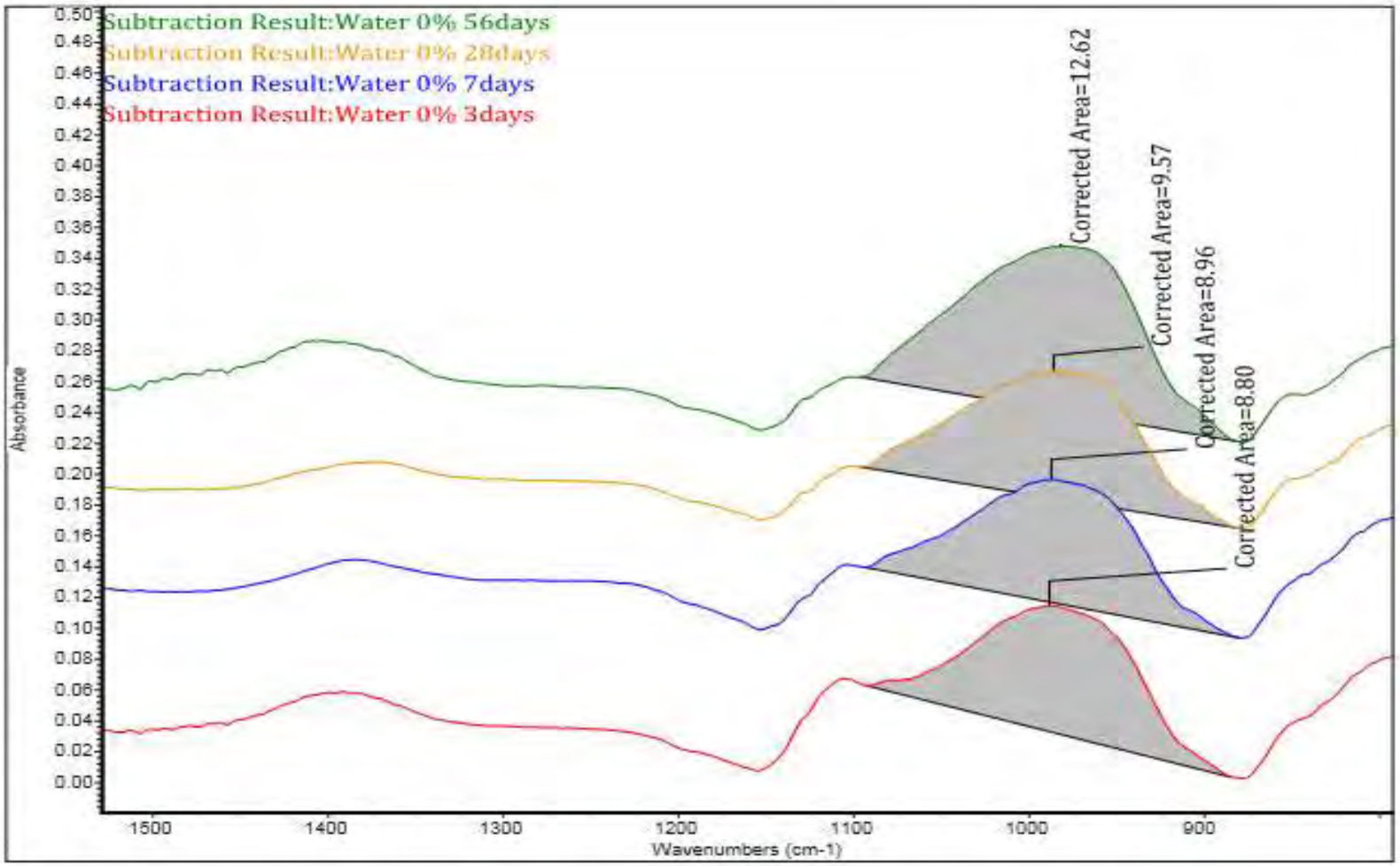

Figure 4.17: Offest spectra of control water cured samples with zoomed CSH area

Using the OMNIC software, the area of the peak region associated with CSH can be exerted by creating a baseline between the two dips neighboring that region. The OMNIC software has icons to help gather and obtain this data, accurately and fast. By choosing the "Area" icon and clicking on the peak in which the area is trying to be found; the software will automatically distinguish the optimum baseline values for the peak region. After selecting the baseline for the desired area, clicking on the "Annotate" command, will enable the software to compute the area under the peak region and within the perimeter of the baseline chosen.

Once obtaining the possible CSH formation from each sample, further analysis can be conducted. Table 4.5 displays the area amounts of CSH formation from each sample tested, for all testing days, percentage of fly ash or silica fume replacement, and both water and vacuum cured.

Table 4.7

Areas of CSH Formation for all Testing Samples at 3, 7, 28, and 56 Days

CSH Area Table									
		Water Cured				Vacuum Cured			
Materials	**Percentages (%)**	**3**	**7**	**28**	**56**	**3**	**7**	**28**	**56**
Control	**0%**	8.8	8.96	9.57	12.62	9.9	10.2	11.18	11.91
Fly Ash	**5%**	10.12	10.24	10.35	10.38	5.69	9.81	10.57	11.16
	10%	8.73	10.63	12.29	12.73	11.23	11.76	12.84	13.32
Silica Fume	**5%**	10.14	10.47	11.18	11.32	11.15	12.33	12.48	12.61
	10%	11.68	12.33	12.6	14.01	11.89	12.04	13.63	14.18

From the data collected, the hydration process can be monitored by determining the change in the CSH area over the course of the 56 days tested. The correction of spectral intensities peaks in spectral data is commonly used with the normalization approach. The Normalize Spectrum feature on the OMNIC software allows corrections according to the intensity and the peak area. Normalization of spectra eliminates length variation and reduces the differences amongst single measurements of samples. The spectra are normalized to the same integrated intensity or intense band in a spectral region. Normalization is used to study the different growth phases of substances, such as bacteria; and used as an advance statistical analysis approach.

4.3 SEM

4.3.1 Imaging. The images in Figure 4.13 and 4.14 illustrate the cement hydration of 28 day cement paste at 1300x magnification without and with a filter, respectively. The filtered image has gone through both the convolution and median filters.

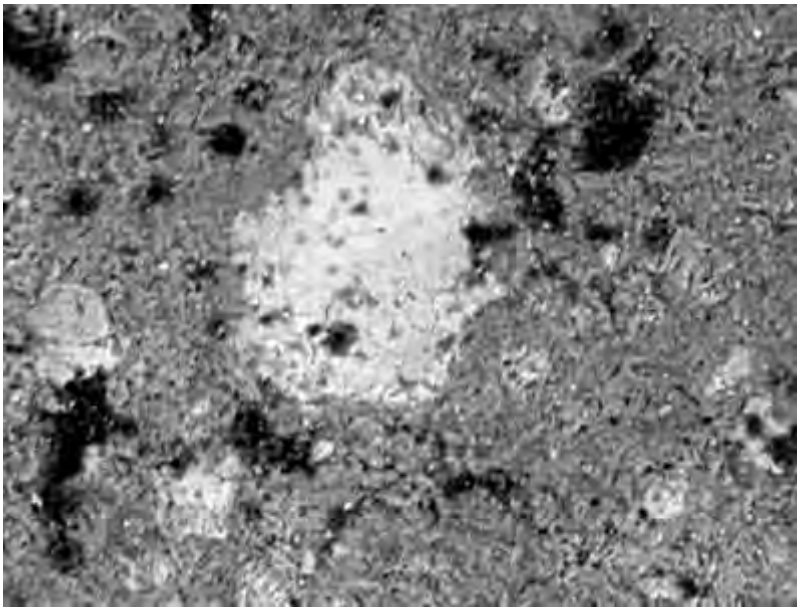

Figure 4.18: SEM image of a 28 day water cured control section

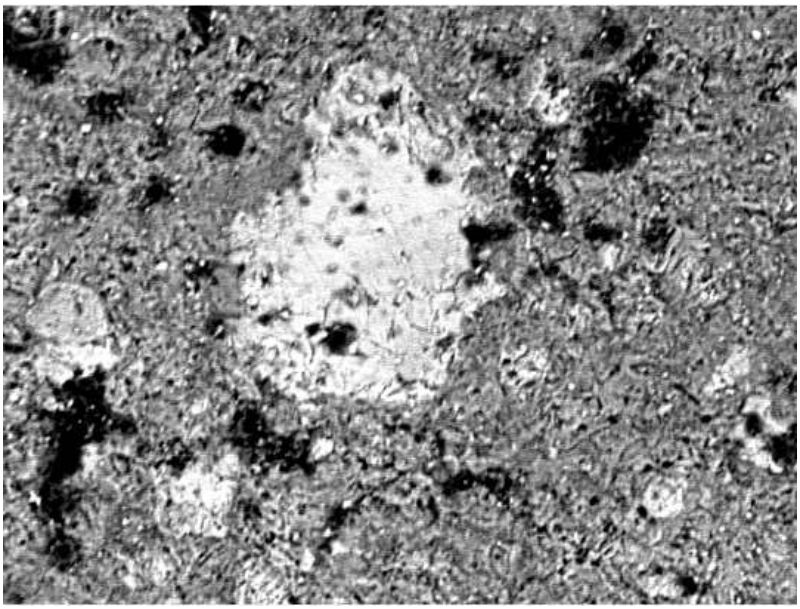

Figure 4.19: Filtered SEM image of a 28 day water cured control section

Comparing Figure 4.13 and 4.14 of the 28 day water cured cement paste SEM image at 1300x magnification, the filter image has a great amount of details for the hydration products with the given area. Whereas the original image is these hydration features are not as prominent.

4.3.2 Hydration phases

4.3.2.1 Area averages. To compare the area percentages, some combinations from the dissertation of Dr. Paulo de Castro Gomes, referred to as the author, will be made to the phases to more accurately correlate to the phases in this research. The major reason for the change is that the number of phases is less in the analysis of this research. That is, only three compared to four or five depending on the presence of the inner product. Then again, there is one phase that fairly remains true to its threshold and that is porosity. The OHP phase holds within it the grayscale intensities that are representative of CSH in the obtained histograms. As such, both OHP and CSH will be considered the same for all area percentage purposes. The CH, IP, and UH phases will all be considered CH for simplicity and will be referred to as the combined phase. The specific samples to use to obtain comparative results are at 20 ° C. The coding reference is

D for three days, J for seven days, and F for 28 days. There is a deficiency of samples to have comparisons to 14 and 56 days. Therefore, only three, seven, and 28 day averages can be used since the dissertation did not look at 14 day and 56 day hydration ages.

The areas for each phase is larger in this research which can be expected since there are less divisions of the total area like slices of a pie. In Table 4.5 and 4.6 the 0.35 and 0.45 water to cement ratios are used from Gomes' results for comparison to the 0.4 ratio that was kept constant in this research, respectively. All values are rounded to the whole number for clarity. The w/c of 0.35 showed a decrease in porosity area from 3 to 28 day from 9% to 5%. The w/c of 0.45 showed a larger decrease in porosity from 3 to 28 day from 15% to 6%.

For example, in Table 4.7, water cured areas for 10% silica fume at seven days are porosity: 14%, CSH: 75%, and CH: 11%. From the average for all ages, 10% fly ash replacement has a higher percentage of porosity, 7% more CSH, but less CH than 5% replacement. Silica fume at 10% replacement has a higher percentage of CSH by two percentage and lower porosity and CH than 5% replacement. Comparing fly ash and silica fume averages at 10%, silica fume had lower porosity, CH, and higher CSH. The control had lower porosity than fly ash and higher than silica fume at 14%. Zero percentage of cement had 65% CSH average which was lower than fly ash and silica fume. The CH of the control at 21% was much larger than fly ash or silica fume averages. Overall areas for water and vacuum curing have CSH percentages that continually grow larger with age.

For example, in Table 4.8, vacuum cured areas for 10% silica fume at 56 days are porosity: 5%, CSH: 80%, and CH: 15%. From the average for all ages, fly ash 10% replacement has a lower percentage of porosity, higher CSH by 4% than 5% replacement but same CH. Silica fume 10% replacement has a higher percentage of CSH by 8% and lower porosity and CH

than 5% replacement. Comparing fly ash and silica fume averages at 10%, silica fume had lower porosity, CH, and higher CSH. The control had higher porosity than fly ash and silica fume but silica fume at 5% was the same at 16%. Zero percentage of cement had 66% CSH which was higher than only 5% fly ash. The CH of the control was higher than silica fume but lower than fly ash averages. Overall areas for water and vacuum curing have CSH percentages that continually grow larger with age.

For the water cured porosity in Table 4.7, the area decreased from 27% and 20%, to 14% and 7% for 10% fly ash and silica fume over the ages of 3 to 56 days, respectively. For the vacuum cured porosity in Table 4.8, the area decreased from 23% and 15%, to 6% and 5% for 5% and 10% fly ash over the ages of 3 to 56 days, respectively.

In the case of CSH, the w/c of 0.35 showed an area increase from 3 to 28 day from 65% to 67%. In the same token, CSH increased at every age for each additive as seen in Figure 4.15 and 4.16. For the water cured CSH, the area increased from 63% and 59%, to 78% and 70% for 10% and 0% fly ash over the ages of 3 to 56 days, respectively. For the vacuum cured CSH, the area increased from 61% and 60%, to 70% and 70% for 0% and 5% fly ash over the ages of 3 to 56 days, respectively.

In the case of CH, the w/c of 0.35 and 0.45 showed an increase in the CH area from 3 to 28 day. For the water cured CH, the area decreased from 25%, to 20% and 17% for 0% and 5% fly ash over the ages of 3 to 56 days, respectively. For the vacuum cured CH, the area decreased from 20%, to 14% and 17% for 0% and 5% fly ash over the ages of 3 to 56 days, respectively.

The tables show the decreasing porosity area with time and other hydrated product area for both the 0.35 and 0.45 water to cement ratios of the dissertation by Paulo de Castro Gomes (1997). Table 4.10 shows the water cured hydration phase area percentages at all ages. The

CSH areas of each material increase with age. Table 4.11 shows the vacuum cured hydration phase area percentages at all ages. The CSH areas of each material increase with age.

Table 4.8*:*

3, 7, & 28 Day Phase Area Percentages of a 0.35 W/C Ratio

W/C Ratio	File Code	Days	P	OHP	Combination
0.35	D	3	9	65	26
	J	7	9	55	35
	F	28	5	67	28

Table 4.9*:*

3, 7, & 28 Day Phase Area Percentages of a 0.45 W/C Ratio

W/C Ratio	File Code	Days	P	OHP	Combination
0.45	D	3	15	65	20
	J	7	7	64	29
	F	28	6	65	29

The Figures 4.20 and 4.21 show the increase in CSH area over time for water and vacuum curing.

4.3.2.2 Phase thresholding. To compare the threshold, some combinations from the dissertation will be made to the phases to more accurately correlate to the phases in this research. The key reason for the change is that the number of phases is less in the analysis of this research. That is, only three compared to four or five depending on the presence of the inner product. Then again, there is one phase that fairly remains true to its threshold and that is porosity. But as

the phase for porosity begins at zero on the grayscale of the histogram there aren't any comparisons needed.

Table 4.10*:*

Water Cured 3, 7, 14, 28, & 56 Day Hydration Phase Area Percentages

Water Cure						
		Control	Fly Ash		Silica Fume	
Days	Area	0%	5%	10%	5%	10%
3	P	17	14	27	18	20
	CSH	59	61	63	71	74
	CH	25	25	10	11	6
7	P	11	15	10	15	14
	CSH	64	62	69	75	75
	CH	25	22	22	10	11
14	P	14	13	18	OUT	OUT
	CSH	66	65	73	OUT	OUT
	CH	19	22	9	OUT	OUT
28	P	17	18	13	10	8
	CSH	67	67	75	76	78
	CH	17	14	12	14	14
56	P	10	14	14	9	7
	CSH	70	69	78	81	84
	CH	20	17	8	10	10

Table 4.11:

Vacuum Cured 3, 7, 14, 28, & 56 Day Hydration Phase Area Percentages

Vacuum Cure						
		Control	Fly Ash		Silica Fume	
Days	Area	0%	5%	10%	5%	10%
3	P	19	19	18	23	15
	CSH	61	60	64	67	75
	CH	20	20	18	11	10
7	P	12	10	12	19	14
	CSH	62	61	65	68	76
	CH	26	29	22	13	10
14	P	17	15	5	OUT	17
	CSH	67	62	69	OUT	77
	CH	16	23	26	OUT	6
28	P	15	20	11	17	13
	CSH	69	69	71	70	79
	CH	16	11	18	13	8
56	P	16	13	11	6	5
	CSH	70	70	72	70	80
	CH	14	17	17	23	15

From Table 4.9, the OHP phase holds within it the grayscale intensities that are representative of CSH in the obtained histograms. As such, both OHP and CSH will be considered the same for all thresholding purposes. The CH, IP, and UH phases will all be considered CH for simplicity and will be referred to as the combined phase. The specific samples

to use to obtain comparative results are at 20 ° C. The coding reference has the same representation of D for 3 days, J for 7 days, and F for 28 days.

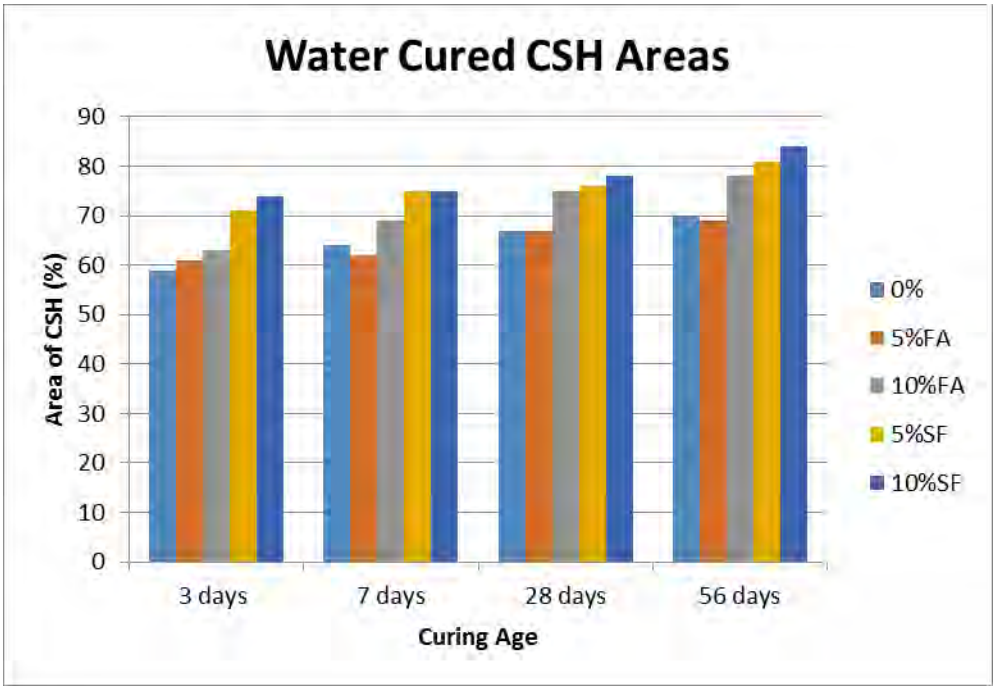

Figure 4.20: Water Cured CSH Areas

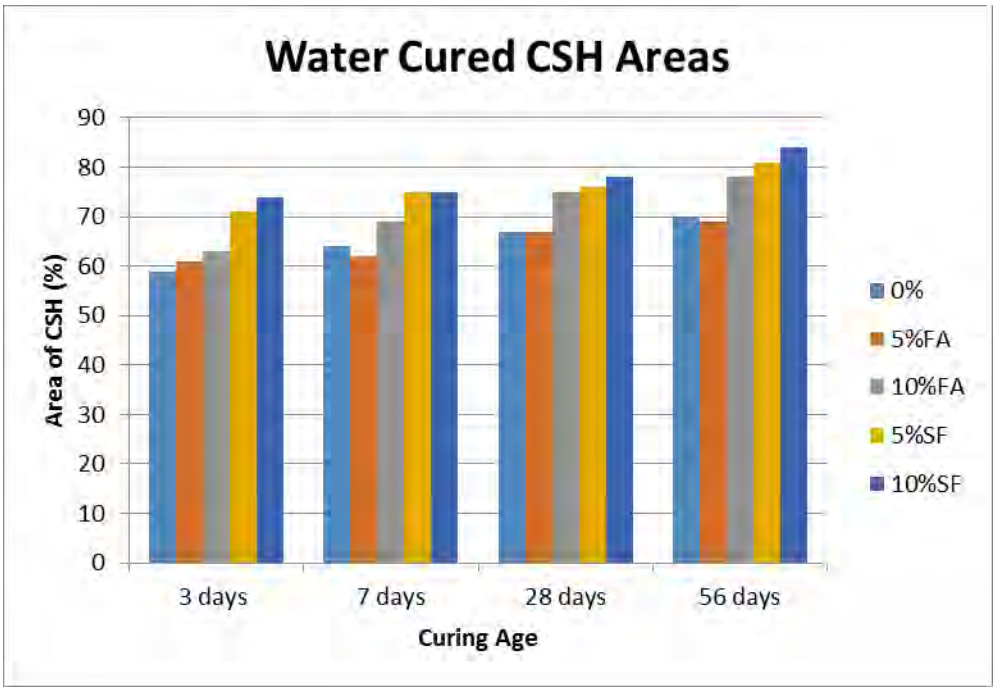

Figure 4.21: Vacuum Cured CSH Areas

Table 4.12:

3, 7, & 28 Day Hydration Phase Thresholds

File Code	Days	OHP	Combination
D	**3**	53	157
J	**7**	48	123
F	**28**	44	134

For three days in relation to the author, the CSH threshold closest is 5% fly ash water cured by 24 and furthest in 10% silica fume water cured by 68 as seen in Table 4.10. The CH threshold closest is 5% fly ash water cured by 36 and furthest in 10% silica fume water cured by 85. For seven days in relation to the author, the CSH threshold was closest is 0% vacuum cured by two and furthest in 5% silica fume vacuum cured by 51 as seen in Table 4.11. The CH threshold closest is 5% fly ash vacuum cured by three and furthest in 5% silica fume vacuum cured by 83. For 28 days in relation to the author, the CSH threshold closest is 5% silica fume water cured by one and furthest in 5% fly ash vacuum cured by 68. The CH threshold closest is 10% silica fume water cured by 35 and furthest in 5% fly ash vacuum cured by 102.

4.3.2.2.1 Water cured thresholding. For example, in Table 4.12, the threshold limits for the 10% silica fume water cured sample at 3 days are observed to be P: 0-120, CSH: 121-241, and CH: 242-255. For all water cured ages, the control had a range of 52-88 for CSH and 151-206 for CH. Fly ash 5% replacement had a range of 63-103 for CSH and 178-202 for CH. Fly ash 10% replacement had a range of 47-114 for CSH and 146-223 for CH. Silica fume 5%

replacement had a range of 43-85 for CSH and 198-200 for CH. Silica fume 10% replacement had a range of 46-121 for CSH and 169-242 for CH.

Table 4.13*:*

3, 7, and 28 Day Water Cured Thresholds

Days	Replacements		CSH	CH-255
3	**Control**	**0%**	88	194
	Fly Ash	**5%**	77	193
		10%	114	218
	Silica Fume	**5%**	85	198
		10%	121	242
7	**Control**	**0%**	53	162
	Fly Ash	**5%**	63	178
		10%	47	146
	Silica Fume	**5%**	76	199
		10%	68	198
28	**Control**	**0%**	70	204
	Fly Ash	**5%**	103	202
		10%	58	171
	Silica Fume	**5%**	43	199
		10%	46	169

4.3.2.2.2 Vacuum cured thresholding. For example, in Table 4.13, the threshold limits for the 10% fly ash vacuum cured sample at 28 days are observed to be porosity: 0-56, CSH: 57-179, and CH: 180-255. For all vacuumed cured ages, the control had a range of 50-101 for CSH and 150-229 for CH. Fly ash 5% replacement had a range of 42-112 for CSH and 120-236 for

CH. Fly ash 10% replacement had a range of 19-100 for CSH and 124-215 for CH. Silica fume 5% replacement had a range of 24-119 for CSH and 133-212 for CH. Silica fume 10% replacement had a range of 46-111 for CSH and 193-222 for CH.

Table 4.14:

3, 7, and 28 Day Vacuum Cured Thresholds

Days	Replacements		CSH	CH-255
3	Control	0%	101	222
	Fly Ash	5%	92	205
		10%	100	204
	Silica Fume	5%	119	212
		10%	87	203
7	Control	0%	50	150
	Fly Ash	5%	42	126
		10%	51	167
	Silica Fume	5%	99	206
		10%	86	205
28	Control	0%	76	196
	Fly Ash	5%	112	236
		10%	57	180
	Silica Fume	5%	92	208
		10%	78	222

Table 4.15*:*

Water Cured Threshold Levels

Water Cured Thresholds		Control	Fly Ash		Silica Fume	
Days	Area	0%	5%	10%	5%	10%

Table 4.15:

Cont.

3	**CSH**	88	77	114	85	121
	CH-255	194	193	218	198	242
7	**CSH**	53	63	47	76	68
	CH-255	162	178	146	199	198
14	**CSH**	52	66	106	OUT	OUT
	CH-255	151	184	198	OUT	OUT
28	**CSH**	70	103	58	43	46
	CH-255	204	202	171	199	169
56	**CSH**	69	69	84	62	49
	CH-255	206	200	223	200	203

Table 4.16:

Vacuum Cured Threshold Levels

Vacuum Cured Thresholds		**Control**	**Fly Ash**		**Silica Fume**	
Days	**Area**	**0%**	**5%**	**10%**	**5%**	**10%**
3	**CSH**	101	92	100	119	87
	CH-255	222	205	204	212	203
7	**CSH**	50	42	51	99	86
	CH-255	150	126	167	206	205
14	**CSH**	93	54	19	OUT	111
	CH-255	177	120	124	OUT	220

Table 4.16:

Cont.

28	**CSH**	76	112	57	92	78
	CH-255	196	236	180	208	222
56	**CSH**	94	71	79	24	46
	CH-255	229	197	215	133	193

Since the samples used in the dissertation were made using multiple w/c ratios and more samples overall, the samples obtained cannot be compared directly. However, an average limit for each offers a better comparison. With the difference in number of phases it is evident that there is a large variation in the threshold levels.

CHAPTER 5

Discussion and Future Research

5.1 Compression Strength

5.1.1 Forney universal testing machine - cylinders. The Forney machine was used to differentiate the compressive strength of Portland cement with and without the addition of fly ash or silica fume. Other studies have considered the compression testing of Portland cement with and without fly ash or silica fume addition. So far, there is an open area of interest for observing the strength alongside the hydration of concrete with fly ash after days of curing. Replacing cement with fly ash is known to lower the early strength. This study uses the Forney machine to view this relation from the compressive strength standpoint. Speculation of concrete cured with the traditional water curing approach arises when in comparison to concrete cured in vacuum environments.

From the bar graph results, what must be noted is the three samples for each mix design are all from the same batch. The results of the cylinders' compressive strength testing will be compared for both water and vacuum cured samples. The controlled cement paste serves as the reference for the comparison of the various replacements. The reference samples depict a continuous increase in strength with age. In the case of the three days results, the reference concrete peaked at 5,219 psi for water cured, and 4,838 psi for vacuum cured. The reference concrete strength continued to increase with each age until to 56 day testing; in which the strength peaked at 10,842 psi and 10,508 psi for water and vacuum curing, respectively.

The change in compressive strength for each additive in comparison to the control for water and vacuum cured are shown in Table 5.1 and 5.2. The largest margin of change for water cured samples of compressive strength is 22% in 5% fly ash at seven days. The smallest margin

of change in water cured samples of compressive strength is 0% that occurs in 5% silica fume at 3 days. The largest change for vacuum cured samples of compressive strength is 34% in 10% fly ash at 28 days. The smallest change for vacuum cured samples of compressive strength is 0% that occurs in 10% fly ash at 56 days.

Table 5.1:

Compressive Strength Variations for Water Cured of Both Additives

Percent Change in Strength (%)					
Replacement (%)	**3 Day**	**7 Day**	**14 Day**	**28 Day**	**56 Day**
0%	0	0	0	0	0
5% FA	-24	22	6	10	15
10% FA	-6	8	9	14	18
5% SF	0	-14	-20	15	10
10% SF	12	3	-6	12	4

The change in elastic modulus strength for each additive in comparison to the control for water and vacuum cured are shown in Table 5.3.

5.1.1.1 Fly ash addition. After the addition of fly ash, the concrete strength showed a drastic increase in comparison to that of the reference concrete in testing over time. Concrete samples with the addition of 10% of fly ash to cement replacement outperformed in concrete strength at all ages except for three day water cured results, in comparison to the control mix. Fly ash concrete of 10% displayed the highest stresses for 56 day tests. The stresses for the 10% fly ash replacement reached to 12,798 psi for the 56 day water cured samples. The 5% fly ash replacement samples obtained peaked stresses at 12,511 psi during the 56 day water cured tests.

Table 5.2:

Compressive Strength Variations for Vacuum Cured of Both Additives

Percent Change in Strength (%)					
Replacement (%)	**3 Day**	**7 Day**	**14 Day**	**28 Day**	**56 Day**
0%	0	0	0	0	0
5% FA	-18	18	24	20	13
10% FA	23	3	31	34	16
5% SF	-4	-9	-8	22	5
10% SF	10	11	7	14	0

Table 5.3:

Elastic Modulus Strength Variations for Vacuum Cured of Both Additives

Percent Change in Strength (%)					
Replacements	**3 Day**	**7 Day**	**14 Day**	**28 Day**	**56 Day**
0% Water	0	0	0	0	0
0% Vacuum	0	0	0	0	0
5% FA Water	4	3	-1	1	5
5% FA Vacuum	3	4	1	1	5
10% FA Water	3	4	2	2	6
10% FA Vacuum	5	5	4	1	6
5% SF Water	-1	1	0	14	10
5% SF Vacuum	-1	4	3	16	10
10% SF Water	2	2	1	15	11
10% SF Vacuum	4	3	3	16	11

However, the 3, 14, 28, and 56 day tests for the 10% fly ash water cured concretes, all performed higher than that of the 5% fly ash water concrete samples. The cylinder testing results indicate the optimum percentage of fly ash to cement replacement is that of the 5%, due to its constant and higher stresses during most of all testing ages.

5.1.1.2 Silica fume addition. After the addition of silica fume, the concrete strength showed an increase in comparison to that of the reference concrete in testing over time. Concrete samples with the addition of 10% of silica fume to cement replacement outperformed in concrete strength at all ages except for three day water cured and 56 vacuum cured results, in comparison to the control mix. For all silica fume samples, 5% displayed the highest stresses for 56 day tests. The stresses for the 5% silica fume replacement reached to 11,920 psi for the 56 day water cured samples. The 10% silica fume replacement samples obtained peaked stresses at 11,329 psi during the 56 day water cured tests. However, the 3, 7, and 14 day tests for the 10% silica fume water and vacuum cured concretes, all performed higher than that of the 5% silica fume concrete samples. At 3 and 28 days, the water cured 5% and 10% silica fume samples outperformed both fly ash replacements. The cylinder testing results indicate the optimum percentage of silica fume to cement replacement is that of the 5%, due to its constant and higher stresses during most of all testing ages.

5.1.2 MTS tests – cubes. This section will discuss the results obtain from the MTS cube testing performed for all testing days for water and vacuum cured samples. The controlled cement paste was used as a reference in comparing fly ash or silica fume percentages and the different methods of curing. The reference samples portray a steady increase in strength over the course of time. For the 3 days results, the reference concrete peaked at 6,149 psi for water cured,

and 5,070 psi for vacuum cured. The reference concrete strength continued to increase with time up to the 56 day test; in which the strength peaked at 12,793 psi and 12,219 psi for water and vacuum curing, respectively.

5.1.2.1 Fly ash addition. With the addition of fly ash, the concrete strength showed a significant increase in comparison to that of the reference concrete at all stages of testing. Concrete samples with the addition of 5% of fly ash to cement replacement, performed consistently better in concrete strength for the 3 day water cured results, in comparison to the control mix. Fly ash concrete of 5% displayed the highest stresses for 28 and 56 day tests. The stresses for the 5% fly ash replacement reached to 12,116 psi and 11,150 psi for the 28 day water and vacuum cured samples, respectively. The 5% fly ash replacement samples obtained peaked stresses at 14,071 psi and 14,282 psi during the 56 day water and vacuum cured tests, respectively. The 10% fly ash concrete samples performed poorly in comparison to the 5% fly ash concretes in nearly all stages of testing. The concrete strength for the 10% fly ash concrete peaked at 12,492 psi for the 56 day vacuum cured test. However, the 7, 28, and 56 day tests for the 10% fly ash water cured concretes, all performed lower than that of the 5% fly ash concrete samples. The results indicate the optimum percentage of fly ash to cement replacement is that of the 5%, due to its consistent and higher stresses during majority of all testing ages.

5.1.2.2 Silica fume addition. With the addition of silica fume, the concrete strength showed a significant increase in comparison to that of the reference concrete at all stages of testing. Concrete samples with the addition of 5% of silica fume to cement replacement, performed consistently better in concrete strength for the 3 day water cured results, in comparison to the control mix. Silica fume concrete of 5% displayed the highest stresses for 28 and 56 day tests. The stresses for the 5% silica fume replacement reached to 14,045 psi and

12,164 psi for the 28 day water and vacuum cured samples, respectively. The 5% silica fume replacement samples obtained peaked stresses at 11,270 psi and 10,042 psi during the 56 day water and vacuum cured tests, respectively. The 10% silica fume concrete samples performed poorly in comparison to the 5% silica fume concretes in nearly all stages of testing. The concrete strength for the 10% silica fume concrete peaked at 11,216 psi for the 56 day vacuum cured test. However, the 28 and 56 day tests for the 10% silica fume water cured concretes, both performed lower than that of the 5% silica fume concrete samples. The results indicate the optimum percentage of silica fume ash to cement replacement is that of the 5%, due to its consistent and higher stresses during majority of all testing ages.

5.1.2.3 Curing method. The two curing methods examined in this study are the commonly used water curing, and a new curing method of vacuum sealing. In this section, the two curing methods are being compared to better understand the effects of vacuum curing and to determine if this method is suitable for curing concrete. In regards to the reference concrete, the vacuum cured samples performed weaker in strength in all testing days in comparison to water curing. Yet, the stresses were not too far apart. Also, it is apparent in the initial portion of the stress-stress curves of the vacuum samples that there is a slight deviation from the slope. This deviation is a representation of increase of strain from possible internal capillary cracking of the cube that is a characteristic of vacuum curing. These internal gaps are closed by the compressive force from the MTS machine then the curve returns to its regular characteristic curve. The water cured reference samples ranged from 6,149 psi to 12,793 psi, from 3 day to 56 day. The vacuum cured reference samples ranged between 5,070 psi to 12,219 psi, from 3 day to 56 day tests. In the cases involving the incorporation of fly ash, results showed decreases in concrete strength

with the 10% of cement replacement compared to 5% amongst testing days. These comparison too shows the optimum fly ash or silica fume to cement replacement for water curing is 5%.

To review, the age and curing that performed similarly both water and vacuum cures at three days and seven day vacuum cured for 5% silica fume. This mix design had the most amount of outstanding sample peaks. On the matter of silica fume, a reaction between silica fume and lime formed during cement hydration does not occur during the early stages of hydration. The presence of silica fume slightly increases the rate of cement hydration during the first few hours of hydration. Likewise, this indicates that silica fume affects hydration by the nucleating effect of its surface when it still exists as a chemically inert filler.

5.2 FTIR

The FTIR was used to monitor the hydration process of Portland cement with and without the addition of fly ash or silica fume between the ranges of 3 to 56 days. Other studies have investigated the early hydration of Portland cement with and without fly ash or silica fume addition. Yet, there is an open area of interest for observing the hydration of cement paste with fly ash after days of curing. This study uses FTIR to view this hydration process over a course of 56 days for cement paste cured with the traditional water curing approach; in comparison to cement paste cured in vacuum environments.

From the results, the areas of possible CSH formation have been determined for all cement paste samples tested. These areas have been recorded and presented in Table 4.5 which portrays data for the water and vacuum cured samples. They portray all of the normalized areas, as in the change in area per time, from the spectrums displayed in the results in regards to the percentage of fly ash or silica fume to cement replacement, corresponding to the age of testing.

There was an increase in CSH areas over time in the control, 5% and 10% fly ash and fume. At 56 days the CSH area was the largest for the silica fume with vacuum curing of 14%. The largest CSH area for the fly ash occurred with 10% replacement vacuum curing at 56 days. The replacement of 5% fly ash water cured had the smallest change of area from three to 56 days, actually less than 1% change of area. The largest increase in CSH area from three days to 56 days was 5% fly ash vacuum cured with an increase of 5%. The controlled cement paste was outperformed by both fly ash and silica in regards to change of CSH area over time. As a whole, the fly ash and silica fume both showed a strong a correlation for growing in CSH area with replacement percentage.

Figures 5.1 and 5.2 show the 0% for the water and vacuum cured samples, respectively. Figure 5.3 illustrates the 5% and 10% fly ash replacement for water cured samples; and Figure 5.4 shows the same for the vacuum cured samples. For the 0% cement paste graphs, additional tests and data was plotted to show the early age or stages of CSH growth in comparison to the days. A small mix of cement and water, following the same experimental procedure as stated before, has been acquired using FTIR for up to 2 hours. The sample was first recorded after 1 min of hydration, then 2 minutes, 15 minutes, 30 minutes, and 1 hour. Since the data was obtained prior to cement hardening, the data was used for comparison in both water and vacuum cured samples. Table 5.4 shows the data obtained from the FTIR test ran during early ages. Table 5.5 includes the change of area data obtained from the FTIR test ran during early and later ages.

Table 5.4:

Area of CSH region for Cement Paste FTIR Monitored for First 2 Hours

Time (minutes)	Area
1	0
2	0
15	0
30	0.73
60	1.86
120	2.01

Table 5.5:

Change of CSH Area for Cement Paste FTIR Monitored Until 56 Days

Time (Minutes)	Δ Area (cm-1)	
	Water	Vacuum
1	0	0
2	0	0
15	0	0
30	0.73	0.73
60	1.13	1.13
120	0.15	0.15
4320	6.79	7.89
10080	0.16	0.3
40320	0.61	0.98
80640	3.05	0.73

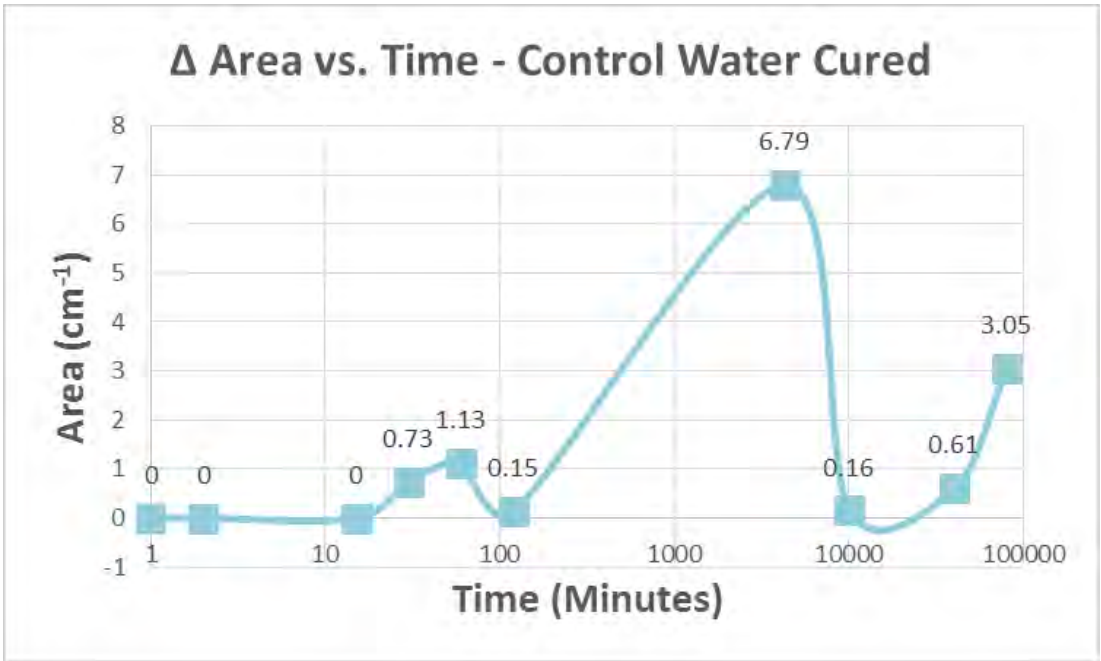

Figure 5.1: Normalized area of CSH in the controlled cement paste after water curing

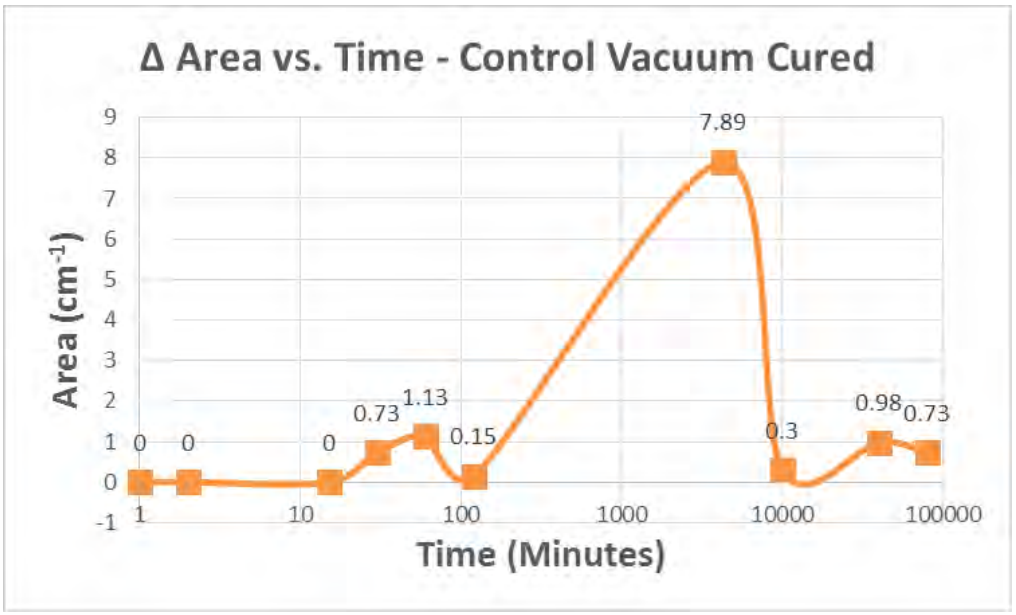

Figure 5.2: Normalized area of CSH in the controlled cement paste after vacuum curing

Knowing that 10080 minutes is 7 days, a comparison can be drawn from the 0% samples. Figures 5.1 and 5.2 signifies the small peaks of CSH formation after 30 minutes of hydration and later after curing, shows the peak of CSH formation around the 3 to 7 day range, before declining

up to the 56 days. The results indicate that the hydration process accelerates in between the early ages and up to about the first week of curing. However, this data doesn't report the CSH formation leading up to the first 3 day test, which may peak high areas of CSH formation. This data does portray a decline in the hydration of CSH formation after the first few days of curing, which is probably cause by the decrease in the amount of water remaining in the cement paste. The formation of polymerized silica is correlated to the incorporation of water. The vacuum cured samples displays similar results to that of the water cured samples. However, the vacuum cured samples show a higher percentage of CSH content in all curing ages in comparison to the water cured samples.

With the incorporation of fly ash or silica fume, the normalized areas of CSH in the respected region varies in comparison to the reference 0% samples. With 5% and 10% of fly ash replacement, the areas of CSH show an increase in vacuum but not in the water cured samples. In all cases of replacement, the areas of CSH increased for the 56 day test for both the water and vacuum cured samples. Also, note that the water cured samples all remain within a close trend of area of the reference CSH. From 3 to 56 days, the vacuum area ranges increased for 5% and 10% fly ash and silica fume.

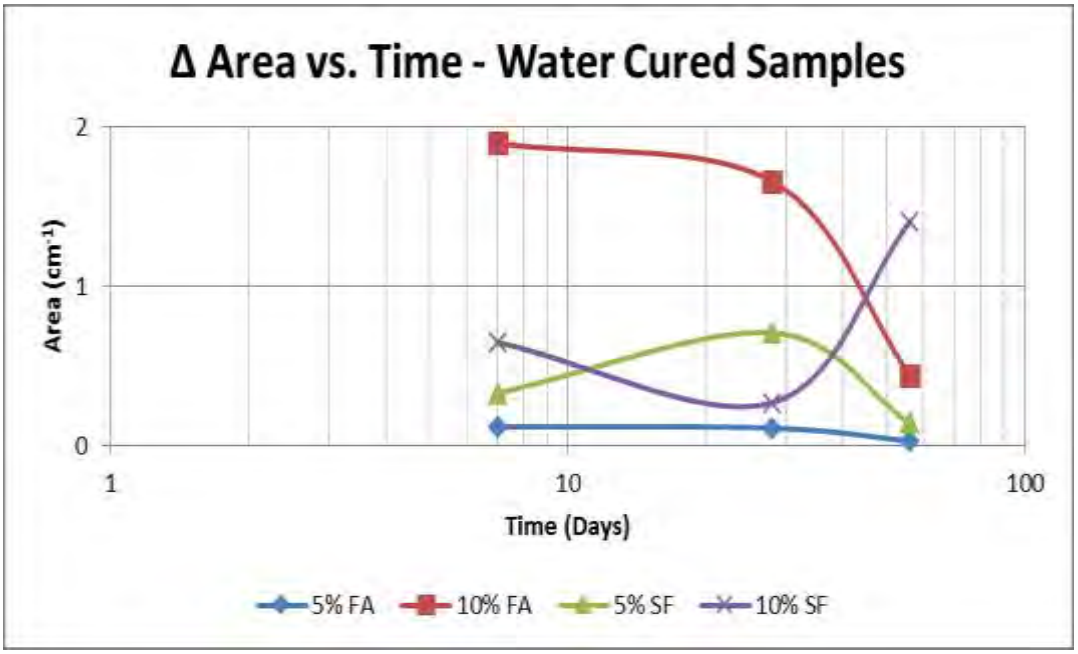

Figure 5.3: Normalized areas for 5% & 10% fly ash and silica fume water cured samples

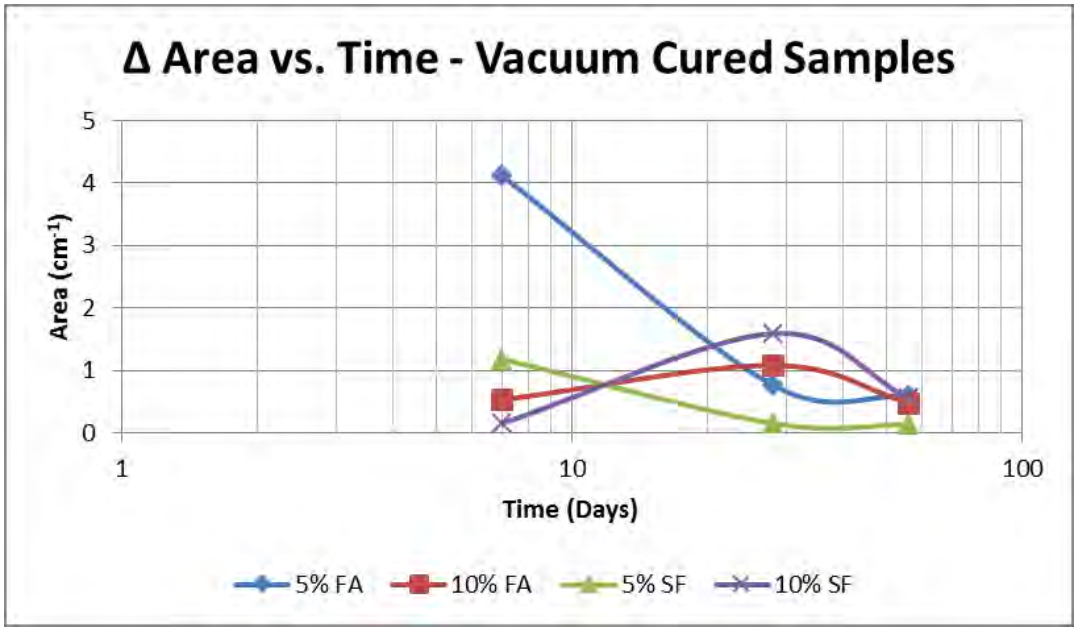

Figure 5.4: Normalized areas for 5% & 10% fly ash and silica fume vacuum cured samples

In all samples of fly ash and silica fume, the normalized area where the CSH formation decreases as the samples cured up to 56 days. However, there are changes in area for 28 days that are higher than the 7 and 56 days. The increase in the change in CSH area at 56 days for the

10% silica fume with water curing could be a result of additional hydration. The prolonged hydration is realized when internal pores filled with trapped water are reached by the growing CSH area during the later ages such as 56 days.

In comparing the 5% fly ash replacement, notice the significant area decrease in change of area in the vacuum cured samples in Figure 5.4 compared to the small change in the water cured samples in Figure 5.3. The peak of 4% in the 5% fly ash vacuum cured case was the highest of the samples in either curing. This peak also creates the largest decrease in all samples. Yet, in the case of the water cured 10% fly ash replacement, note the large decrease in change of area. Another reason for the various changes of CSH areas among the 5% and 10% of fly ash and silica fume to cement replacement can be due to the mixing method of materials. Since large batches of cement paste were created and such a small sample of cement paste is tested on the FTIR, the lack of the batch mixture being completely homogeneous may perchance be the cause to such discrepancies.

5.3 SEM

All samples were prepared using the same procedure. However the samples produced hydration results that varied with age. Water is the key ingredient, which when mixed with cement, forms a paste that binds the aggregate together. The water causes the hardening of cement paste through the hydration process. Hydration is a chemical reaction in which the major compounds in cement form chemical bonds with water molecules and become hydration products. The role of water is important because the water to cement ratio is the most critical factor in the production of optimal cement paste. Too much water reduces cement paste strength, while too little will make the cement paste unworkable. Because cement paste must be both strong and workable, a careful balance of the cement to water ratio is required when making

cement paste. With an increase of water to cement ratio of 0.2 from 0.2 to 0.4, the degree of hydration rises by 40% after 28 days (Lam, 2000).

A reason for the variability in the strength results is that the fly ash attained could have of poor quality since it was offered at no charge. Another observation, as the Hobart mixer mixed some cement is left unmixed at the bottom and lodged in the baffle. So manual stirring is required to have a more uniform mixture. The cement paste needs moisture to hydrate, cement paste with too little water may be dry but is not fully reacted. The properties of such a cement paste would be less than that of a wet cement paste. The reaction of water with the cement in cement paste is extremely important to its properties so that reactions may continue into late ages. Upon the addition of water, tricalcium silicate rapidly reacts to release calcium, hydroxide, and a large amount of heat. The reaction slowly continues producing calcium and hydroxide until the system becomes saturated. Once this occurs, the CH starts to crystallize. Simultaneously, CSH begins to form. The formation of the CH and CSH propel more CSH to form. The speed of the reaction is now controlled by the rate at which water molecules diffuse through the calcium silicate hydrate coating. This coating thickens over time causing the production of calcium silicate hydrate to become much slower.

In the original images and interpreted images are a representation of the products of hydration. The formation of pores, CSH and CH is apparent in each image. The hydration has begun to occur in the very early stages such as the three day samples. During this age the hydration process is transporting at its most rapid. Hydration continues throughout the following 7, 14, 28, and 56 day durations. But it is progressively diminishing with age. Fewer pore spaces exist over time as the majority of space is filled with CSH. The hydration will continue as long as water is present and there are still unhydrated compounds in the cement paste. Even though

the CSH grows in the vacuum samples over time the curing method does not prove to be better than water curing. Variability in the seal of the bags lead to cracks in the vacuum samples which support the decrease in compressive strength over time.

The expectations from the SEM derived images was to have focused images at a consistent magnification of 1300x. The beam would turn on as directed in the procedures every time that it showed it did in the SEM software. It was expected to be able to analyze a maximum of three sections for a total of nine areas in one session since three sections was the limit on the sample holder. It was looked forward to having beam that would not drift off by shifting or tilting. The lower the brightness and the higher the contrast would lead to expect a lower grayscale intensity on the histogram. What was learned was to expect charging of the sample if the beam was kept at a constant location over time. It was expected to find the center of the sample once it was selected the location on the stage navigation window. The samples are not to move once they placed on the stage in the SEM. The stage was also to be calibrated to show exactly where each sample was according to its orientation in the software. In each area of the sample, it was expected to be able to locate many physical features of the hydration reactions. A slower scan speed was to display a clearer image once it was frozen or captured. Occasionally, it was would expect required maintenance on the SEM. For example, the tungsten aperture would need changing which can be a reason that the beam does not turn on.

From the Matlab analysis, it was expected to generate histograms with three or more peaks with all samples. Once the name of the image was changed, the script was to output five figures in total. Those figures were the original image, filtered image, interpreted image, filtered histogram, and that same histogram with colors coding the phase bands. Changes to the threshold were expected to be seen in the adjusted histogram after running the Matlab script once

again. If there was ever an error in the script, it was expected to be shown as an error and its location to be able to find a solution.

There was also a better understanding of the proper way to capture an image like Figure 5.5. The beam shifted and tilted over time but was not aware of this until later. What was done to compensate is to acknowledge that the shift occurred as the research went on. Vacuum stabilization duration is longer than the SEM shows. Since the vacuum is still adjusting for up to an hour, the images have shown to get better once the vacuum finally is stable. The features that provide a five peak is the tricalcium cross weaving fibers that look like a fiberglass web. To resolve the lack in peaks, the image could have had an increase in the contrast to make gray areas darker. Another solution could have been to only use the convolution filter as seen in the Figure 5.6. Also, not stretching the histogram too far past the ends which will cut it off. The research group didn't have training from the US Army Corps of Engineers - Engineer Research & Development Center (ERDC) in Vicksburg, Alabama and only had a quick course with the SEM. Therefore, the lack of training could have had an impact on the quality of the images especially earlier on in the research.

5.4 Discussion Summary

5.4.1 Compressive strength. To review, the number of samples in each day in the Forney machine results reached a maximum of three for one mix design twice at three and seven days, both water and vacuum cured for 5% silica fume. Then another three samples exceeded all others once again in the controlled cement paste at 28 day water cured. For the peak compressive strength, the age and curing that performed similarly both water and vacuum cures at three days and seven day vacuum cured for 5% silica fume.

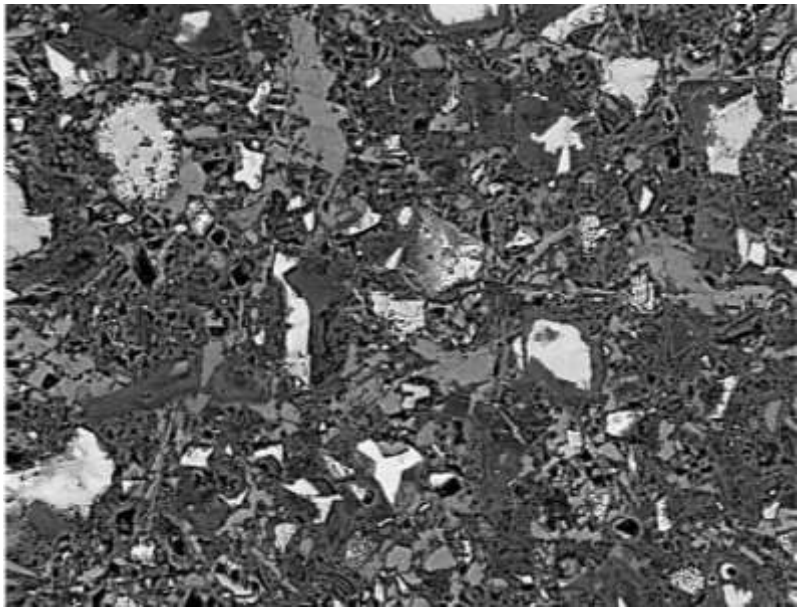

Figure 5.5: Previously researched SEM image of a 28 day water cured control section

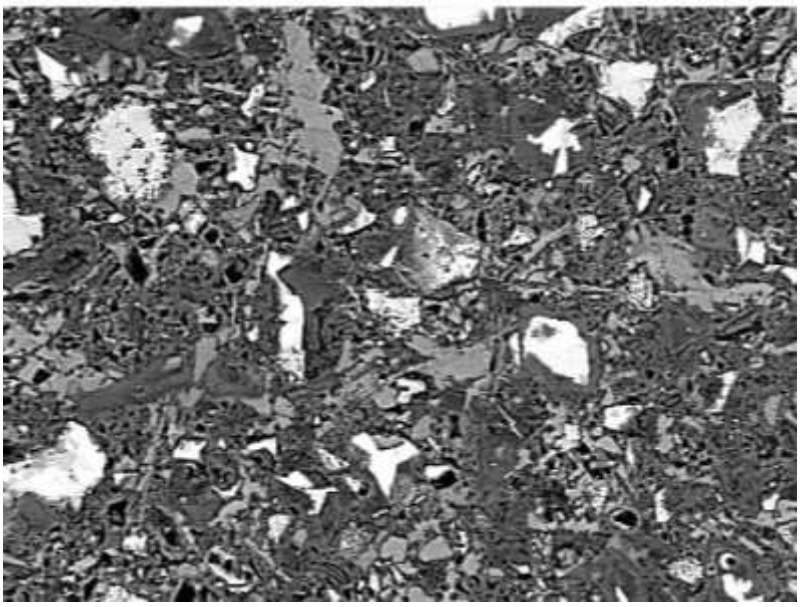

Figure 5.6: Previously researched filtered SEM image of a 28 day water cured control section

This mix design had the most amount of outstanding sample peaks. In the case of the 5% fly ash, the age and curing that performed similarly are seven, 14, and 56 day ages all water cured. Controlled cement paste had noteworthy peaks in each of the curing methods for 28 days.

At this age the water cured peak was an astounding 1900 psi while the vacuum cure was 1650 psi. Both the 10% silica fume and fly ash had one peak, vacuum cured 56 and 14 days respectively.

Likewise, the highest standalone ultimate compressive strength peak for silica fume is in the 28 day 5% water cured sample for the MTS testing. It is evident that both fly ash and silica fume both have the best stress-strain curves at 56 days. Whereas more specifically, 5% fly ash water cured ultimate strength 14000 psi with 0.008 strain and 5% silica fume water cured peaks at 12500 psi with 0.0081 strain at 56 days.

5.4.2 CSH areas. As a whole, FTIR's area values for all ages of controlled cement paste and replacements were smaller for both curing methods. As reviewed, hydrating under sealed conditions as opposed to saturated conditions increases the inherent hydration rate by about 20% which could be result of high concentrations of alkali ions in a pore solution (Bentz, 2006).

In observing the Hobart mixer mix, some cement is left unmixed at the bottom and lodged in the baffle. So manual stirring is required to have a more uniform mixture. The reaction of water with the cement in cement paste is extremely important to its properties so that reactions may continue into late ages. Fly ash showed to have increased hydration in later ages. The formation of pores, CSH and CH is apparent in each image. Fewer pores exist over time as the majority of the volume is filled with CSH. Even though the CSH grows in the vacuum samples over time the curing method does not prove to be better than water curing. It was looked forward to having beam that would not drift off by shifting or tilting. Vacuum stabilization duration is longer than the SEM shows. A better quality image would be producible if there had been more in depth training and practice of the SEM procedures.

From FTIR and SEM tested water cured controlled cement paste, the change in CSH areas was most similar at 56 days with a 3% increase in both tests. FTIR and SEM tested vacuum cured controlled cement paste exhibited a change in CSH areas that was most similar at 56 days as well with a 1% increase in both tests. In comparison of CSH area, the three day change in area will not be considered since there was not a prior age to compare. In water curing for both additives, the largest increase in CSH area was with 10% fly ash at seven and 28 days with 6% in SEM testing. In vacuum curing for both additives, the largest increase in CSH area was 5% fly ash with 8% in SEM testing. The largest increase in CSH area out of all ages for both curing methods in silica fume was 6% in 10% replacement.

CHAPTER 6

Conclusion and Future Research

6.1 Conclusion

In this present study, the hydration process of Portland cement with additives of fly ash or silica fume silica has been monitored. With the use of FTIR and SEM, signatures of CSH which produce most of the concretes' strength, has been determined and examined from 3 to 56 days. Also, using Forney and MTS testing equipment, the overall strength and modulus of elasticity of the harden cement pastes at all testing ages were determined and recorded for analysis. The objective of this report was to demonstrate how all these tests can give more insight on the hydration of cement, with and without the incorporation of fly ash or silica fume, during the later ages or stages of hydration. The integration of the two additives were studied to analyze their effect in accelerating C_3S. To fulfill this objective a total of 350 samples were prepared and tested. Through this search, the development of the concretes strength was also relevant and determined to better understand the process of cement hydration. From this study and results obtained, several conclusion have been drawn from analysis:

6.1.1 Hydration process. The appearance of an absorption peak between the approximate ranges of 875 – 1080 cm^{-1} was correlated with the formation of calcium silicate hydrate, CSH. The area at which the possible formation of CSH was determined from each sample tested, has increased with respect to time; signifying the increase in strength over the course of testing days.

After determining the possible CSH area rate of change, results show small increases in the hydration of cement throughout the testing days. This results can be due to the non-hydrogen bonded O-H groups, or capillary water, reacting to the anhydrate cement causes the hydration

process to pick back up. In comparison to the water cured method, the vacuum cured samples perform identically to that of the water cured when monitoring the hydration. Results indicate similar increases and decrease in hydration over time between both methods. The results show credibility to the vacuum curing method as a suitable form of curing.

In all cases of replacement, the total area of CSH increased most for the 56 day FTIR test for both the water and vacuum cured samples. The largest decrease in normalized area from FTRI testing occurred for the vacuum cured 5 % fly ash replacement. Increases in the change of CSH area in later ages could be due to prolonged hydration of the cement paste. The prolonged hydration is realized when internal pores filled with trapped water are reached by the growing CSH area.

Controlled cement paste water cured had 65% CSH average which was lower than fly ash and silica fume. Overall areas for water and vacuum curing have CSH percentages that continually grow larger with age for SEM. This trend aligns very well with the amount of CSH area growth for FTIR testing as well. The exact values of CSH area for both testing does not match up. This can be due to the divisions of the FTIR not being the same as the SEM where there were only three thresholds: porosity, CSH, and CH that made up the whole. Or possibly by the different methods of gathering the data by wavelength for the FTIR and freezing an image for the SEM. Undesirably, the units for the areas also do not match, the FTIR has cm-1 while the SEM is pixels. Nonetheless, the area is normalized to show the change of area over time with the FTIR, unlike the SEM which is cumulative.

6.1.2 Compressive strength. Fly ash and silica fume in all percentages of cement replacements studied, shows a significant increase in compressive strength in all ages of testing.

When comparing the amount of fly ash or silica fume replacement, results shown the optimal percentage of cement replacement is that of the 5% silica fume, followed close by the 5% fly ash addition. 10% fly ash replacement results portrayed a decrease in strength in comparison to that of the 5% fly ash or silica fume additions. Water curing proved to be the beneficial form of curing by displaying higher overall strength values than that of the vacuum cured method. Yet, the strength of concretes vacuum cured saw a small reduction in compressive strength of about 5%, compared to the water cured.

This study provided insight on the hydration process monitored by FTIR with the incorporation of fly ash and silica fume. In doing so, the strength of the concrete was analyzed and compared to changes of these additives to cement replacement. The study also looked into vacuum curing as an alternate form of curing concrete, and found suitable results for future research and possible incorporation.

The three day water and vacuum cured samples showed to have the highest compressive strength in all three samples of the Forney Machine in the 5% silica fume. The 56 day water cured samples had the highest and lowest compressive strength in the 5% fly ash with 1100 psi and 100 psi.

For the peak compressive strength, the 5% silica fume mix design had the most amount of outstanding sample peaks. It is evident that both fly ash and silica fume both have the best MTS stress-strain curves at 56 days.

To conclude, the collection of experience that have been gathered from this research has much to offer in continuation. A variety of magnifications would have also made a greater impact in determining the hydration of the cement paste and its additives. A lower magnification has a larger area that allows a better representation for the investigation of hydration.

6.2 Future Research

To follow the work, there can an analytical model that uses that images for each specimen among various others to develop a 3-D model. The model could be built using each image as a two dimensional cross section taken at all levels of the specimen, then stacked on one another. This would serve as a replica of the specimen with the chemical components all identified throughout the volume of the specimen. Constructing the model would require a stitching of the images derived from the SEM. The images could be organized using a coordinate system to do the stitching. As a suggestion, AutoCAD software could be a tool that would assist with viewing this model and identifying the structural properties. Components of the model will all be able to be turned off and on like layers that can be color coordinated.

References

Artioli, G. & Bullard, J.W. (2013). Cement hydration: the role of adsorption and crystal growth. Crystal Research Technology, 903-918.

Bentz, D.P. (2006). Influence of water-to-cement on hydration kinetics: Simple models based on spatial considerations. Cement and Cement paste Research, 238-244.

Berodier, E., & Scrivener, K. (2012). Impact of filler on hydration kinetics. 32nd Cement and Cement Paste Science Conference,

Bjornstrom, J. et al. (2004). Accelerating effects of colloidal nano-silica for beneficial calcium–silicate–hydrate formation in cement. Chemical Physics Letters, 242-248.

Bullard, J.W. et al. (2011). Mechanisms of cement hydration. Cement and Cement paste Research, 1208-1223.

Cervera, M. (2002). Numerical modeling of cement paste curing, regarding hydration and temperature phenomena. Computers and Structures, 1511-1521.

Cheung, J et al. (2011). Impact of Admixtures on the Hydration Kinetics. Cement and Cement paste, 1289-1309.

Diamond, S. (2004). The microstructure of cement paste and cement paste- a visual primer. Cement & Cement paste Composites, 919-933.

Diamond, S. & Kjellsen, K.O. (2006). Resolution of fine fibrous CSH in backscatter SEM examination. Cement & Cement paste Composites, 130-132.

Ferron, R.D et al. (2013). Aggregation and breakage kinetics of fresh cement paste. Cement and Cement Paste Research, 1-10.

Garcia-Mate, M. et al. (2013). Hydration studies of calcium sulfoaluminate cements blended with fly ash. Cement and Cement paste Research, 12-20.

Kadri, E & Duval, R. (2009). Hydration heat kinetics of cement paste with silica fume, 3388-3392.

Kirby, D. & Biernacki, J. (2012). The Effect of Water to Cement Ratio on the Hydration Kinetics of Tricalcium Silicate Cements: Testing the Two Step Hydration Hypothesis. Cement and Cement paste Research, 1147-1156.

Kjellsen, K.O. et al. (1999). On the compressive strength development of high-performance cement paste and paste-effect of silica fume. Materials and Structures, 63-69.

Kjellsen, K.O. & Justnes, H. (2004). Revisiting the microstructure of hydrated tricalcium silicate- a comparison to Portland cement. Cement & Cement paste Composites, 947-956.

Krstulovic, R. & Dabic, P. (2000). A conceptual model of the cement hydration process. Cement and Cement paste Research, 693-698.

Lam, L et al. (2000). Degree of hydration and gel/space ratio of high-volume fly ash/cement systems. Cement and Cement paste Research, 747-756.

Lin, F., Meyer, C. (2009). Hydration kinetic modeling of Portland cement considering the effects of curing temperature and applied pressure. Cement and Cement paste Research, 255-265.

Luttge, A. (2011). Experimental techniques for cement hydration studies. Studia UBB Geologia, 3-15.

Monteagudo, S.M. et al. (2014). The degree of hydration assessment of blended cement pastes by differential thermal and thermogravimetric analysis. Morphological evolution of the solid phases. Thermochimica Acta, 37-51.

Narmluk, M & Nawa, T. (2011). Effect of Fly Ash on the Kinetics of Portland Cement Hydration at Different Curing Temperature. Cement and Cement paste Research, 579-589.

Pang, X et al. (2013). A Comparison Study of Portland Cement Hydration Kinetics as Measured by Chemical Shrinkage and Isothermal Calorimetry. Cement & Cement paste Composites, 23-32.

Paulo de Castro Gomes, J. (1997). Mathematical models for assessing hydration and microstructure of cement pastes. Dissertation,

Pavia, D., & Lampman, G. (2008). Introduction to spectroscopy (Fifth ed.).

Poole, J.L. et al. (2007). Methods for calculating activation energy for Portland cement. ACI Materials Journal, 303-311.

Richardson, I.G. (1991). The nature of CSH in hardened cements. Cement & Cement paste Research, 1131-1147.

Scrivener, K. L. (2004). Backscattered electron imaging of cementitious microstructures: understanding and quantification. Cement & Cement paste Composites, 935-945.

Scrivener, K.L. & Nonat, A. (2011). Hydration of cementitious materials, present and future. Cement and Cement paste Research, 651-665.

Termkhajornkit, P. & Barbarulo, R. (2012). Modeling the Coupled Effects of Temperature & Fineness of Portland Cement on the Hydration Kinetics in Cement Paste. Cement and Cement Paste Research, 526-538.

Thomas, J.J. (2007). A new approaching to modeling the nucleation and growth kinetics of tricalcium silicate hydration. Journal of American Ceramic Society, 3282-3288.

Thomas, J.J. (2009). Hydration kinetics and microstructure development of normal CaCl2-accelerated tricalcium silicate pastes. Journal of Physical Chemistry, 19836-19844.

Thomas, J.J. & Jennings, H.M. (1999). Effects of D20 and mixing on the early hydration kinetics of tricalcium silicate. Chemical Materials, 1907-1914.

Trapote-Barreira, A. et al. (2013). Dissolution kinetics of CSH gel. Flow-through experiments. Physics and Chemistry of the Earth,

Ylmén, R. (2009). Early hydration and setting of Portland cement monitored by IR, SEM and Vicat techniques. Cement and Cement Paste Research, 433-439.

Zelic, J et al. (2000). The role of silica fume in the kinetics and mechanisms during the early stage of cement hydration. Cement and Cement paste Research, 1655-1662.

Zhang, Y.M et al. (2000). Hydration of High-Volume Fly Ash Cement Paste. Cement and Cement Paste Composites, 445-452.

Appendix A: Matlab Analysis

Script:

```
%%%%%%%%%%%%%%%%%%%%%%%%%%%%%%%%%%%%%%%%%%%%%%%%%%%%%%%%%%%%%%%%%%%%%%%%%
%%%%%%%%%%%%%%%%%%%%%%%%%
clc; close all; clear all;
%CHANGE THE IMAGE
  uiopen('0w_28_1300x_mid_area1_2.tif',1);
I=imread('0w_28_1300x_mid_area1_2.tif');
figure(1);imshow(I,'InitialMagnification',30)   % original image  <<<<<<<<
%CHANGE THRESHOLD LIMITS: T2;T3;T4;T5 (T1=0; T6=255;)
T2=16;T4=198; T3=1+T2; T5=1+T4;   %use find to put in T's in _findmed


PIX=8000;
sig=0.4; h=zeros(3,3);
for ii=1:3  % gaussian matrix
    for jj=1:3
        h(ii,jj)=1/(2*pi*sig^2)*exp(-(((ii-2))^2+((jj-2))^2)/2/sig^2);  %1/(2*pi*sig^2)*;
    end
end
% h=[0 0 0;0 1 0;0 0 0];                    % without convolution
Iconvol=imfilter(I,h,'conv');               % convolution or neutral density(N-D) filter


Imed=medfilt2(Iconvol(:,:,1));              % 2D median filter
```

```
figure(2);
imshow(Imed,'InitialMagnification',30);          % convol, median filtered image (to compare)

[counts1,v1]=imhist(Imed);counts(256)=0;  %pixel count, at grays of the scale(0-255)

SS=size(counts1);SSS=SS(1);v3=0;vL=0;vH=0;

for jj=1:SSS
   if counts1(jj)<500
      counts1(jj)=0;
      if v1(jj)<125
         vL=vL+1;
      else
         vH=vH+1;
      end
   else
      v3=v3+1;
      counts2(v3)=counts1(jj);
   end
end
vL;
vH;
```

```
v3;
N2=nnz(counts1);
% v4=1:v3;
r=255/v3;
% v5=v4*N1/v3;
for xx=1:768
   for yy=1:1024
      if Imed(xx,yy)<vL
         Imed(xx,yy)=0;
      elseif Imed(xx,yy)>255-vH
         Imed(xx,yy)=255;
      else
%           one=Imed(xx,yy)
%           round((Imed(xx,yy)+1-vL)*1.25)
         ImedS(xx,yy)=round((Imed(xx,yy)+1-vL)*r); %Median Stretched
      end
   end
end


%%%%%%%%%%%%%%%%%%%%%%%%%%%%%%%%%%%%%%%%%%%%%%%%%%%%%%%%%%%%%
%%%%%%%%%%%%%%%%%%%%%%%%%%%
```

```
%Pseudo of Convolution and Median filter


inputimage=Imed;
siz =size(inputimage);
for i=1:siz(1,1)
   for j=1:siz(1,2)
      if inputimage(i,j,:) < T2      % black
         inputimage(i,j,1) = 0;     % blue coded by RGB
         inputimage(i,j,2) = 0;
         inputimage(i,j,3) = 255;
      elseif inputimage(i,j,:) < T4 % dark grey
         inputimage(i,j,1) = 0;     % green coded by RGB
         inputimage(i,j,2) = 255;
         inputimage(i,j,3) = 0;
      else                          % light grey
        inputimage(i,j,1) = 255;    % red coded by RGB
        inputimage(i,j,2) = 0;
        inputimage(i,j,3) = 0;
      end
   end
end
%%%%%%%%%%%%%%%%%%%%%%%%%%%%%%%%%%%%%%%%%%%%%%%%%%%%%
%%%%%%%%%%%%%%%%%%%%%%%
```

```
figure(3);imshow(inputimage,'InitialMagnification',30);          % pseudo of median

%histograms

figure(4)
imhist(ImedS)
xlabel('Grayscale'),ylabel('Pixels')       % histrogram of Median Stretched
axis([0 255 0 PIX])

figure(5)                          % colored histrogram of Median Stretched colored
[counts,v]=imhist(ImedS(:,:,1));N=size(counts);N1=N(1);
p = imhist(ImedS(:,:,1));
x1=1:T2; x2=T3:T4; x3=T5:255;          %THRESHOLD CHANGE

stem(x1,p(1:T2),'b'); hold on;         %THRESHOLD CHANGE
stem(x2,p(T3:T4),'g'); hold on;
stem(x3,p(T5:255),'r');

xlabel('Grayscale'),ylabel('Pixels')
axis([0 255 0 PIX])

%THRESHOLD CHANGE
[counts,v]=imhist(ImedS);N=size(counts);N1=N(1); %counts for Median Stretched phases
```

```
A1S=0;ii=0;A2S=0;A3S=0;
for ii=1:N1
   if v(ii)< T2
      A1S=A1S+counts(ii);
   elseif v(ii)< T4
      A2S=A2S+counts(ii);
   else
      A3S=A3S+counts(ii);
   end
end
Area1S=A1S;    % area 1  0~74
Area2S=A2S;    % area 2  75~160
Area3S=A3S;    % area 3  161~255

AP1S=A1S/(A1S+A2S+A3S)*100;    % area 1  0~74
AP2S=A2S/(A1S+A2S+A3S)*100;    % area 2  75~160
AP3S=A3S/(A1S+A2S+A3S)*100;    % area 3  161~255
R1S=round(AP1S);
R2S=round(AP2S);
R3S=round(AP3S);
D1S=['Porosity is ',num2str(R1S), '%'];disp(D1S)
D2S=['CSH is ',num2str(R2S), '%'];disp(D2S)
D3S=['CH is ',num2str(R3S), '%'];disp(D3S)
```

%%

Phase Thresholding for Both Curing Methods:

Water Cure Threshold Levels						
		Control	Fly Ash		Silica Fume	
Days	Area	0%	5%	10%	5%	10%
3	CSH	88	77	114	85	121
	CH-255	194	193	218	198	242
7	CSH	53	63	47	76	68
	CH-255	162	178	146	199	198
14	CSH	52	66	106	OUT	OUT
	CH-255	151	184	198	OUT	OUT
28	CSH	70	103	58	43	46
	CH-255	204	202	171	199	169
56	CSH	69	69	84	62	49
	CH-255	206	200	223	200	203

Vacuum Cure Threshold Levels						
		Control	Fly Ash		Silica Fume	
Days	Area	0%	5%	10%	5%	10%
3	CSH	101	92	100	119	87
	CH-255	222	205	204	212	203
7	CSH	50	42	51	99	86
	CH-255	150	126	167	206	205
14	CSH	93	54	19	OUT	111
	CH-255	177	120	124	OUT	220
28	CSH	76	112	57	92	78
	CH-255	196	236	180	208	222
56	CSH	94	71	79	24	46
	CH-255	229	197	215	133	193

Appendix B: SEM Image Analysis via Matlab

Control Cement Paste Vacuum Cured at 3 Days

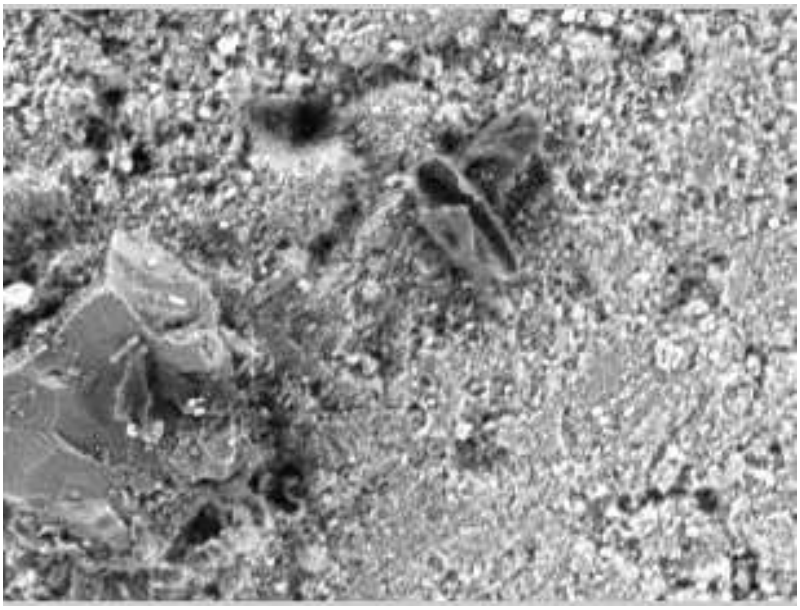

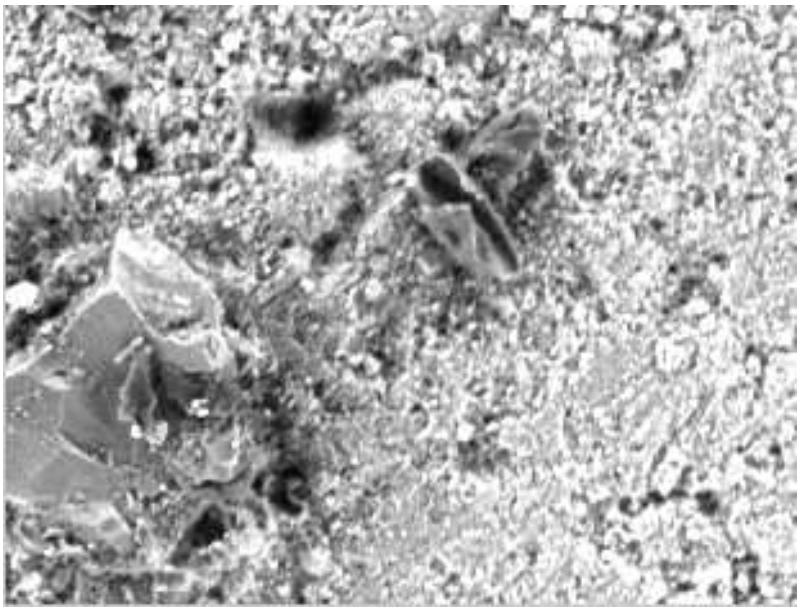

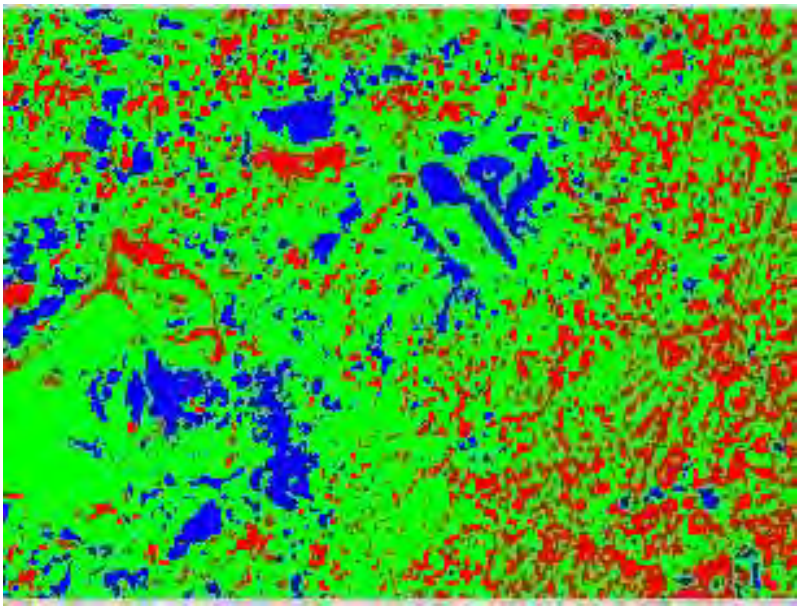

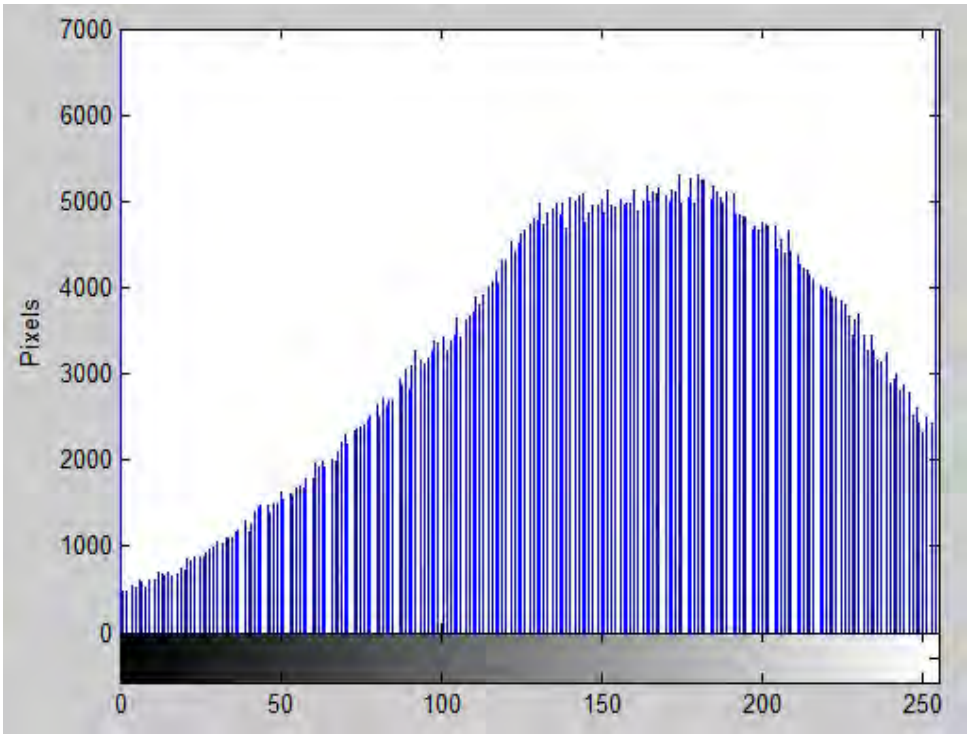
Pixels
7000
6000
5000
4000
3000
2000
1000
0
0
50
100
150
200
250

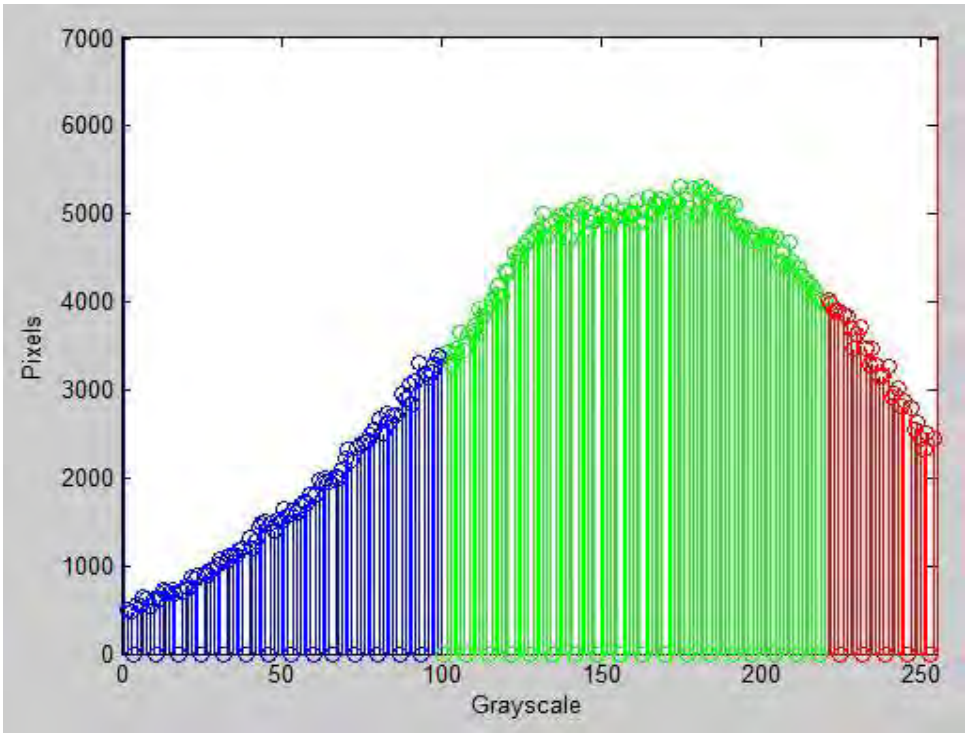

Porosity is 19%

CSH is 61%

CH is 20%

Control Cement Paste Vacuum Cured at 7 Days

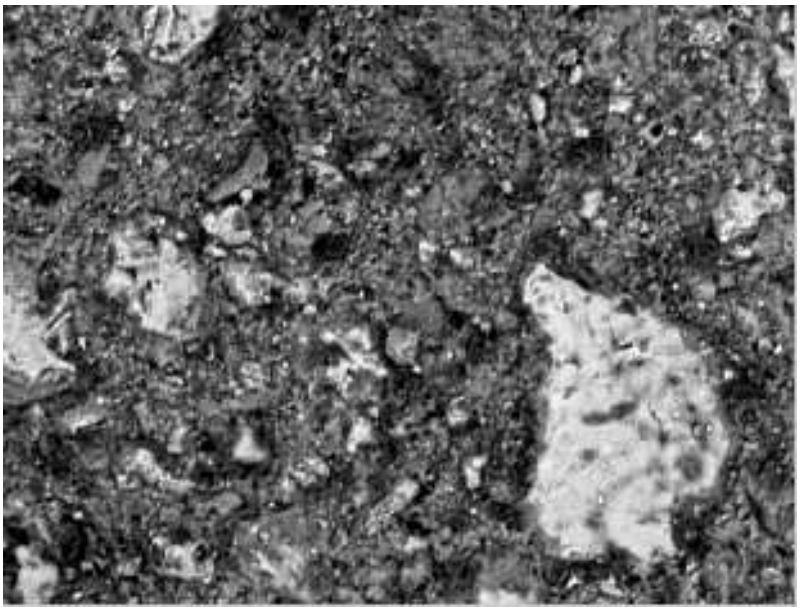

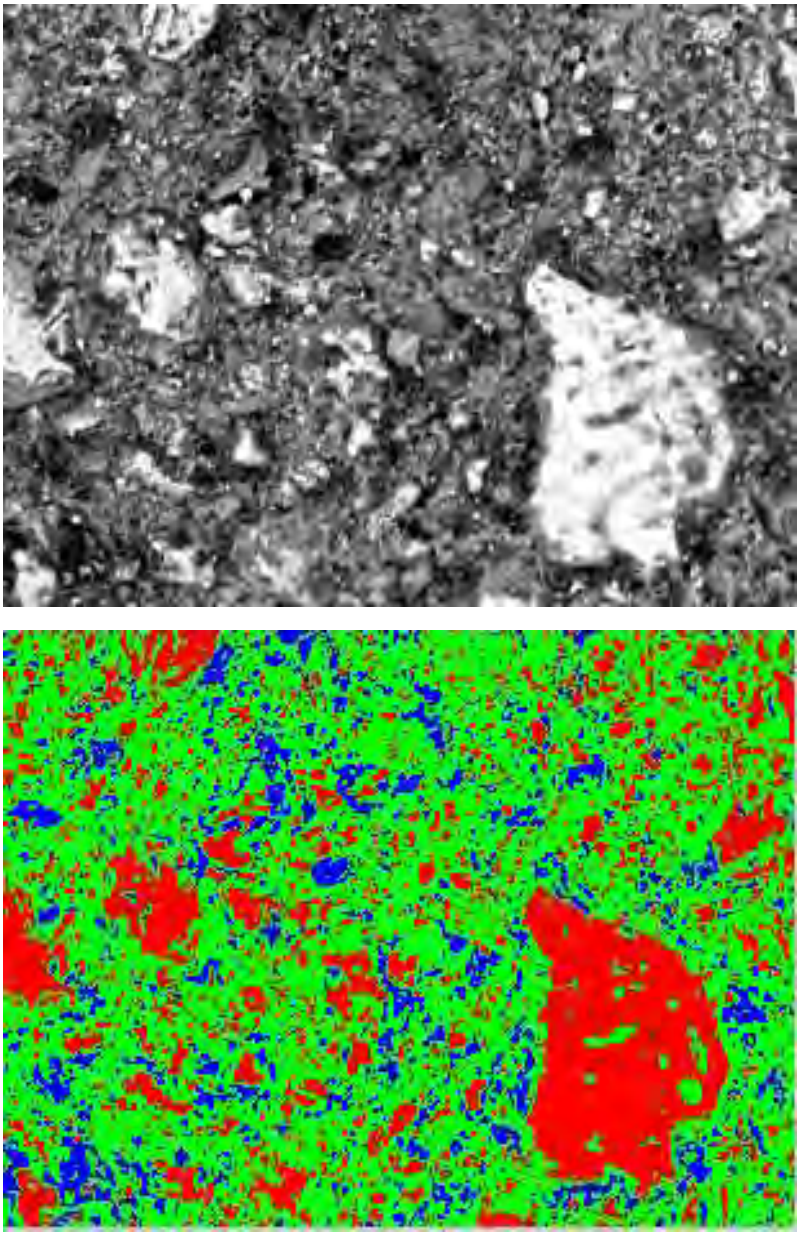

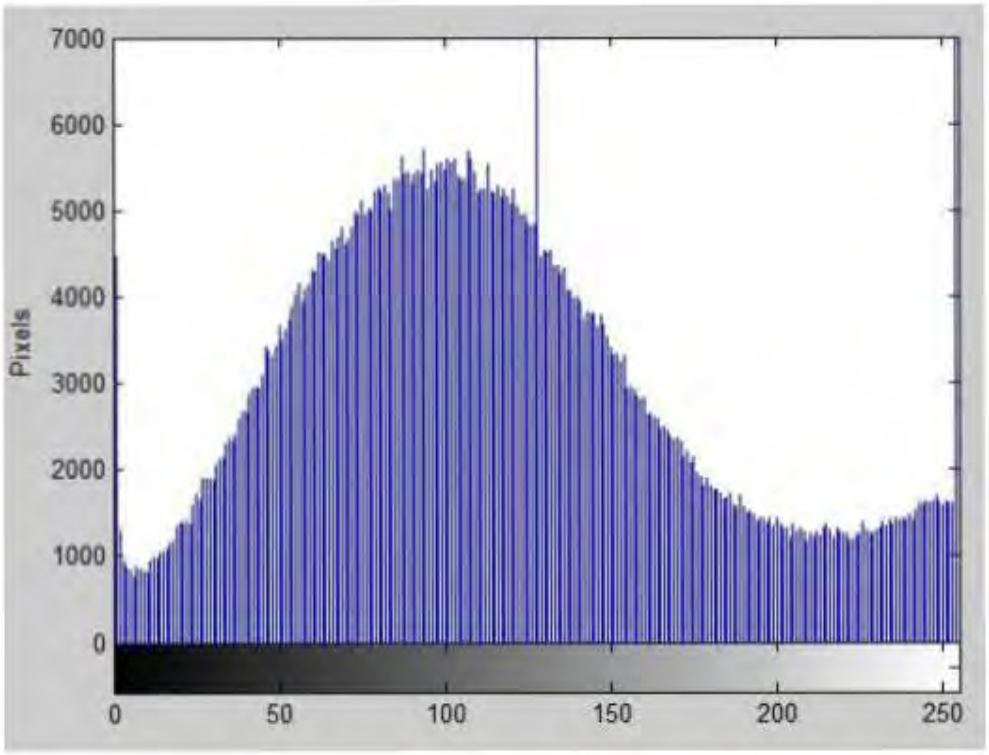

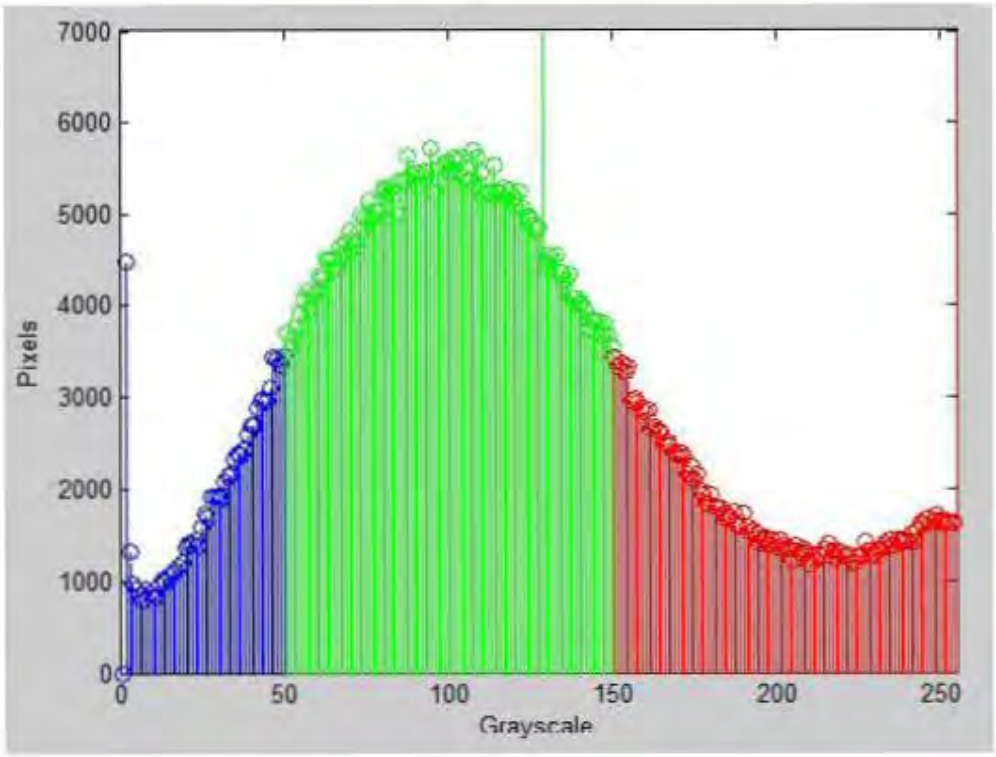

Porosity is 12%

CSH is 62%

CH is 26%

Control Cement Paste Vacuum Cured at 14 Days

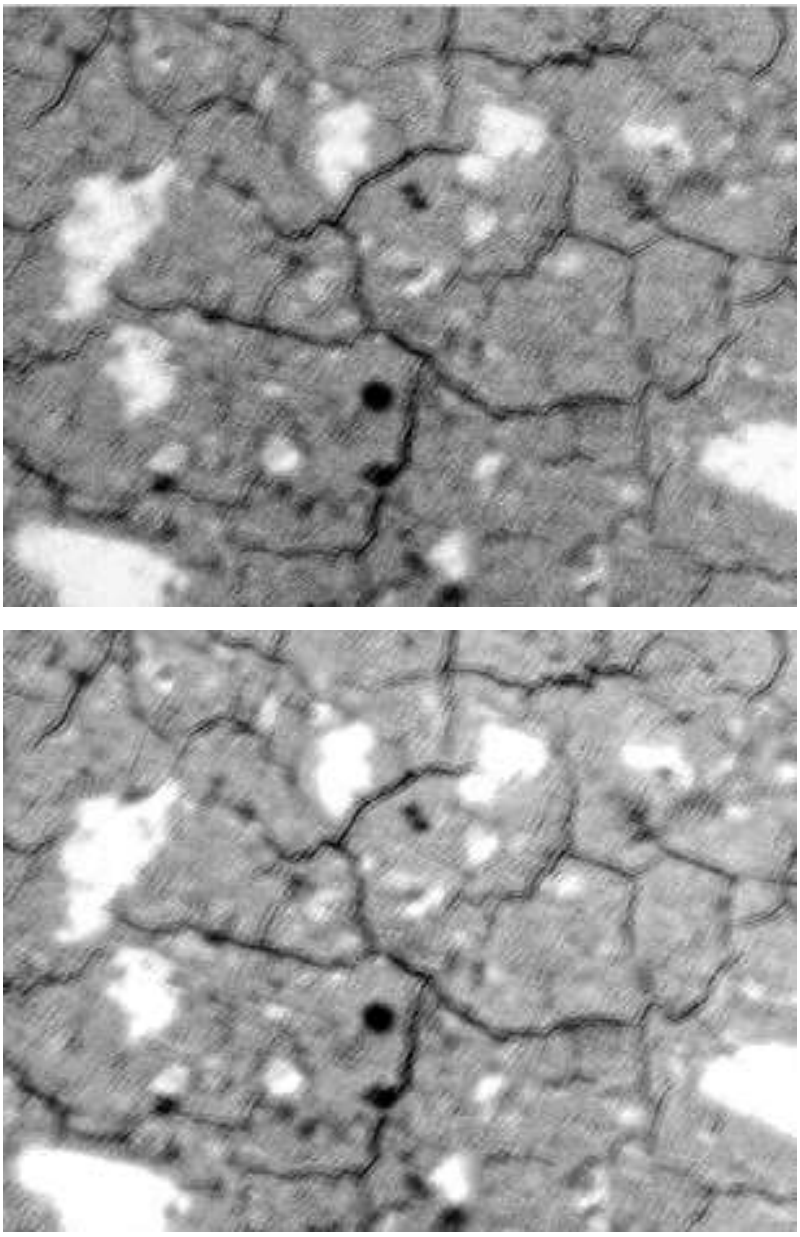

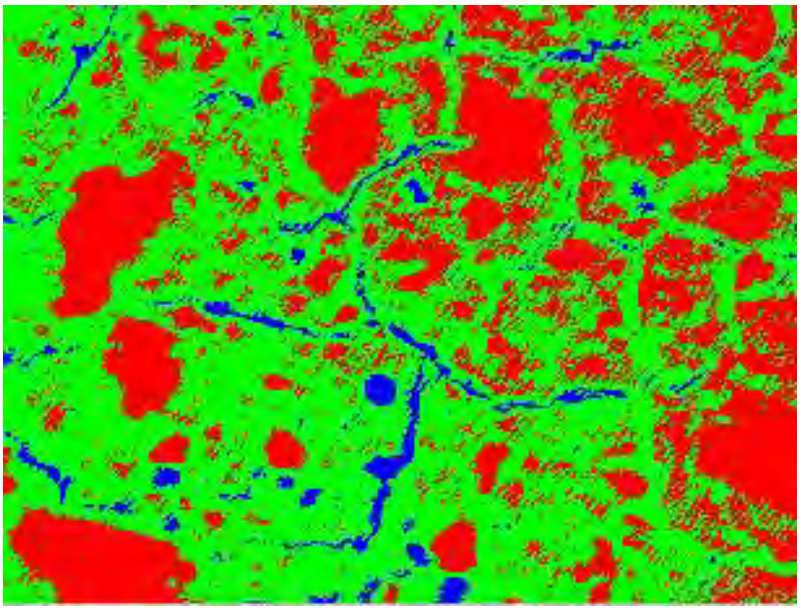

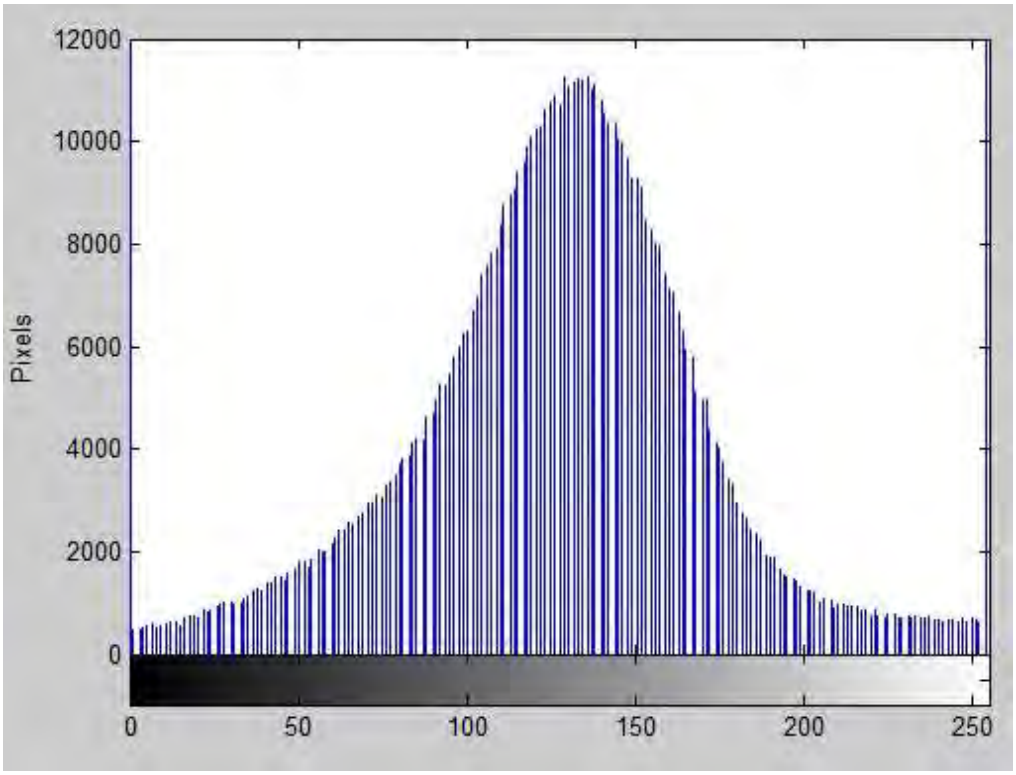
12000
10000
8000
6000
4000
2000
0
Pixels
0
50
100
150
200
250

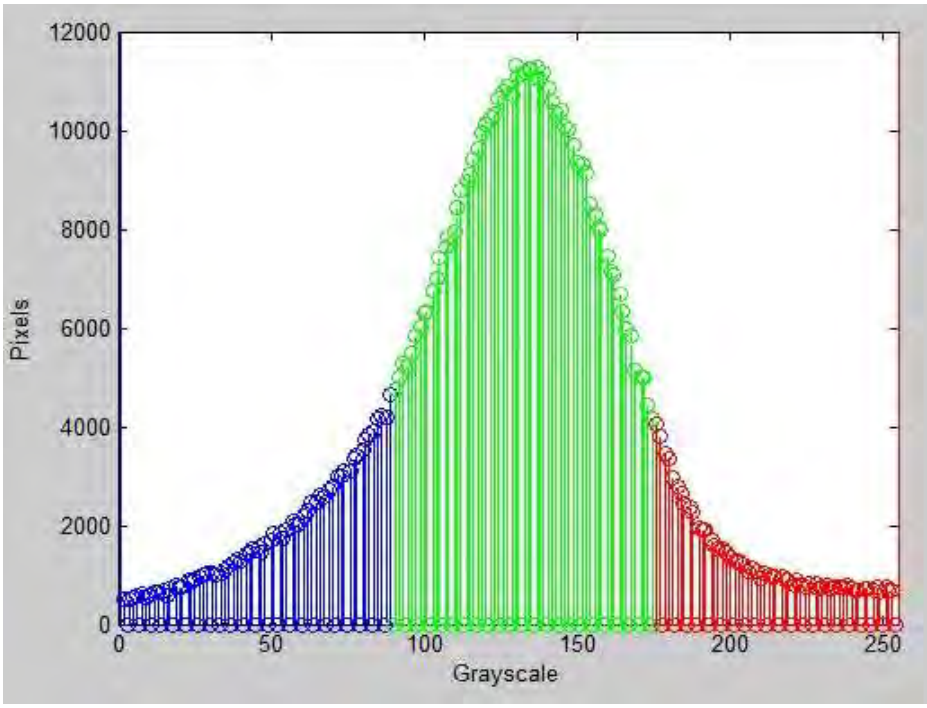

Porosity is 17%

CSH is 67%

CH is 16%

Control Cement Paste Vacuum Cured at 28 Days

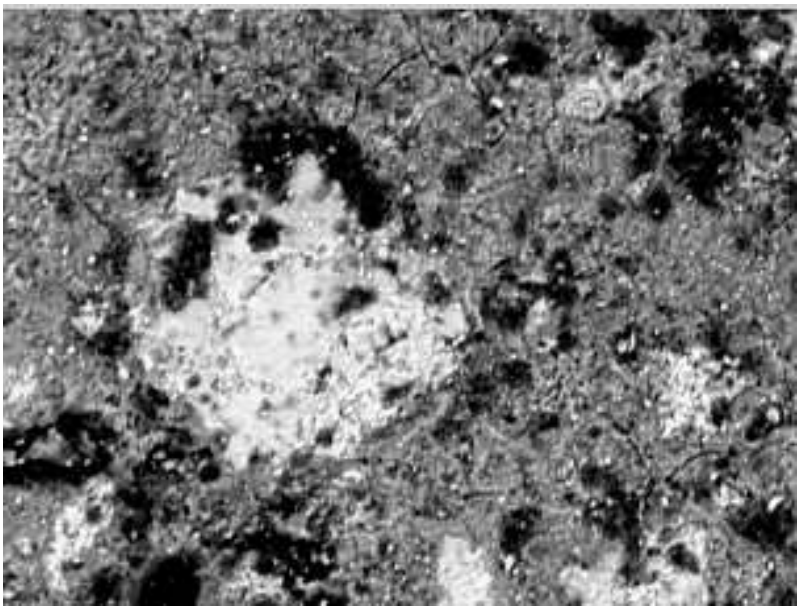

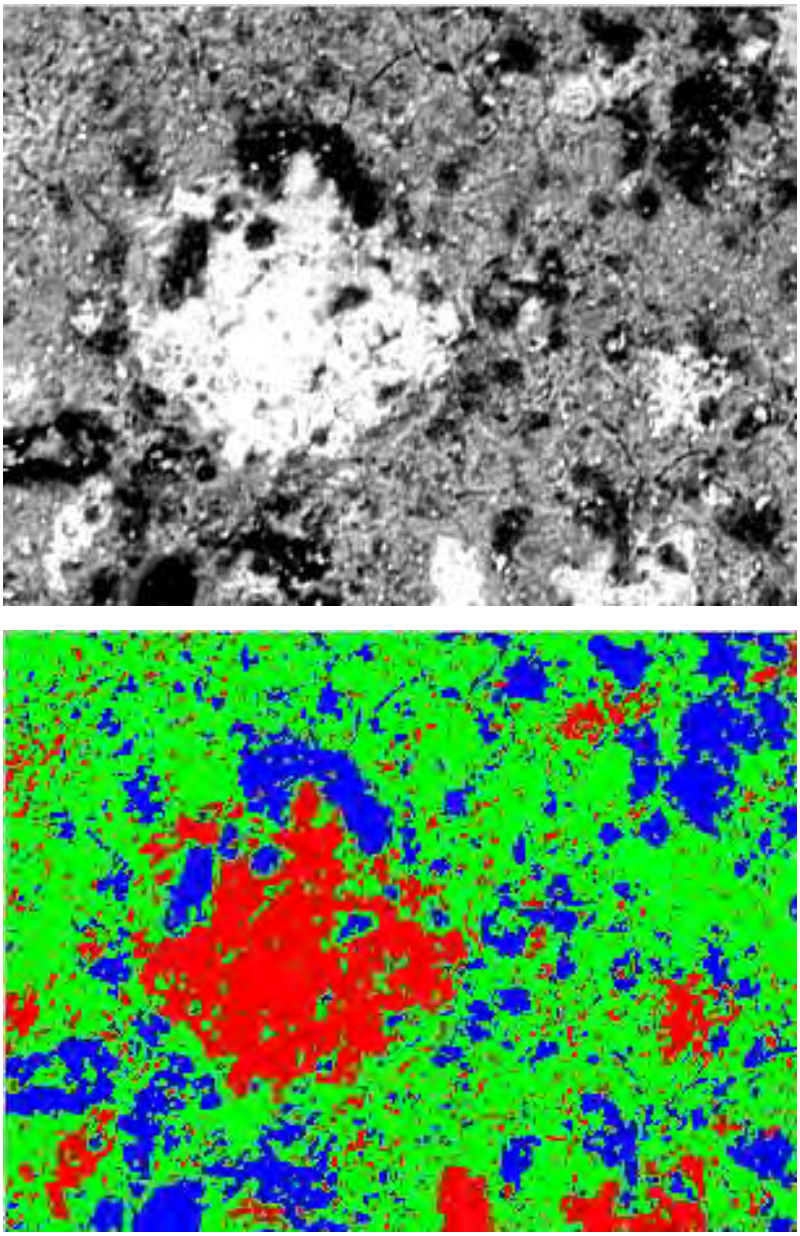

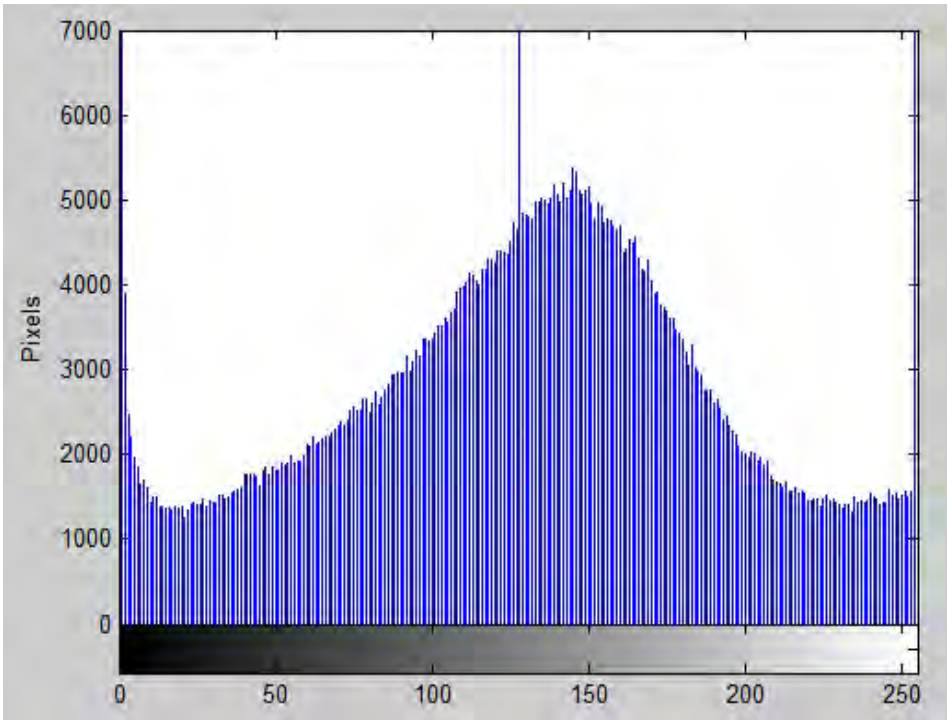

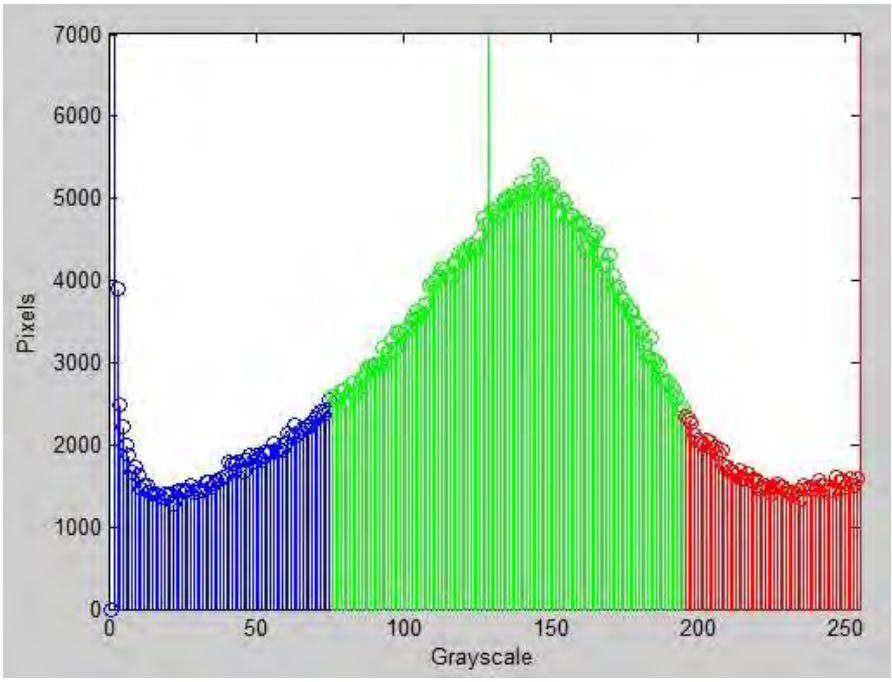

Porosity is 15%

CSH is 69%

CH is 16%

Control Cement Paste Vacuum Cured at 56 Days

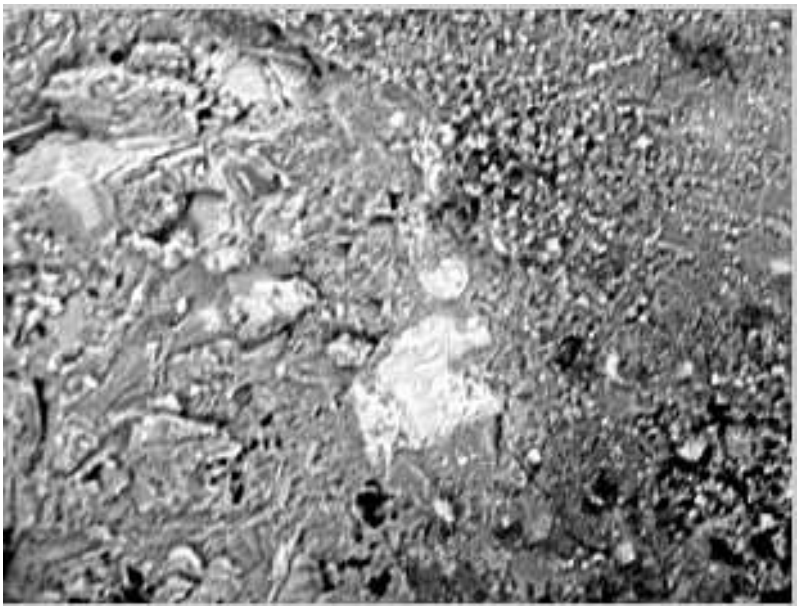

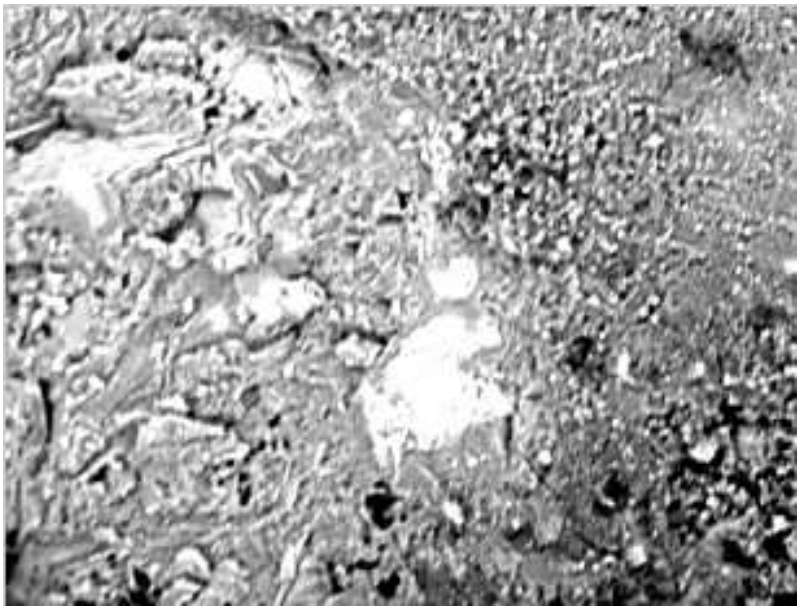

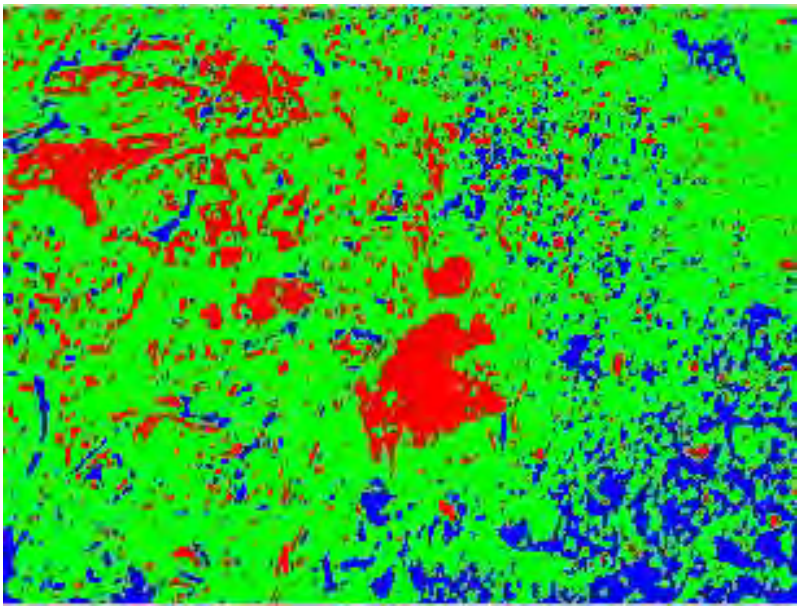

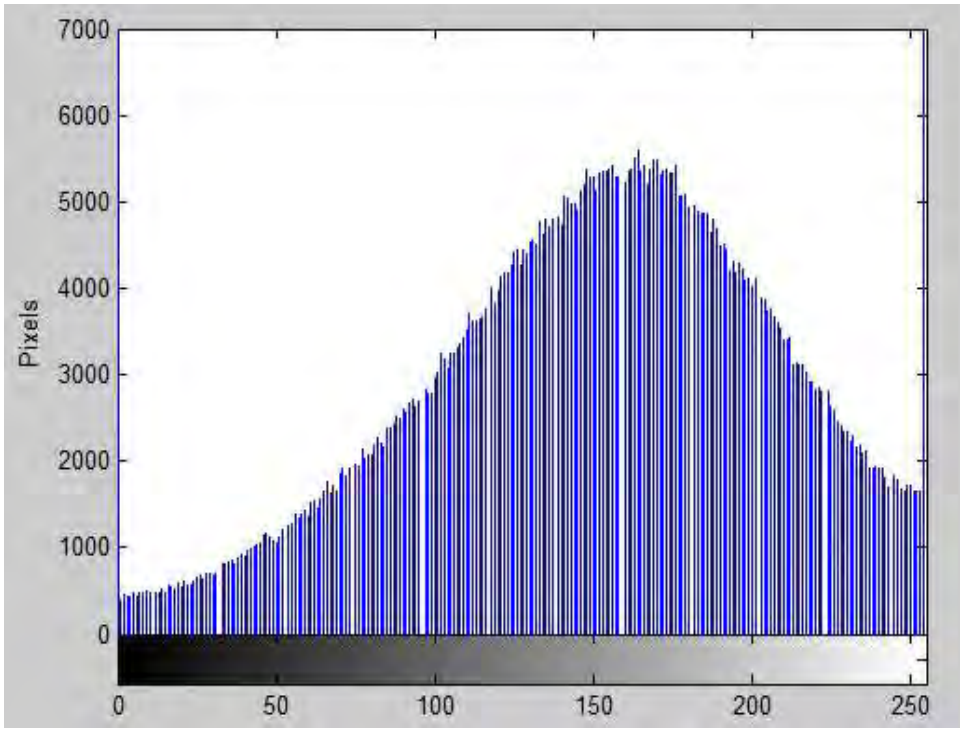
Pixels
7000
6000
5000
4000
3000
2000
1000
0
0
50
100
150
200
250

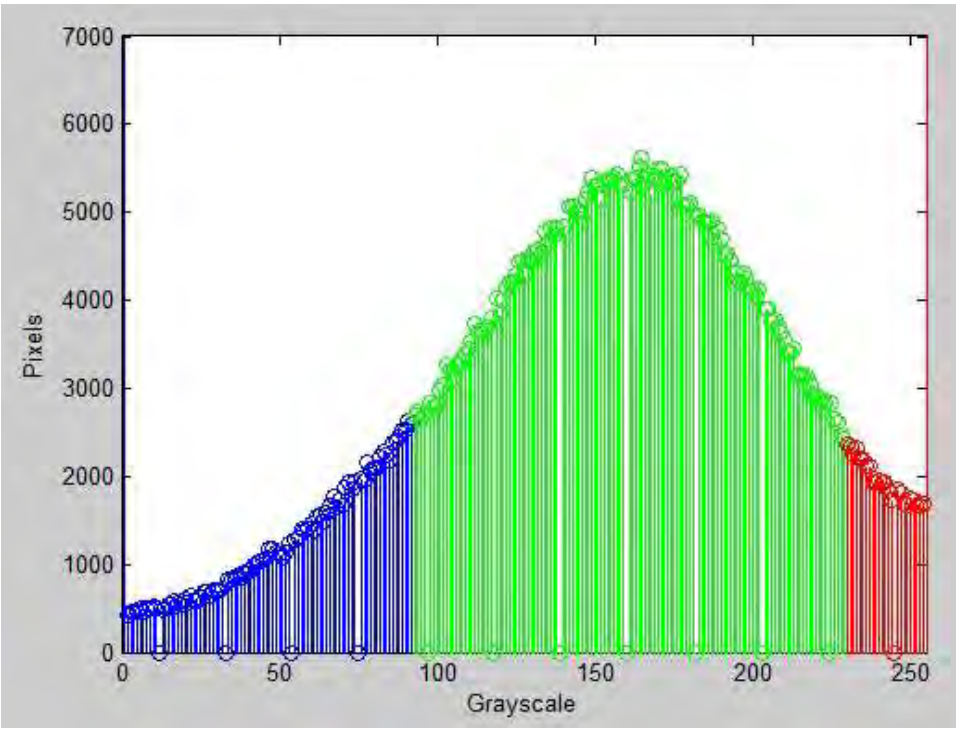

Porosity is 16%

CSH is 70%

CH is 14%

Control Cement Paste Water Cured at 3 Days

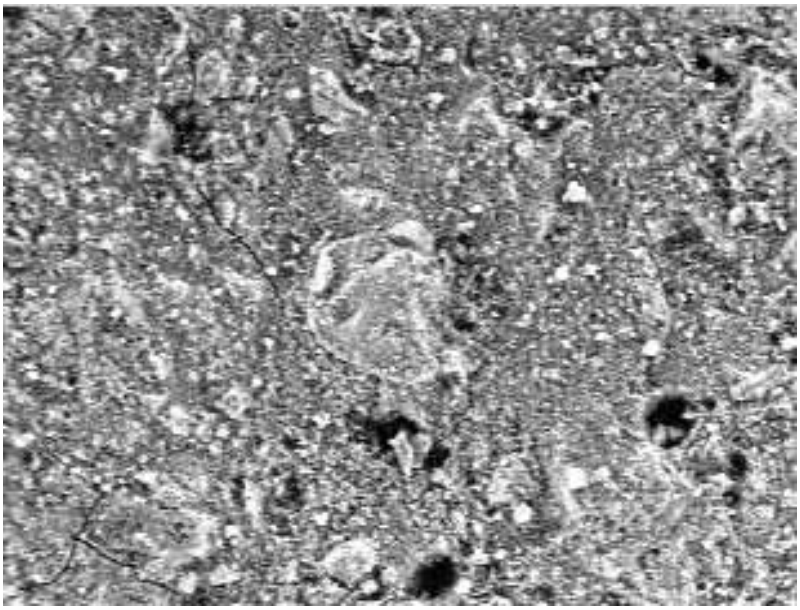

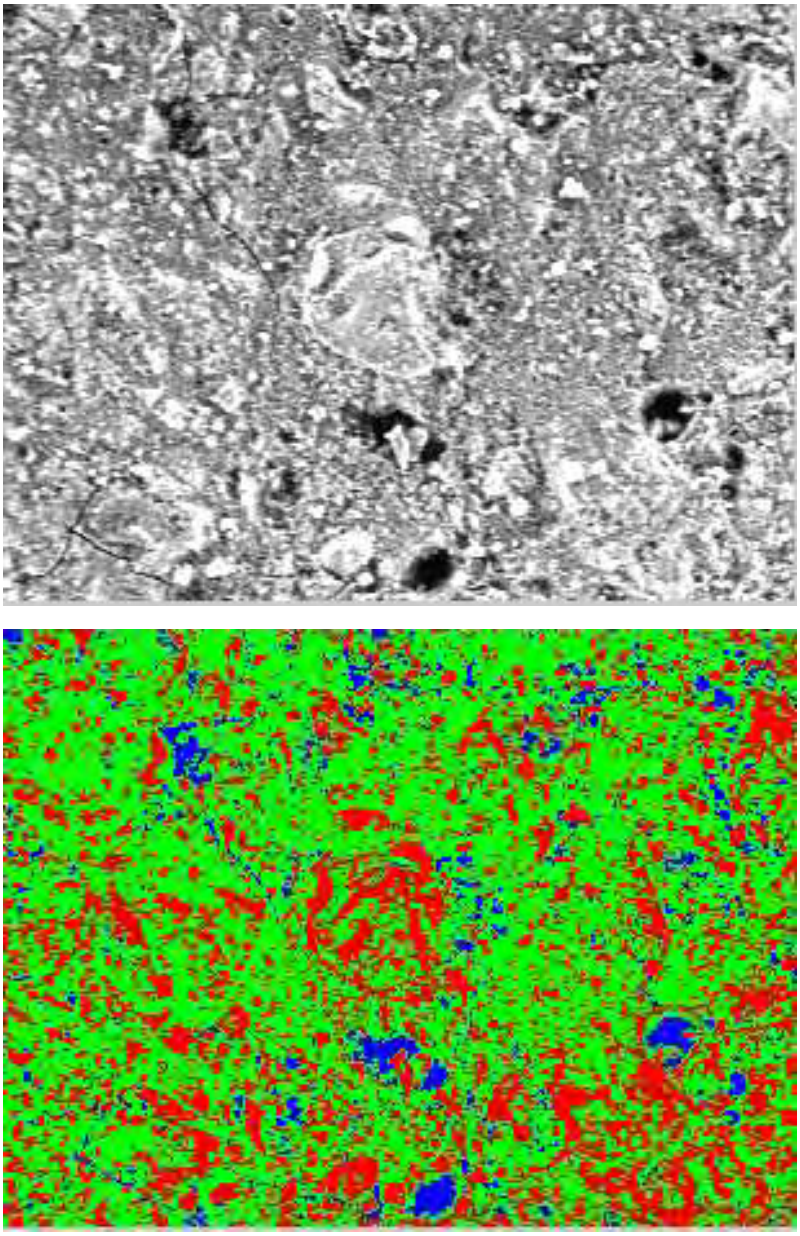

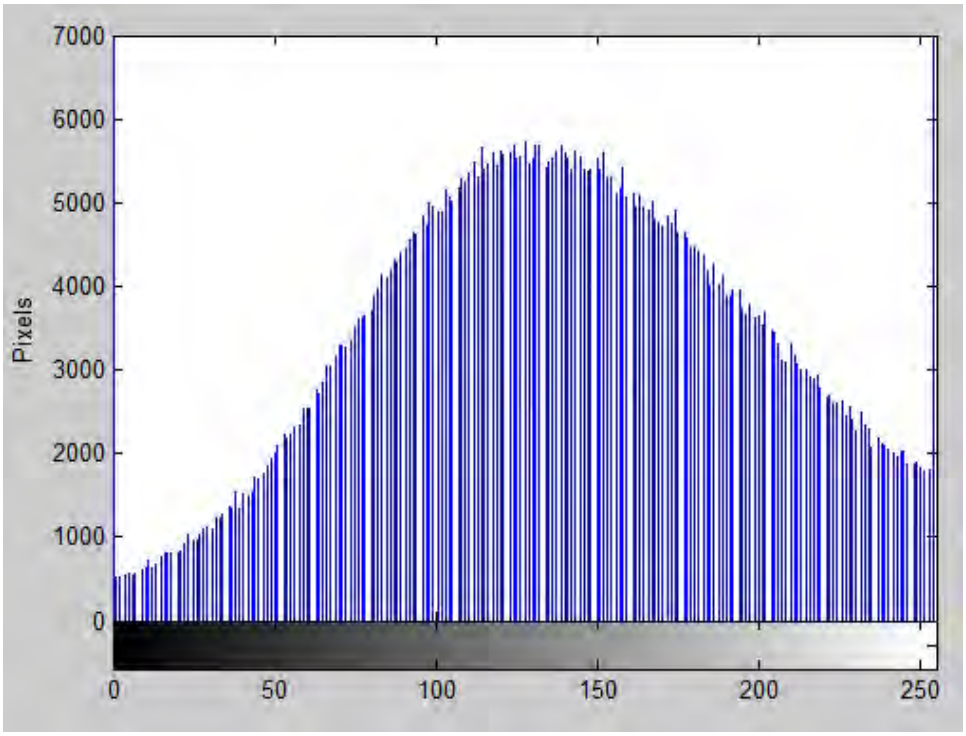

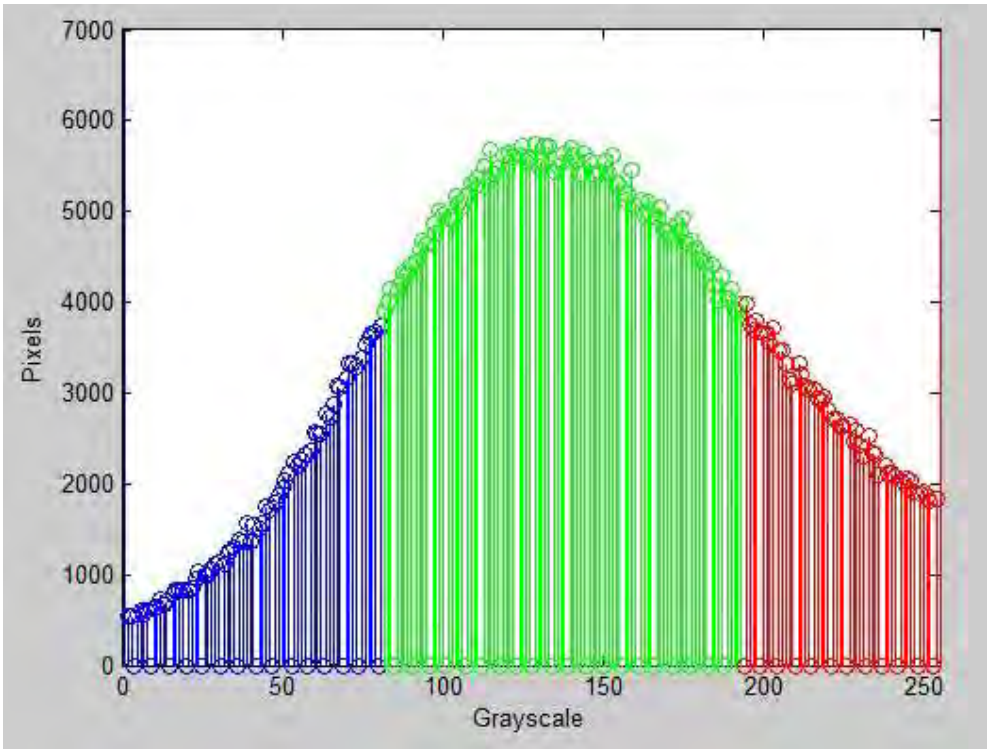

Porosity is 17%

CSH is 59%

CH is 25%

Control Cement Paste Water Cured at 7 Days

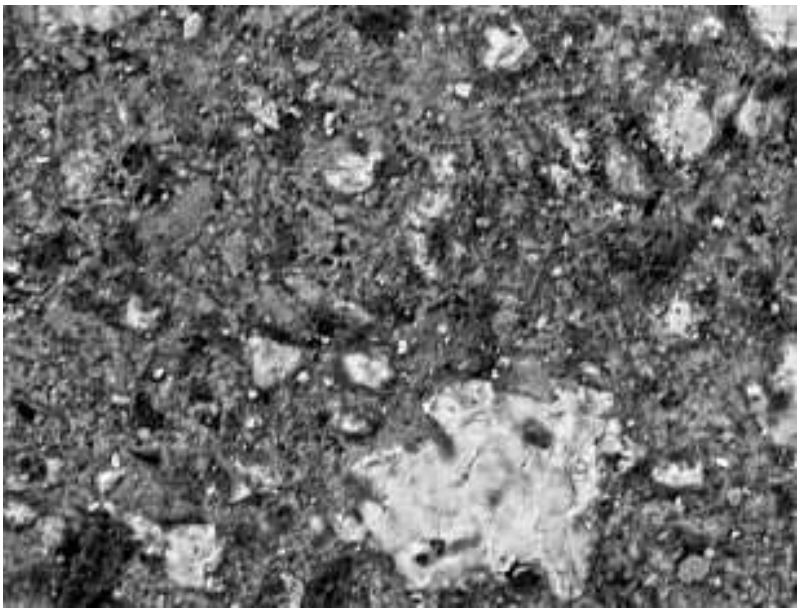

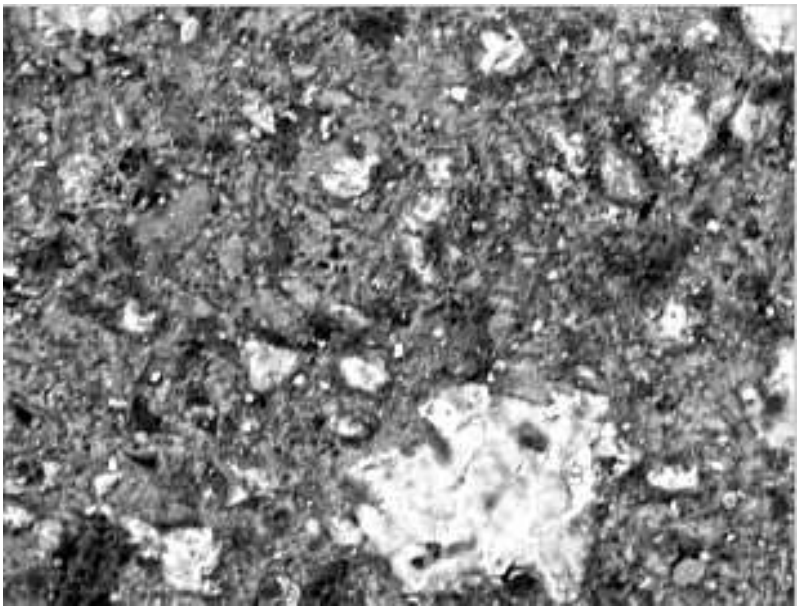

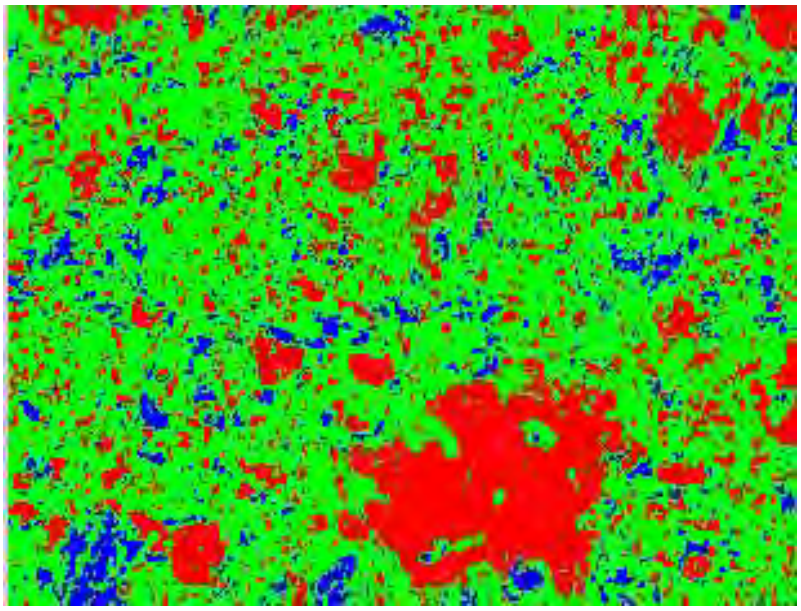

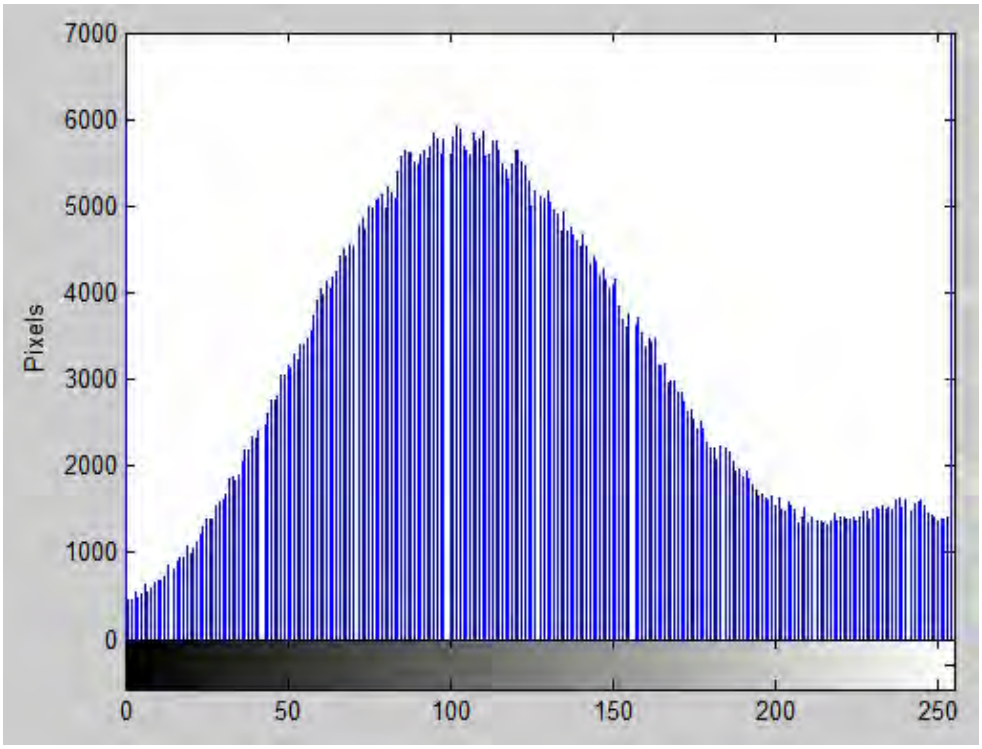
Pixels
7000
6000
5000
4000
3000
2000
1000
0
0
50
100
150
200
250

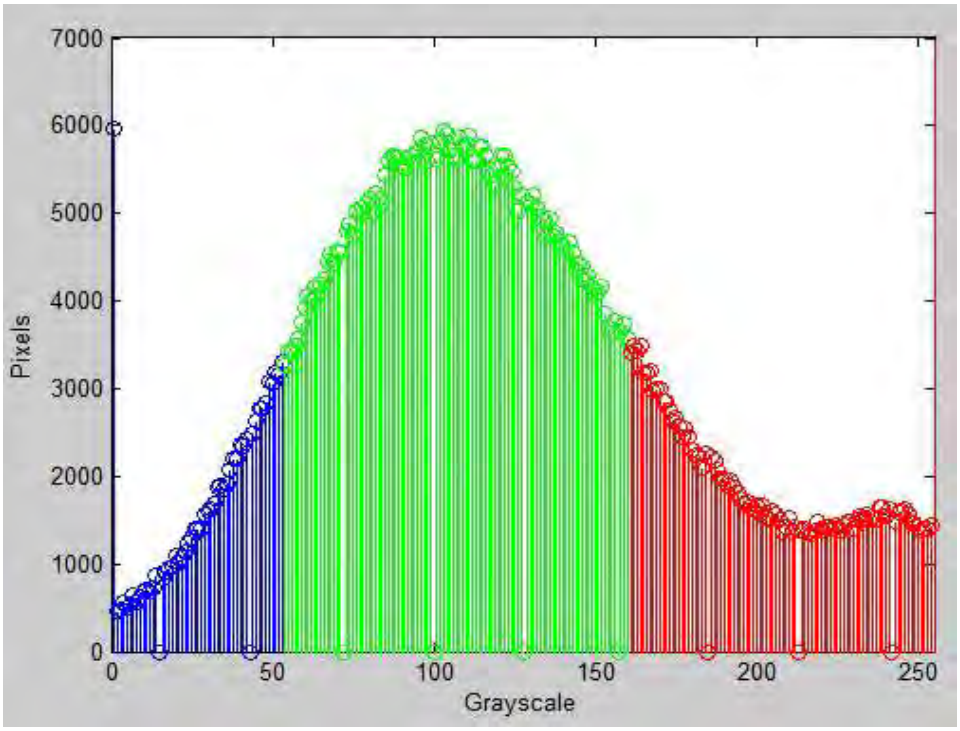

Porosity is 11%

CSH is 64%

CH is 25%

Control Cement Paste Water Cured at 14 Days

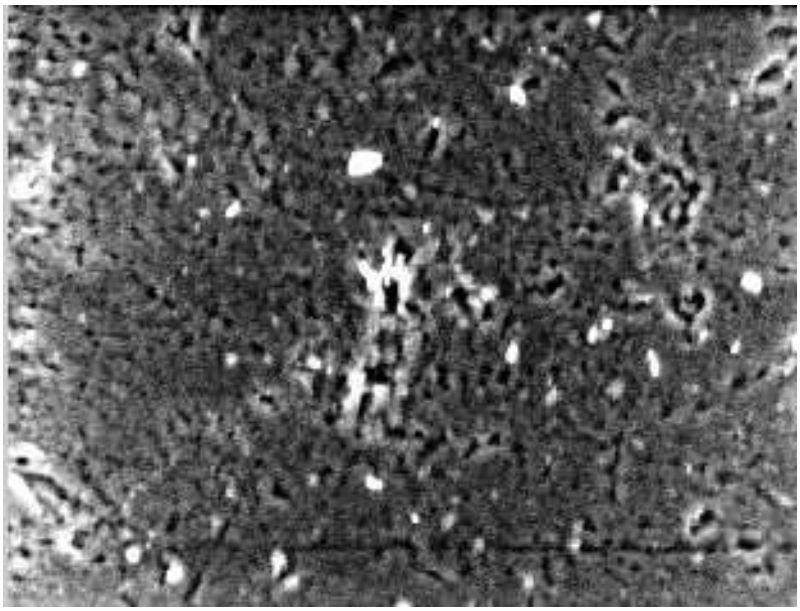

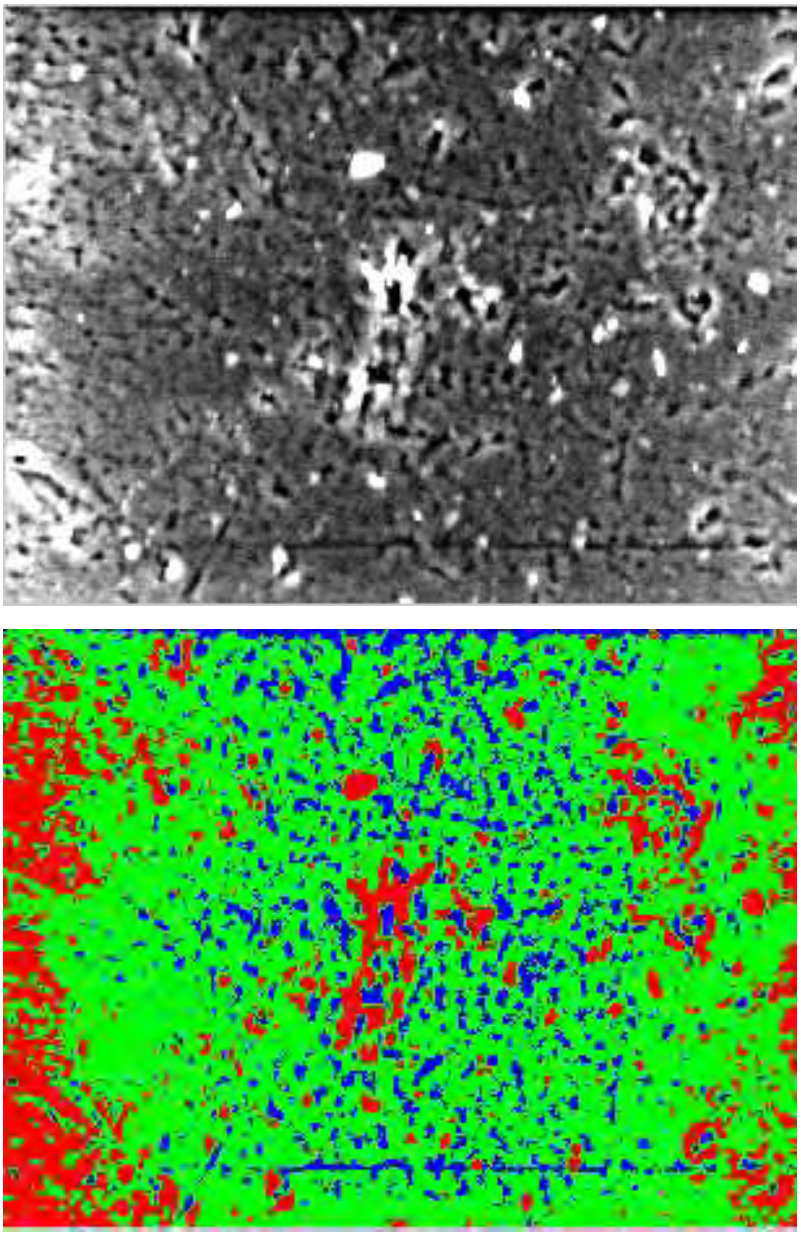

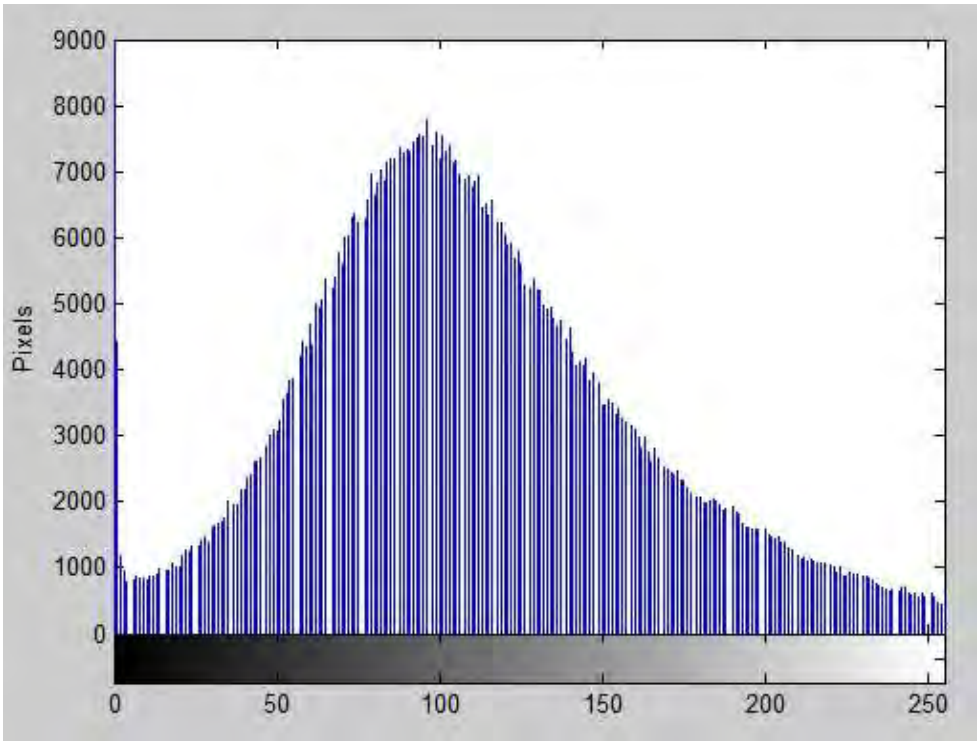

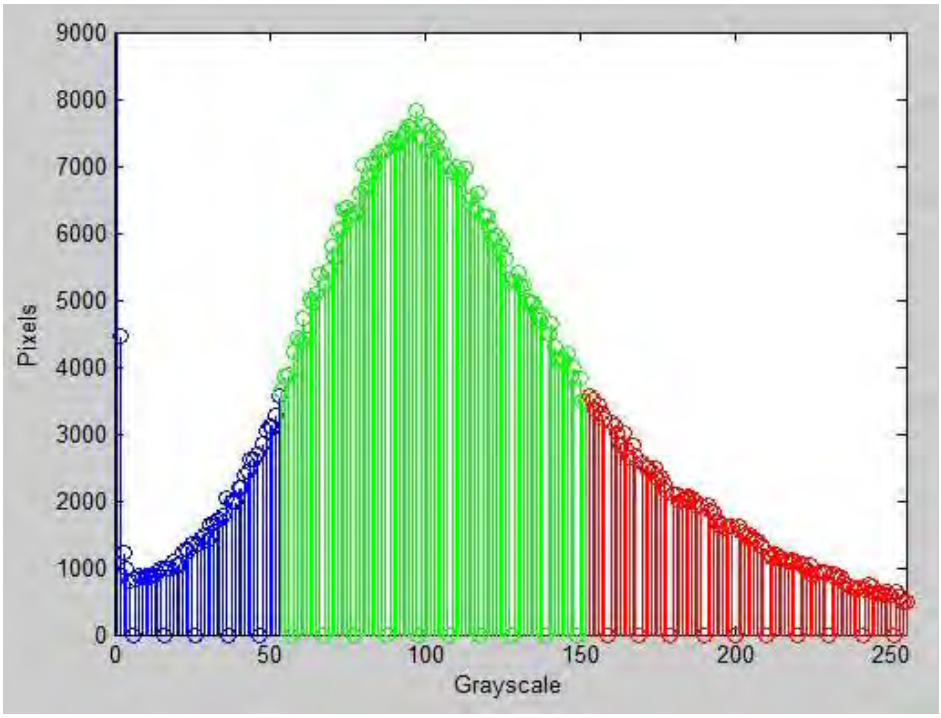

Porosity is 14%

CSH is 66%

CH is 19%

Control Cement Paste Water Cured at 28 Days

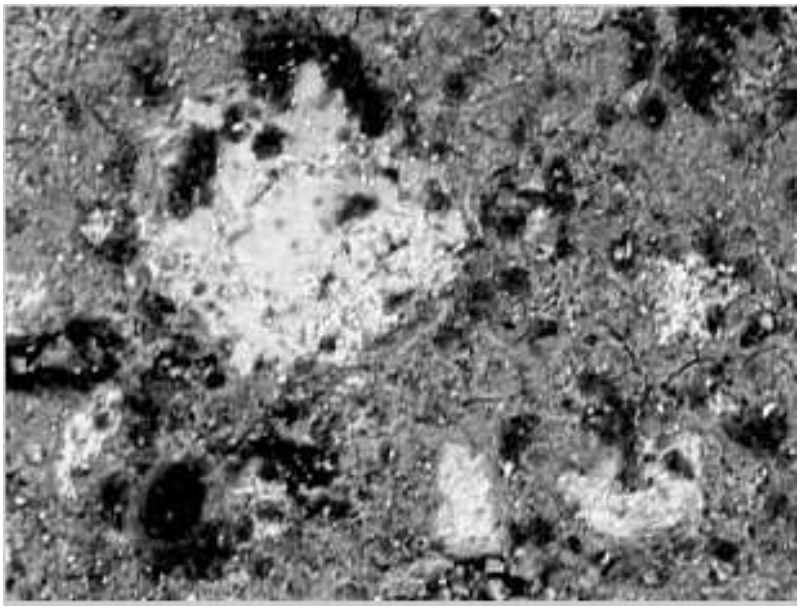

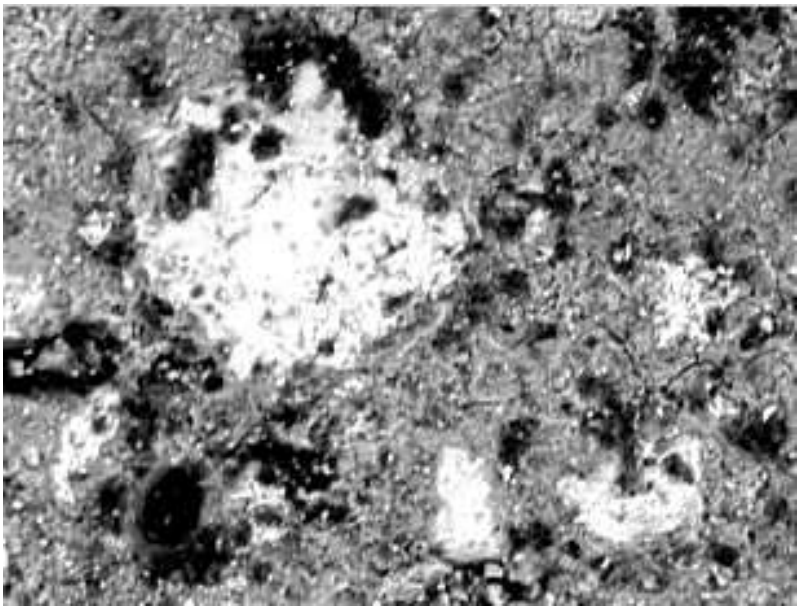

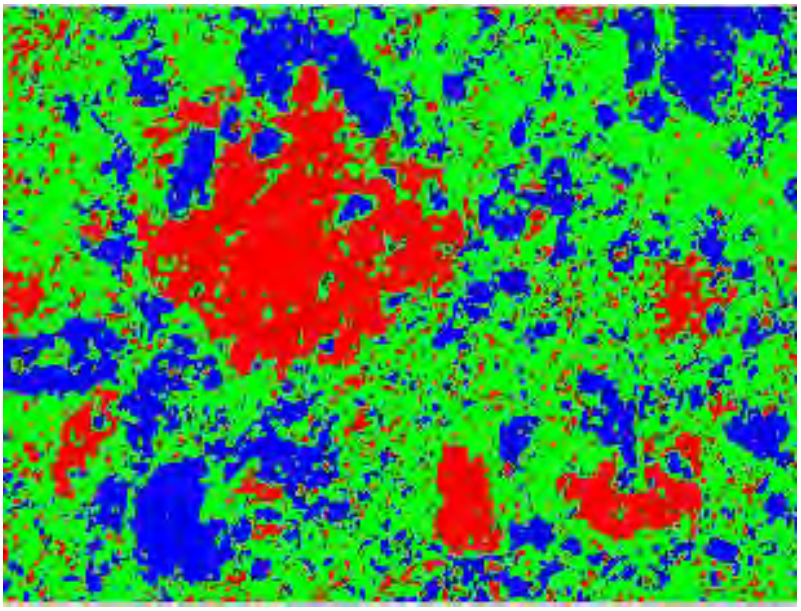

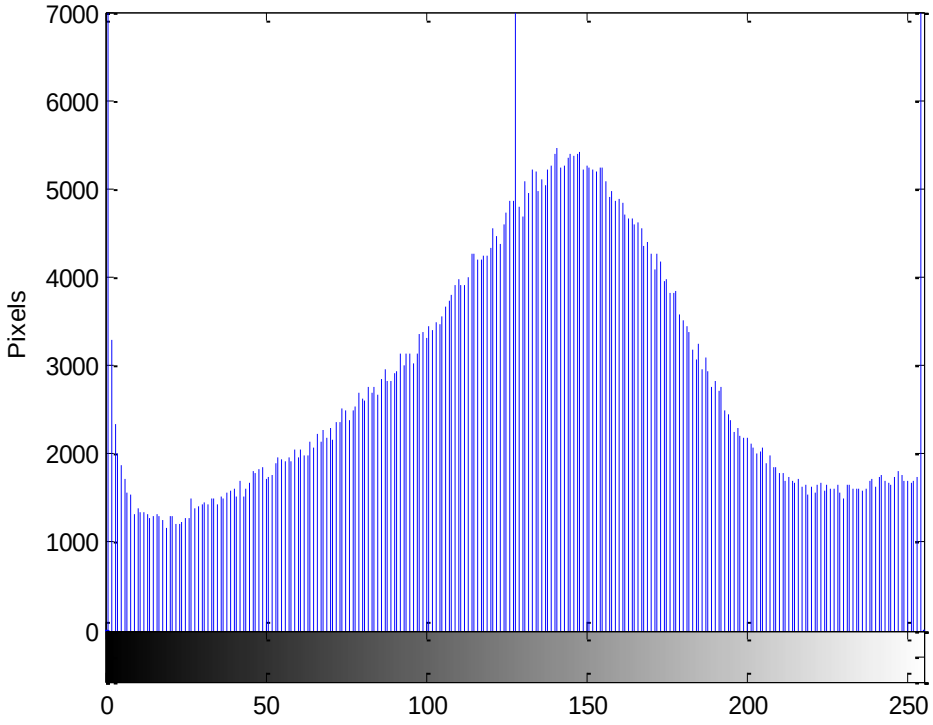
Pixels
7000
6000
5000
4000
3000
2000
1000
0
0
50
100
150
200
250

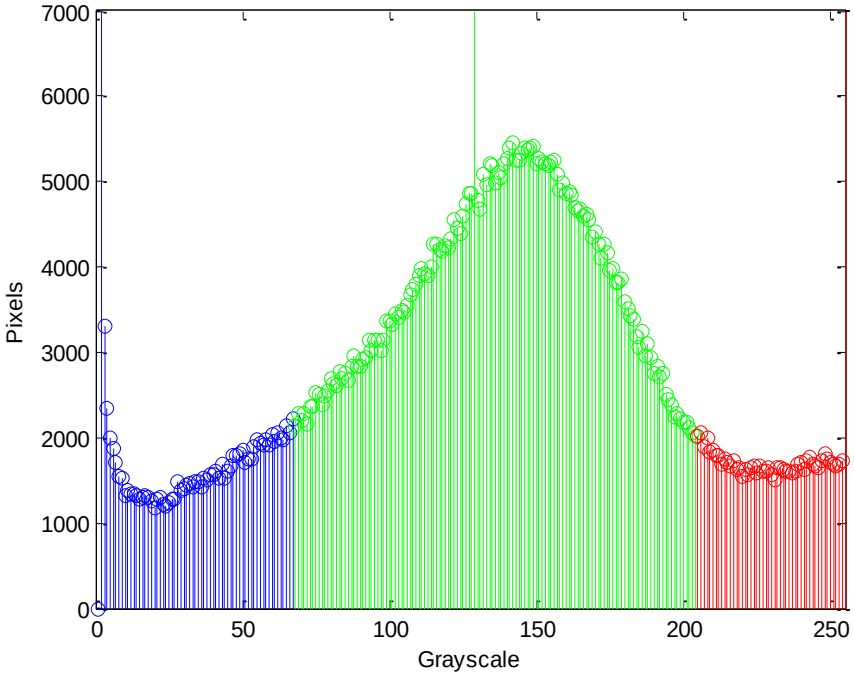

Porosity is 17%

CSH is 67%

CH is 17%

Control Cement Paste Water Cured at 56 Days

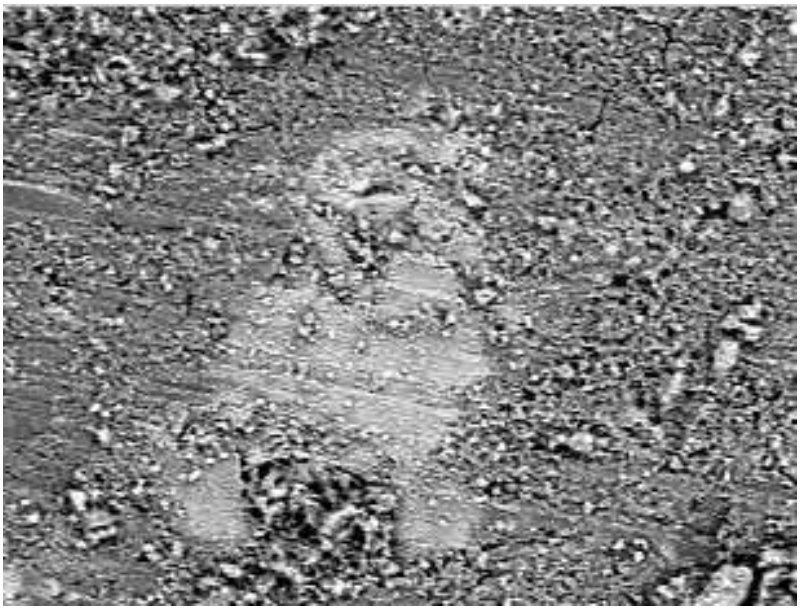

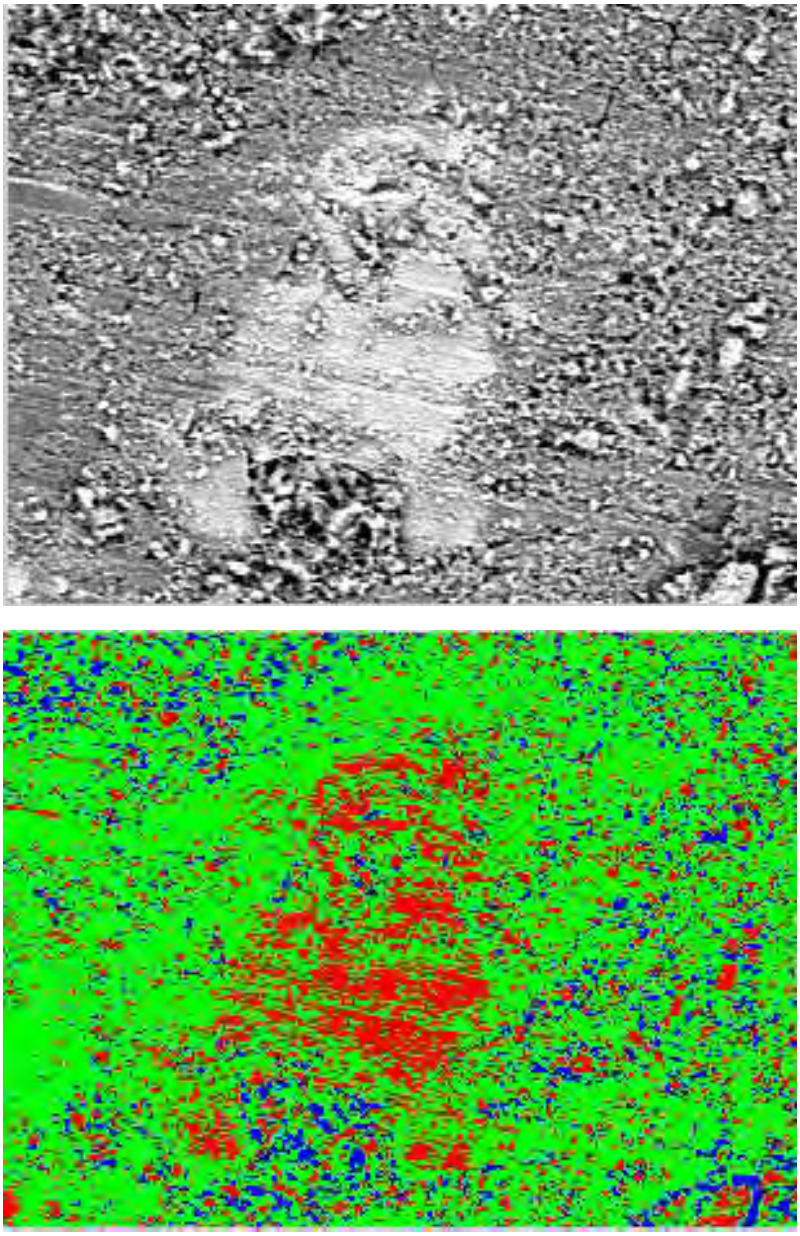

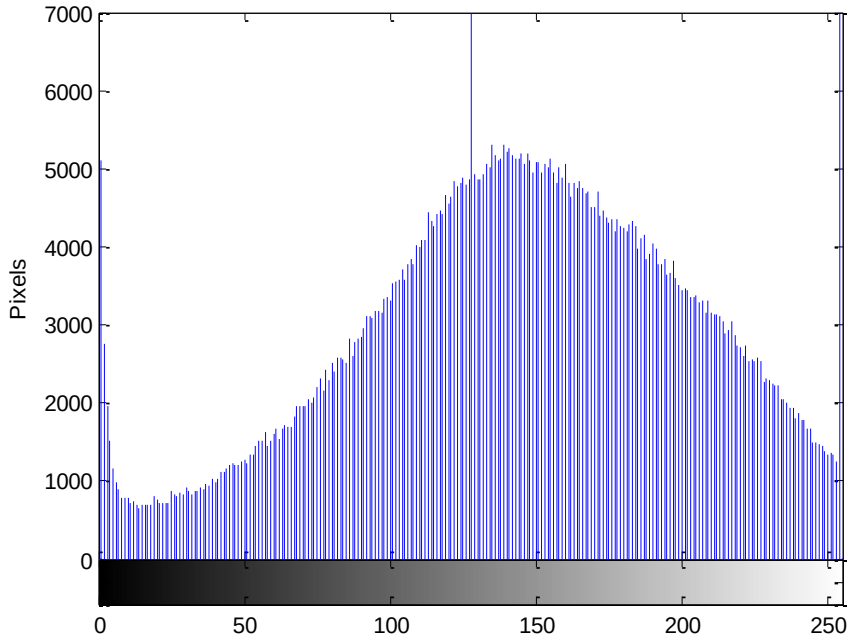

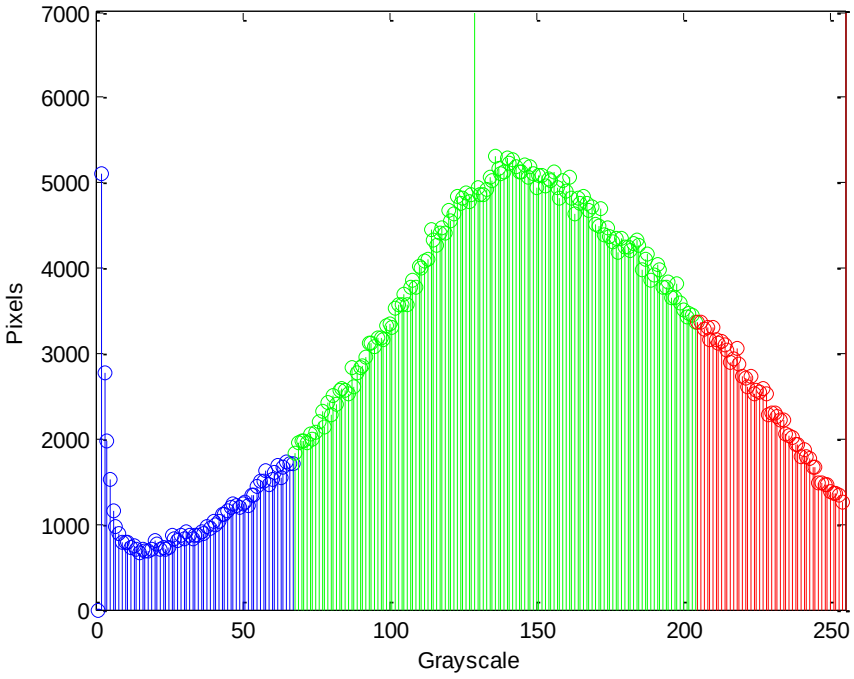

Porosity is 10%

CSH is 70%

CH is 20%

5% Fly Ash Vacuum Cured at 3 Days

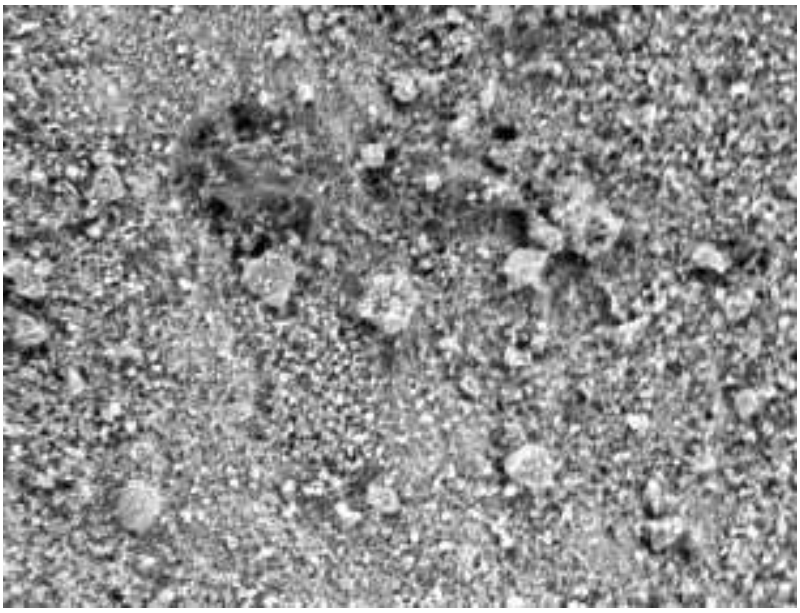

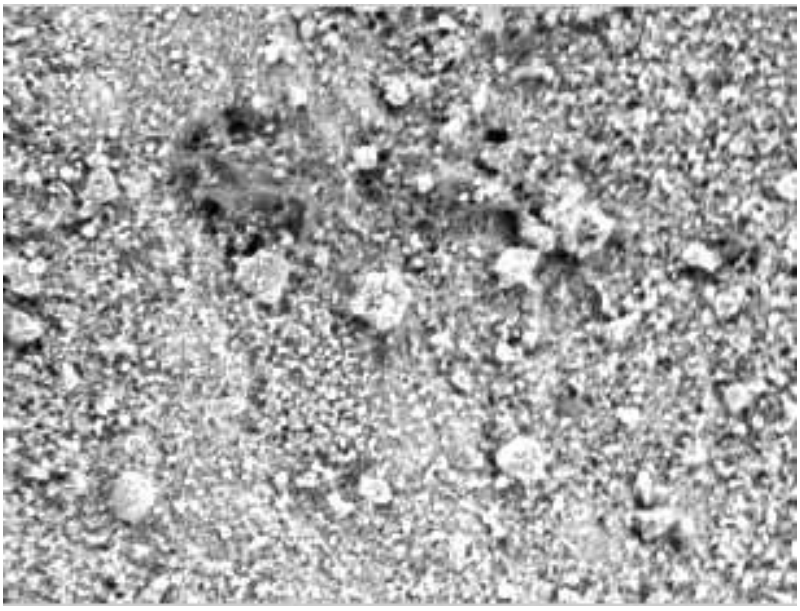

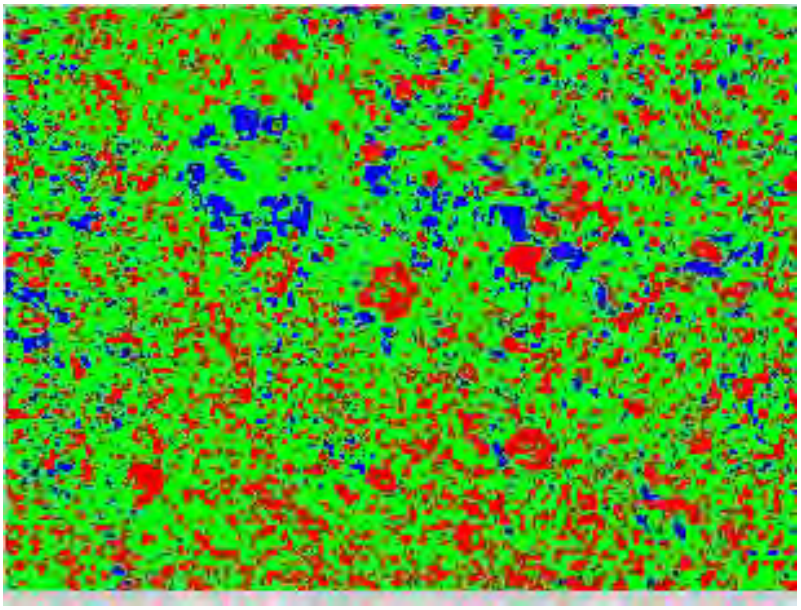

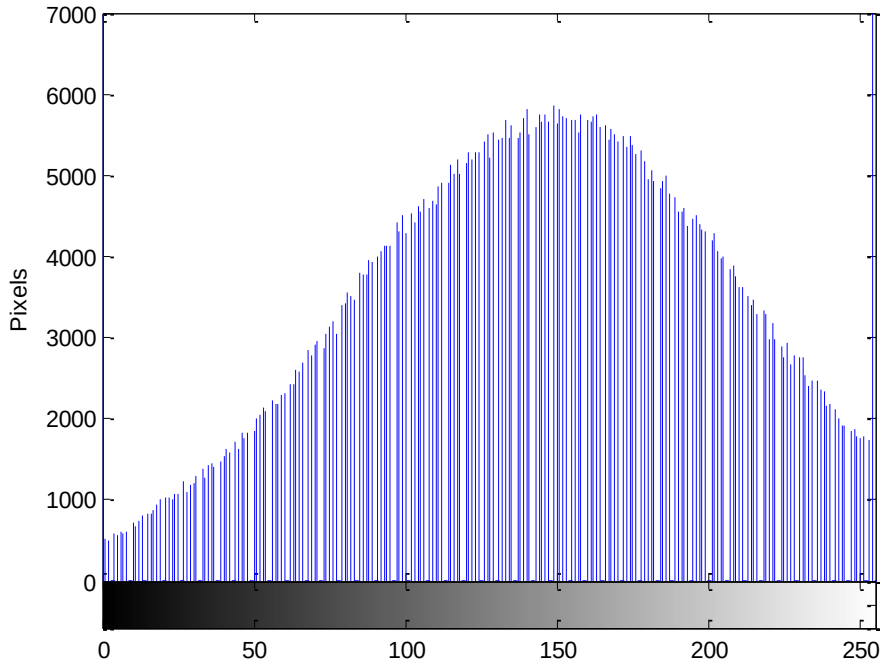
Pixels
7000
6000
5000
4000
3000
2000
1000
0
0
50
100
150
200
250

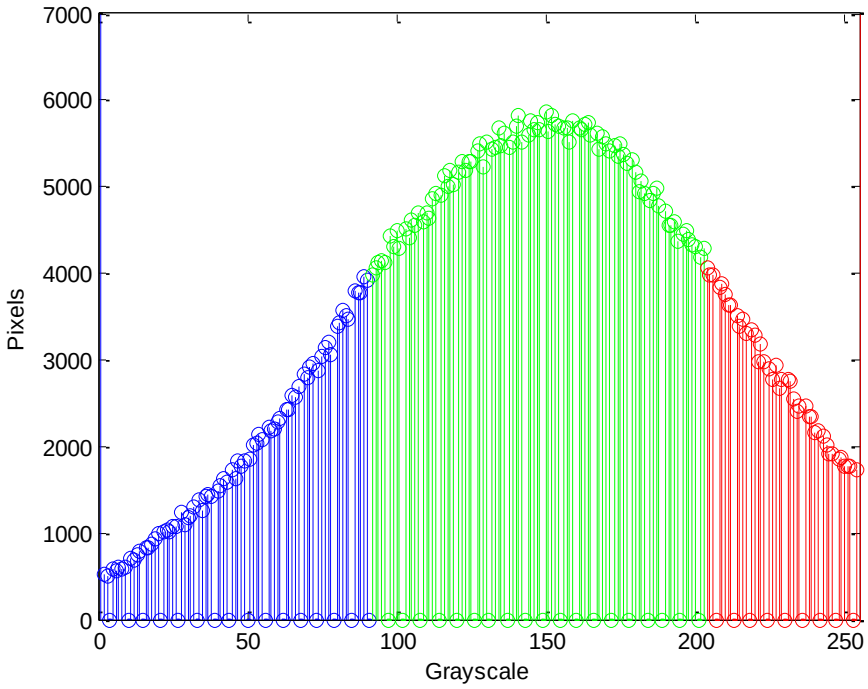

Porosity is 19%

CSH is 60%

CH is 20%

5% Fly Ash Vacuum Cured at 7 Days

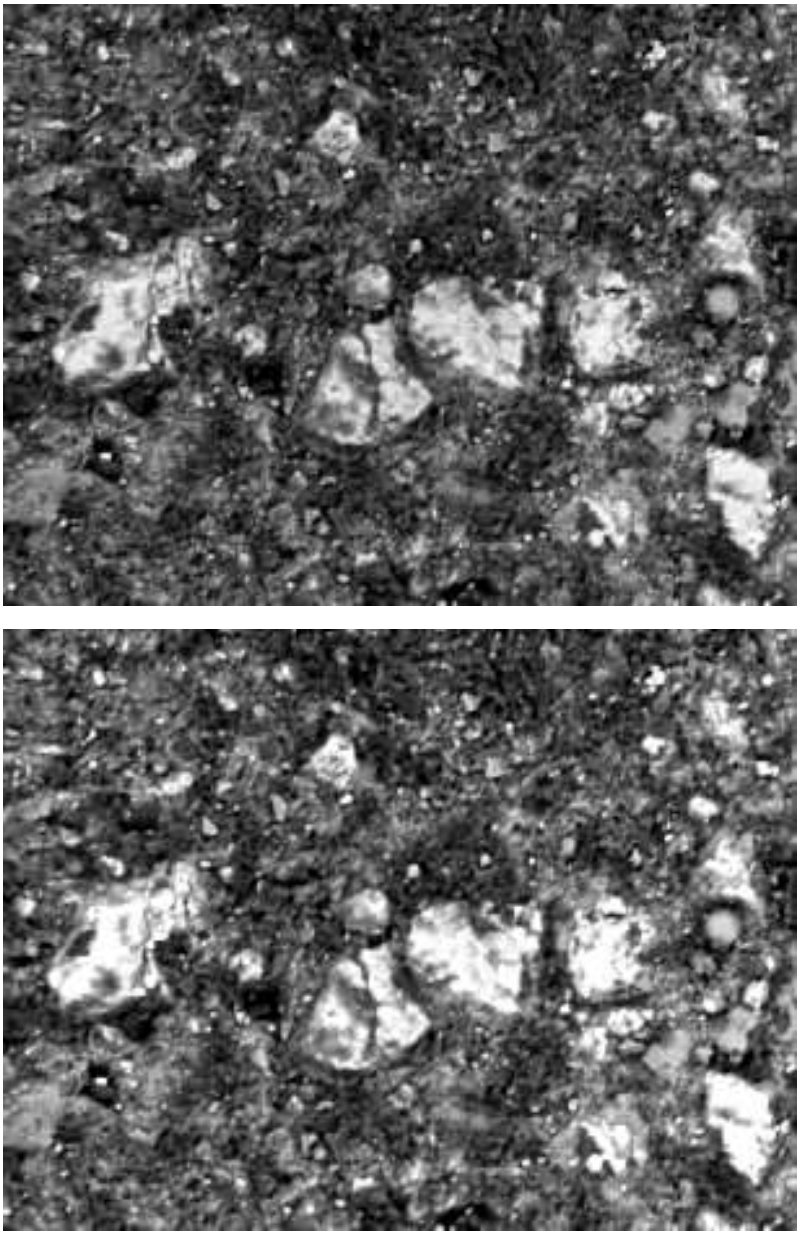

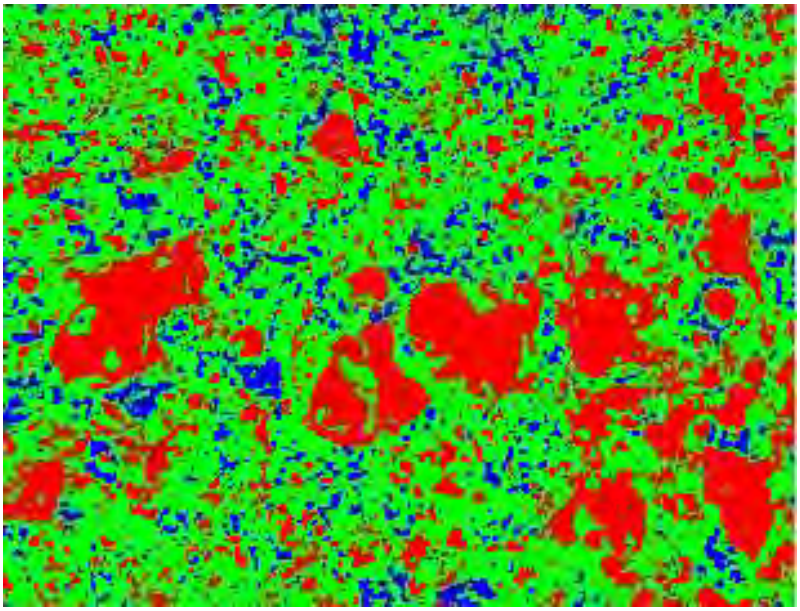

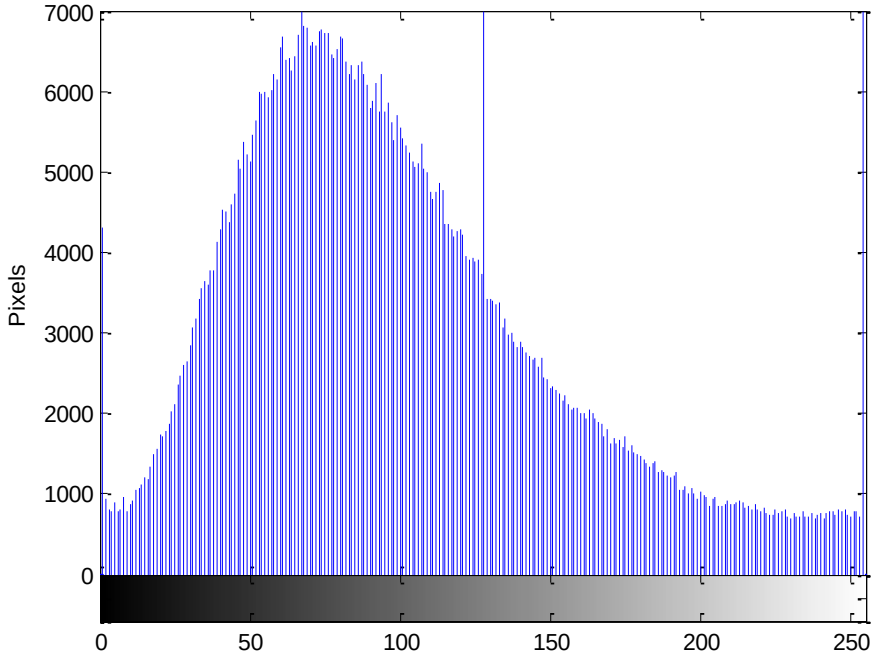
Pixels
7000
6000
5000
4000
3000
2000
1000
0
0
50
100
150
200
250

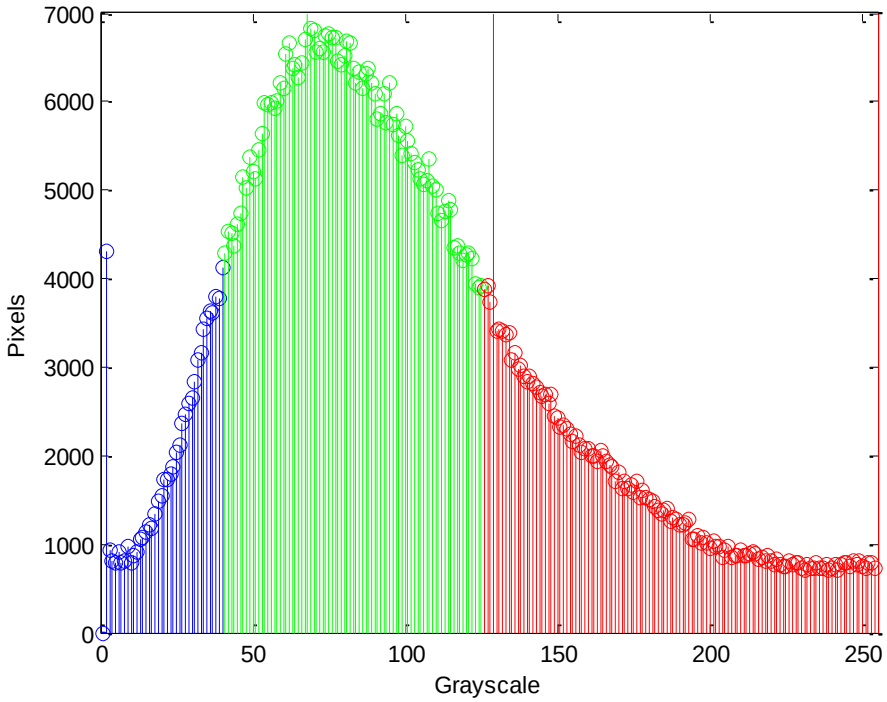

Porosity is 10%

CSH is 61%

CH is 29%

5% Fly Ash Vacuum Cured at 14 Days

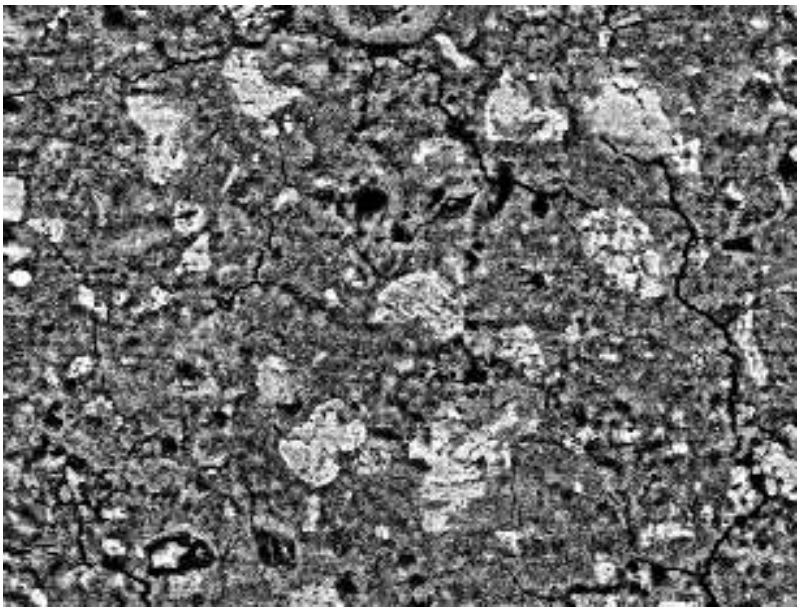

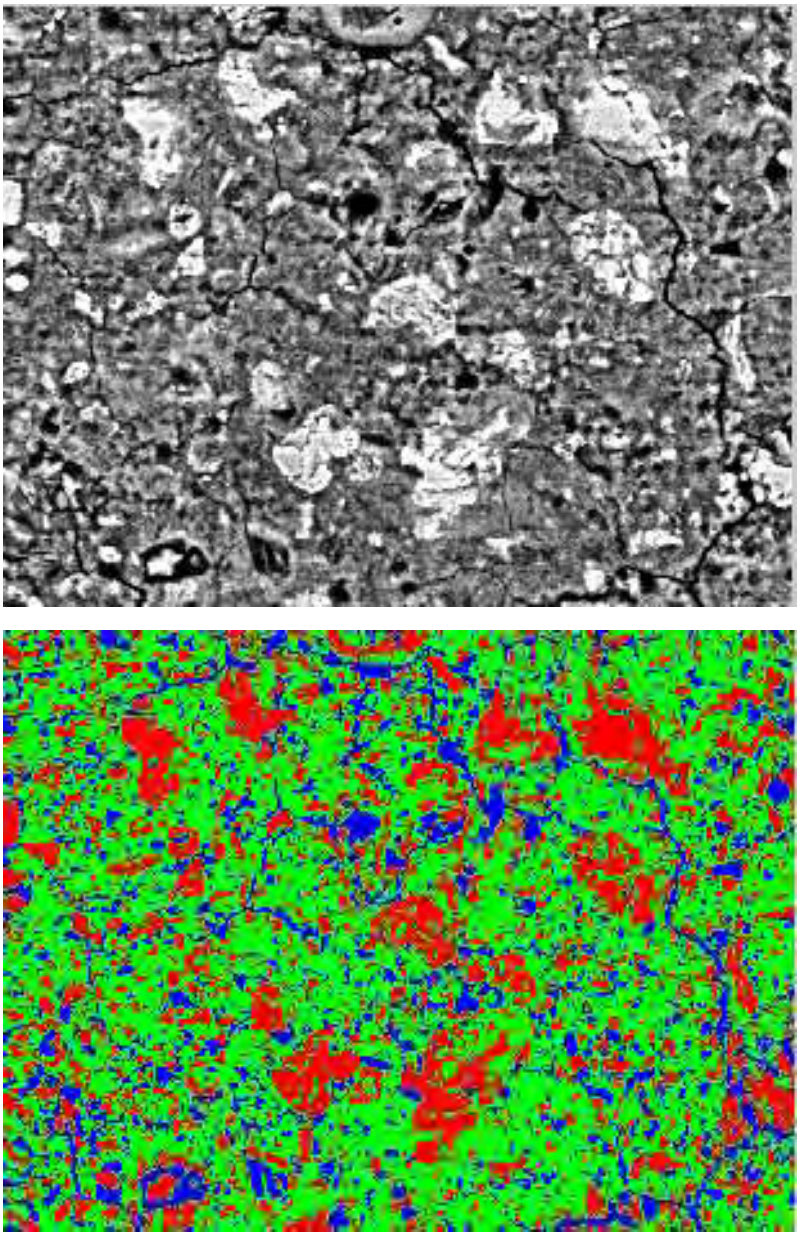

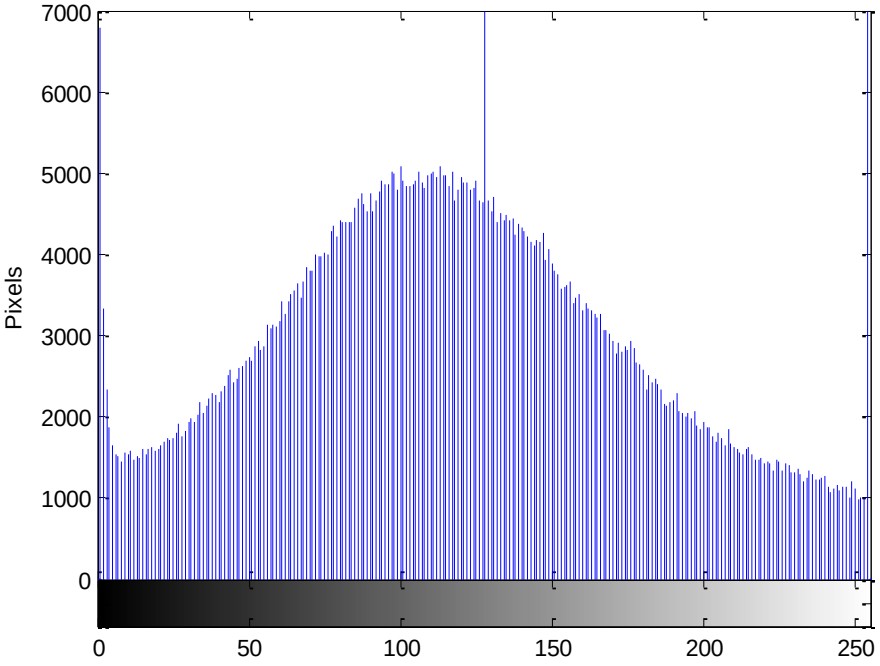

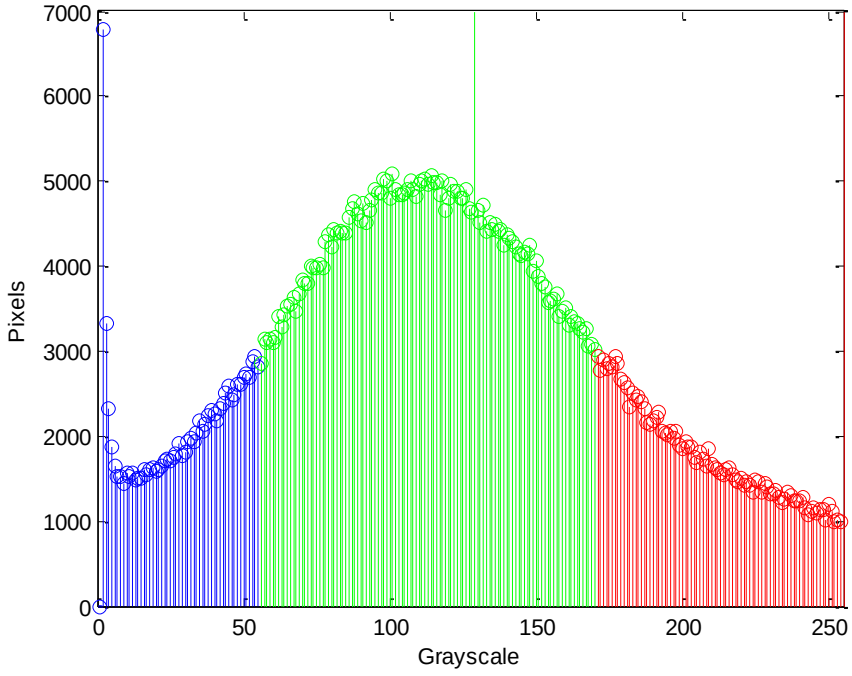

Porosity is 15%

CSH is 62%

CH is 23%

5% Fly Ash Vacuum Cured at 28 Days

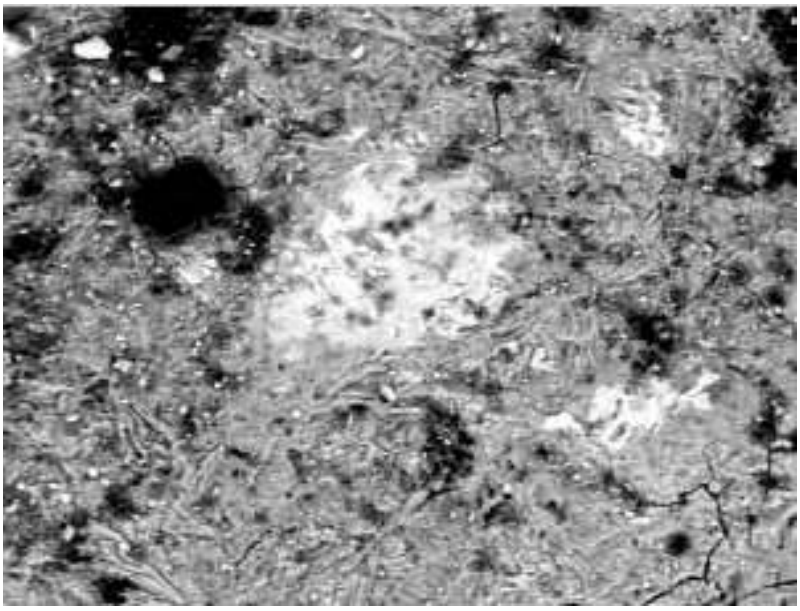

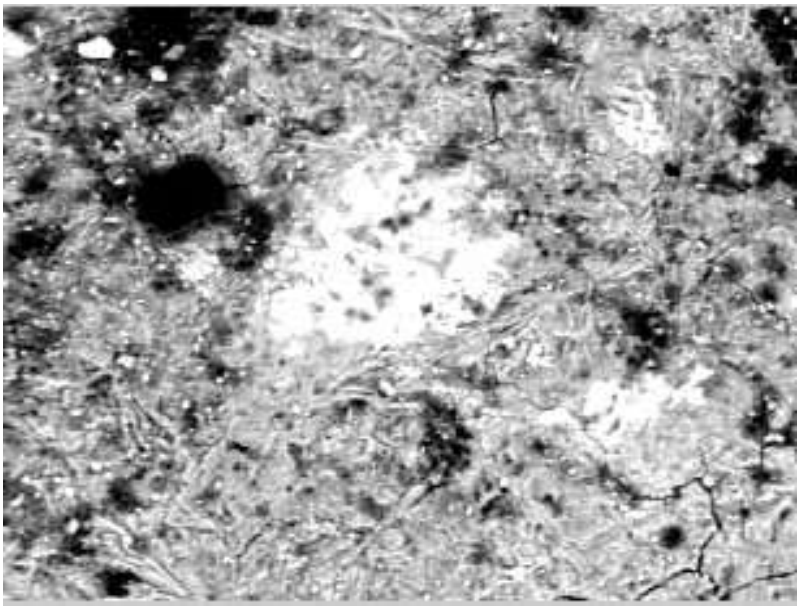

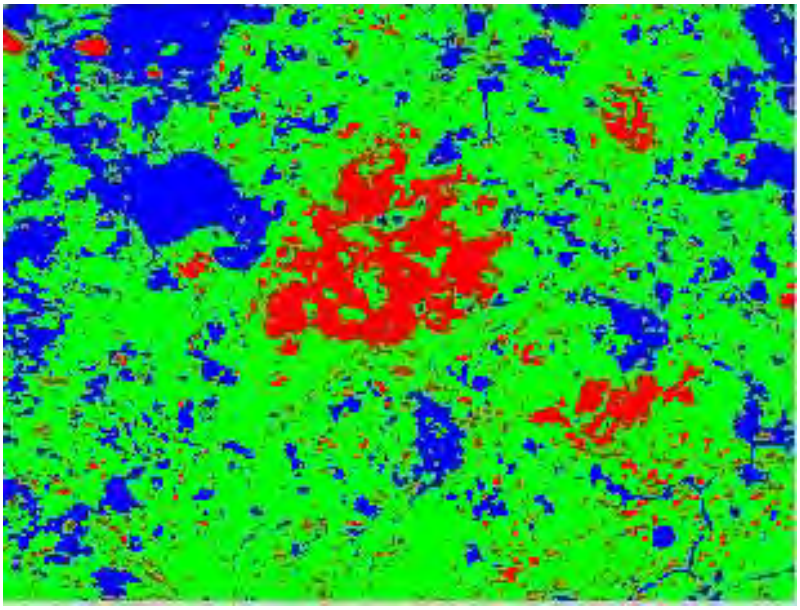

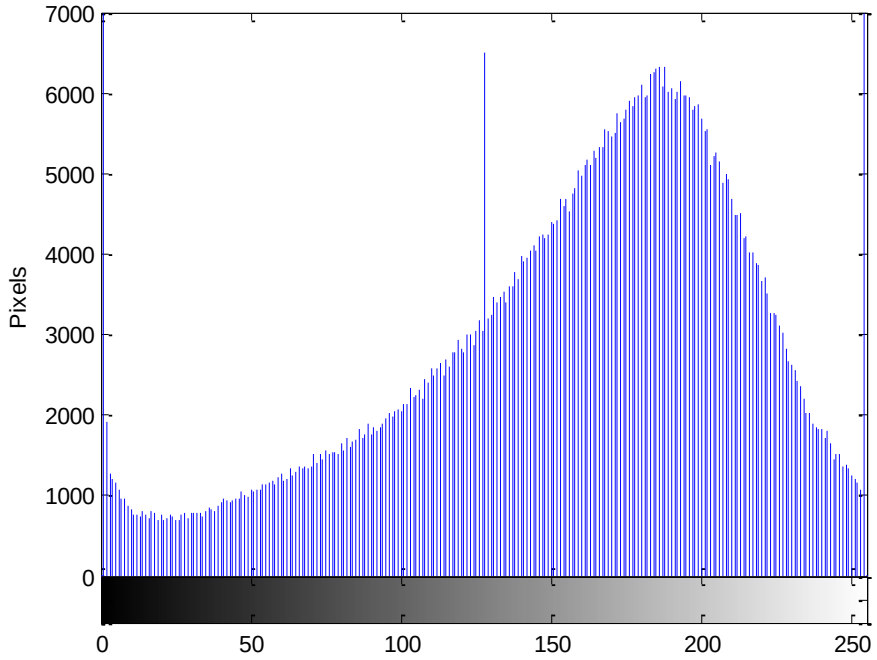
Pixels
7000
6000
5000
4000
3000
2000
1000
0
0
50
100
150
200
250

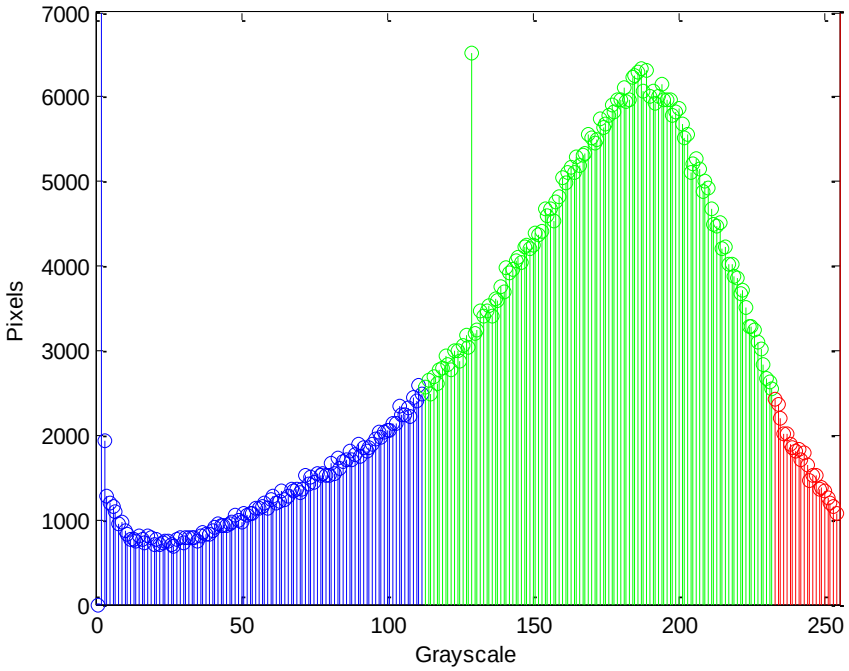

Porosity is 20%

CSH is 69%

CH is 11%

5% Fly Ash Vacuum Cured at 56 Days

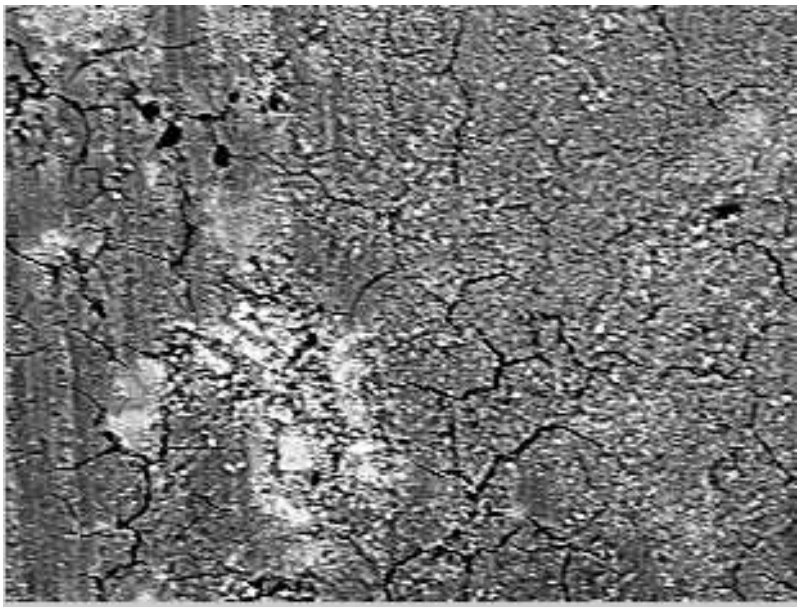

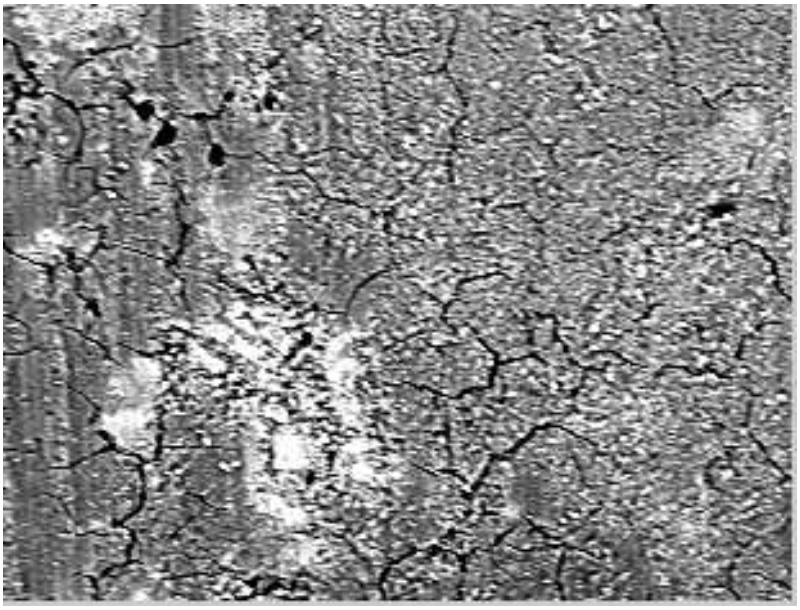

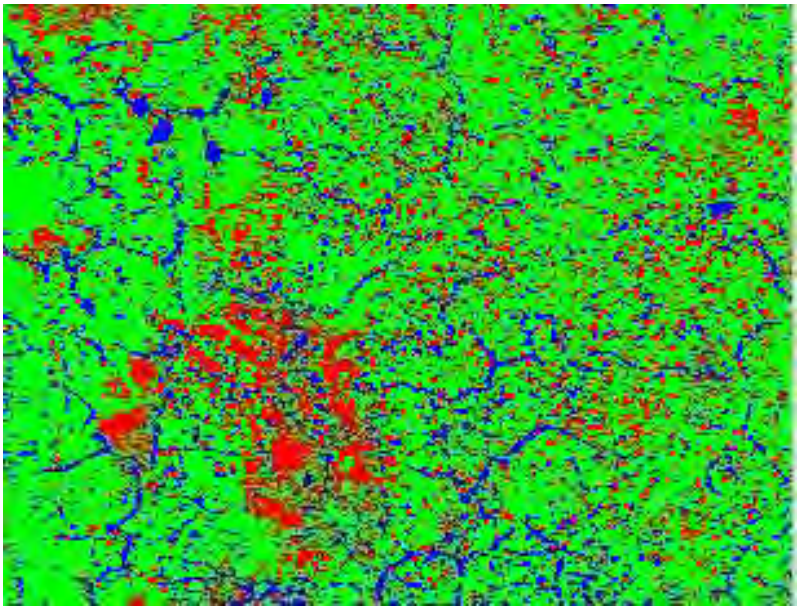

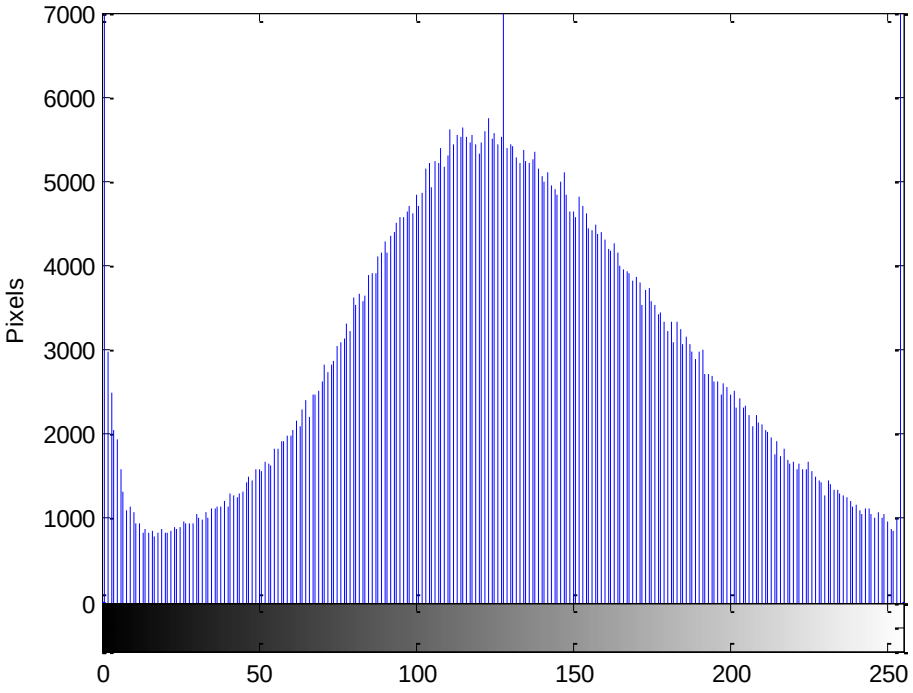

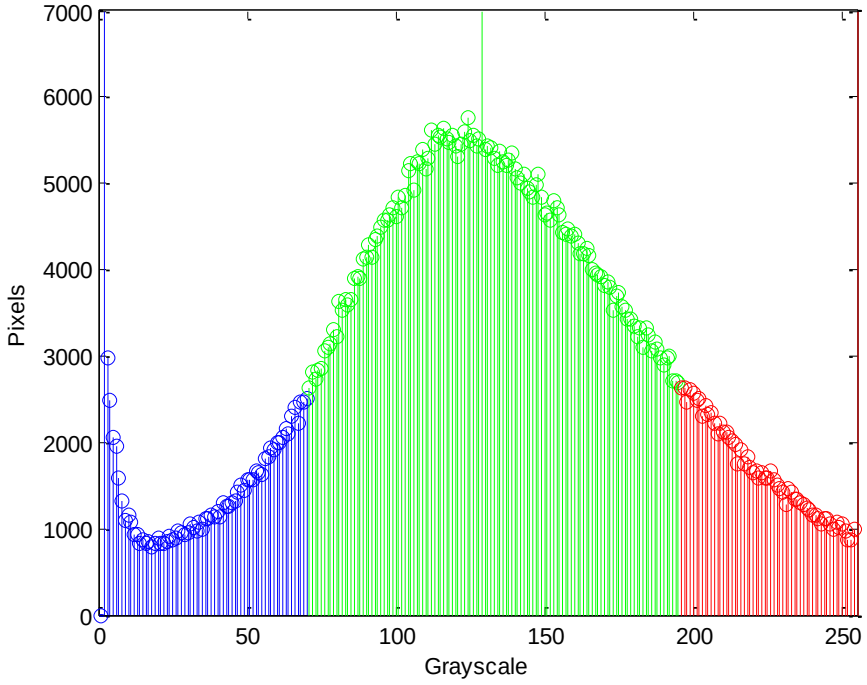

Porosity is 13%

CSH is 70%

CH is 17%

5% Fly Ash Water Cured at 3 Days

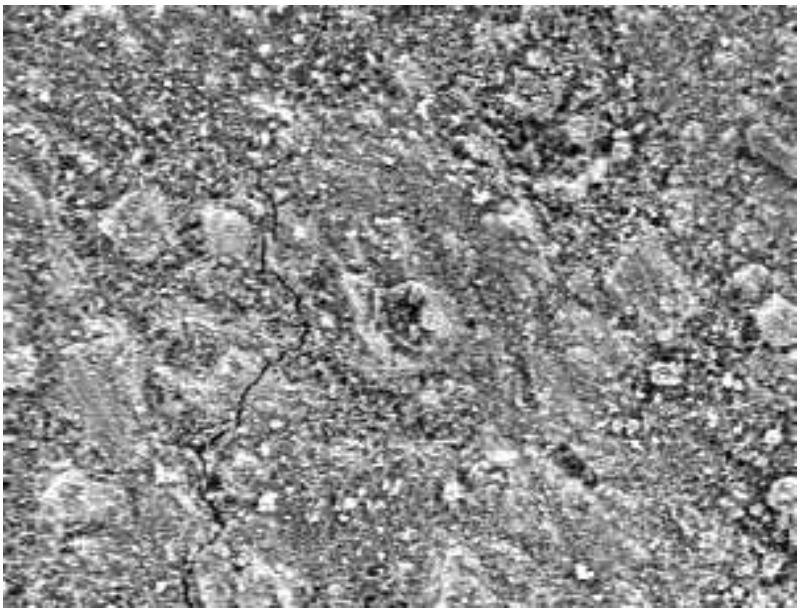

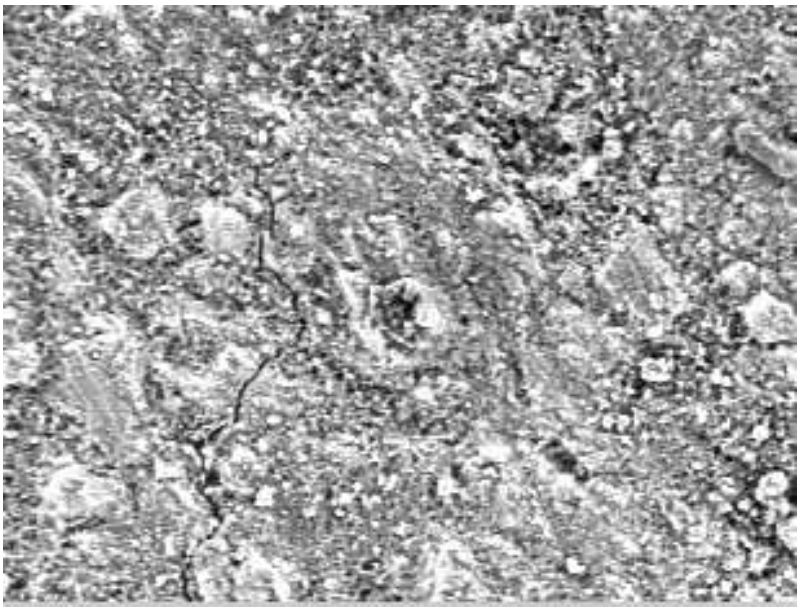

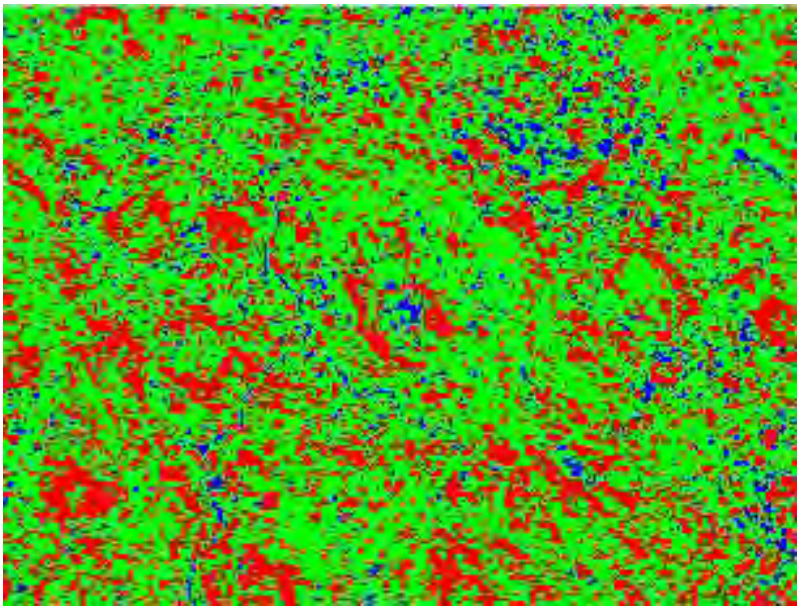

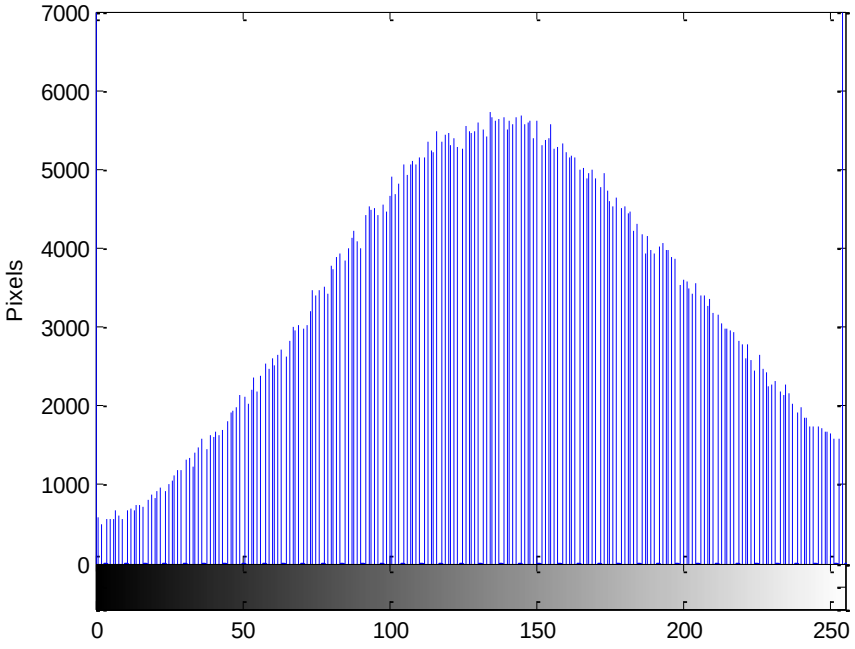
Pixels
7000
6000
5000
4000
3000
2000
1000
0
0
50
100
150
200
250

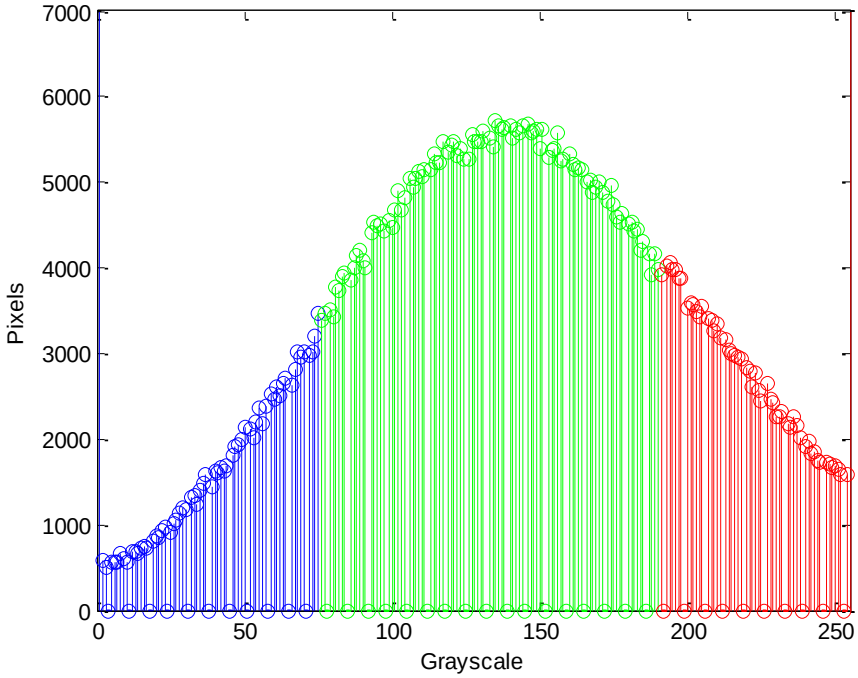

Porosity is 14%

CSH is 61%

CH is 25%

5% Fly Ash Water Cured at 7 Days

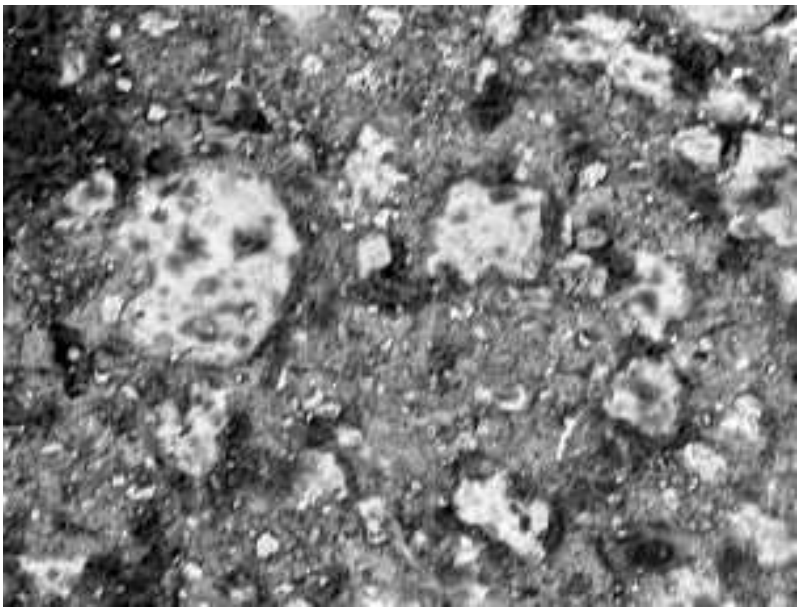

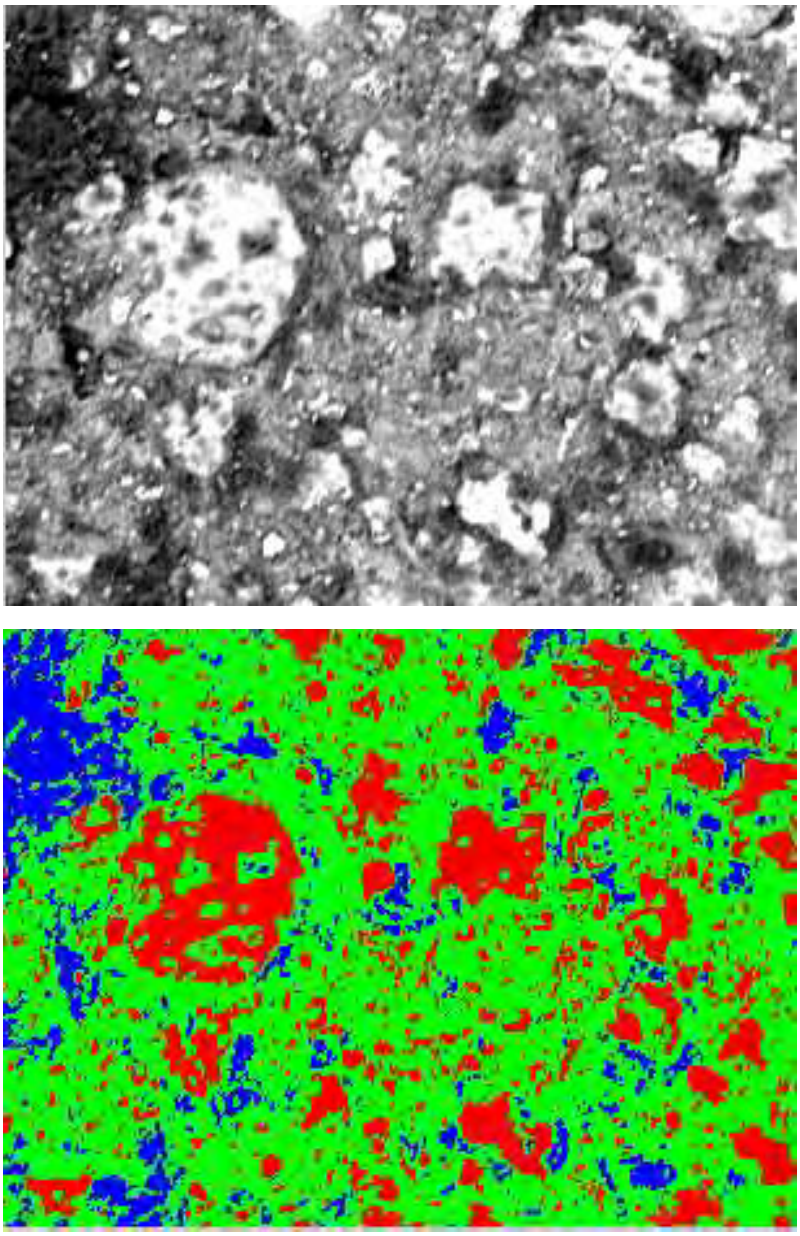

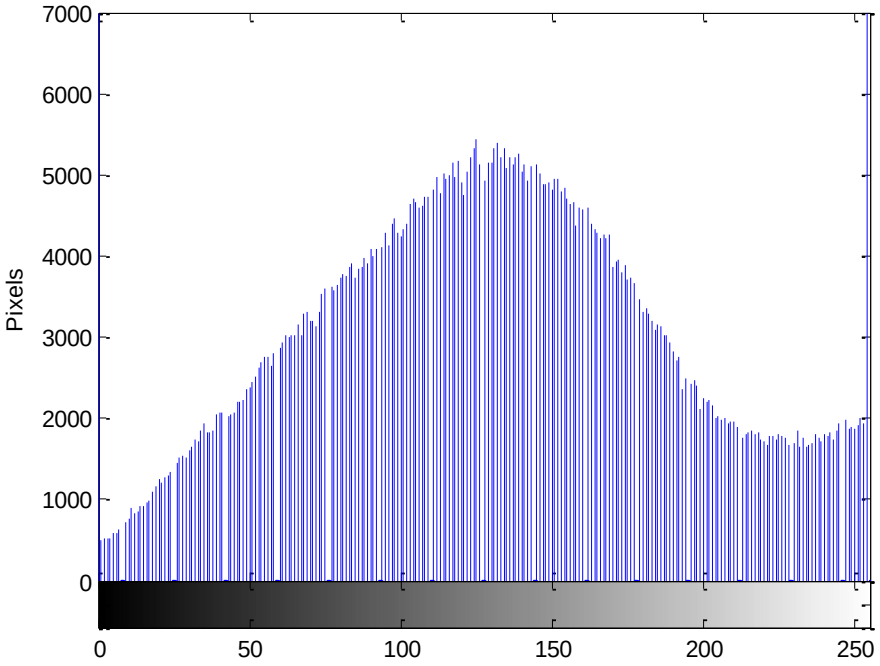

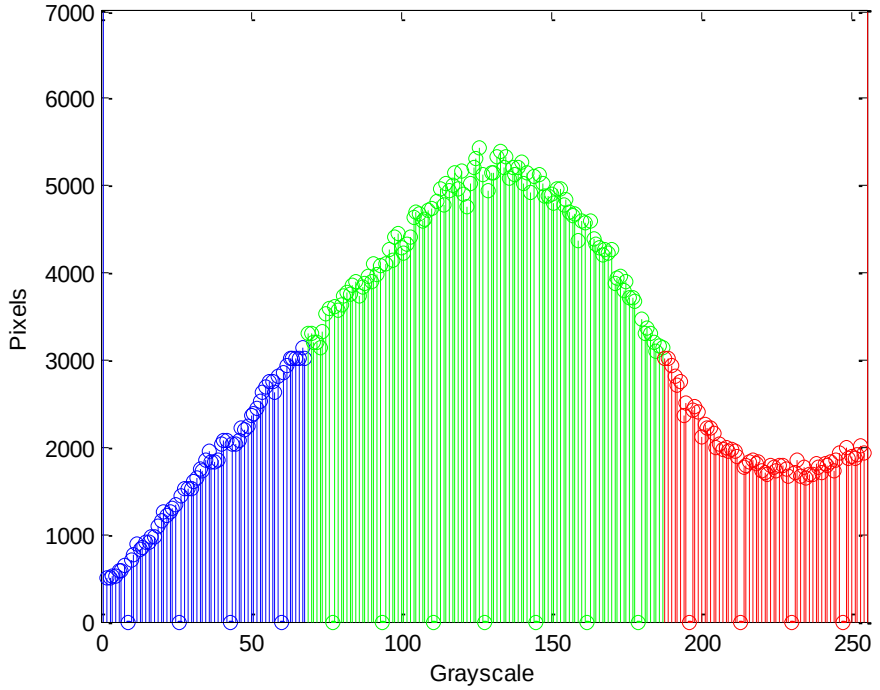

Porosity is 15%

CSH is 62%

CH is 22%

5% Fly Ash Water Cured at 14 Days

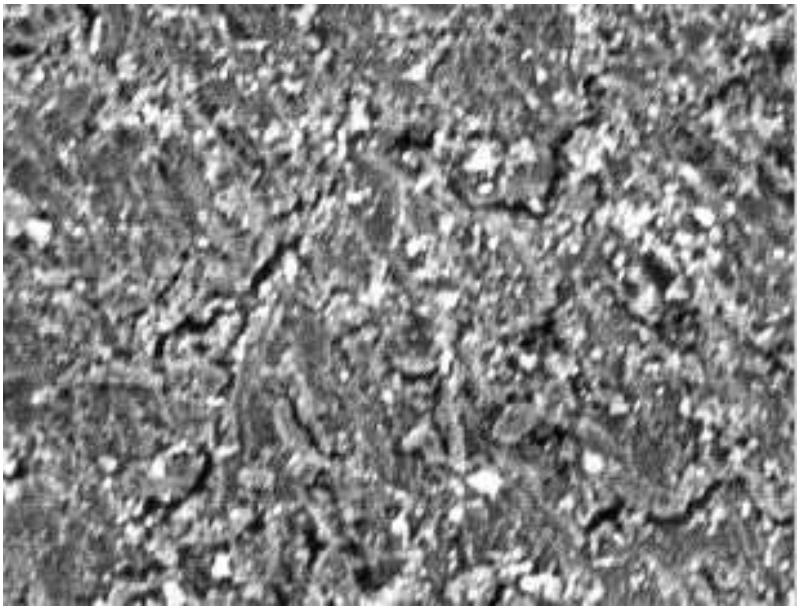

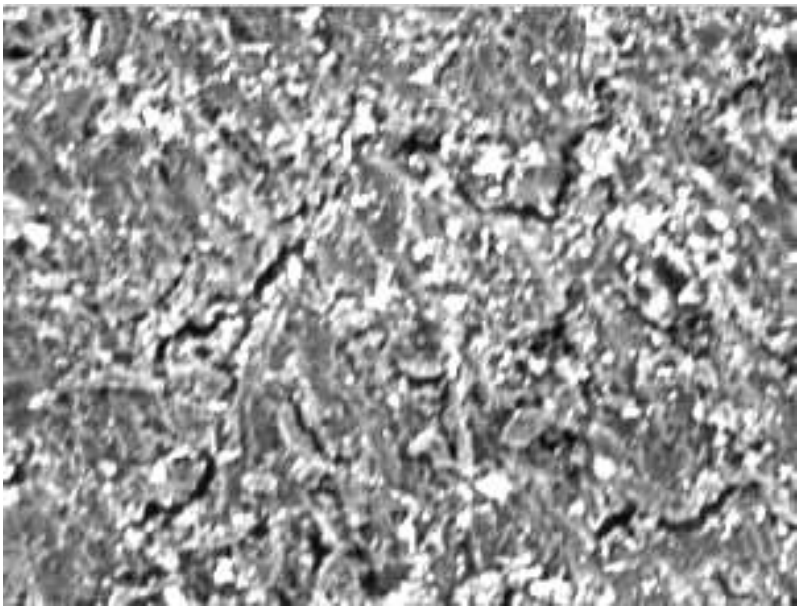

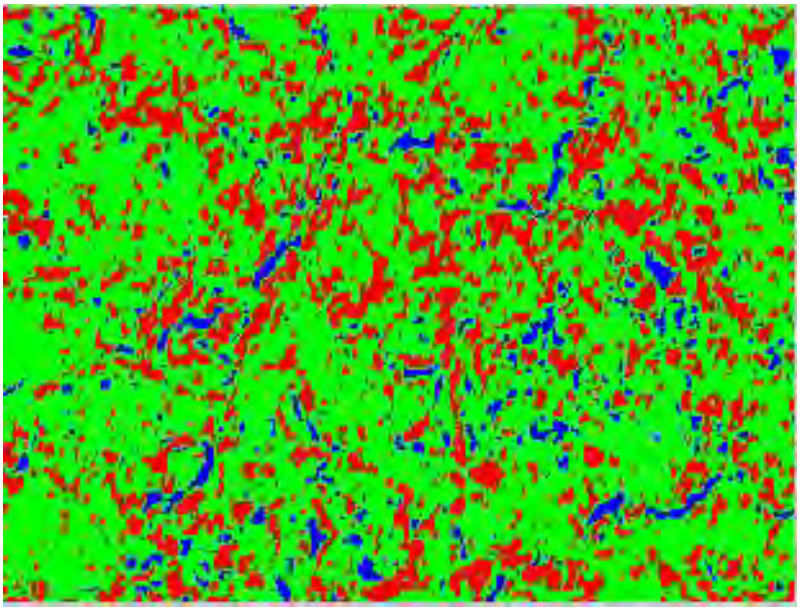

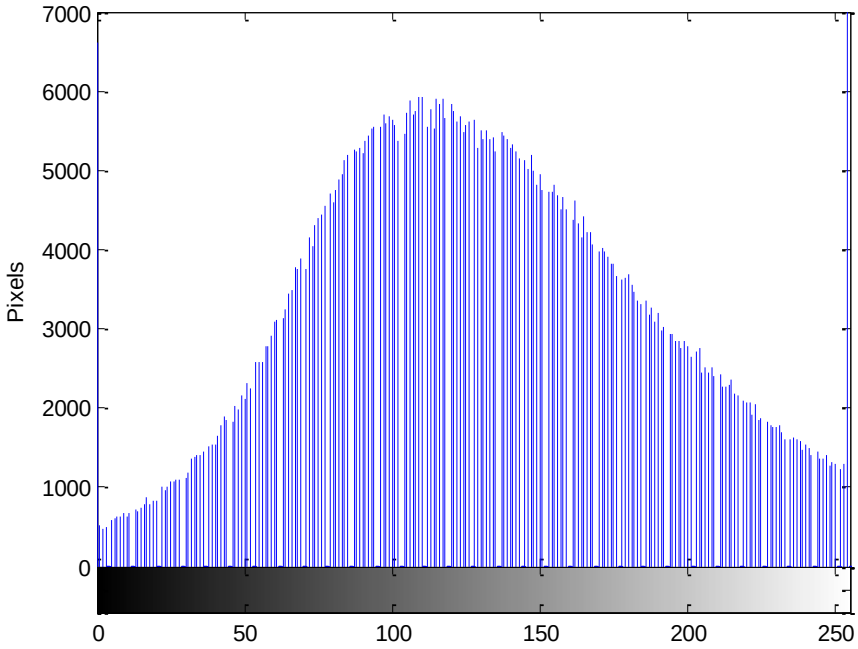
Pixels
7000
6000
5000
4000
3000
2000
1000
0
0
50
100
150
200
250

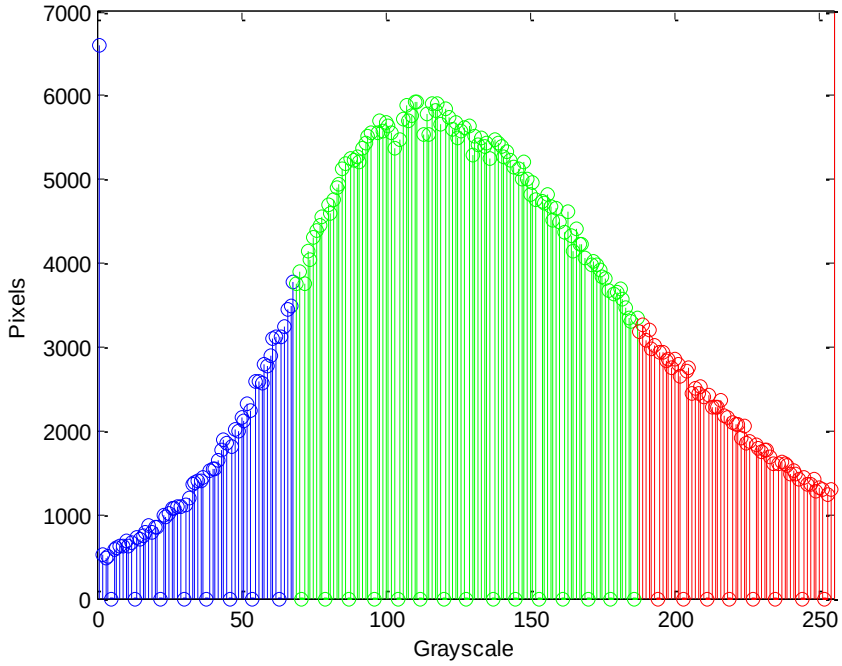

Porosity is 13%

CSH is 65%

CH is 22%

5% Fly Ash Water Cured at 28 Days

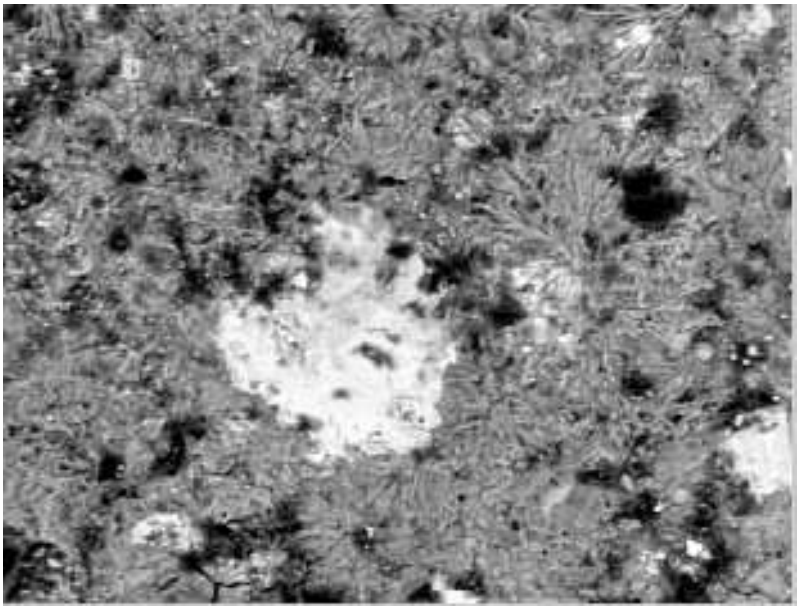

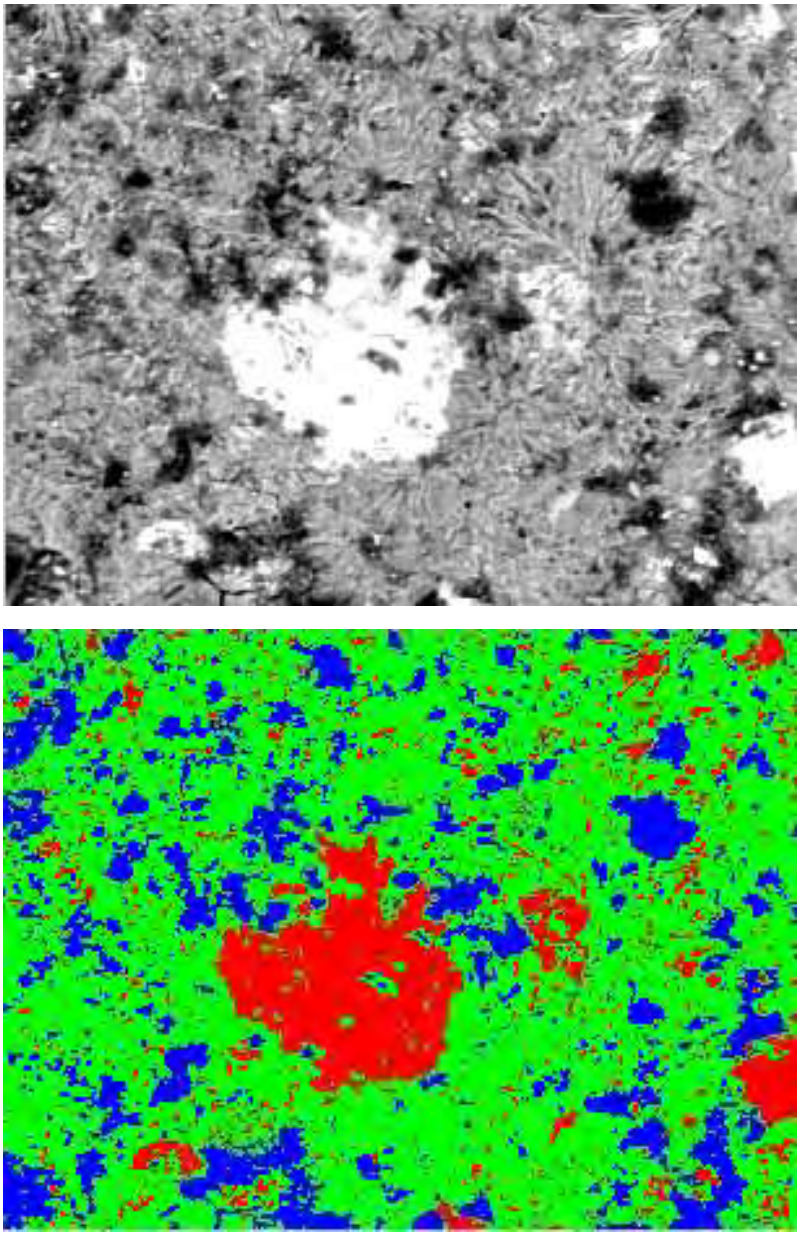

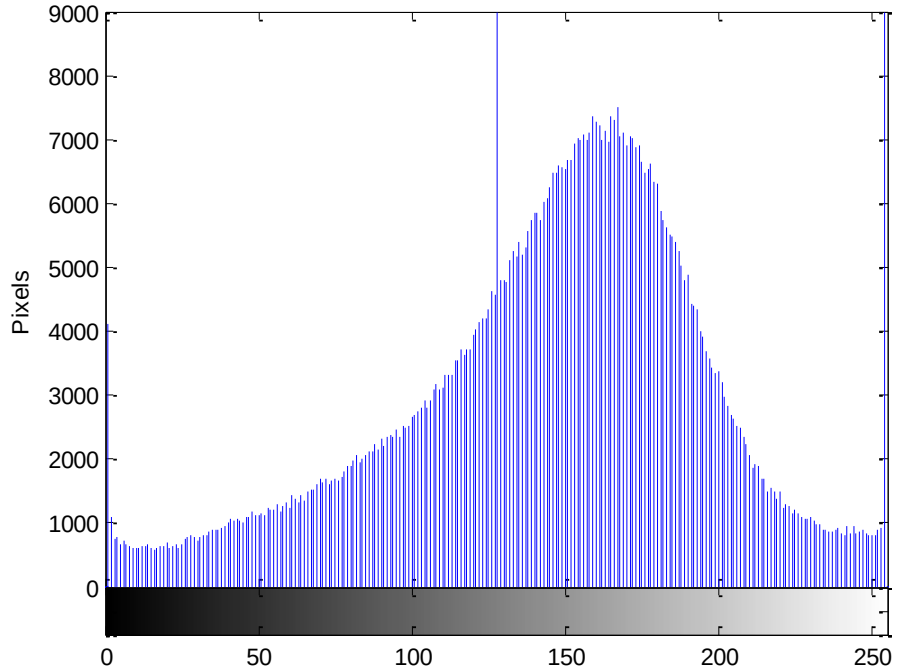

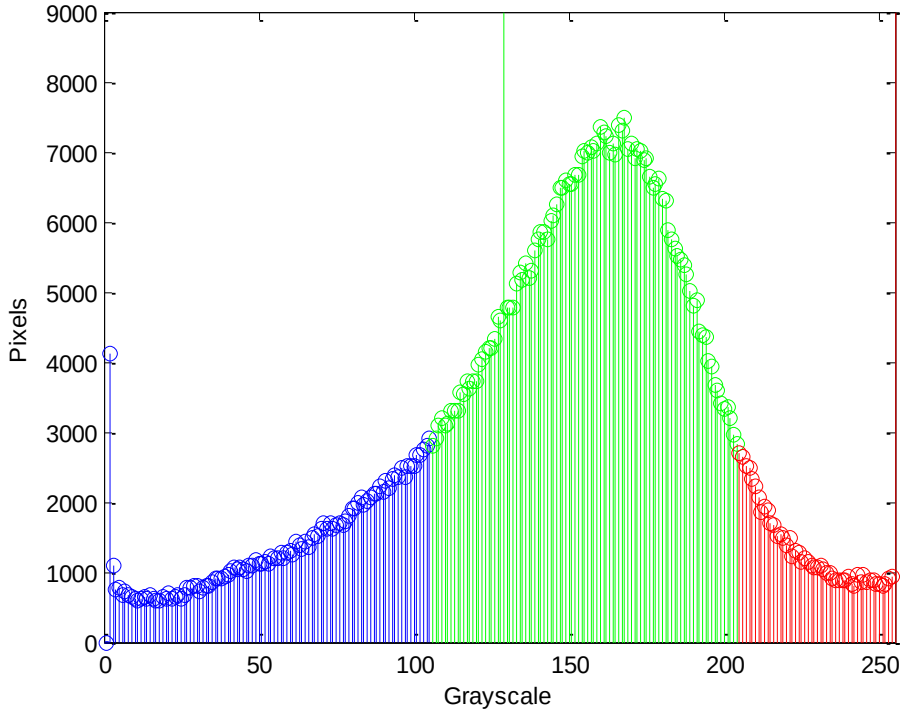

Porosity is 18%

CSH is 67%

CH is 14%

5% Fly Ash Water Cured at 56 Days

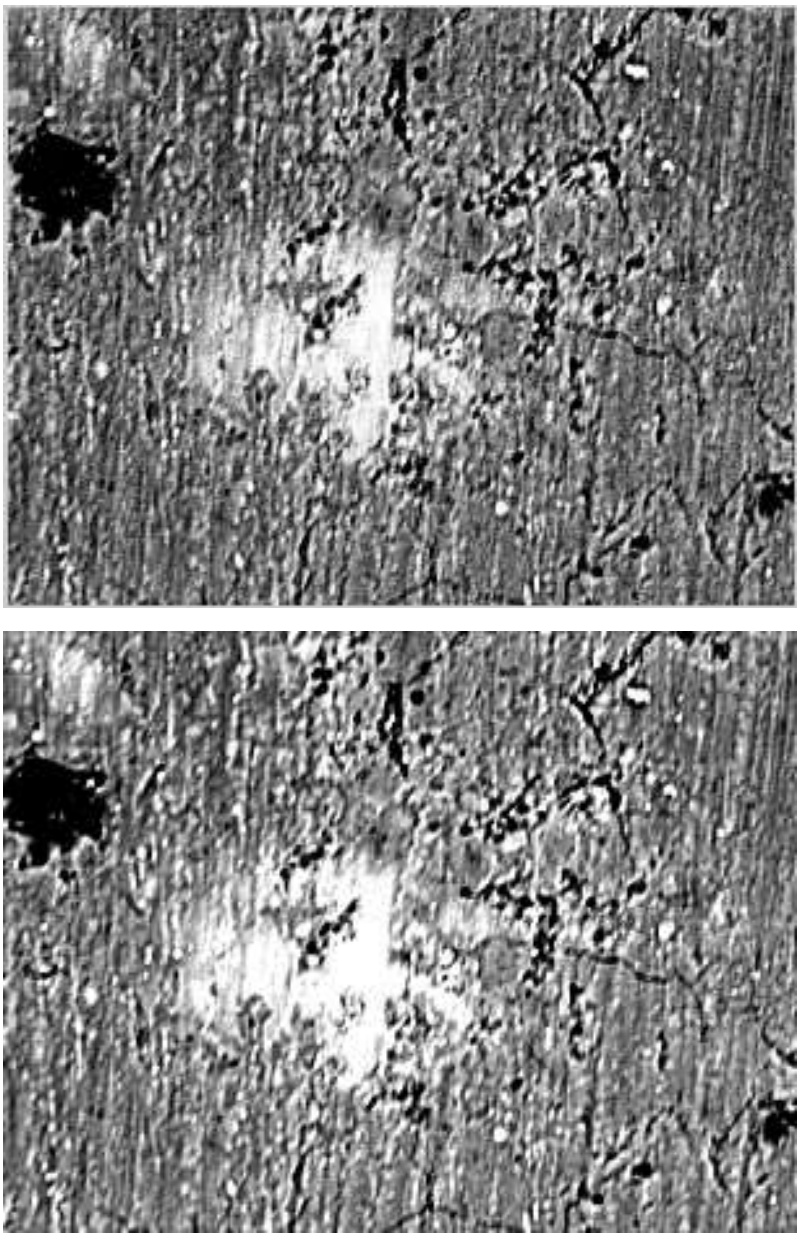

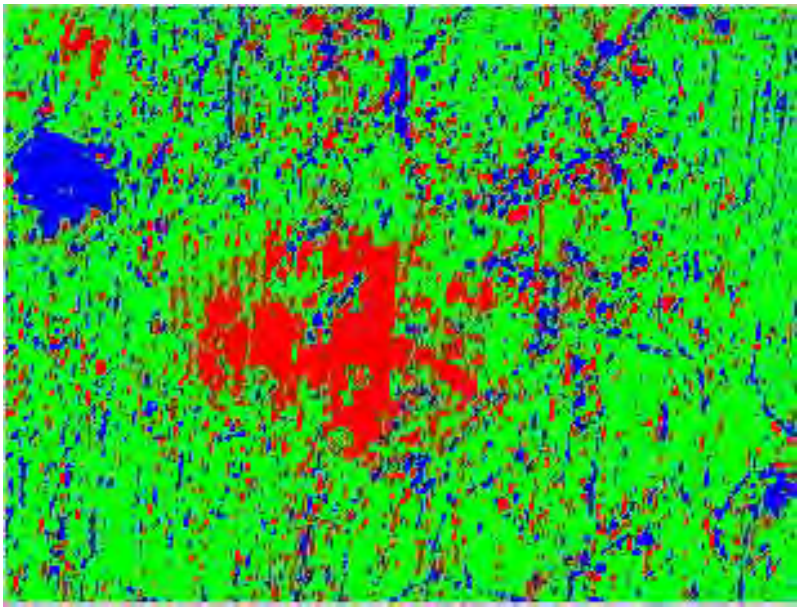

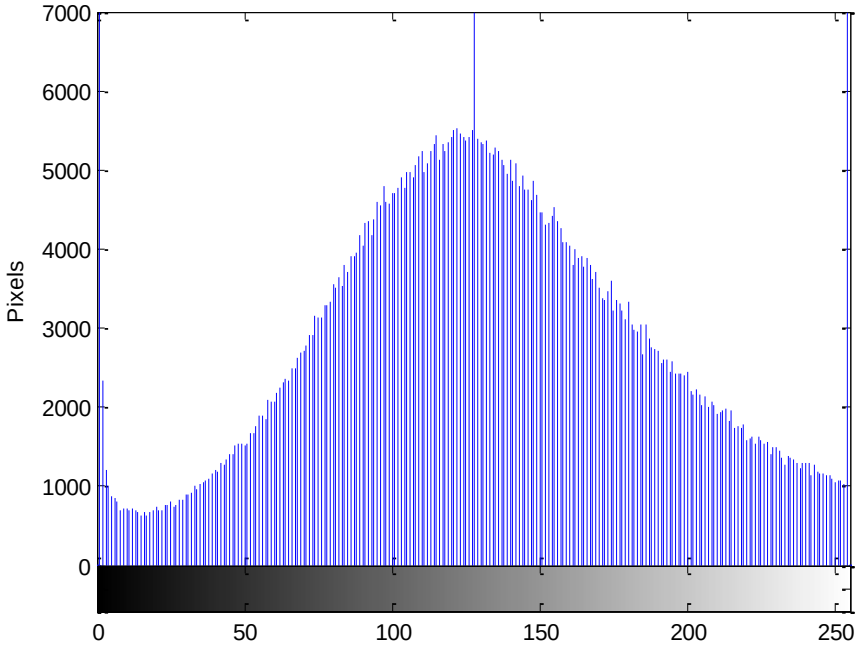
Pixels
7000
6000
5000
4000
3000
2000
1000
0
0
50
100
150
200
250

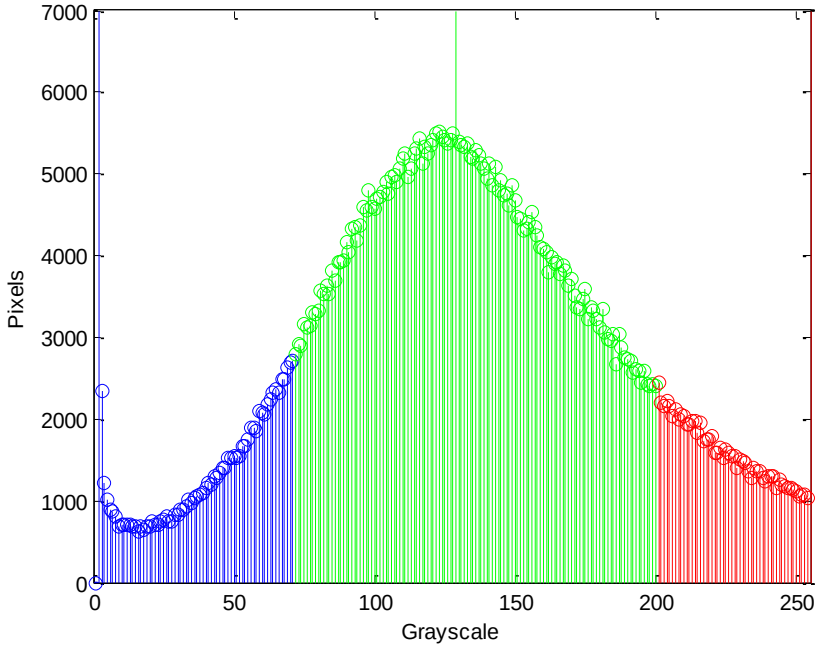

Porosity is 14%

CSH is 69%

CH is 17%

10% Fly Ash Vacuum Cured at 3 Days

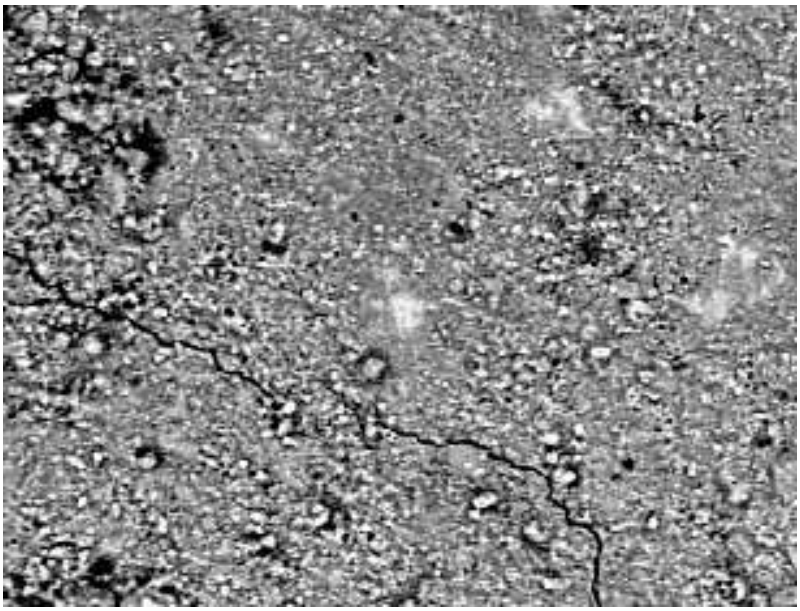

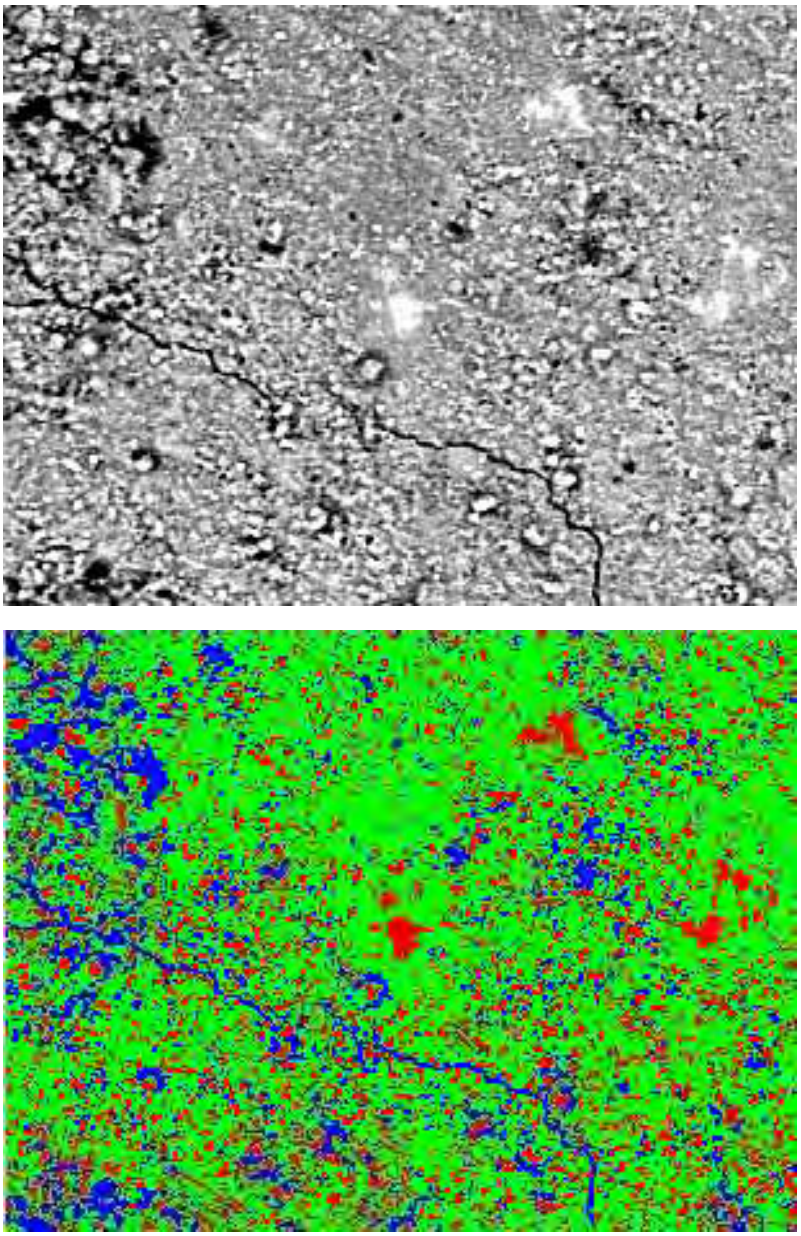

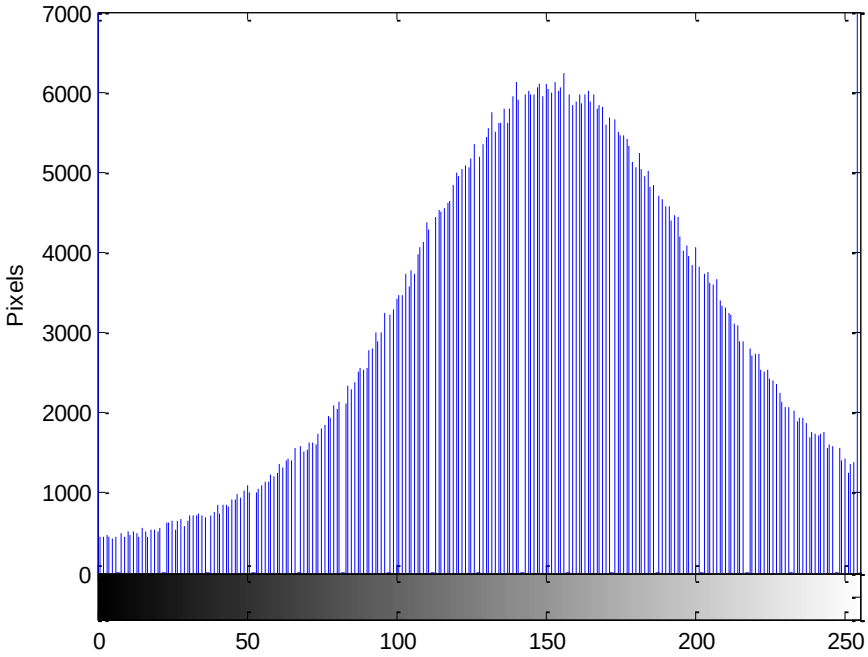

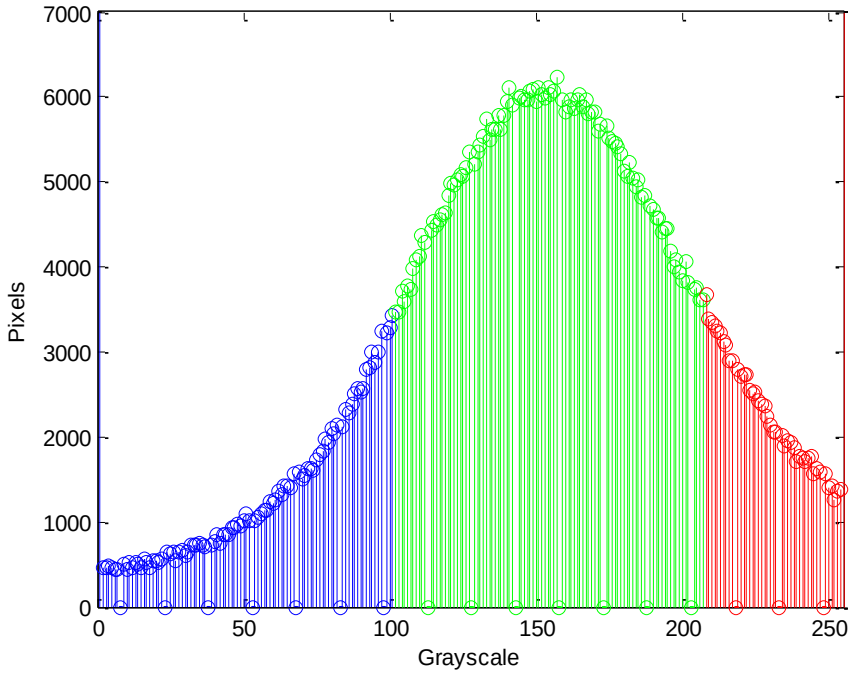

Porosity is 18%

CSH is 64%

CH is 18%

10% Fly Ash Vacuum Cured at 7 Days

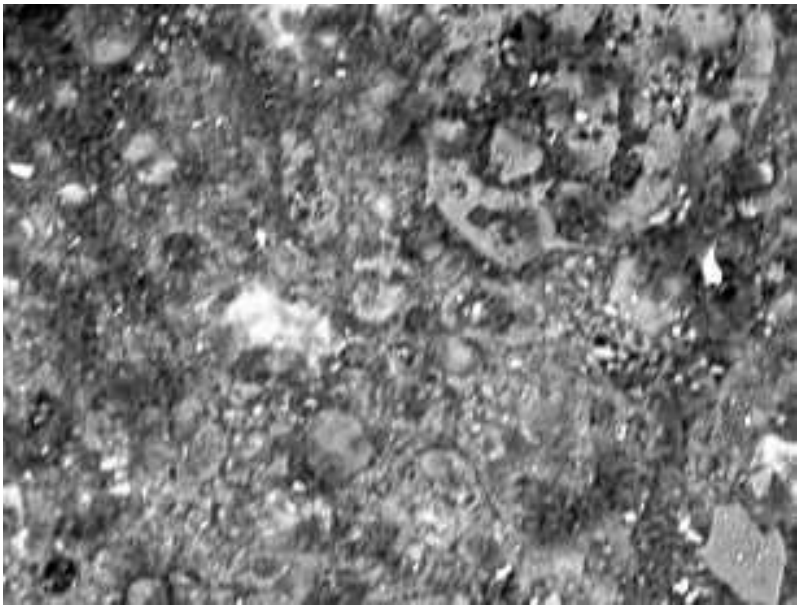

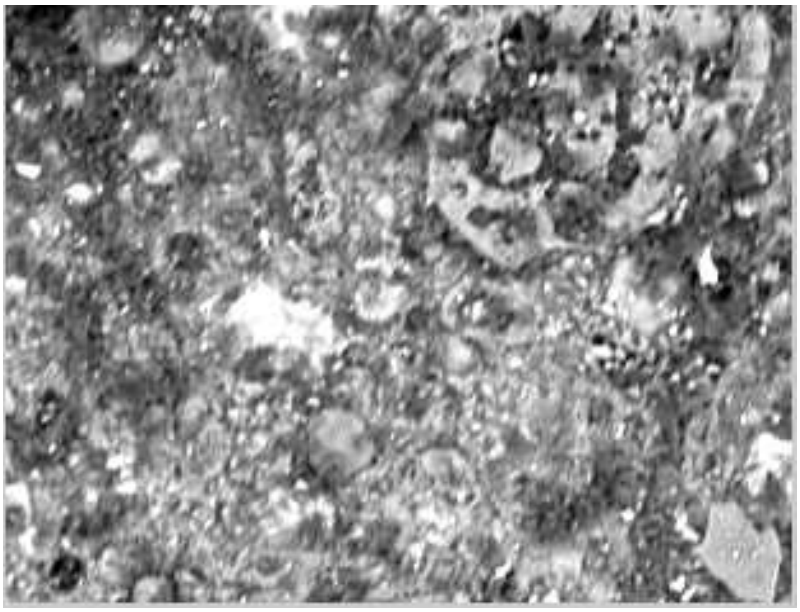

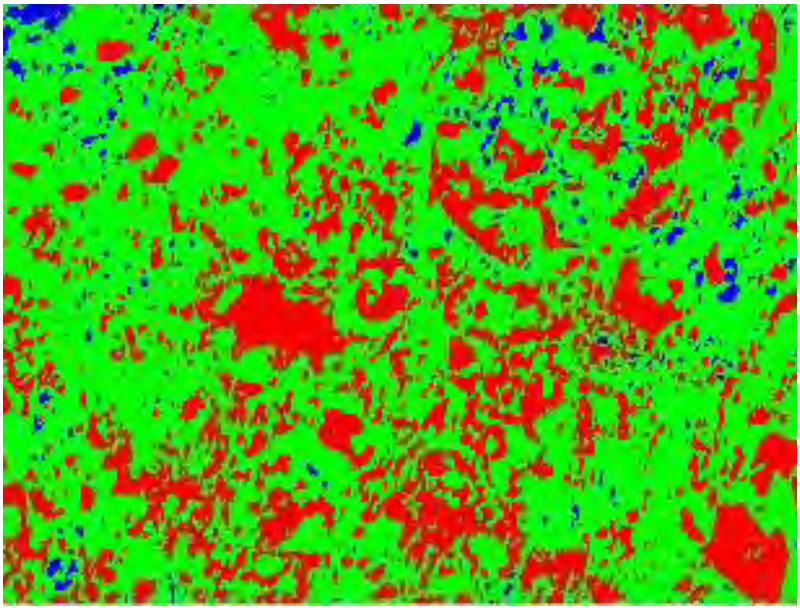

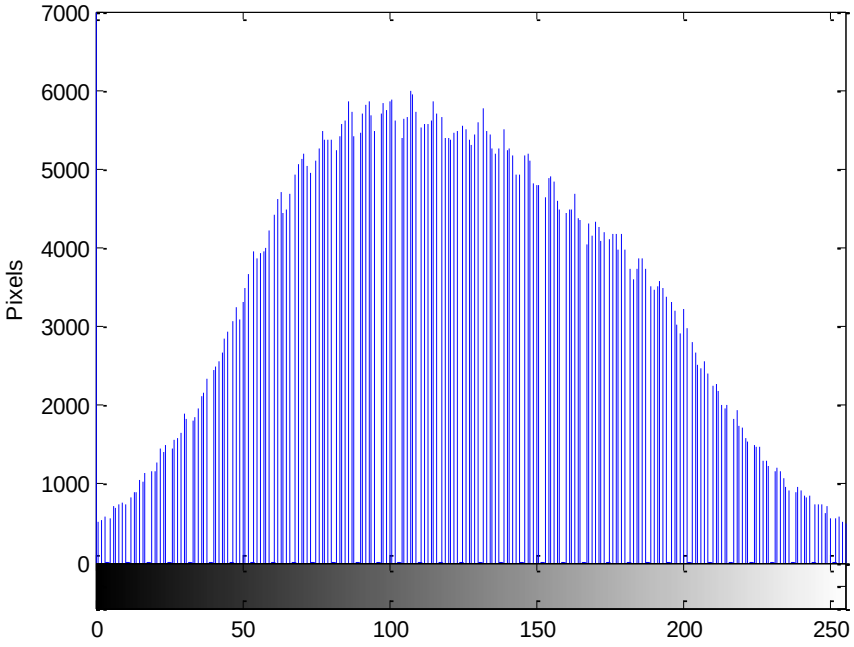
Pixels
7000
6000
5000
4000
3000
2000
1000
0
0
50
100
150
200
250

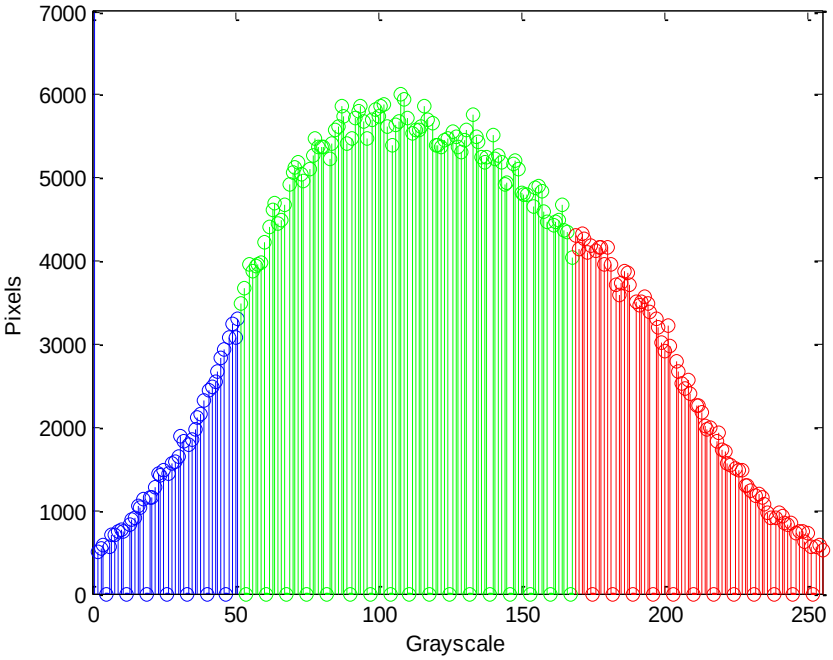

Porosity is 12%

CSH is 65%

CH is 22%

10% Fly Ash Vacuum Cured at 14 Days

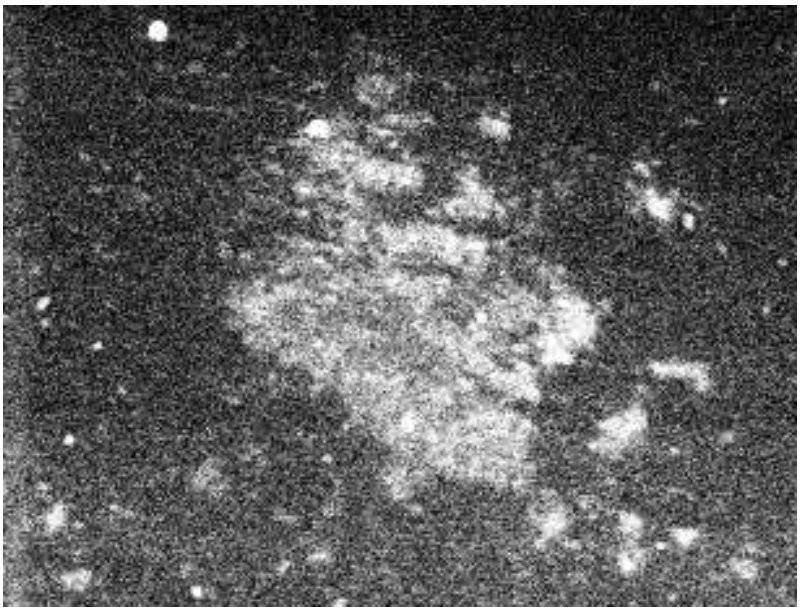

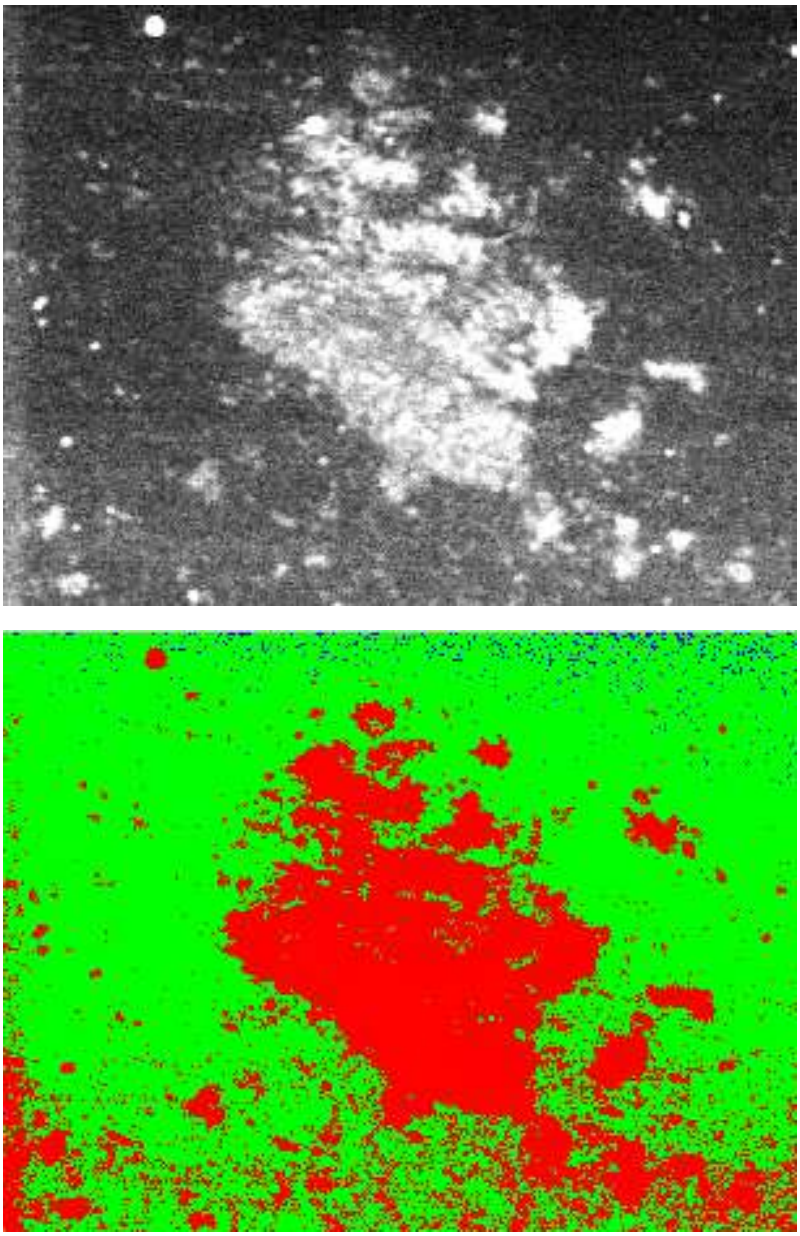

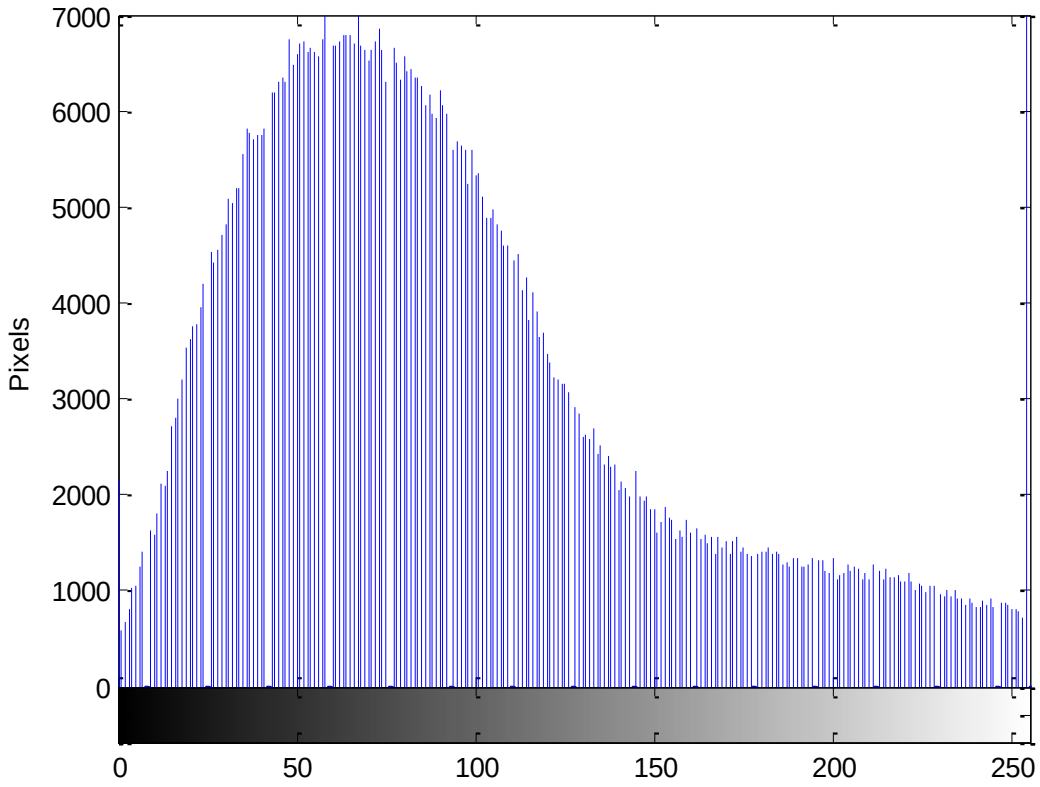
Pixels
7000
6000
5000
4000
3000
2000
1000
0
0
50
100
150
200
250

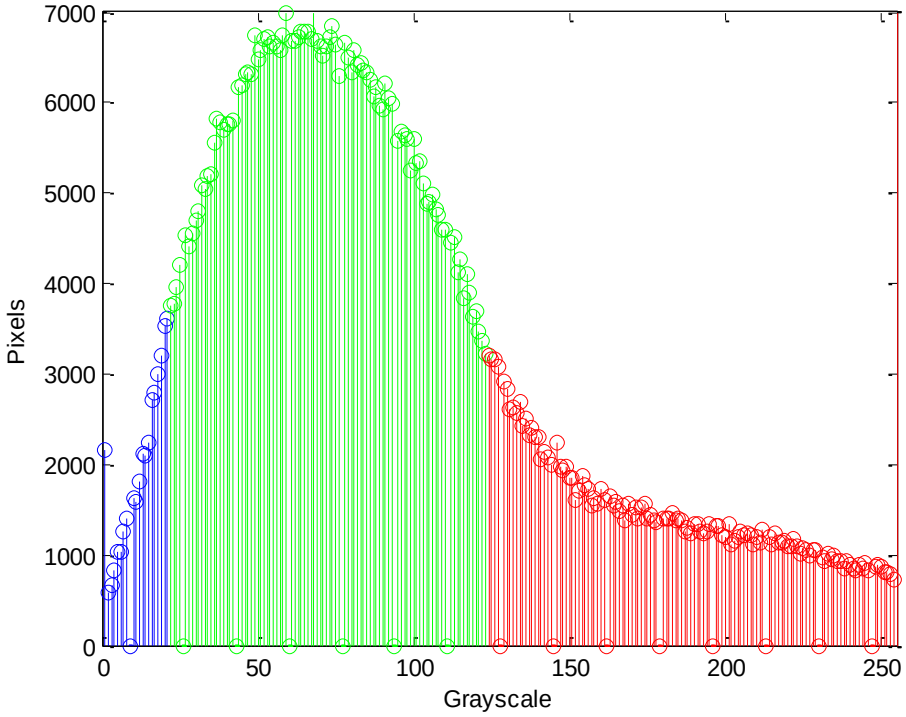

Porosity is 5%

CSH is 69%

CH is 26%

10% Fly Ash Vacuum Cured at 28 Days

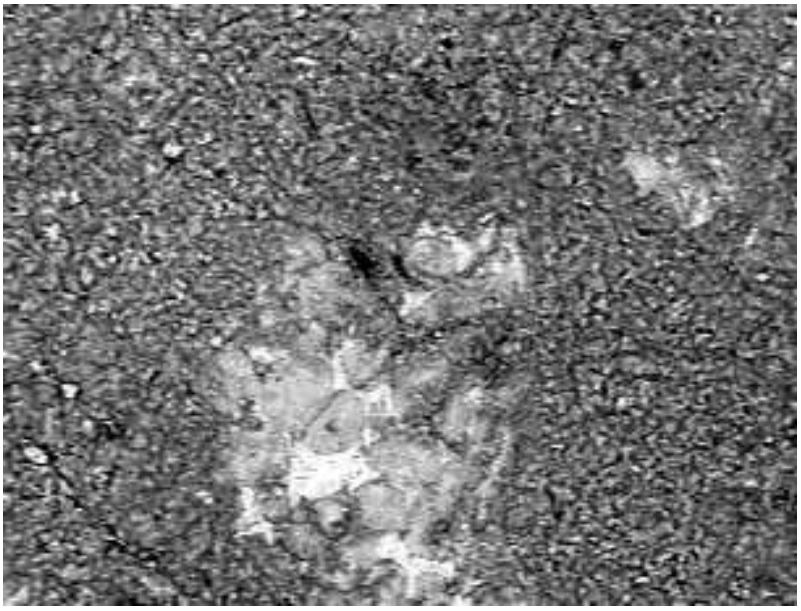

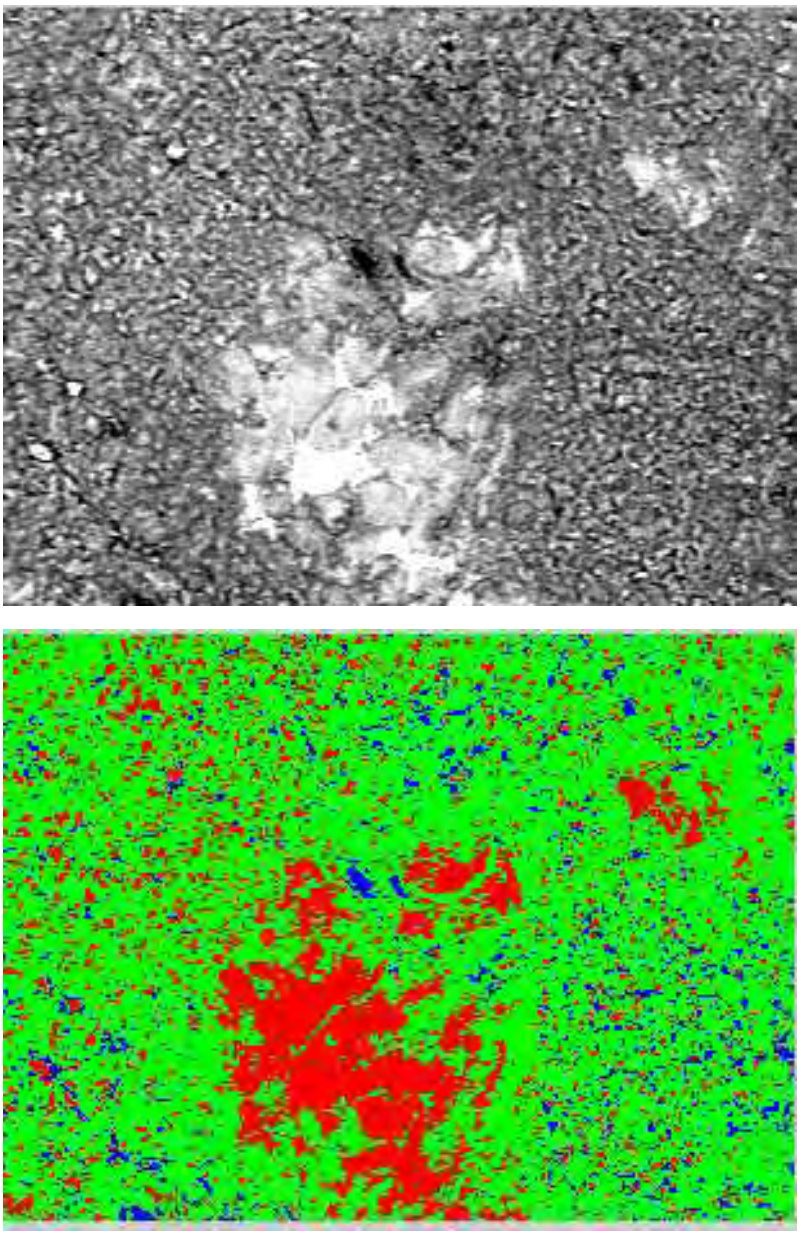

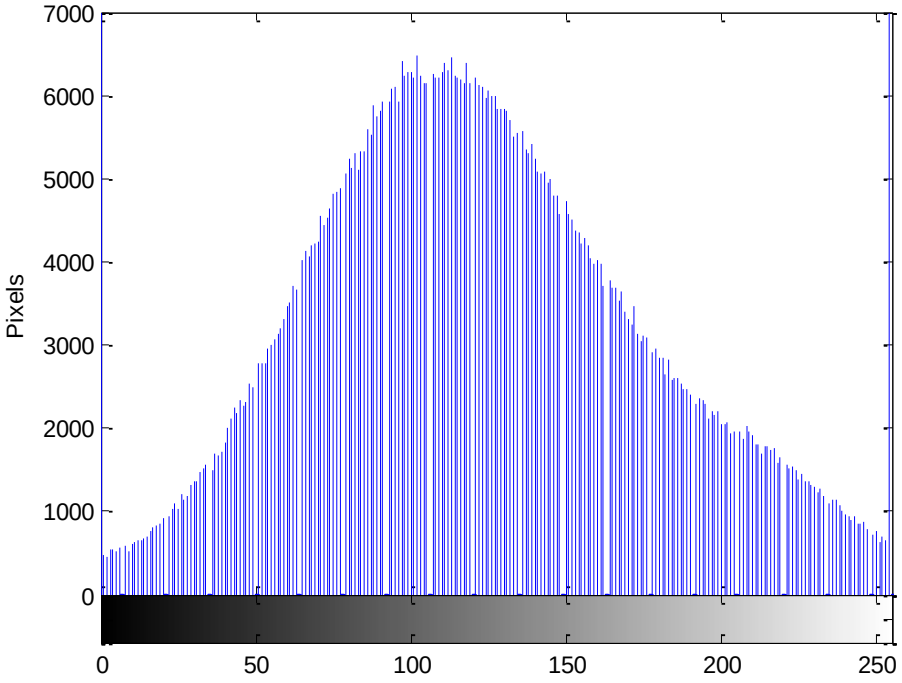

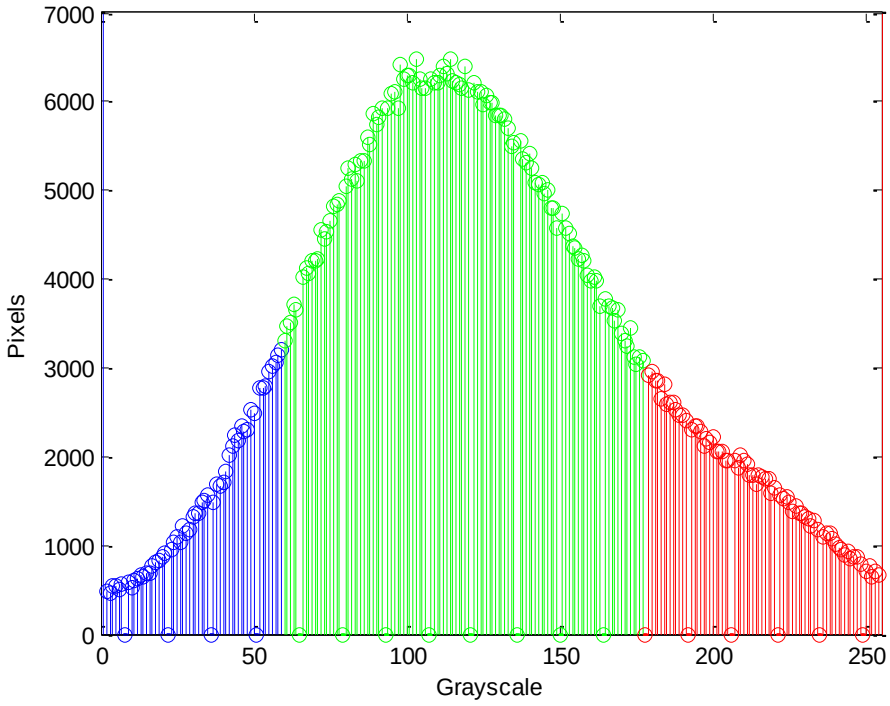

Porosity is 11%

CSH is 71%

CH is 18%

10% Fly Ash Vacuum Cured at 56 Days

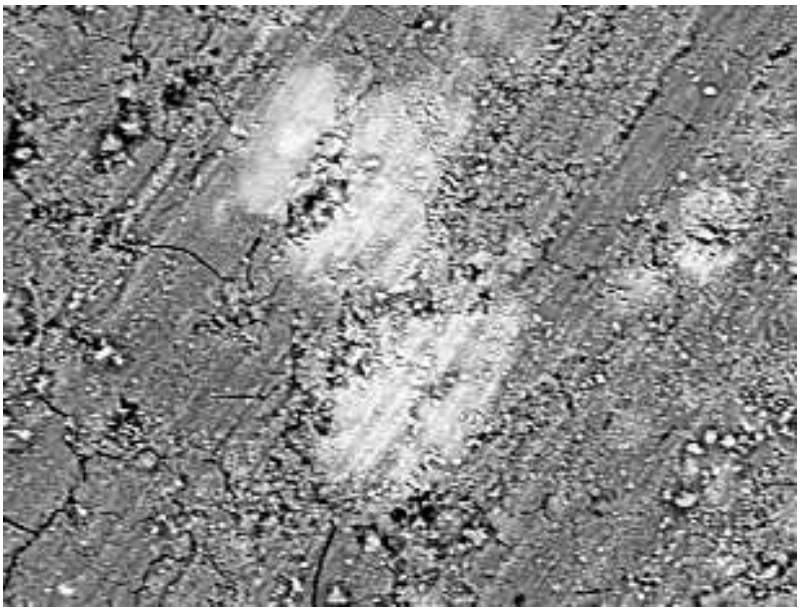

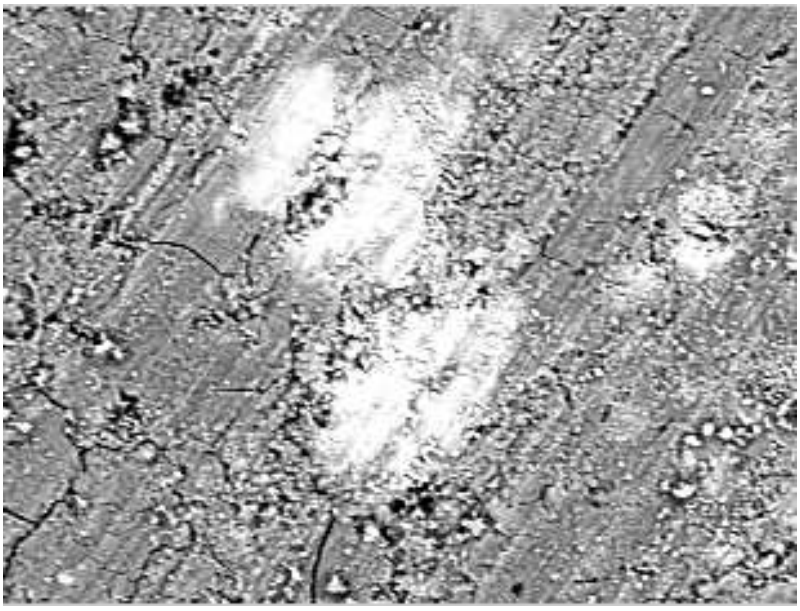

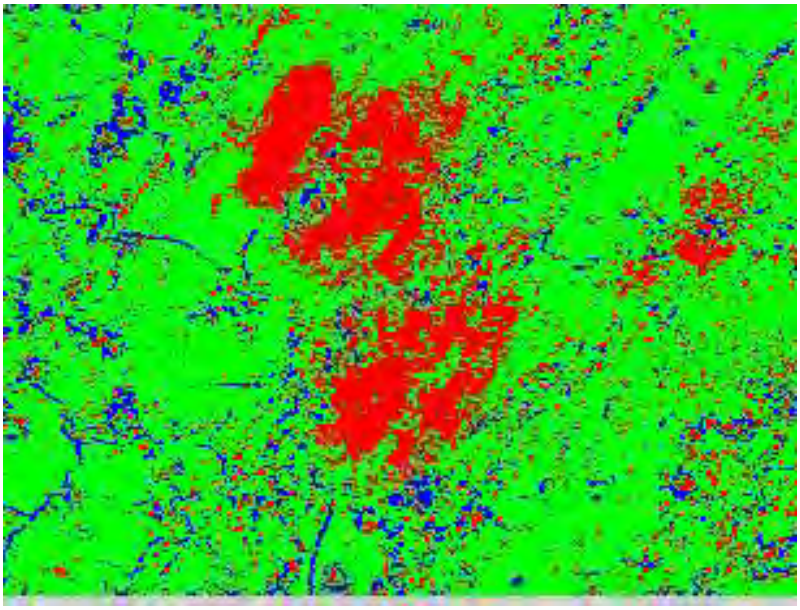

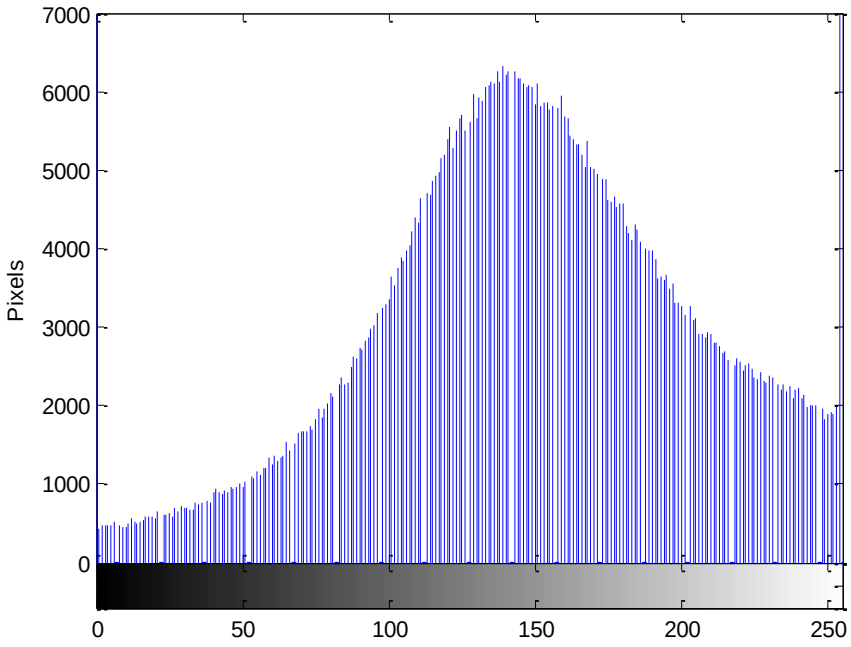
Pixels
7000
6000
5000
4000
3000
2000
1000
0
0
50
100
150
200
250

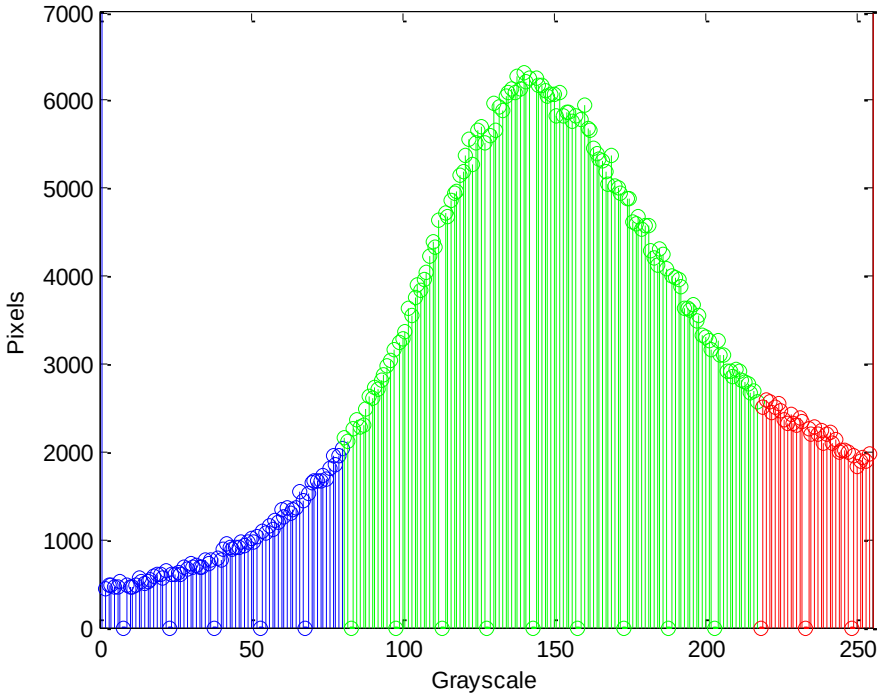

Porosity is 11%

CSH is 72%

CH is 17%

10% Fly Ash Water Cured at 3 Days

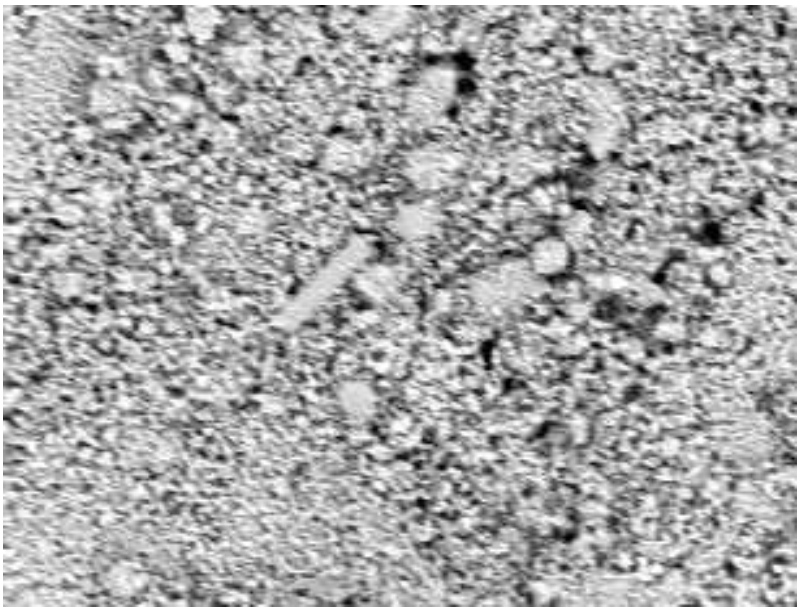

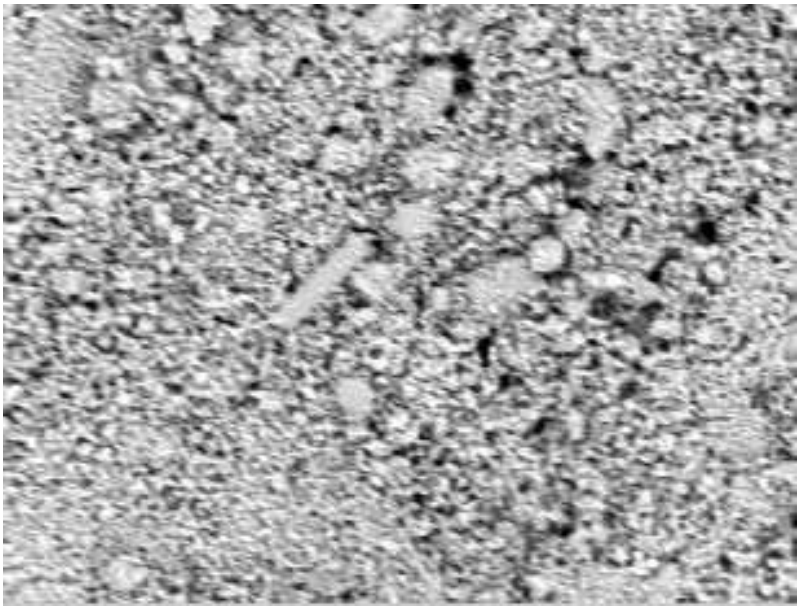

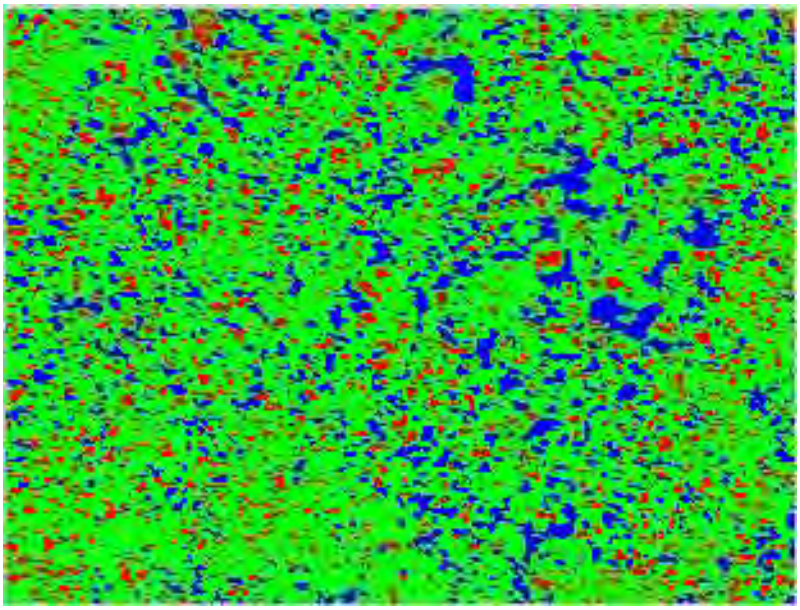

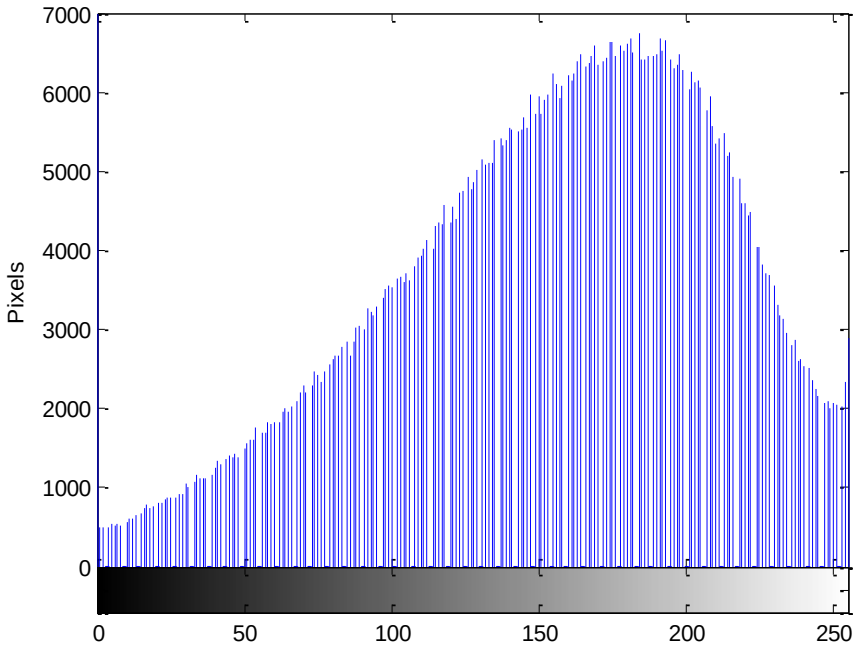

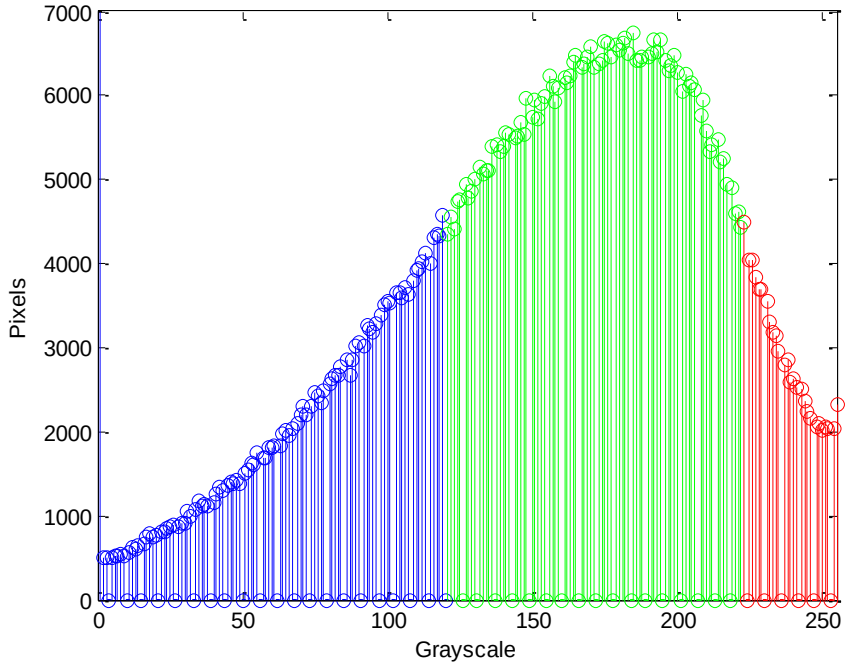

Porosity is 27%

CSH is 63%

CH is 10%

10% Fly Ash Water Cured at 7 Days

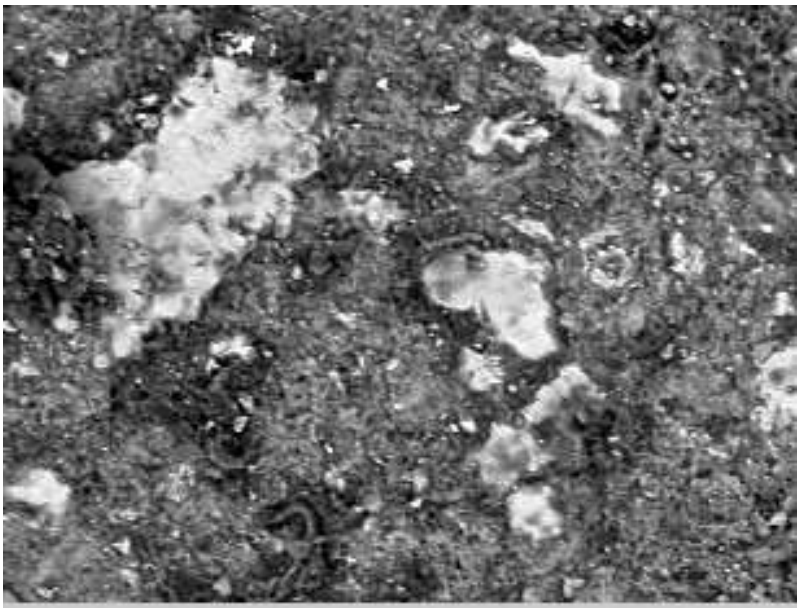

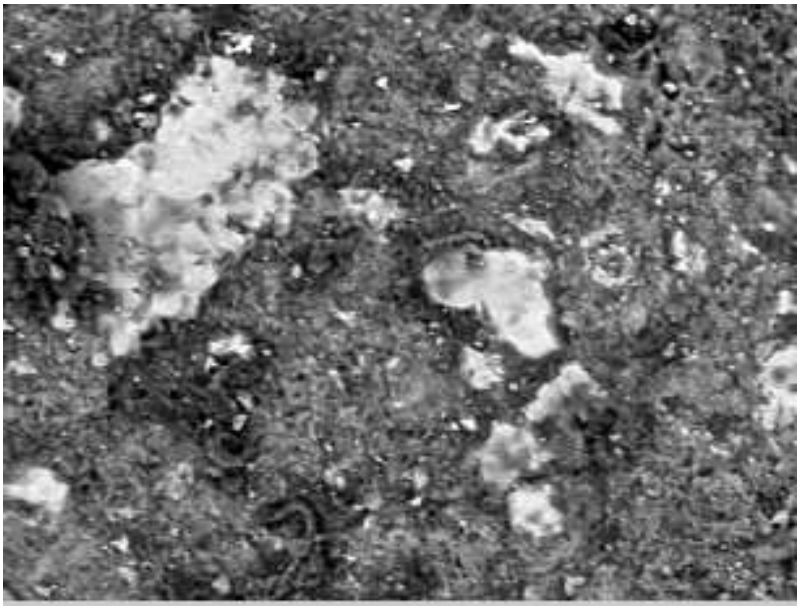

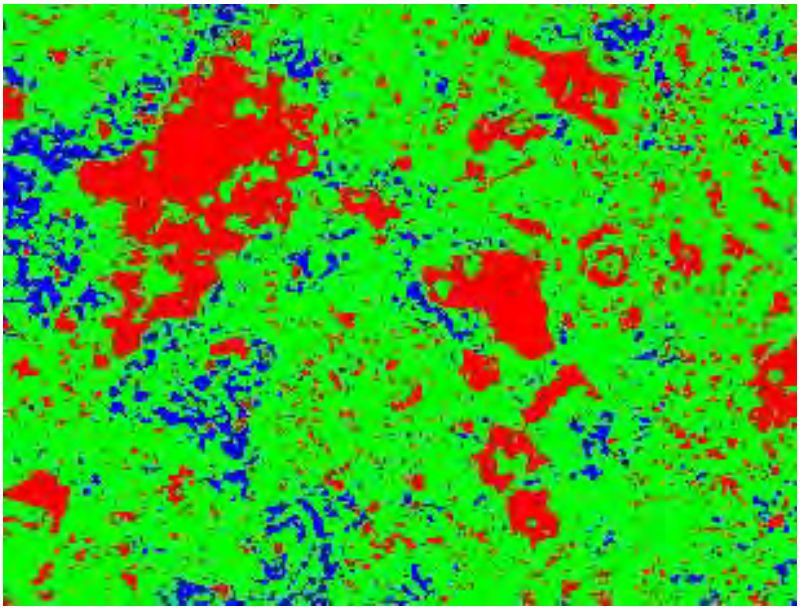

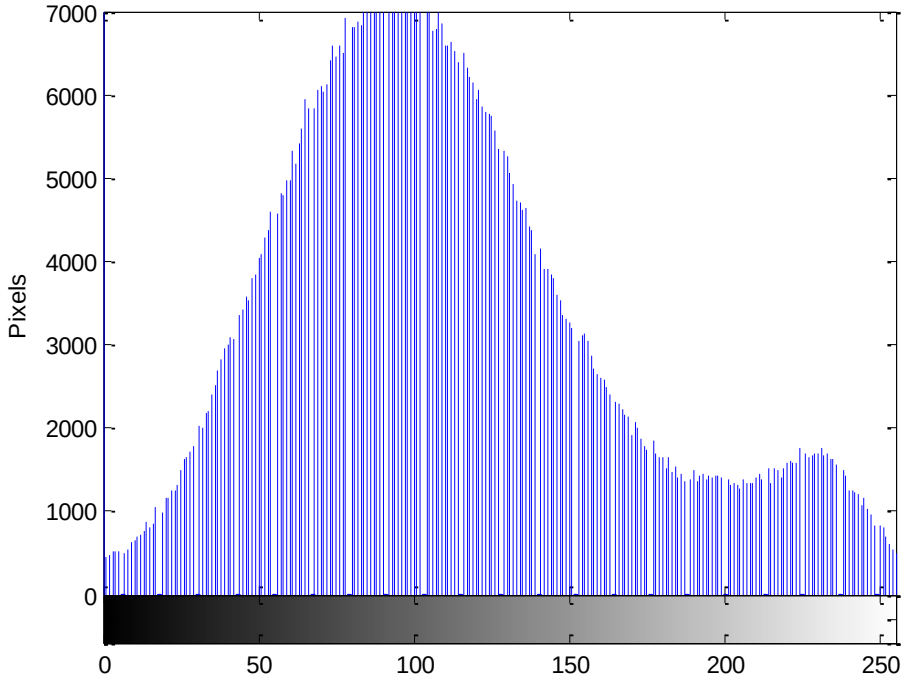
Pixels
7000
6000
5000
4000
3000
2000
1000
0
0
50
100
150
200
250

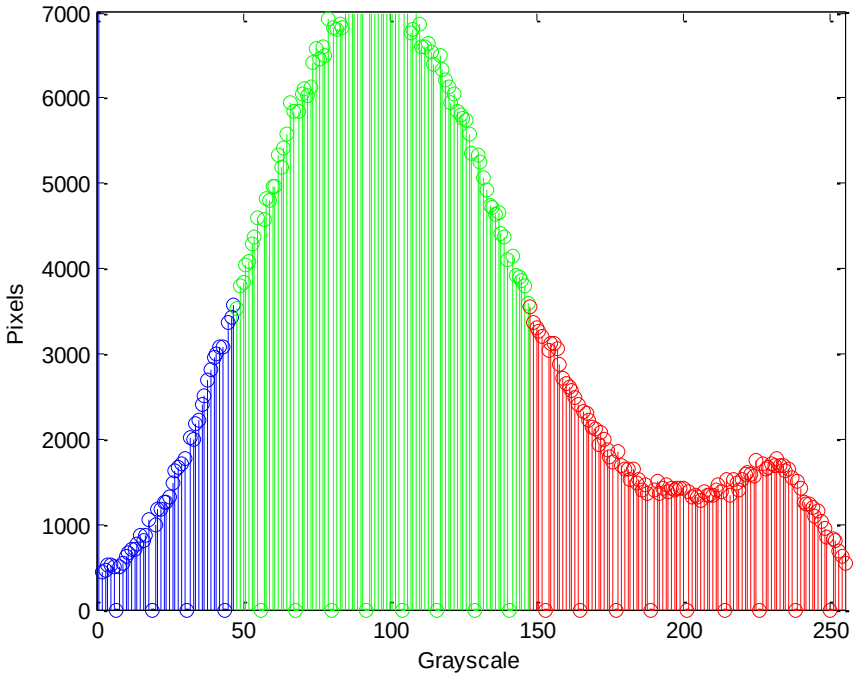

Porosity is 10%

CSH is 69%

CH is 22%

10% Fly Ash Water Cured at 14 Days

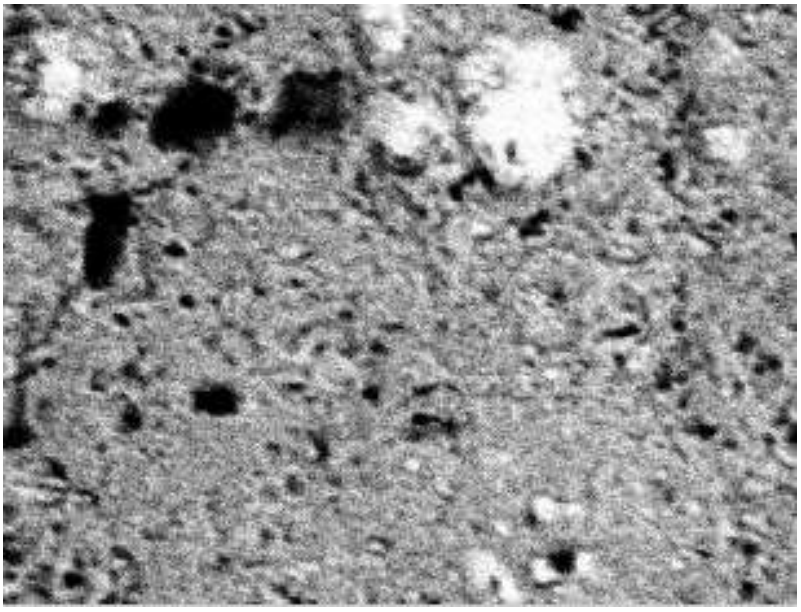

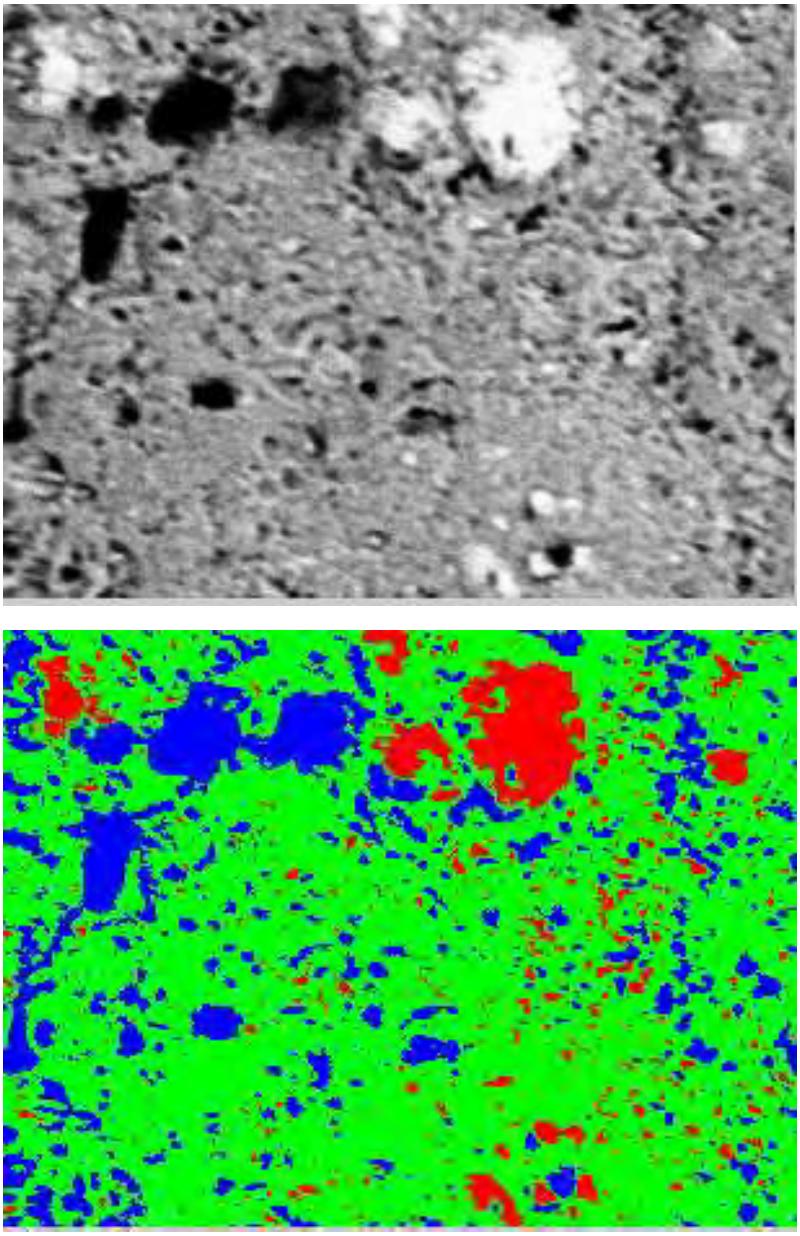

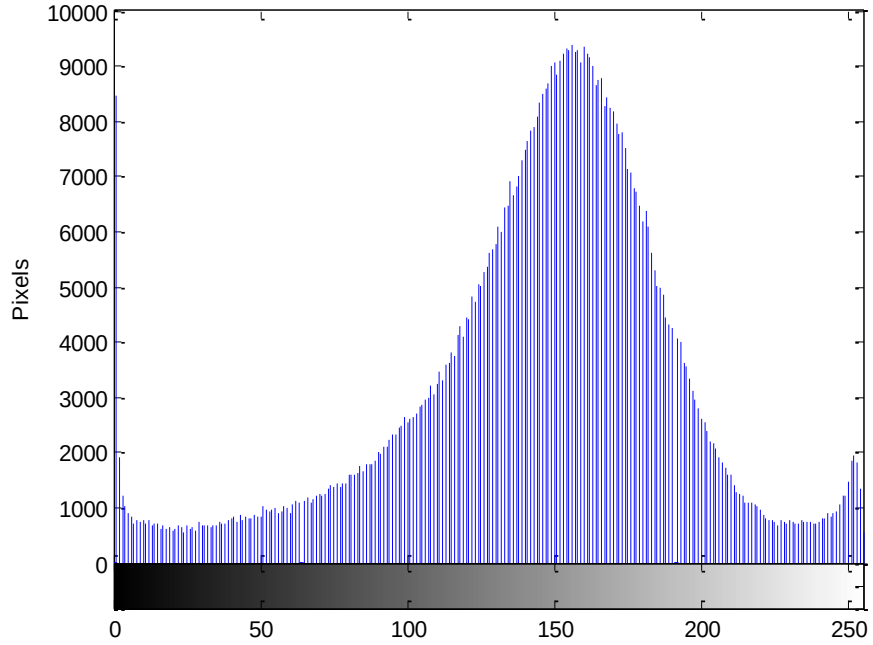

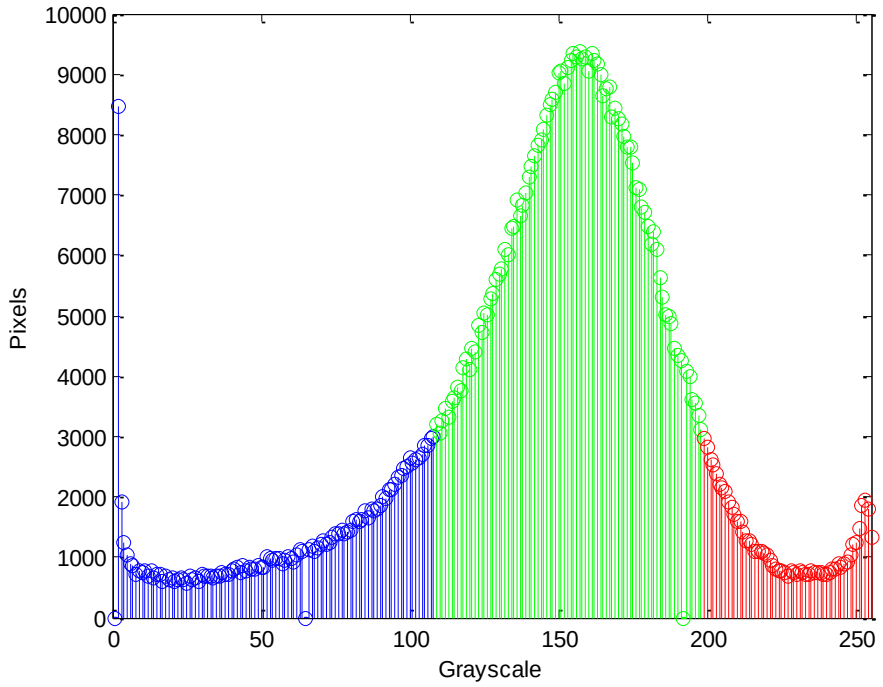

Porosity is 18%

CSH is 73%

CH is 9%

10% Fly Ash Water Cured at 28 Days

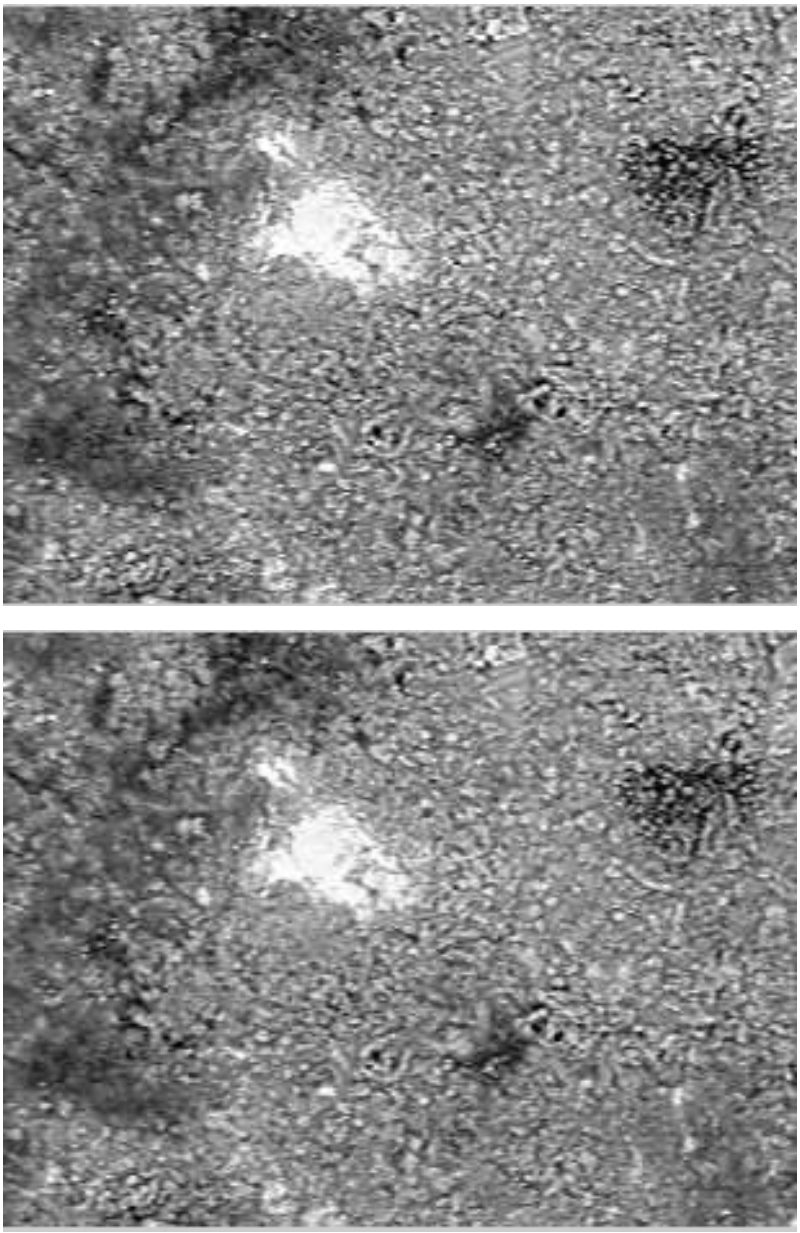

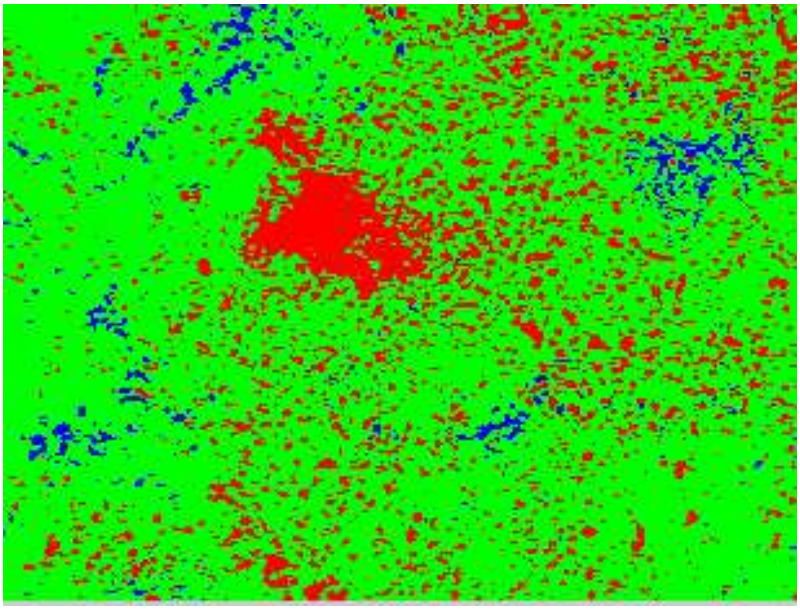

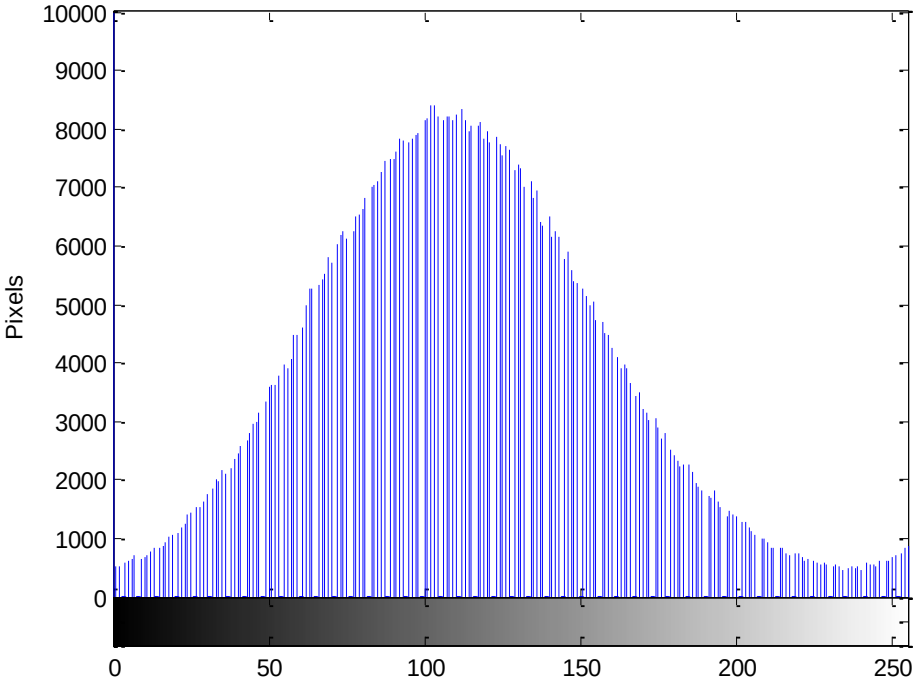
Pixels
10000
9000
8000
7000
6000
5000
4000
3000
2000
1000
0
0
50
100
150
200
250

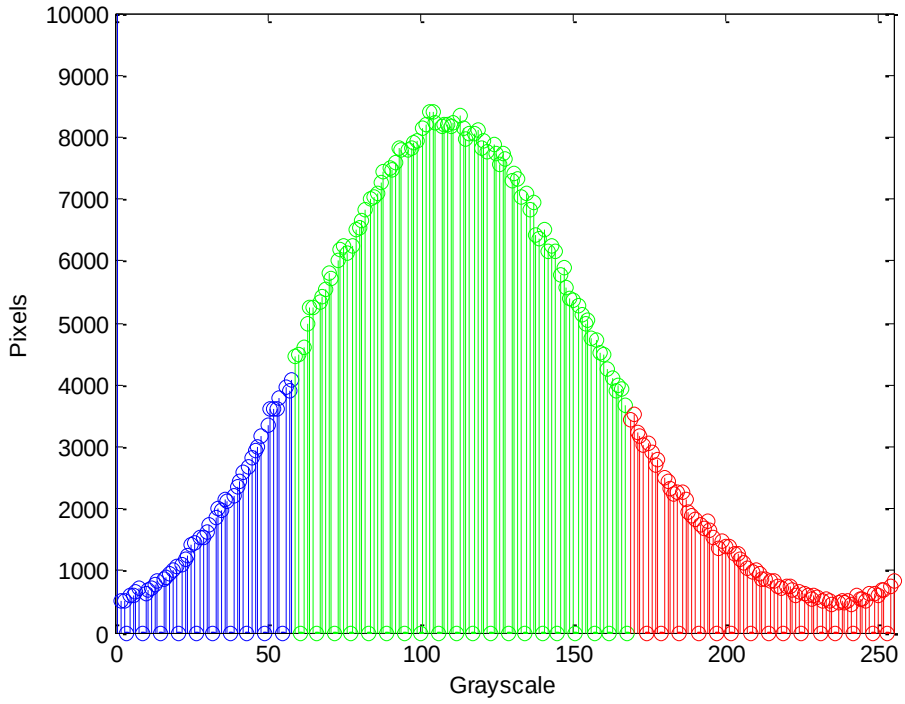

Porosity is 13%

CSH is 75%

CH is 12%

10% Fly Ash Water Cured at 56 Days

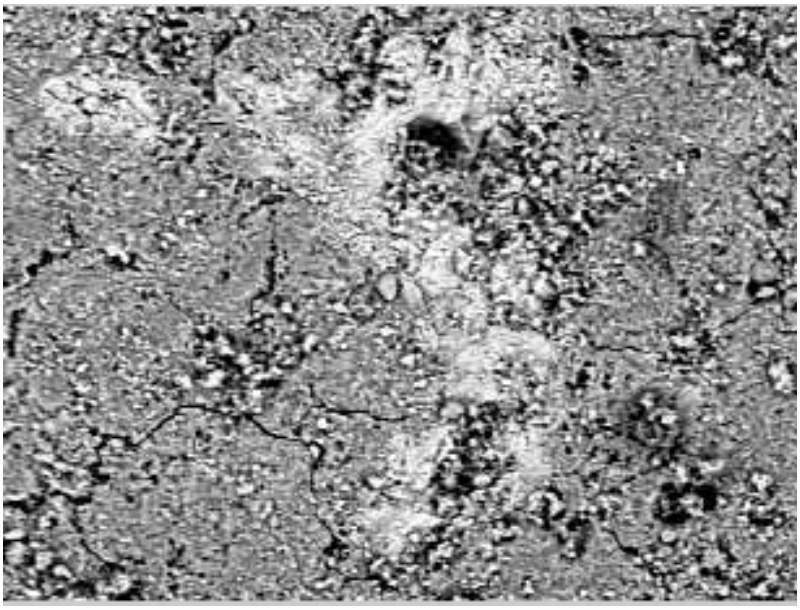

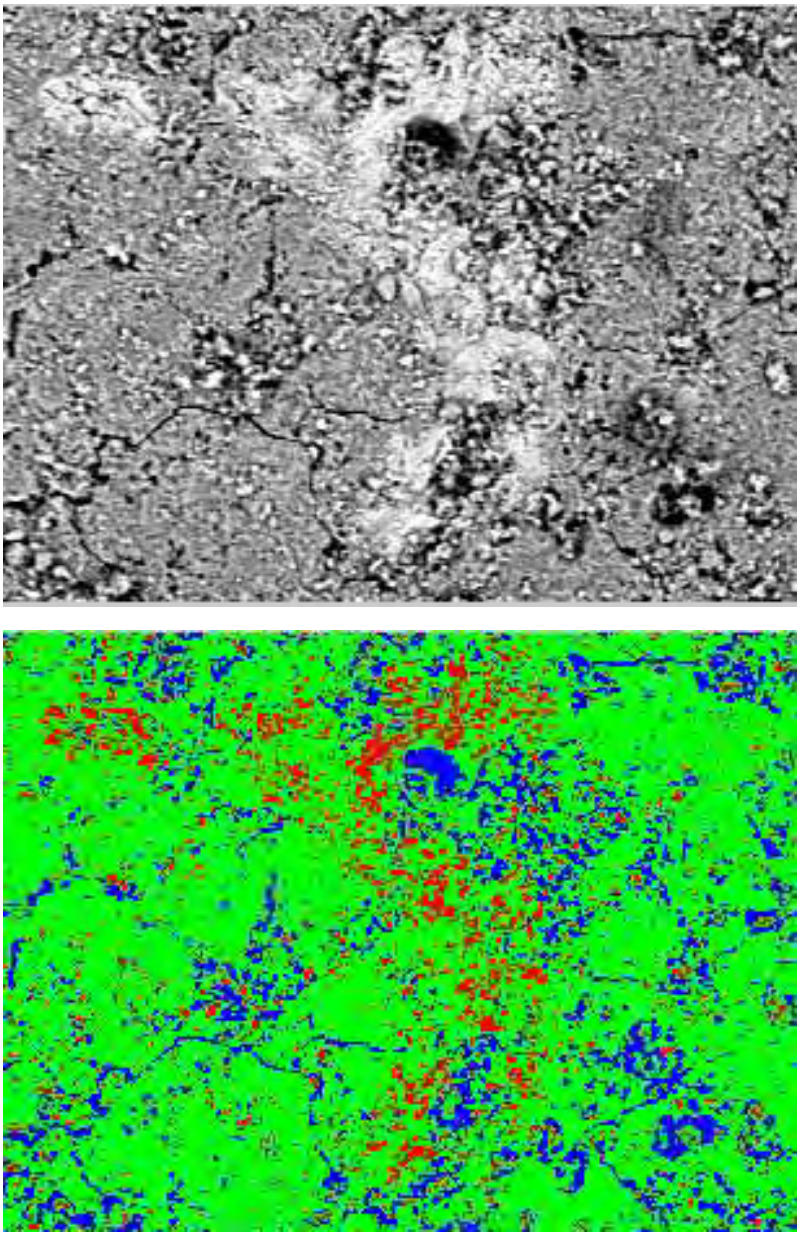

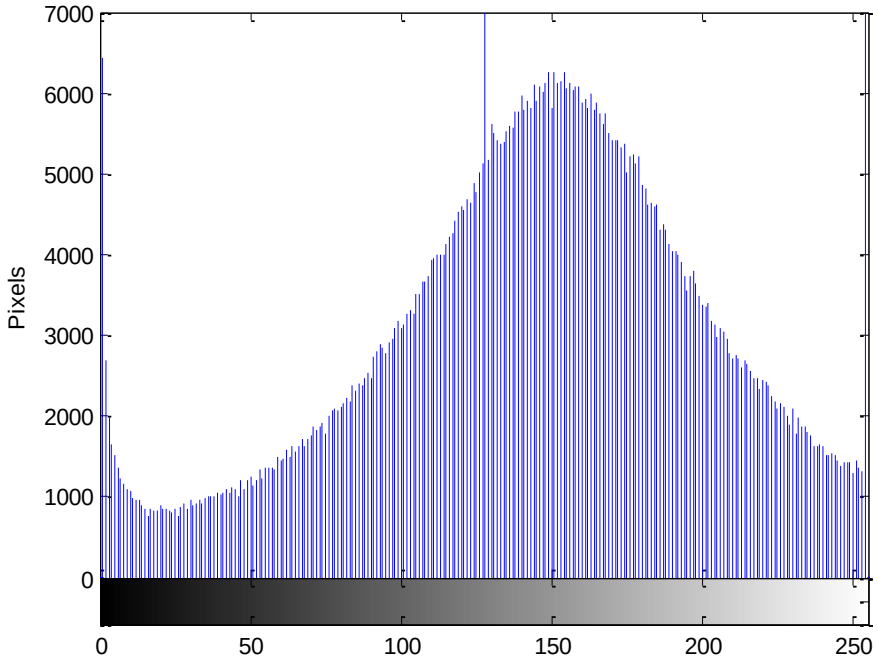

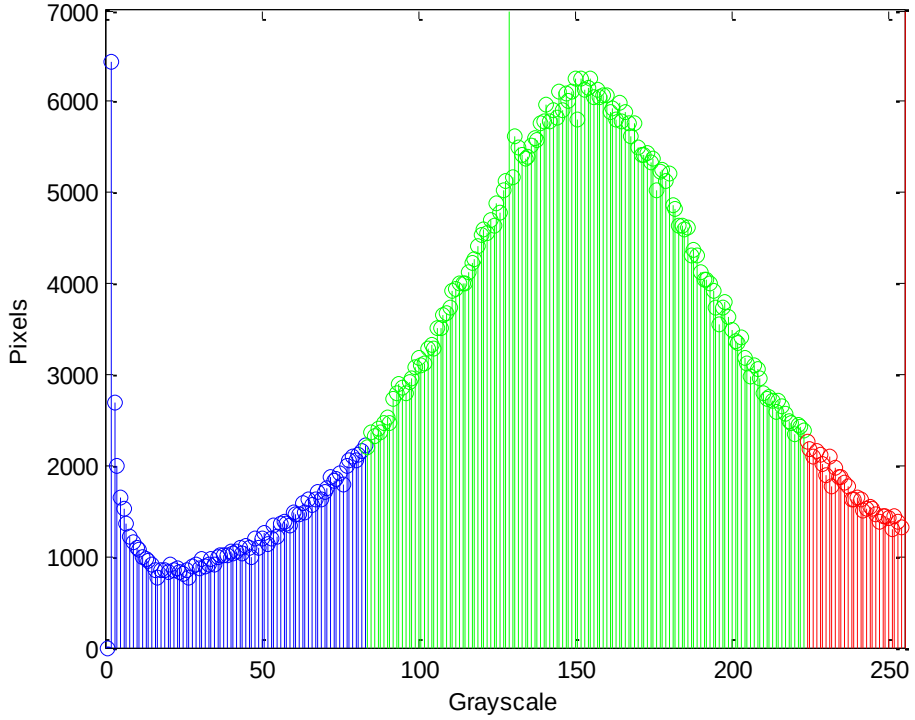

Porosity is 14%

CSH is 78%

CH is 8%

5% Silica Fume Vacuum Cured at 3 Days

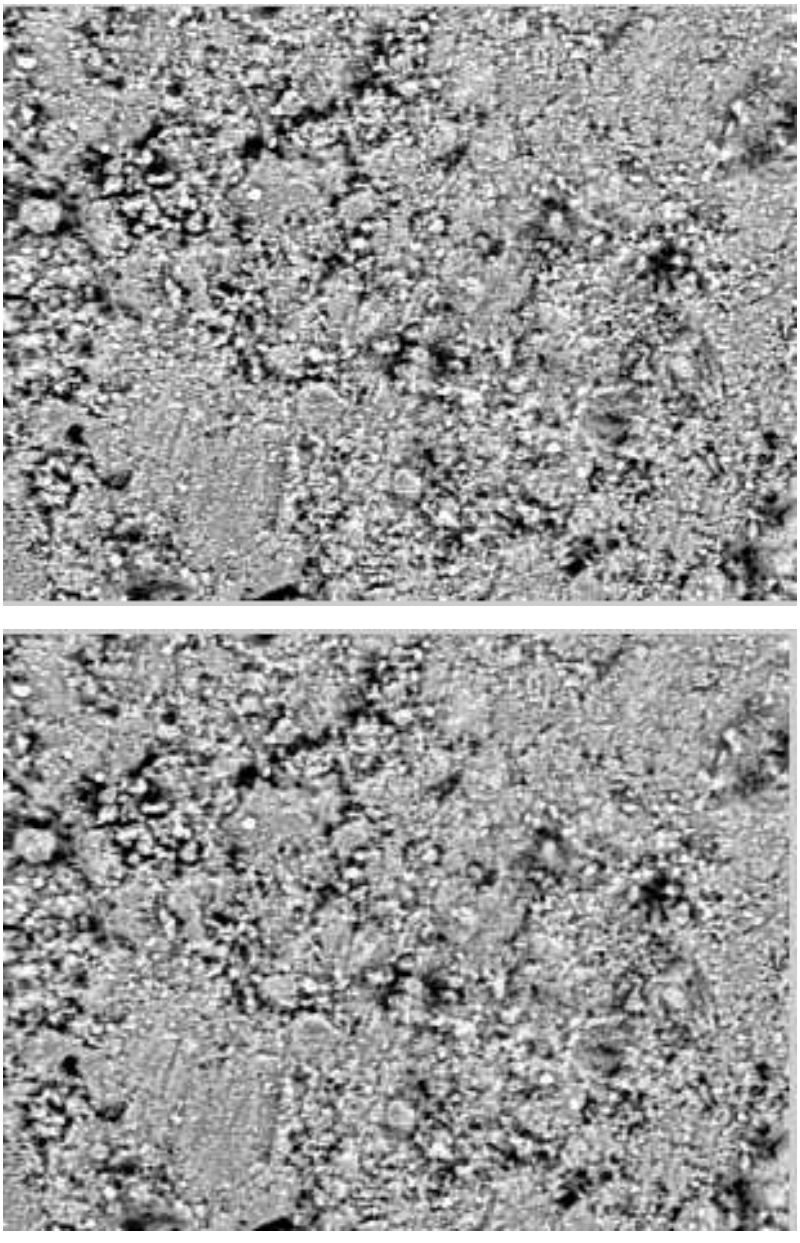

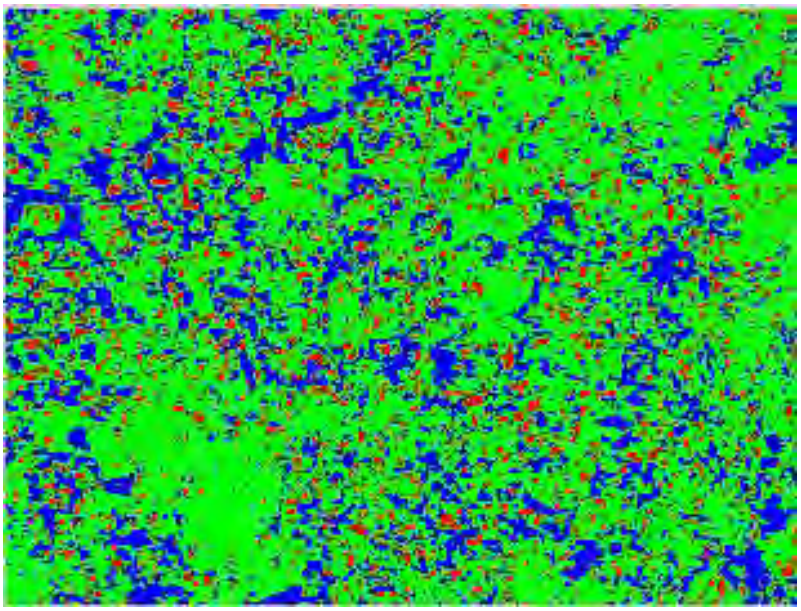

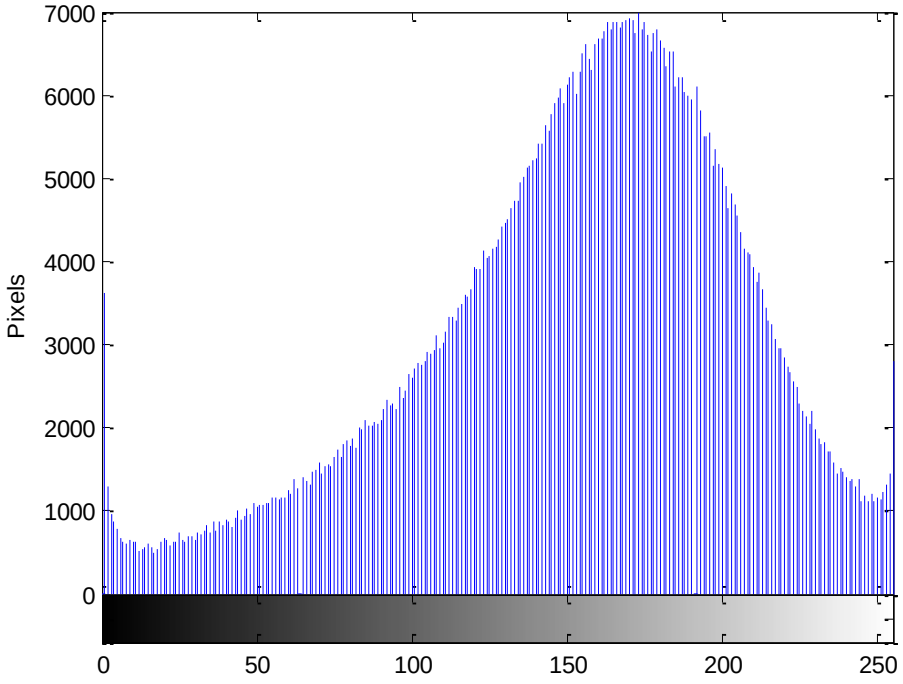
Pixels
7000
6000
5000
4000
3000
2000
1000
0
0
50
100
150
200
250

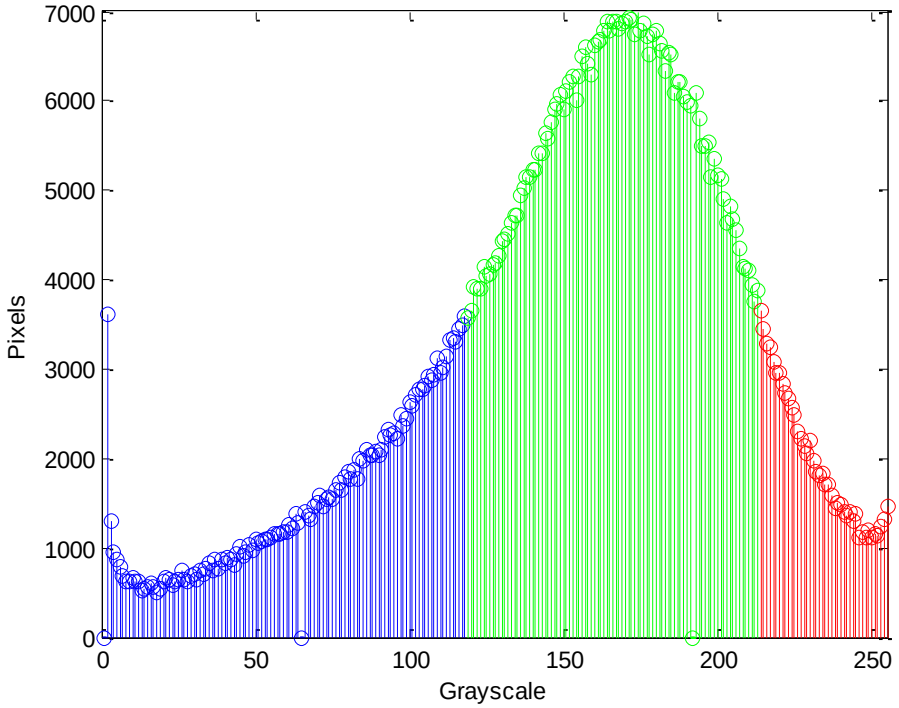

Porosity is 23%

CSH is 67%

CH is 11%

5% Silica Fume Vacuum Cured at 7 Days

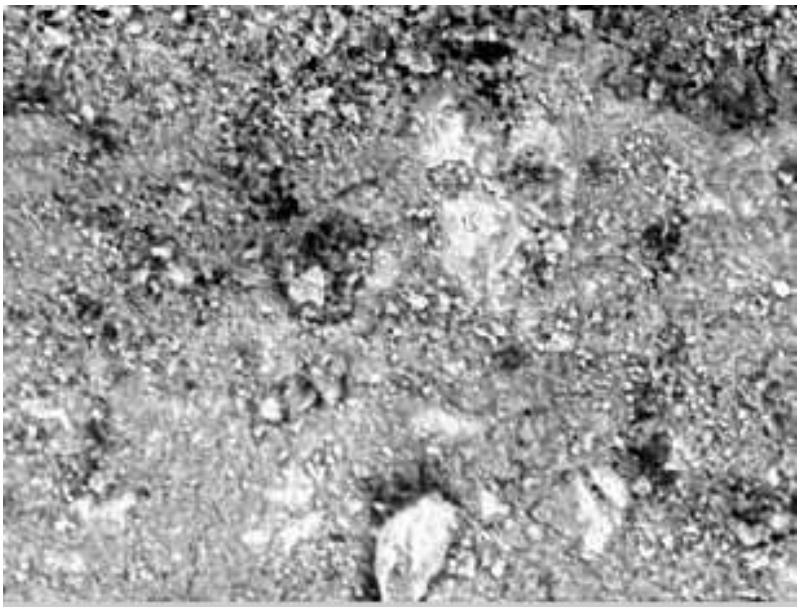

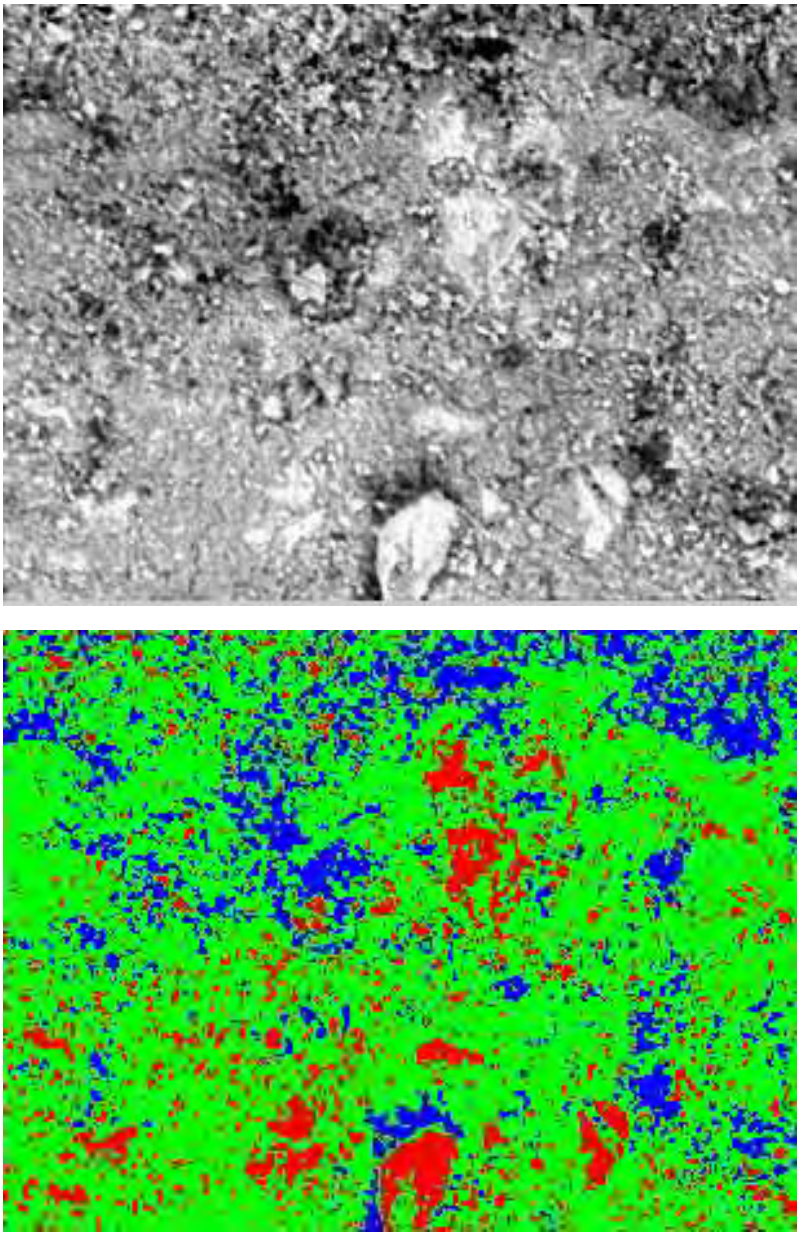

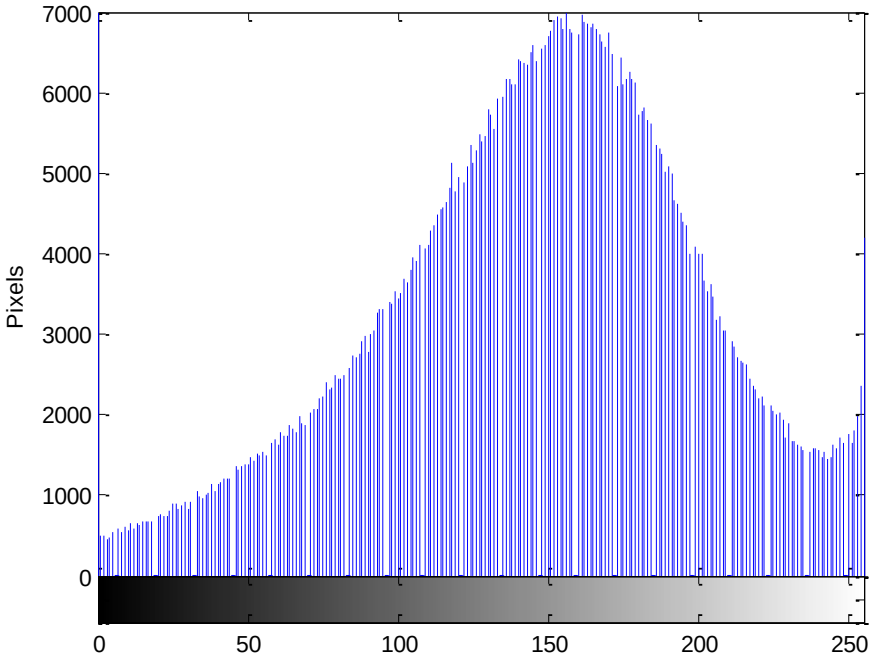

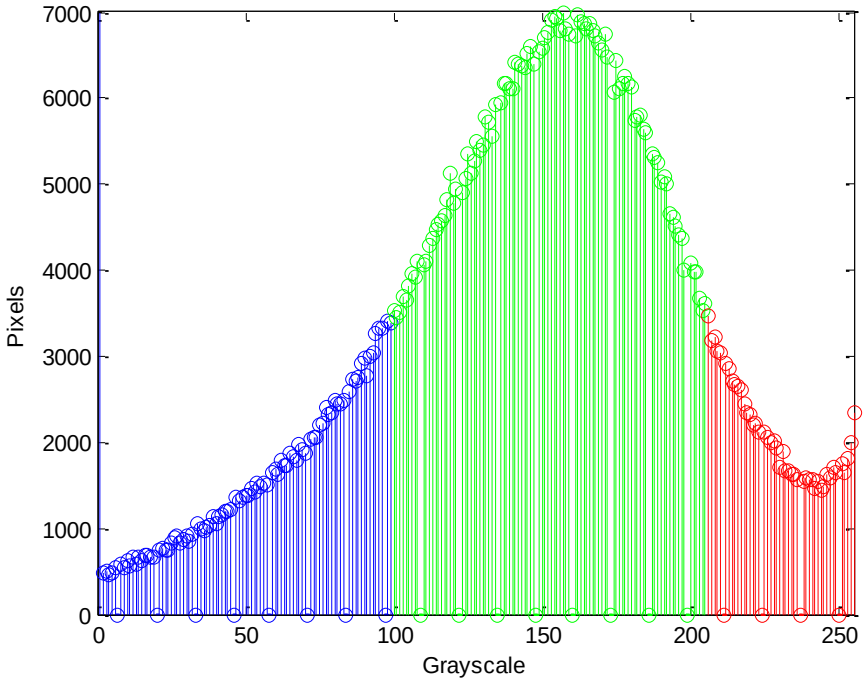

Porosity is 19%

CSH is 68%

CH is 13%

5% Silica Fume Vacuum Cured at 14 Days

OUT

5% Silica Fume Vacuum Cured at 28 Days

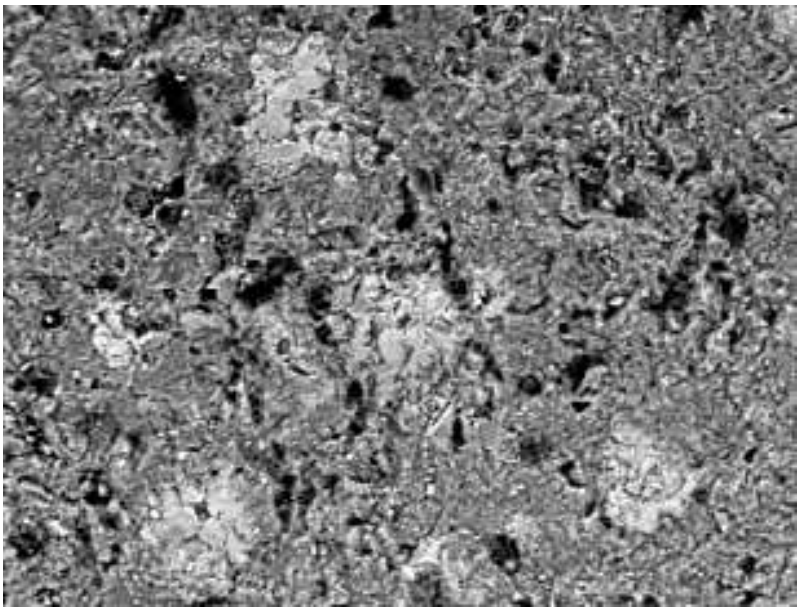

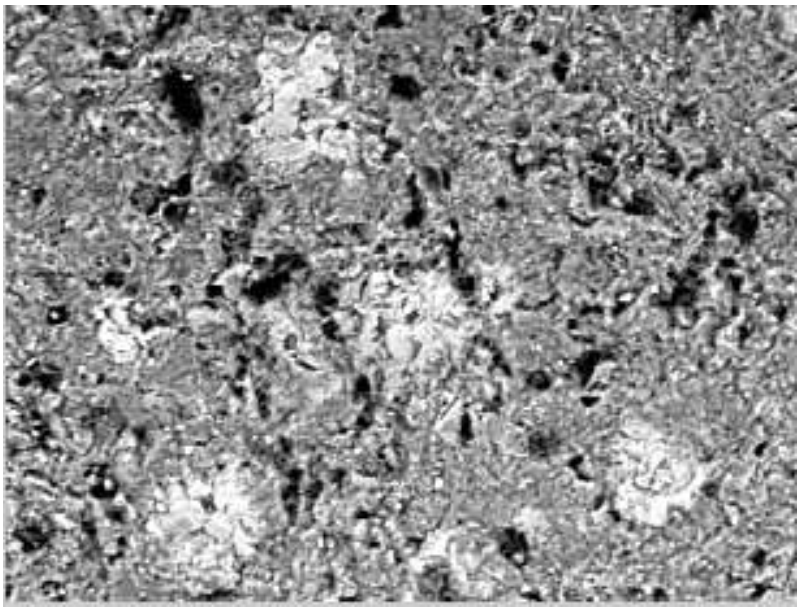

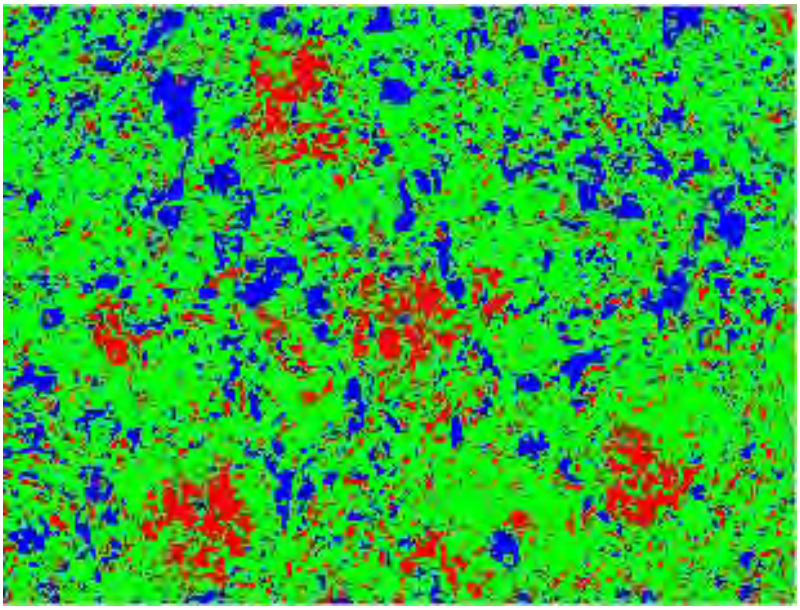

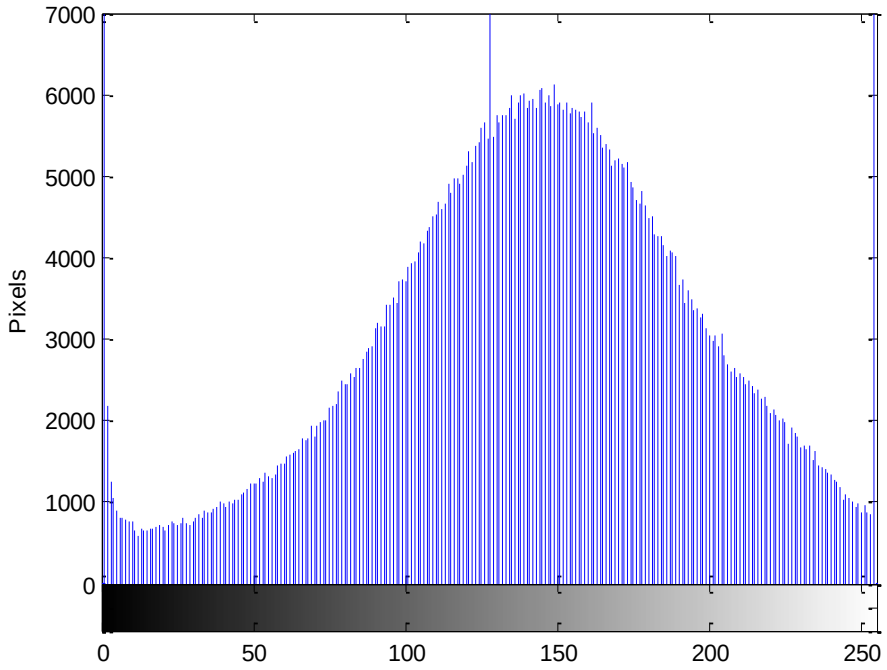
Pixels
7000
6000
5000
4000
3000
2000
1000
0
0
50
100
150
200
250

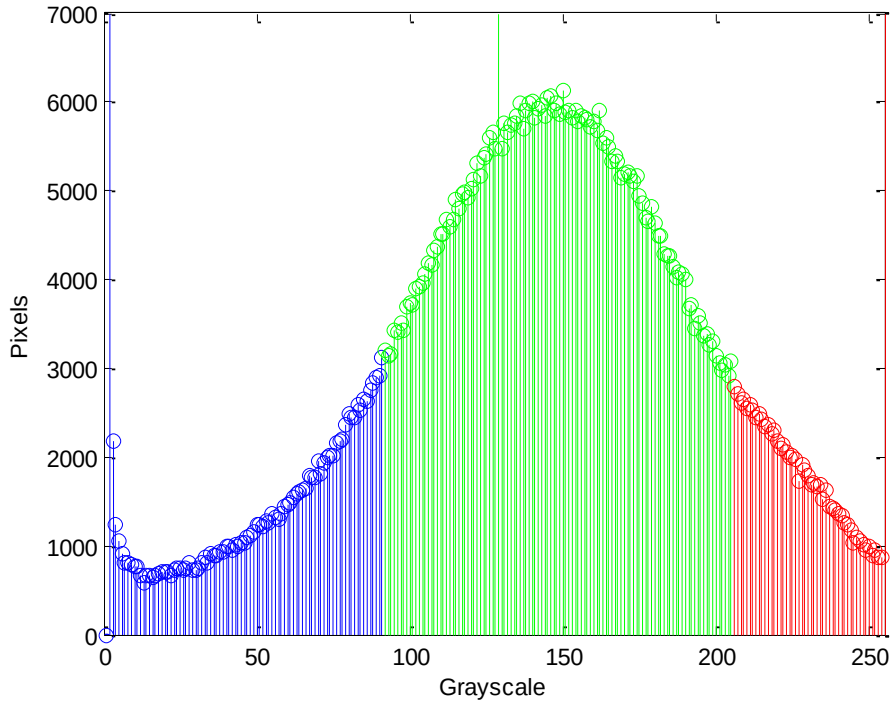

Porosity is 17%

CSH is 70%

CH is 13%

5% Silica Fume Vacuum Cured at 56 Days

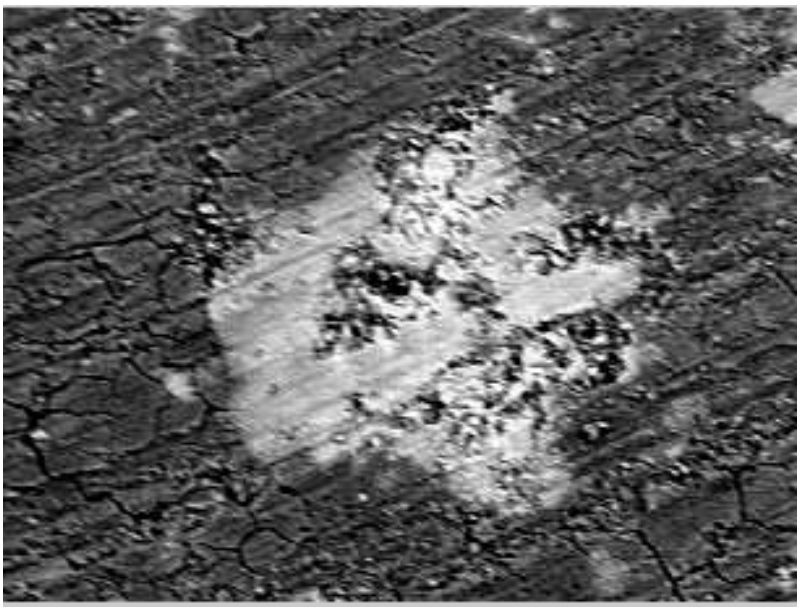

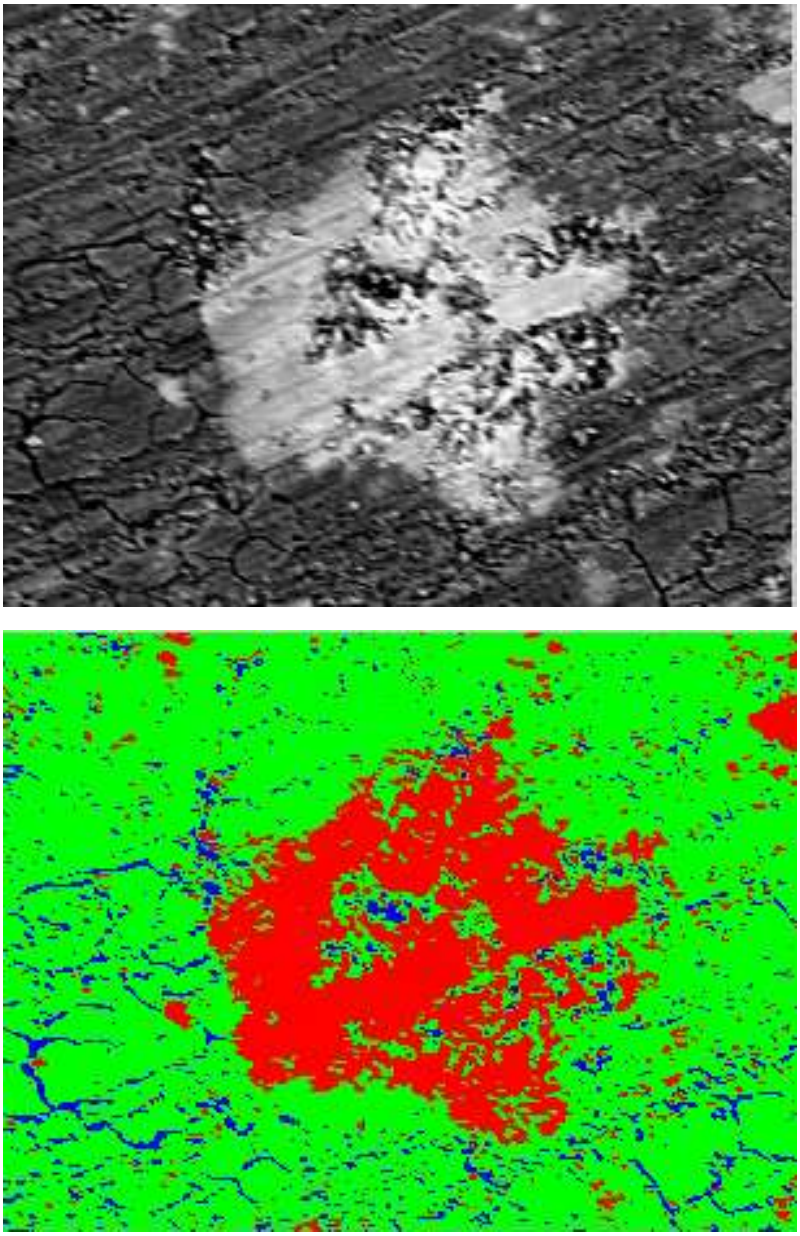

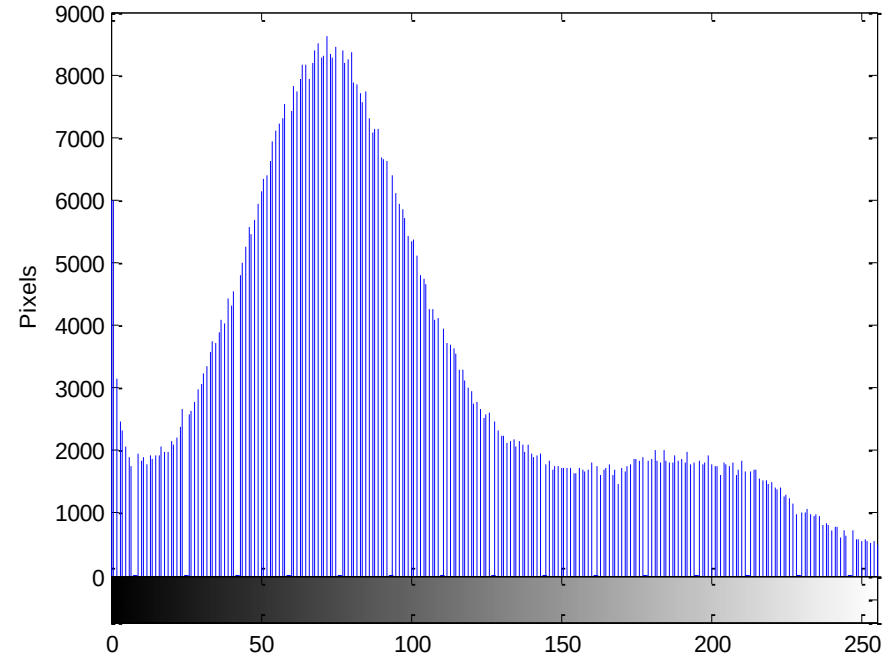

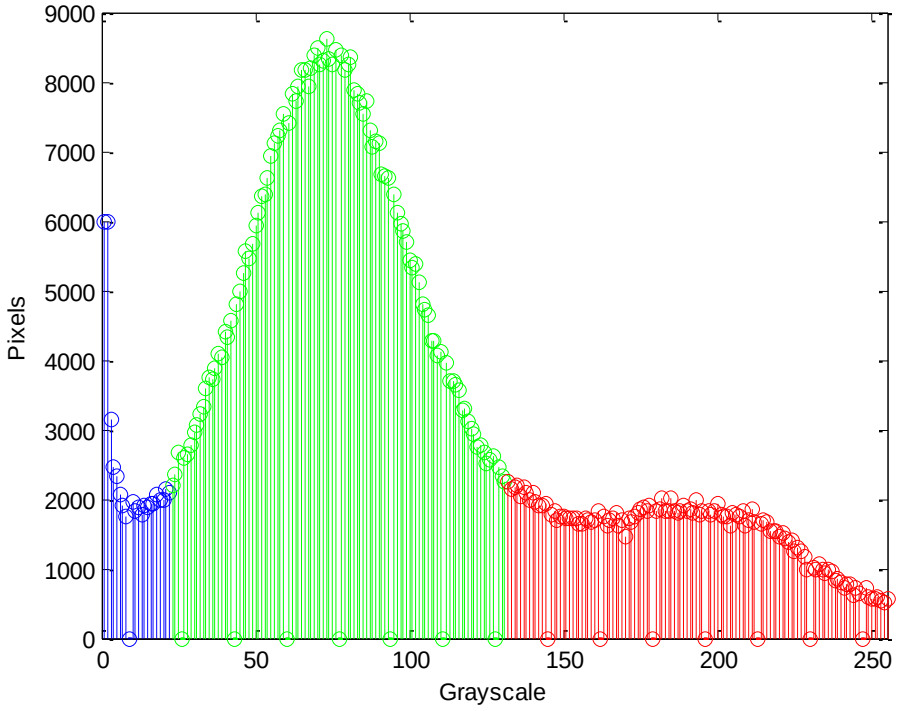

Porosity is 6%

CSH is 70%

CH is 23%

5% Silica Fume Water Cured at 3 Days

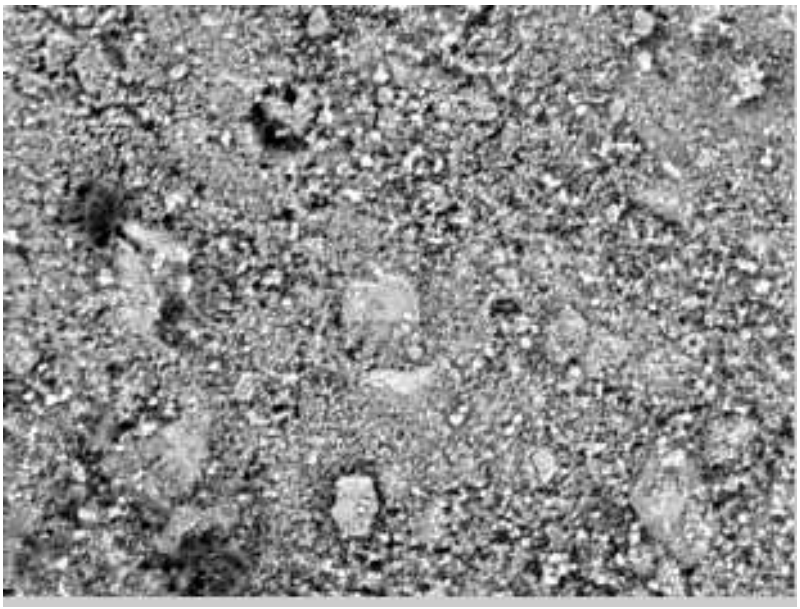

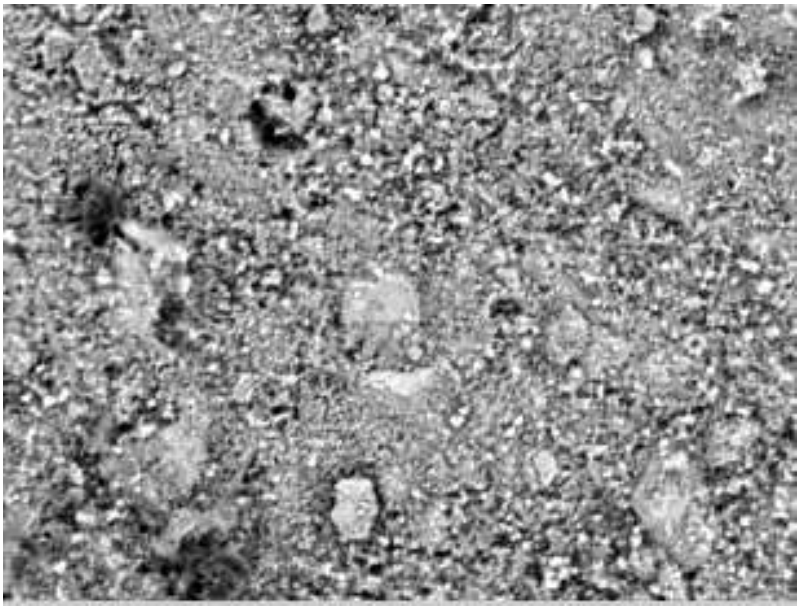

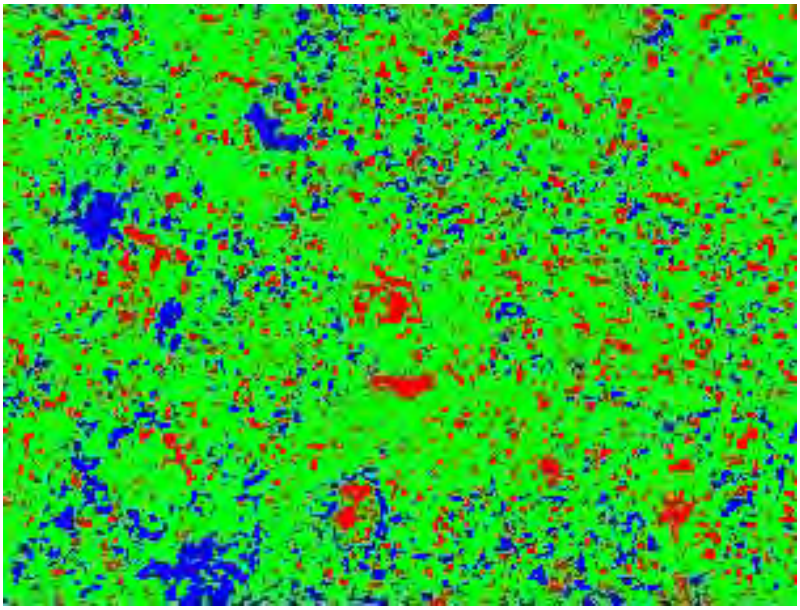

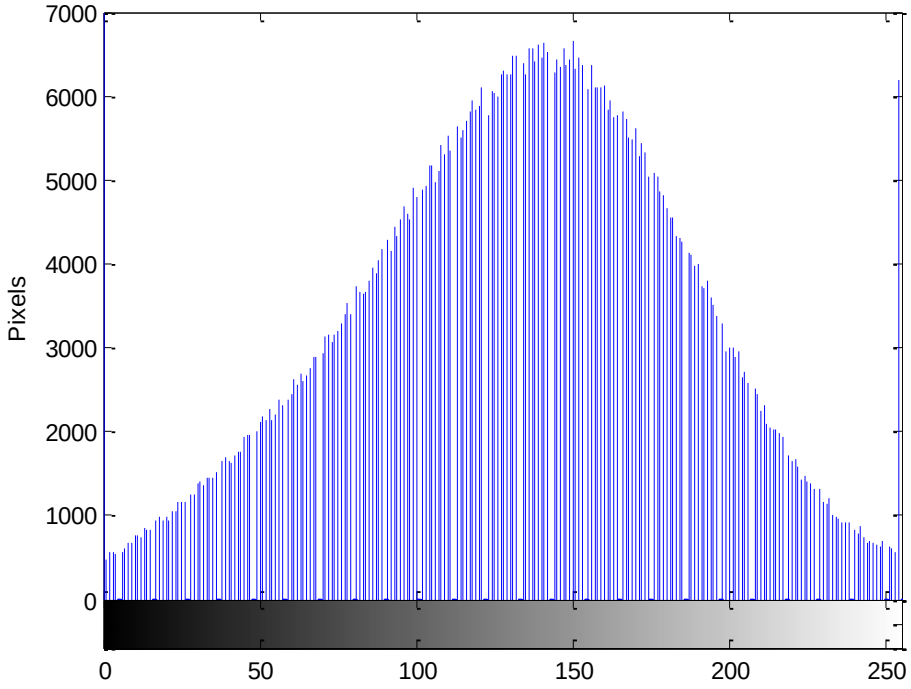
Pixels
7000
6000
5000
4000
3000
2000
1000
0
0
50
100
150
200
250

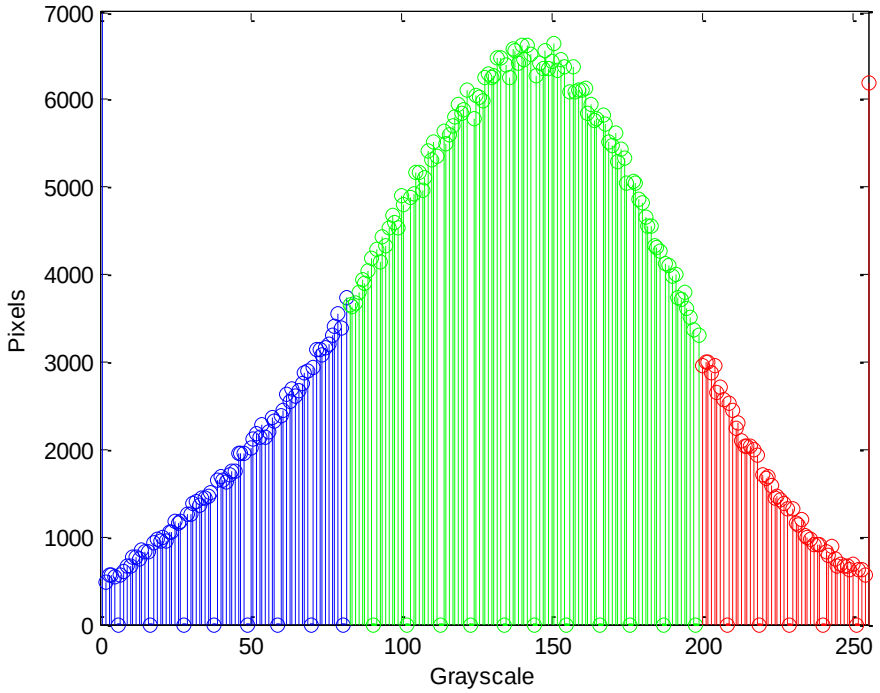

Porosity is 18%

CSH is 71%

CH is 11%

5% Silica Fume Water Cured at 7 Days

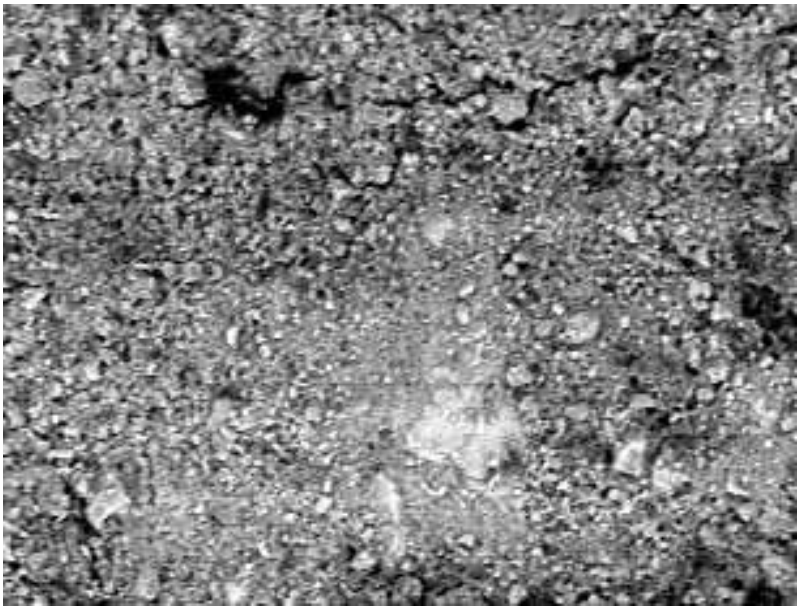

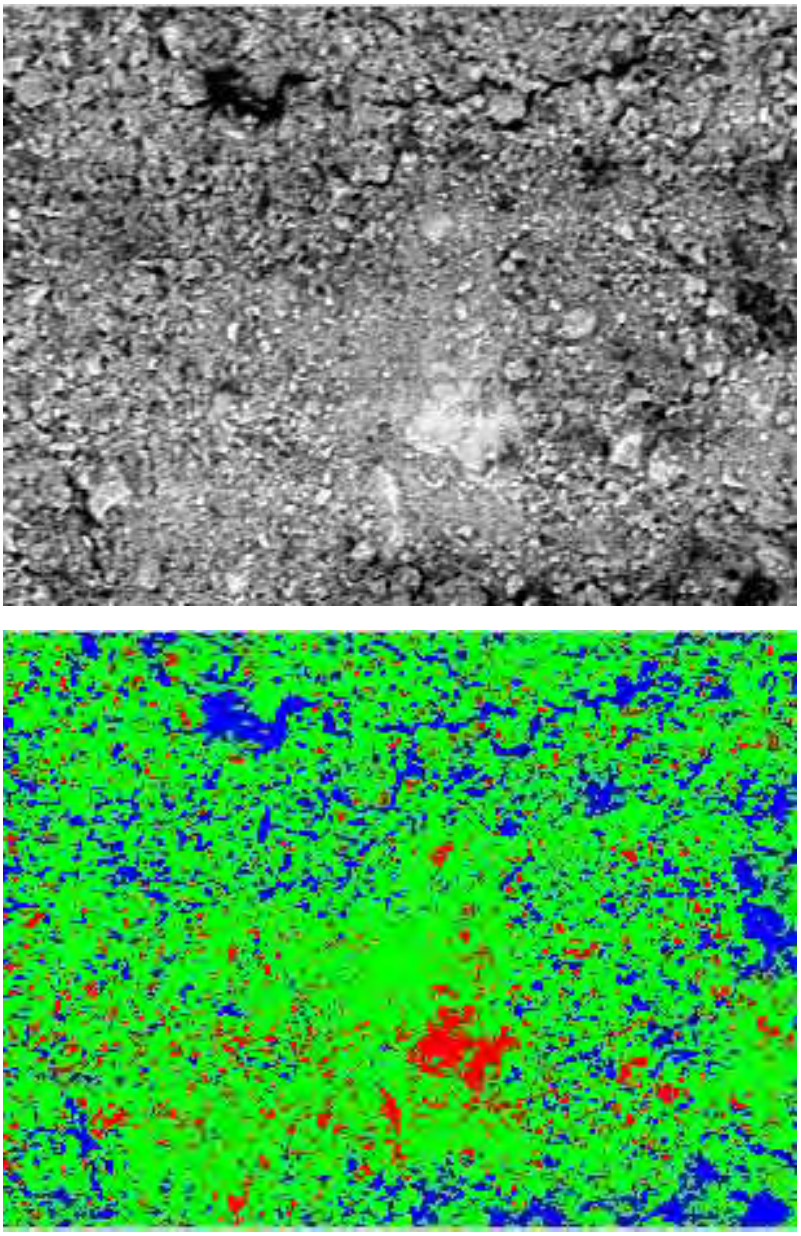

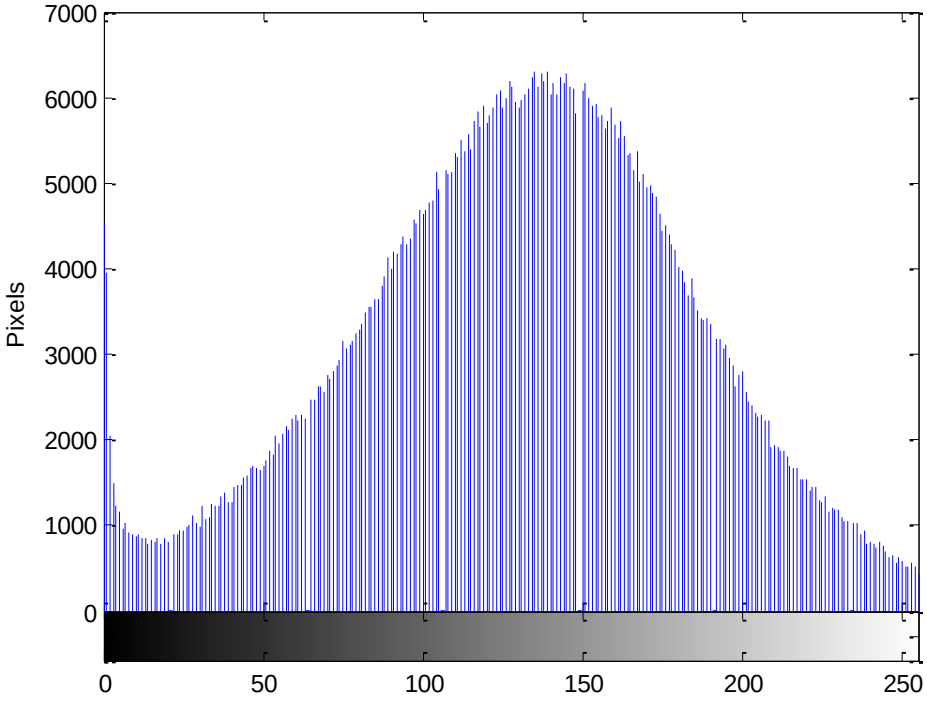

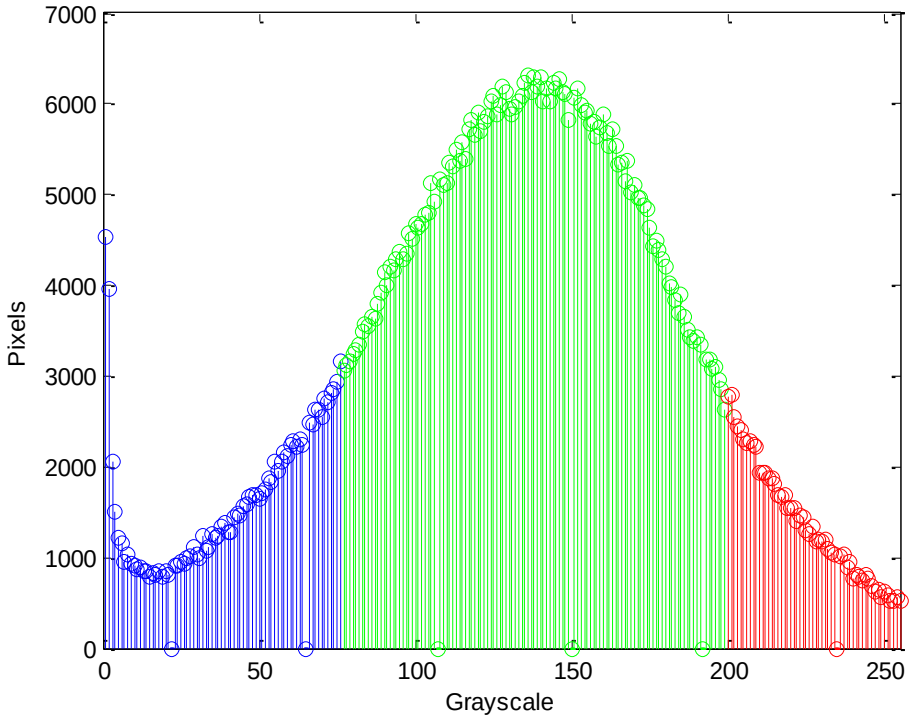

Porosity is 15%

CSH is 75%

CH is 10%

5% Silica Fume Water Cured at 14 Days

OUT

5% Silica Fume Water Cured at 28 Days

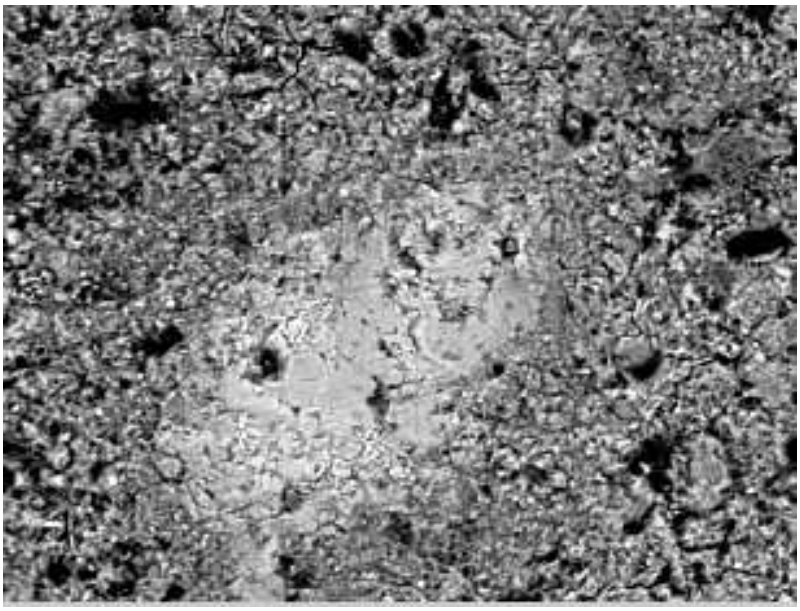

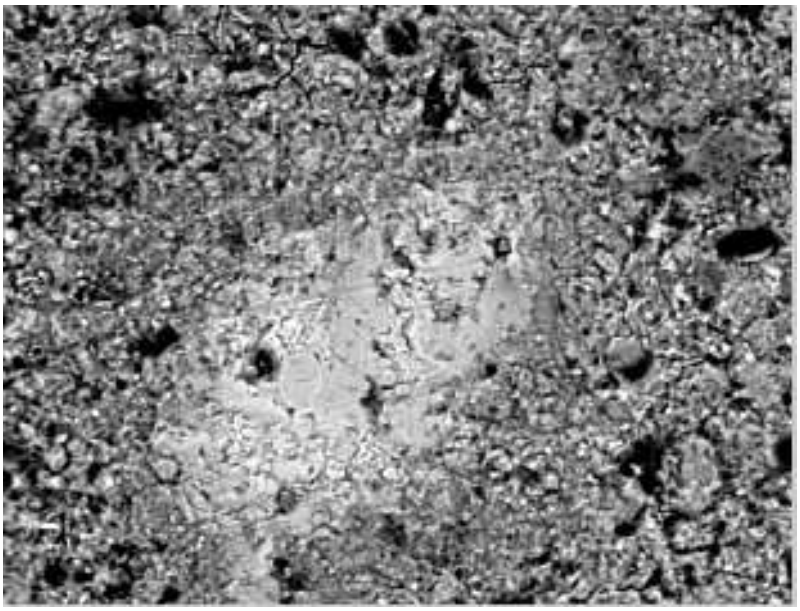

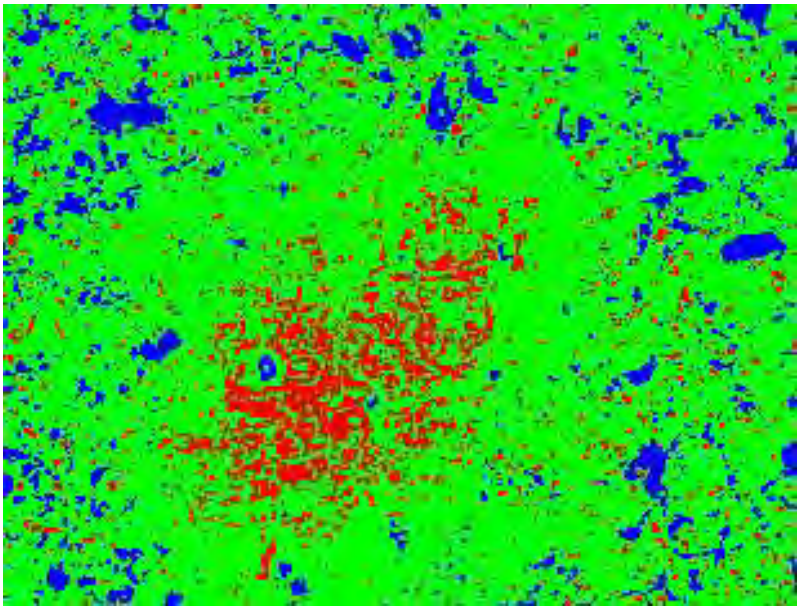

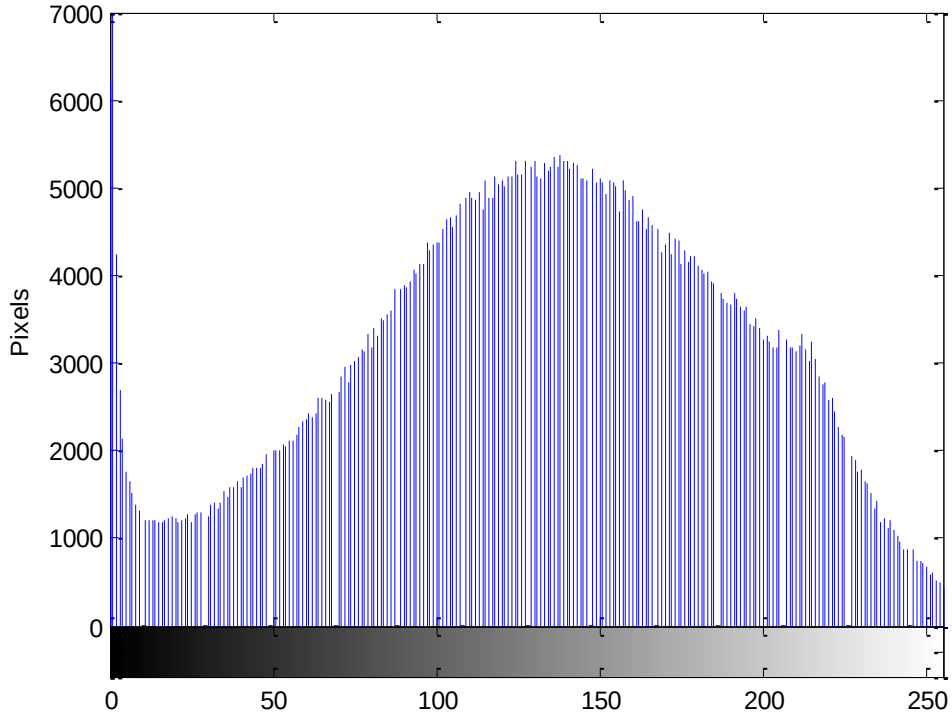
Pixels
7000
6000
5000
4000
3000
2000
1000
0
0
50
100
150
200
250

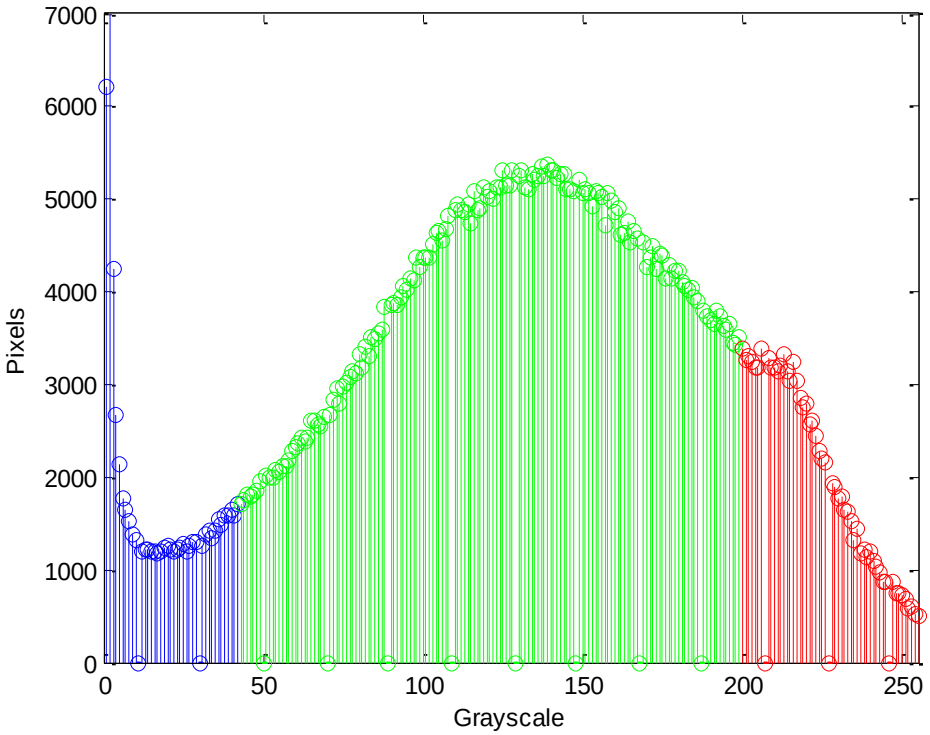

Porosity is 10%

CSH is 76%

CH is 14%

5% Silica Fume Water Cured at 56 Days

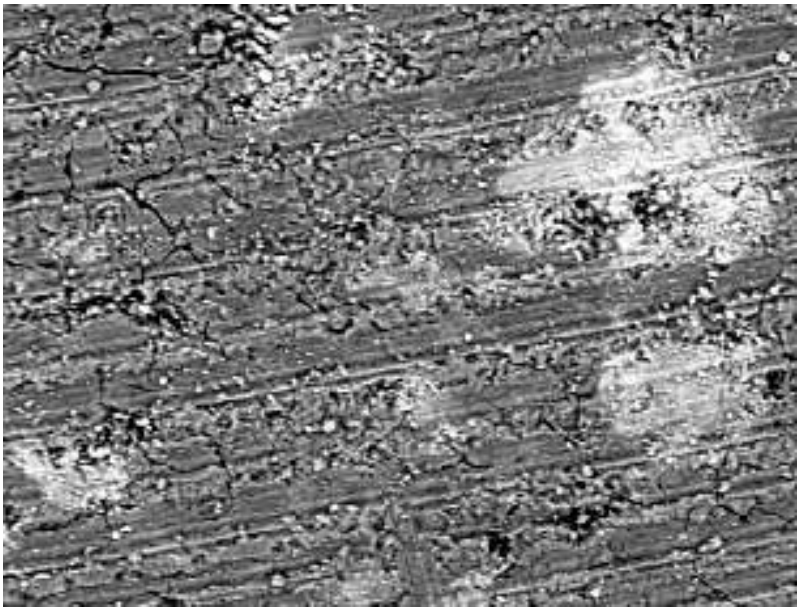

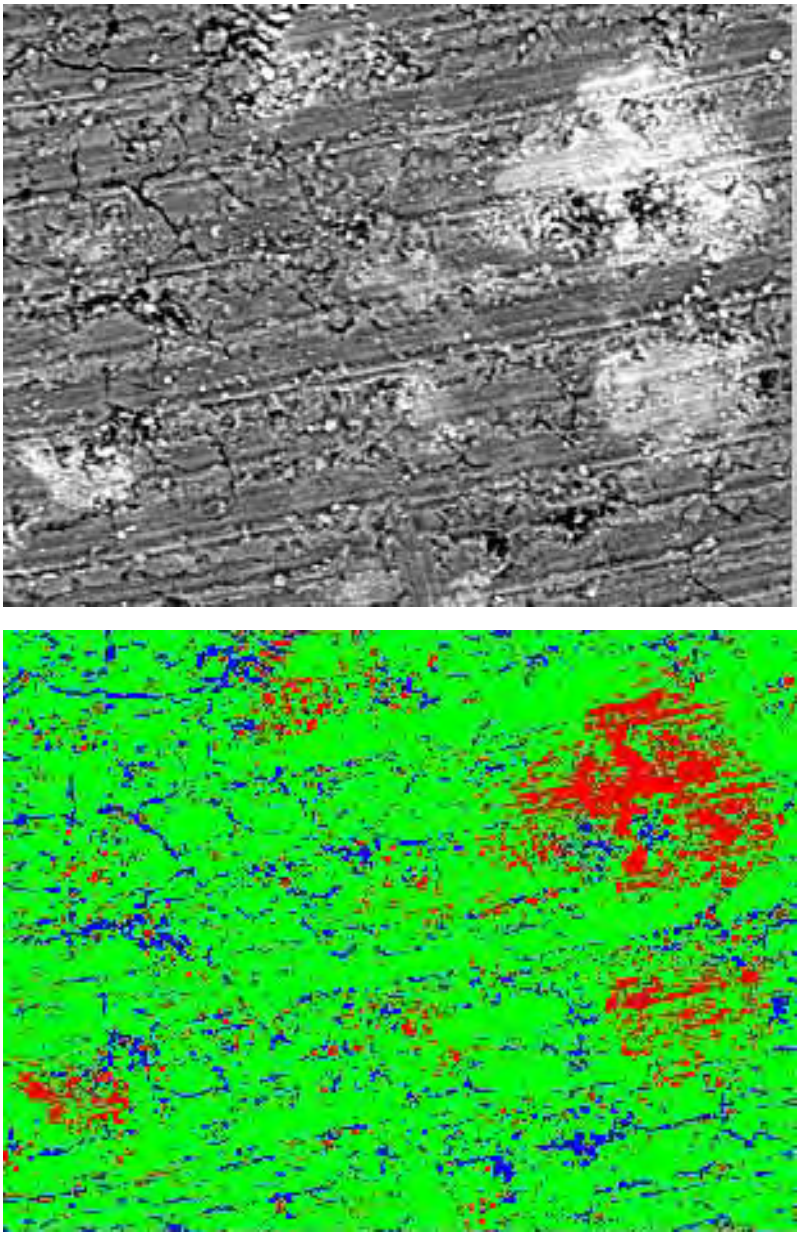

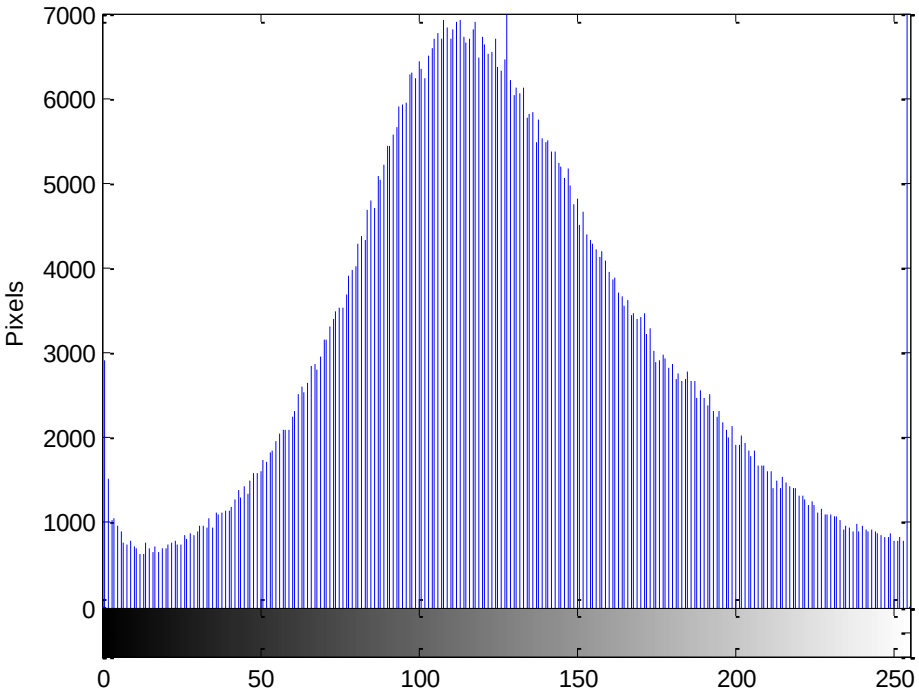
7000
6000
5000
4000
3000
2000
1000
0
Pixels
0
50
100
150
200
250

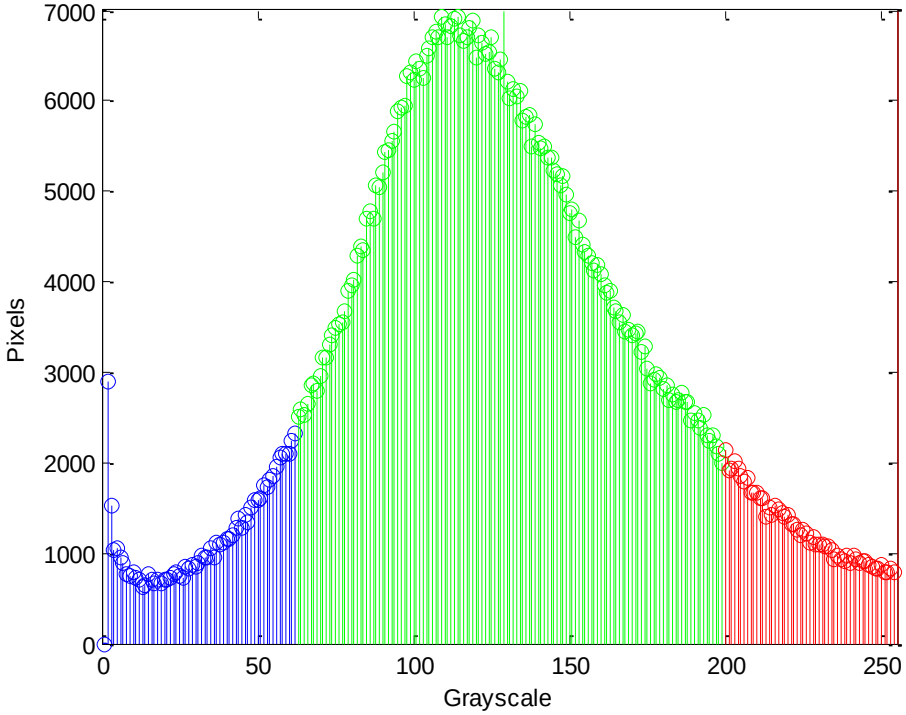
7000
6000
5000
4000
3000
2000
1000
0
Pixels
0
50
100
150
200
250
Grayscale

Porosity is 9%

CSH is 81%

CH is 10%

10% Silica Fume Vacuum Cured at 3 Days

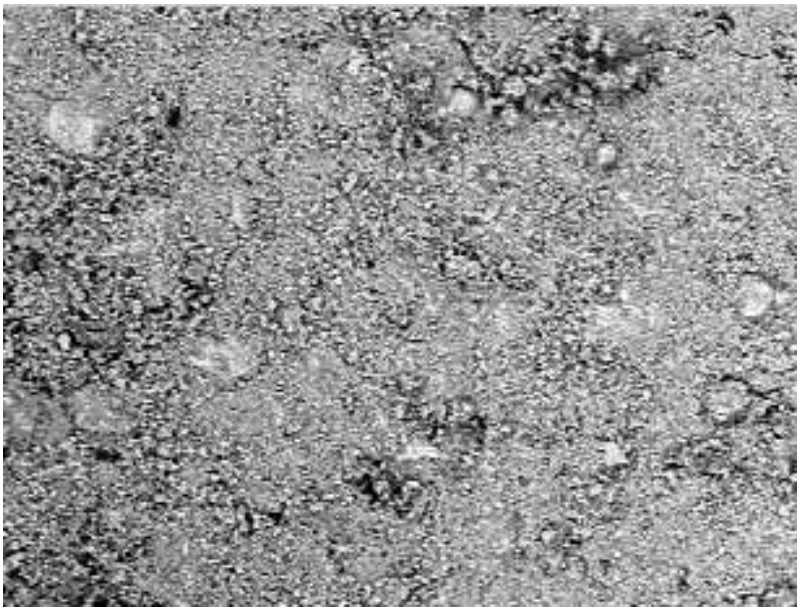

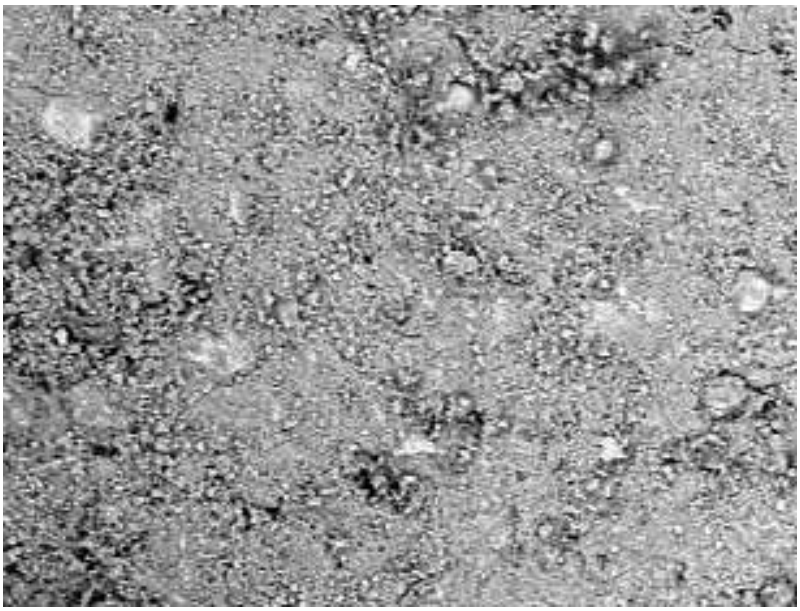

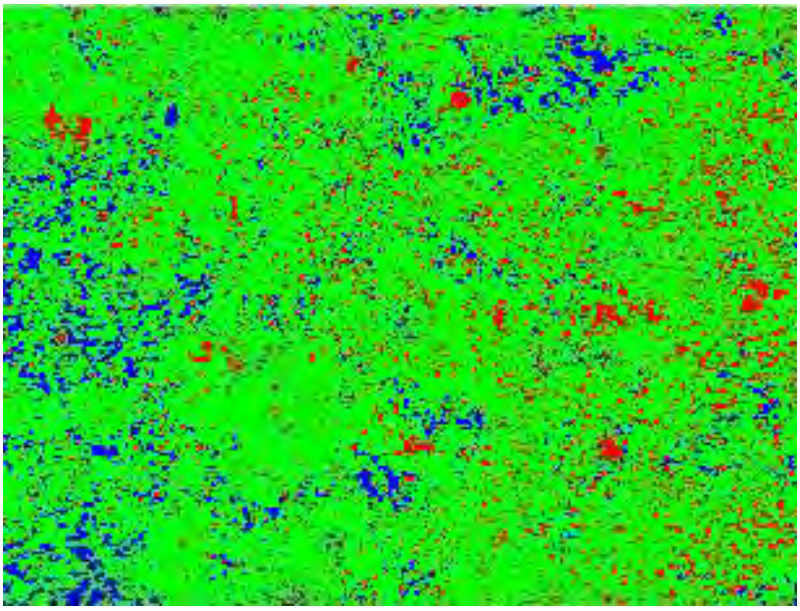

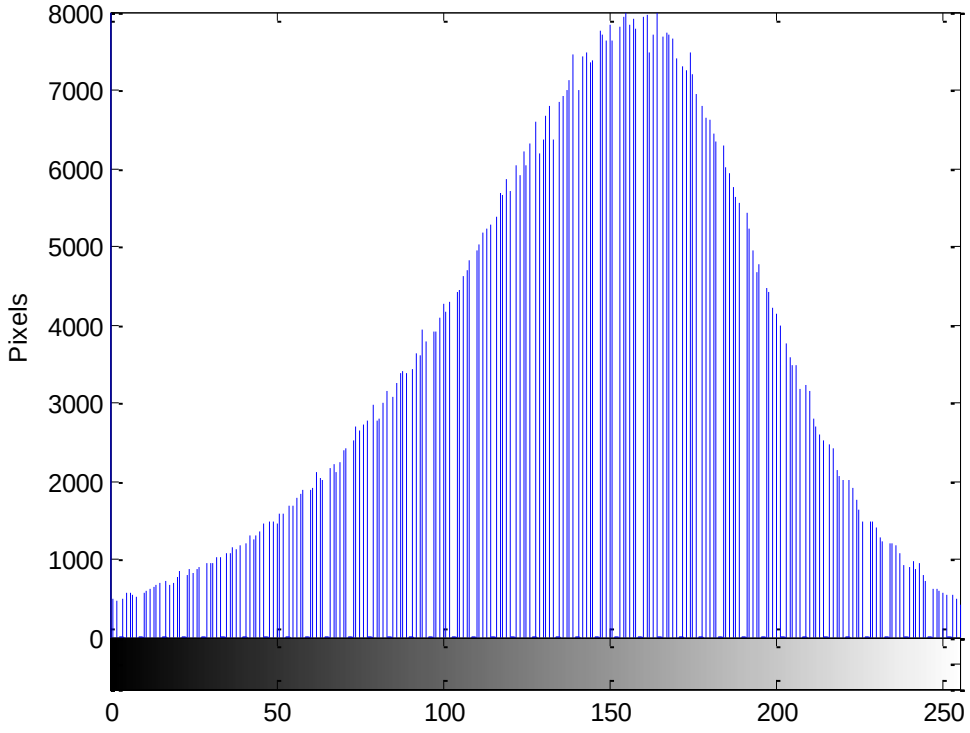
Pixels
8000
7000
6000
5000
4000
3000
2000
1000
0
0
50
100
150
200
250

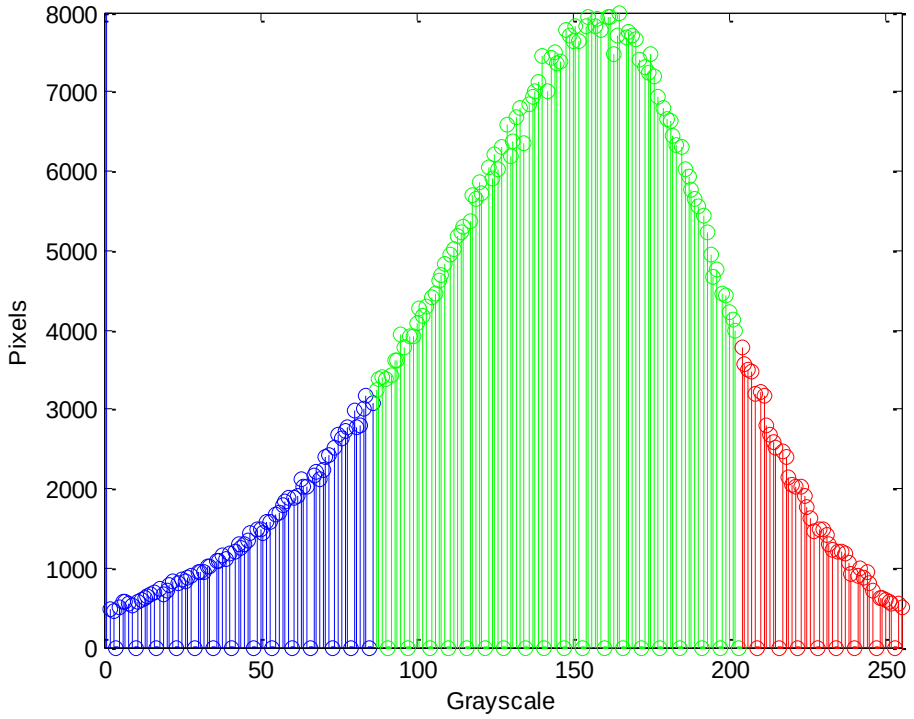

Porosity is 15%

CSH is 75%

CH is 10%

10% Silica Fume Vacuum Cured at 7 Days

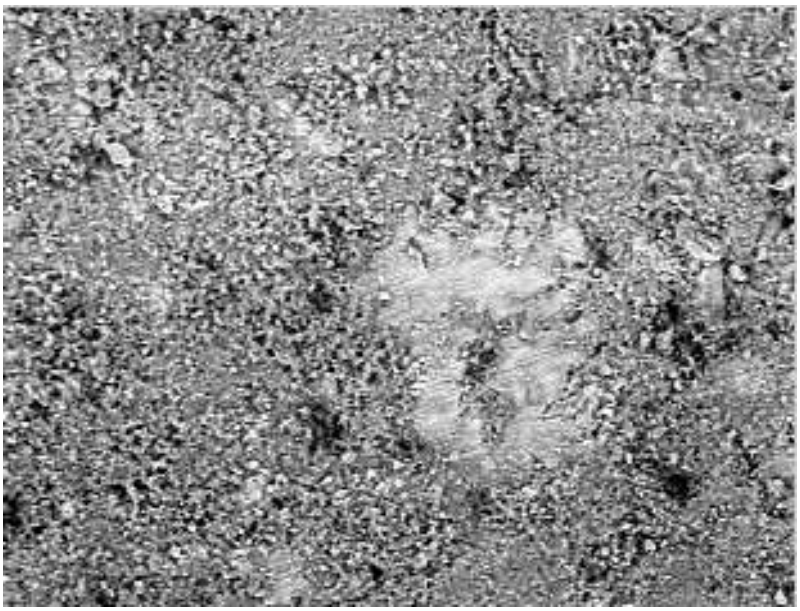

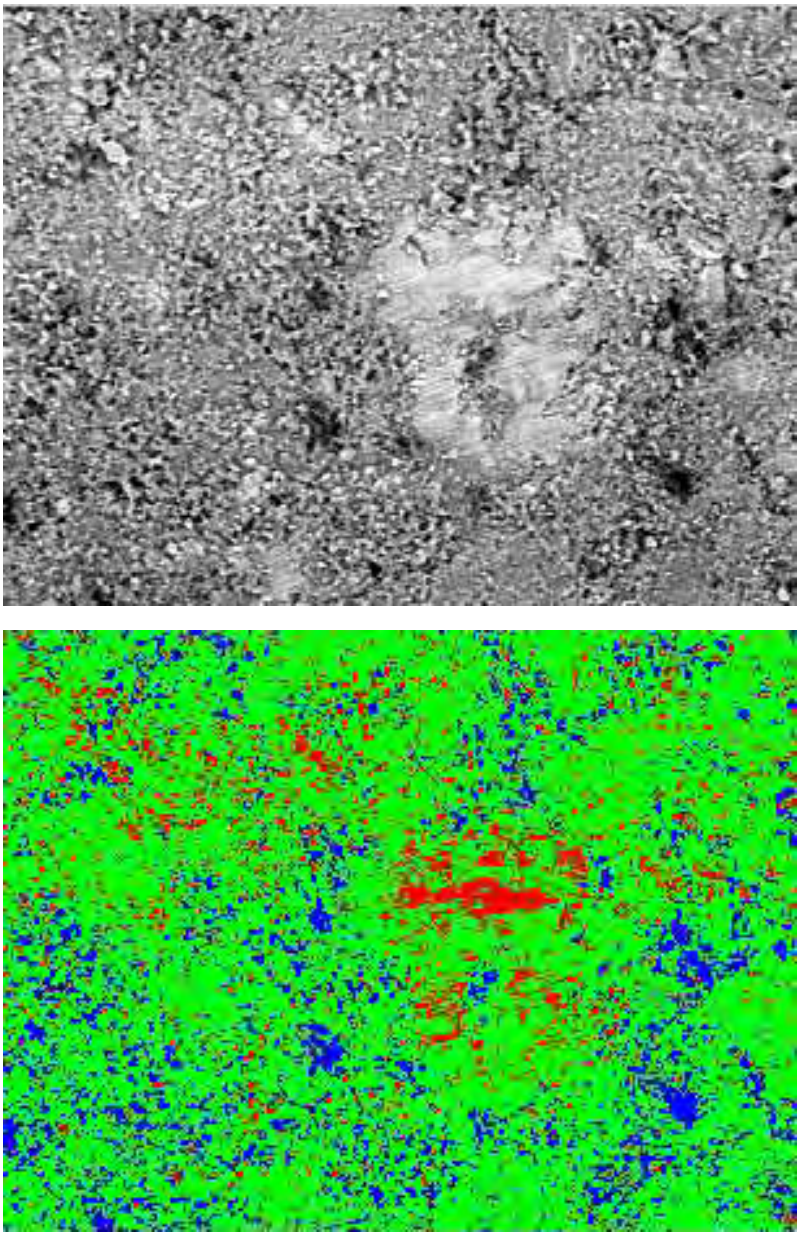

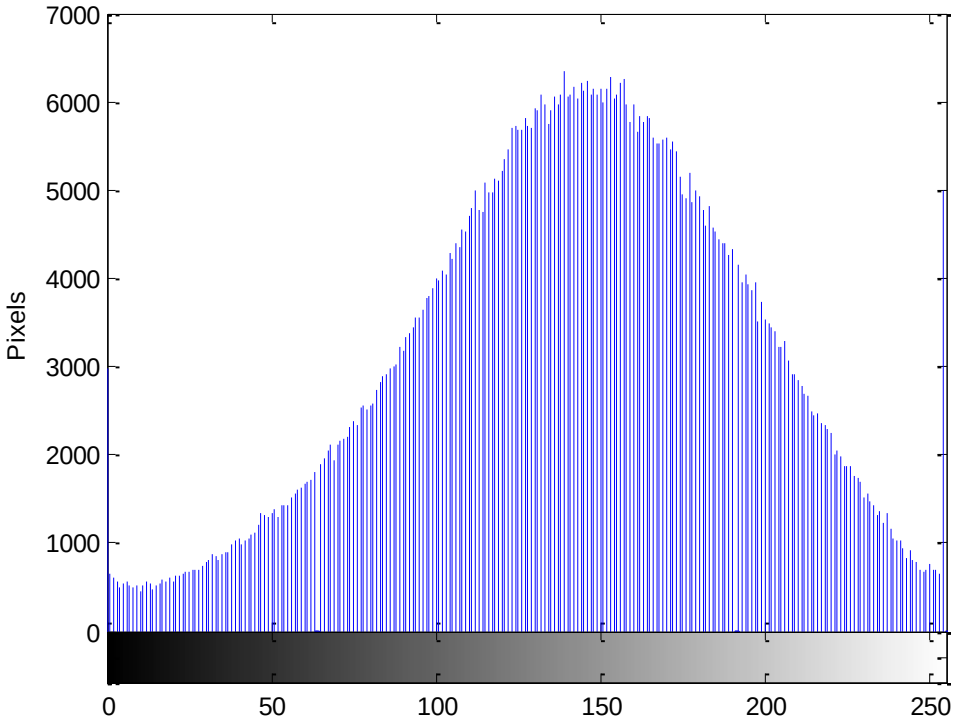
7000
6000
5000
4000
3000
2000
1000
0
Pixels
0
50
100
150
200
250

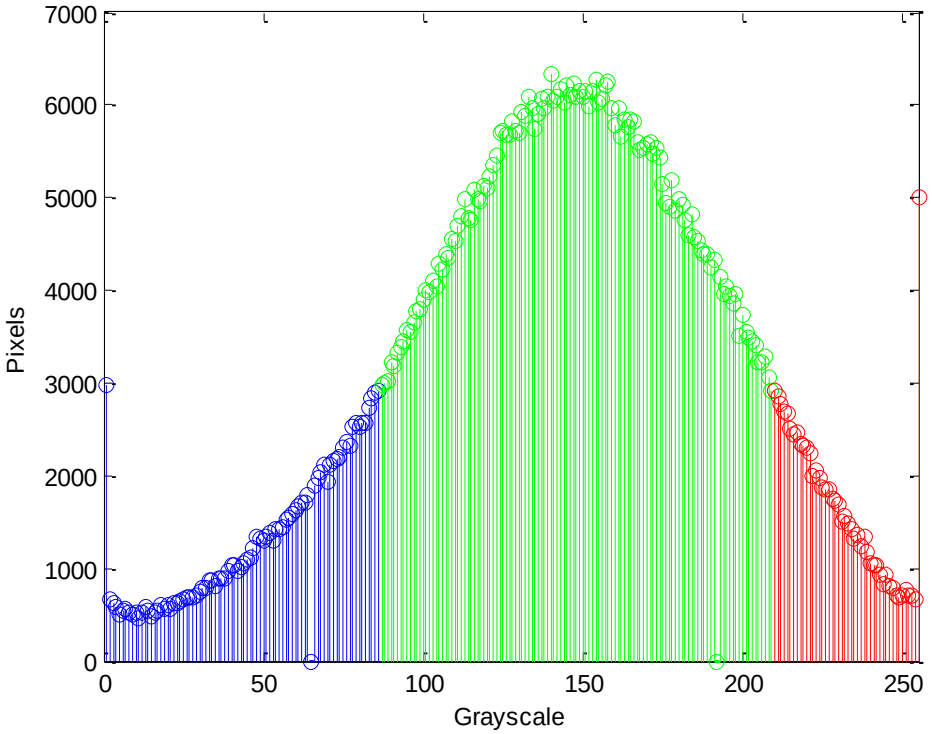
7000
6000
5000
4000
3000
2000
1000
0
Pixels
0
50
100
150
200
250
Grayscale

Porosity is 14%

CSH is 76%

CH is 10%

10% Silica Fume Vacuum Cured at 14 Days

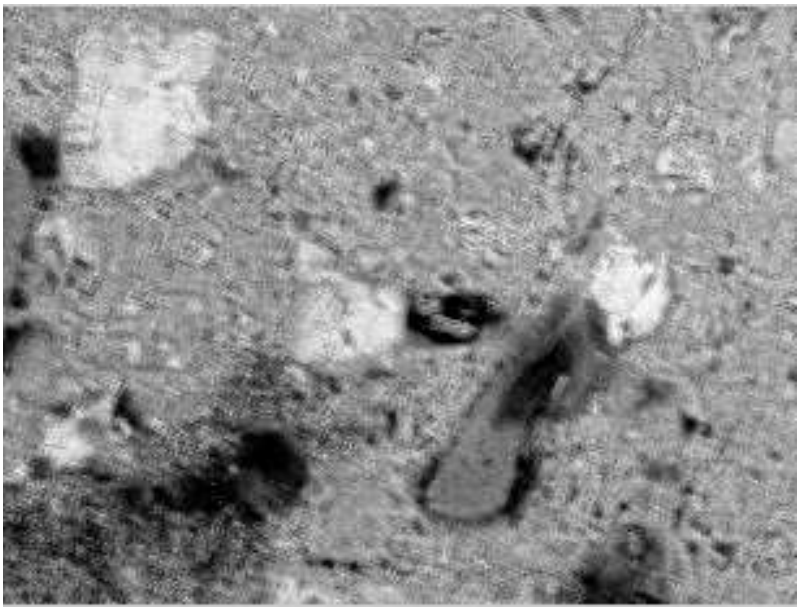

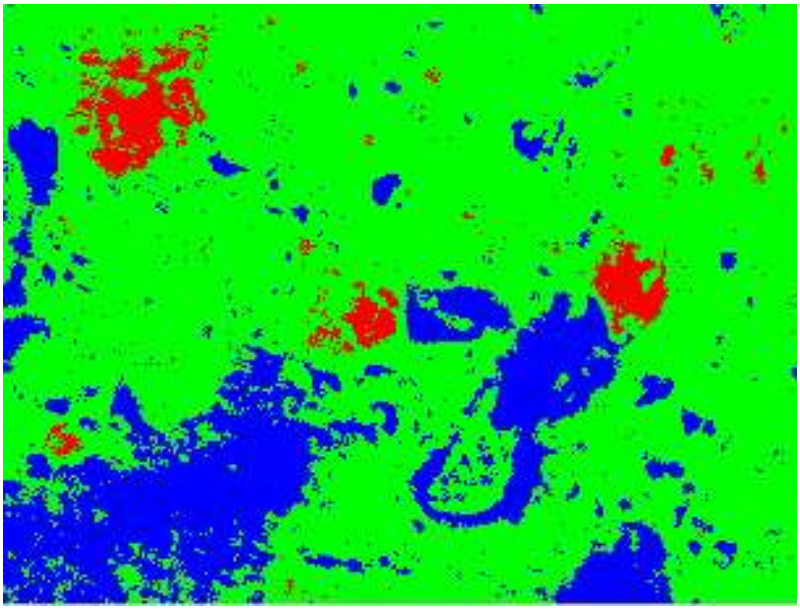

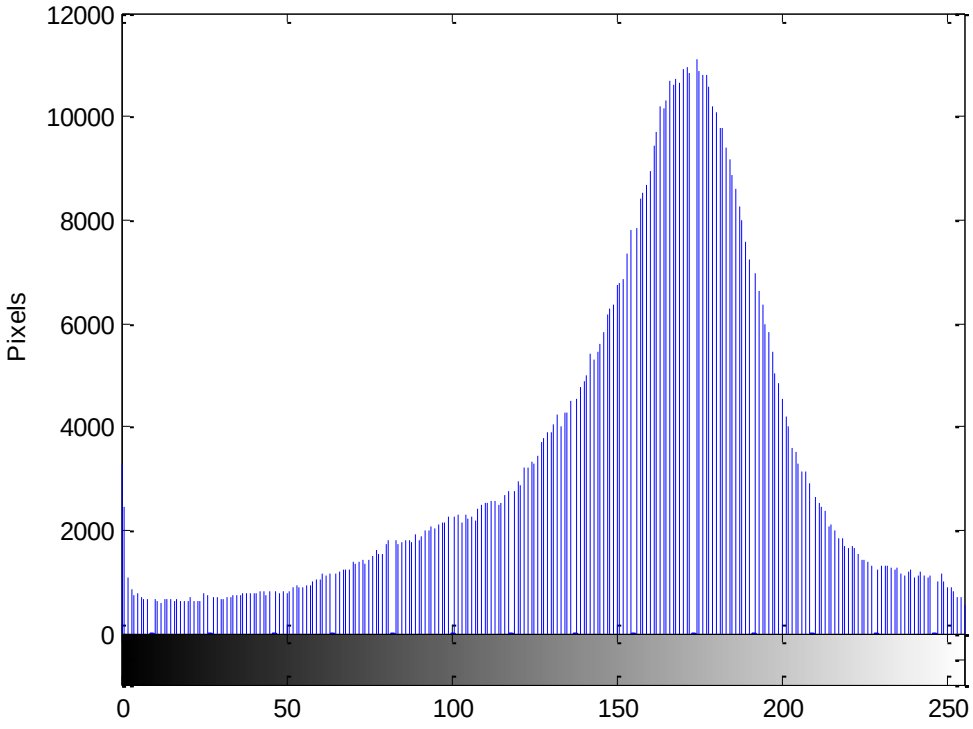
12000
10000
8000
6000
4000
2000
0
Pixels
0
50
100
150
200
250

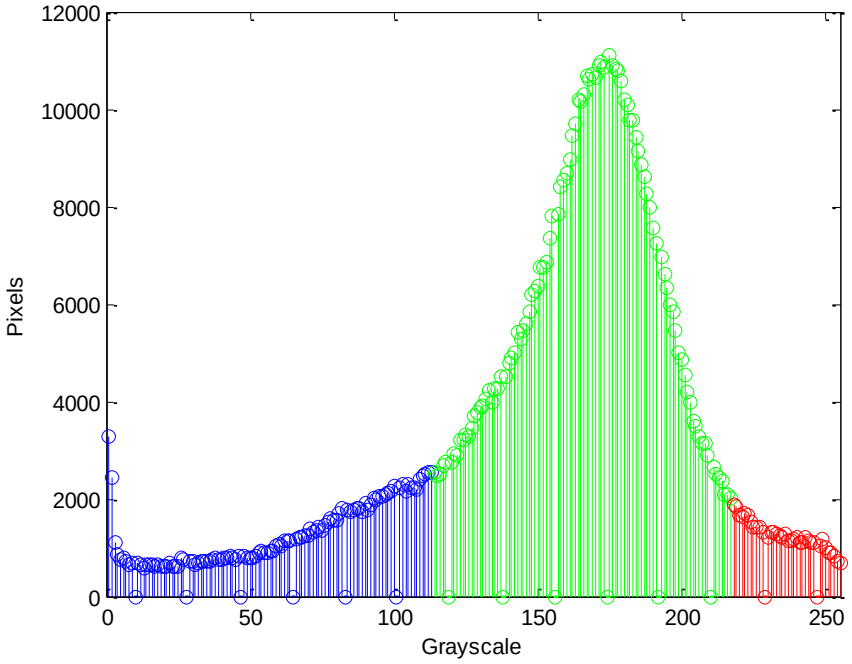

Porosity is 17%

CSH is 77%

CH is 6%

10% Silica Fume Vacuum Cured at 28 Days

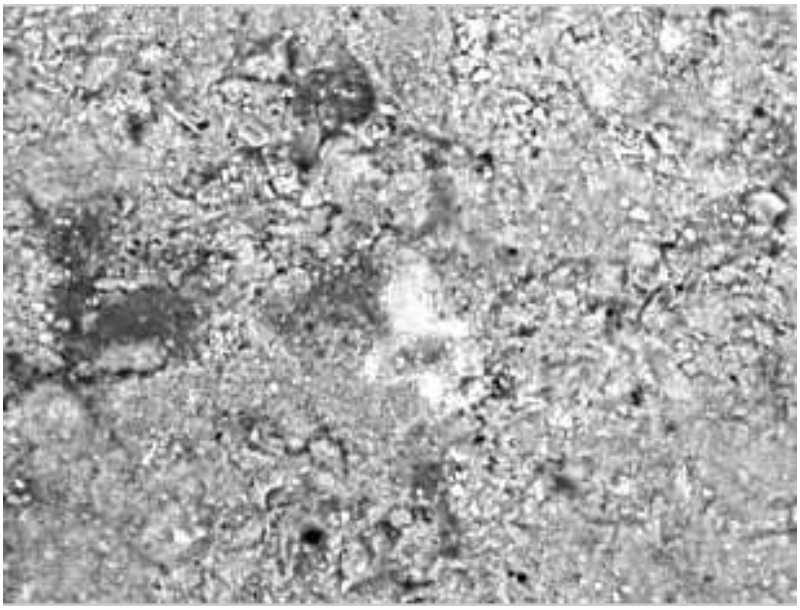

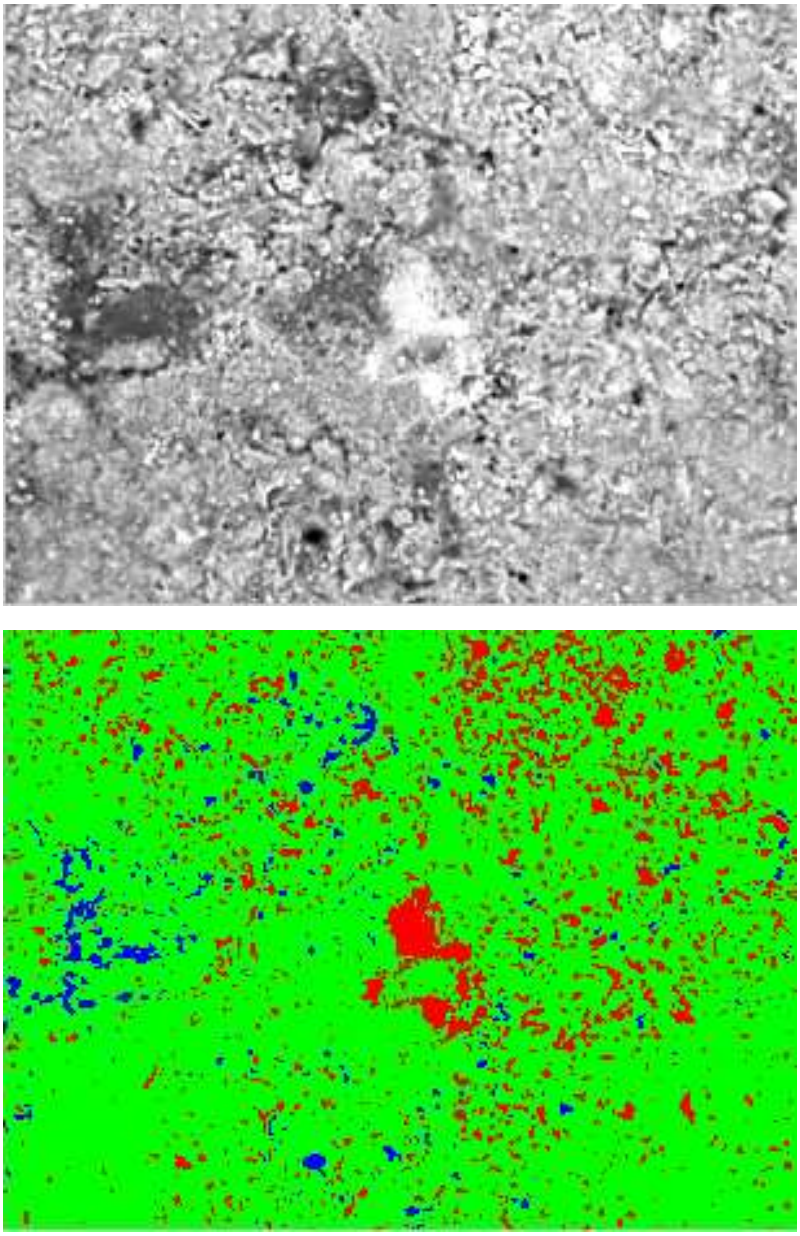

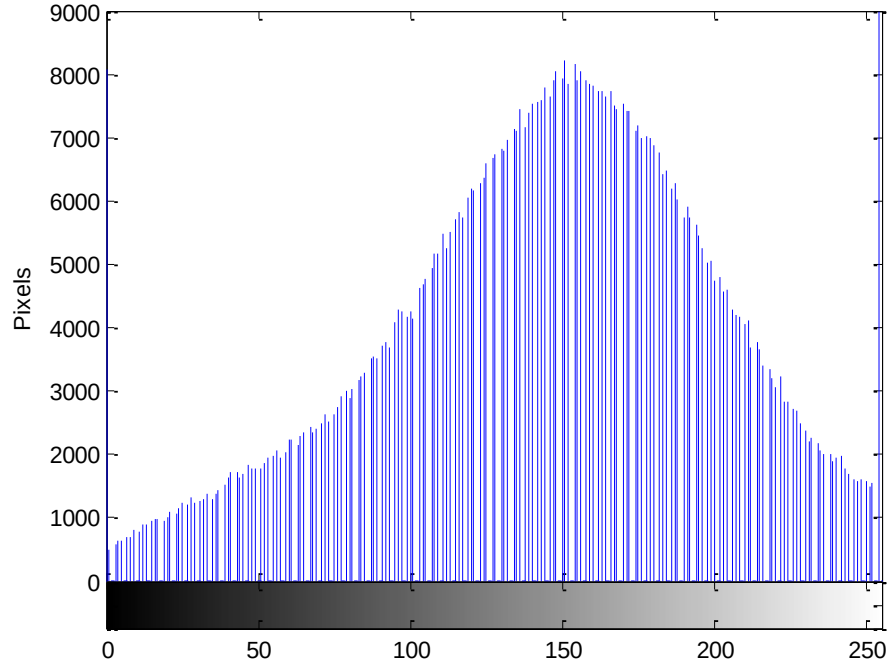

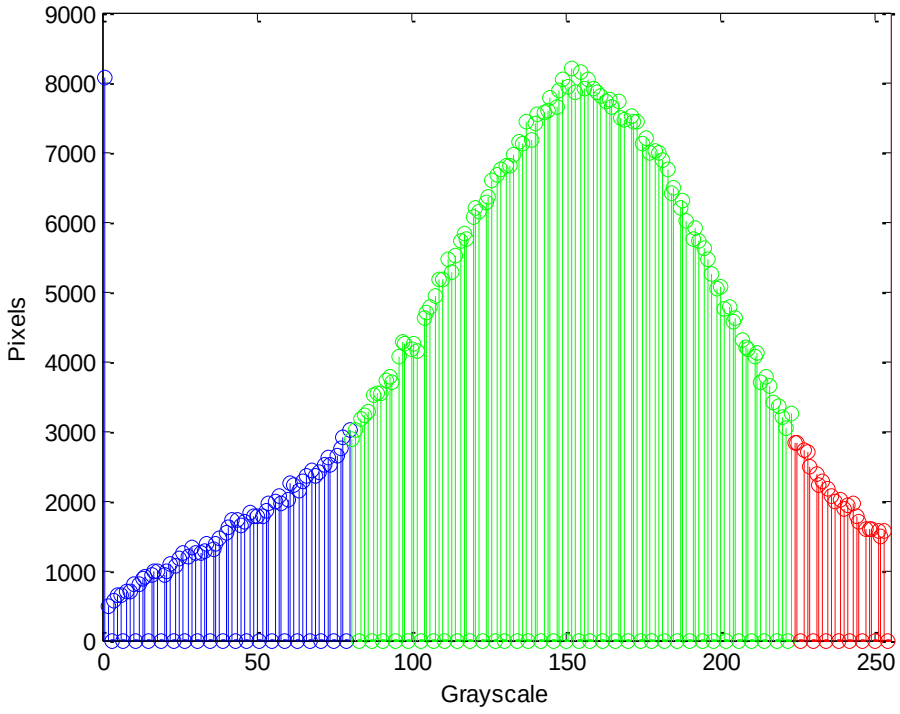

Porosity is 13%

CSH is 79%

CH is 8%

10% Silica Fume Vacuum Cured at 56 Days

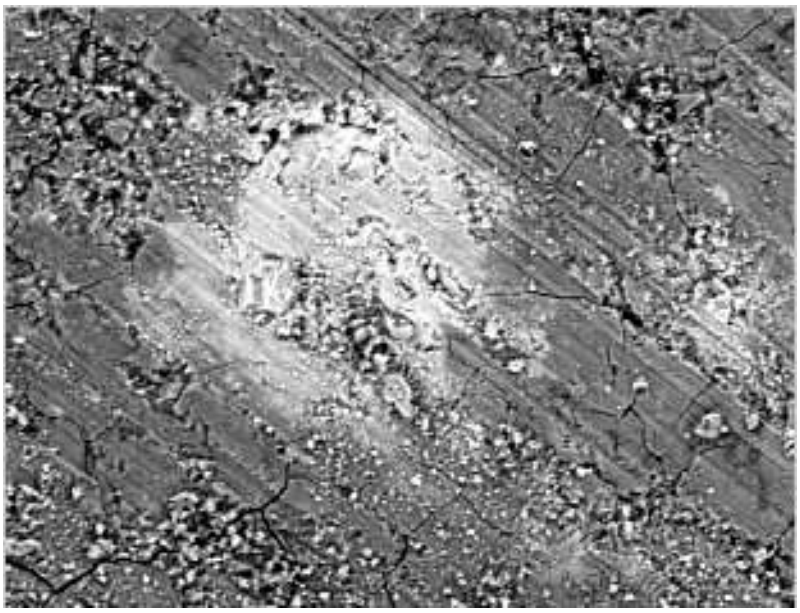

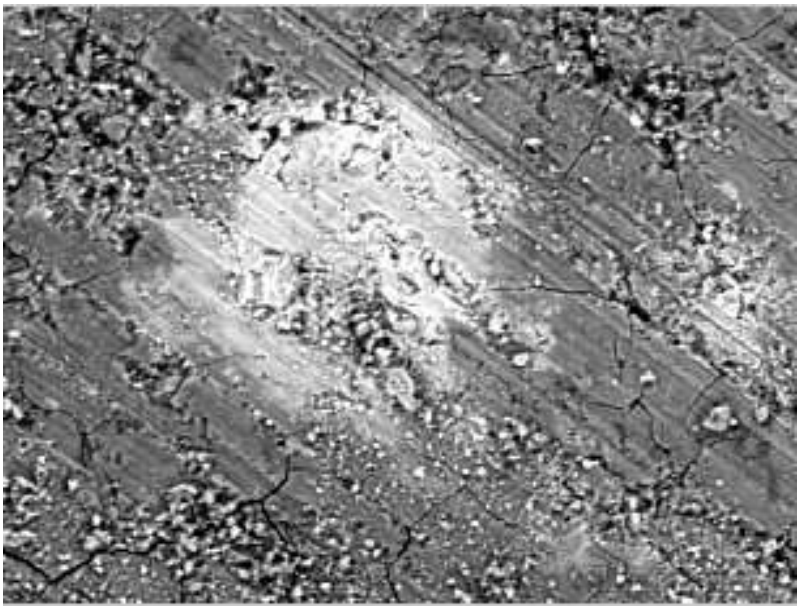

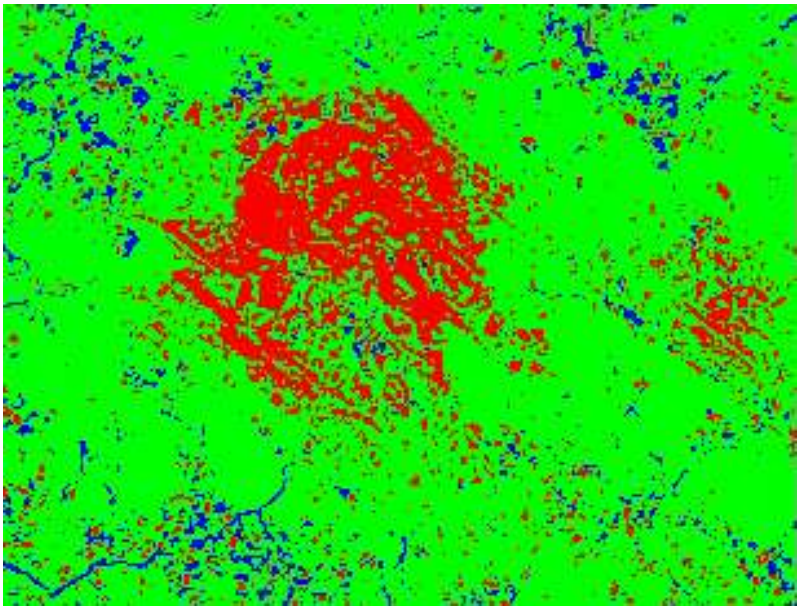

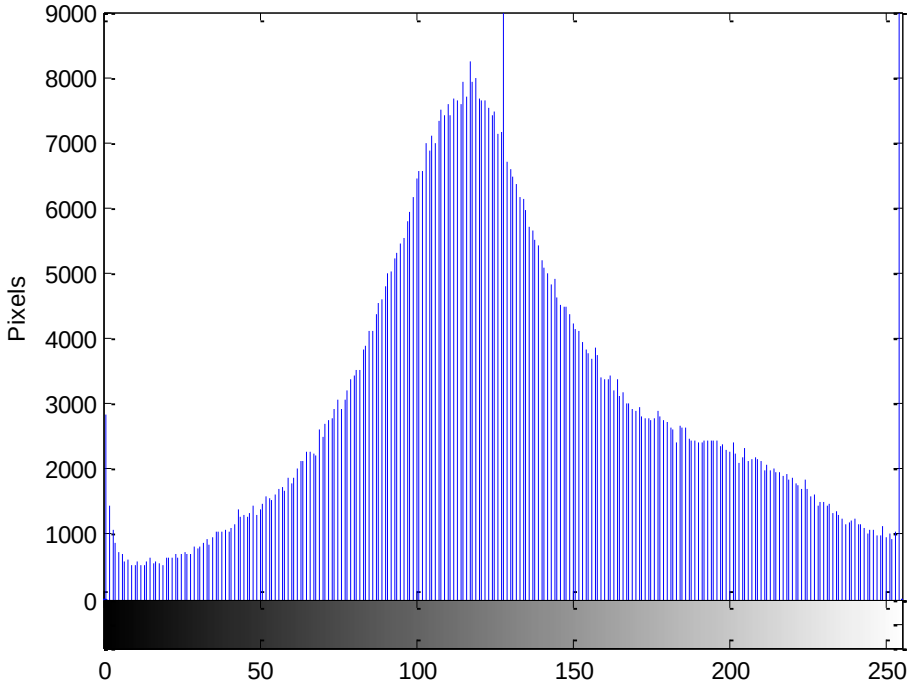
Pixels
9000
8000
7000
6000
5000
4000
3000
2000
1000
0
0
50
100
150
200
250

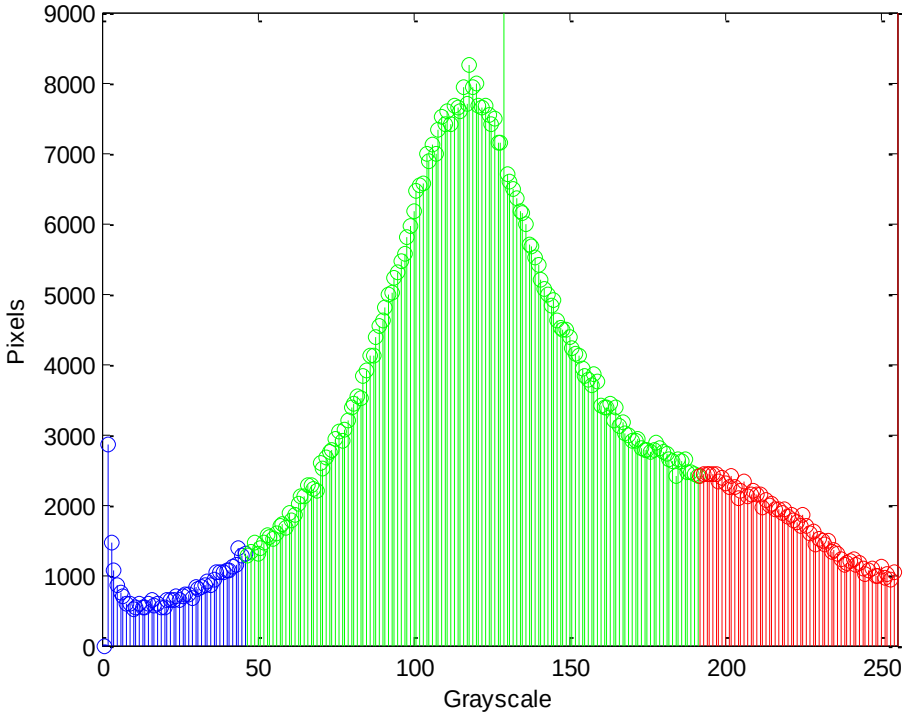

Porosity is 5%

CSH is 80%

CH is 15%

10% Silica Fume Water Cured at 3 Days

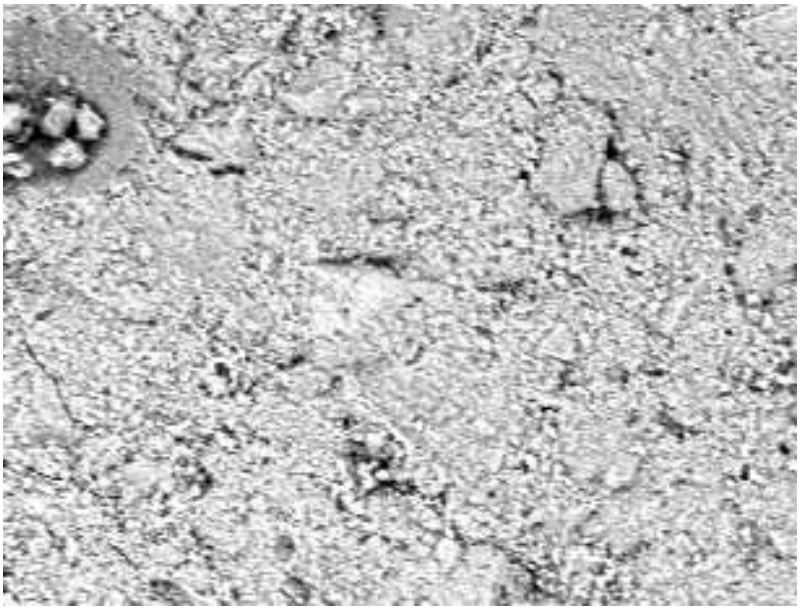

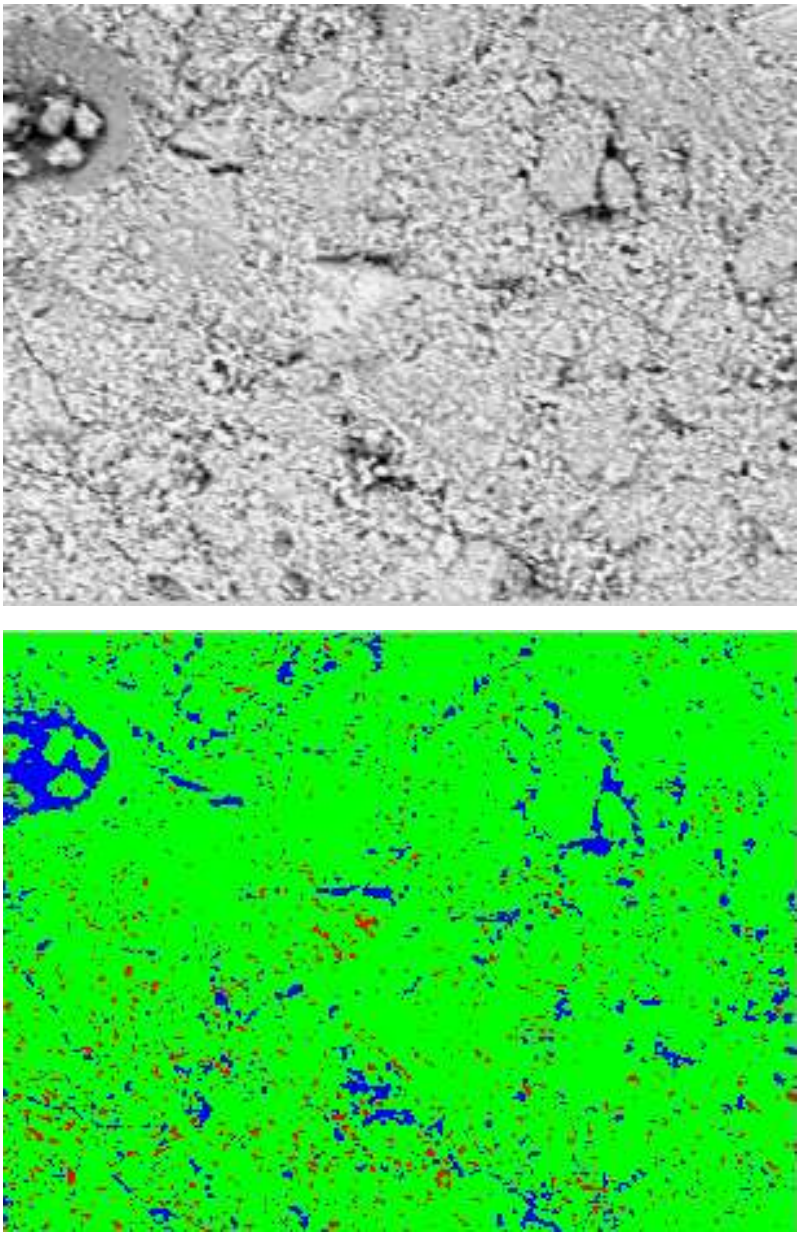

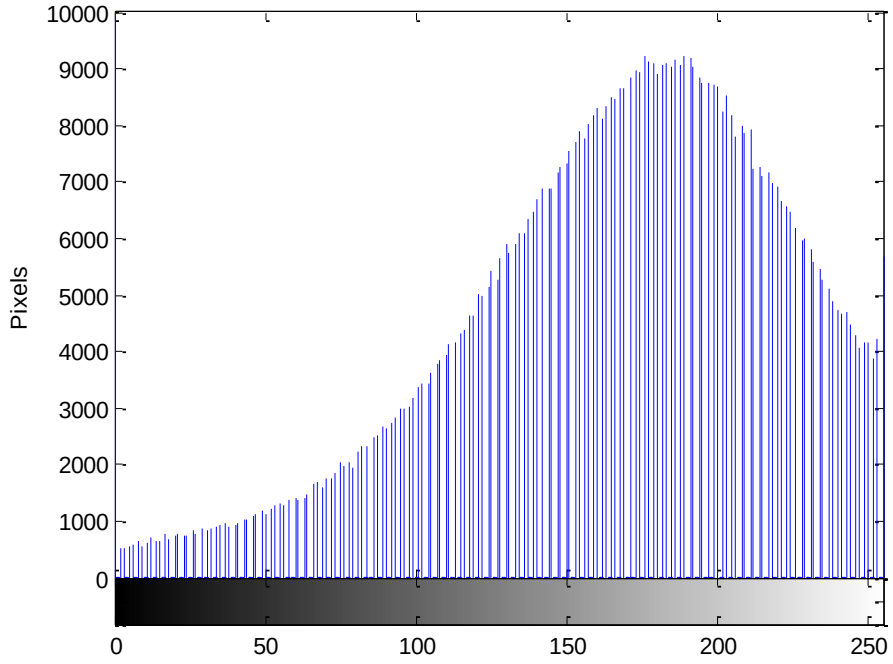

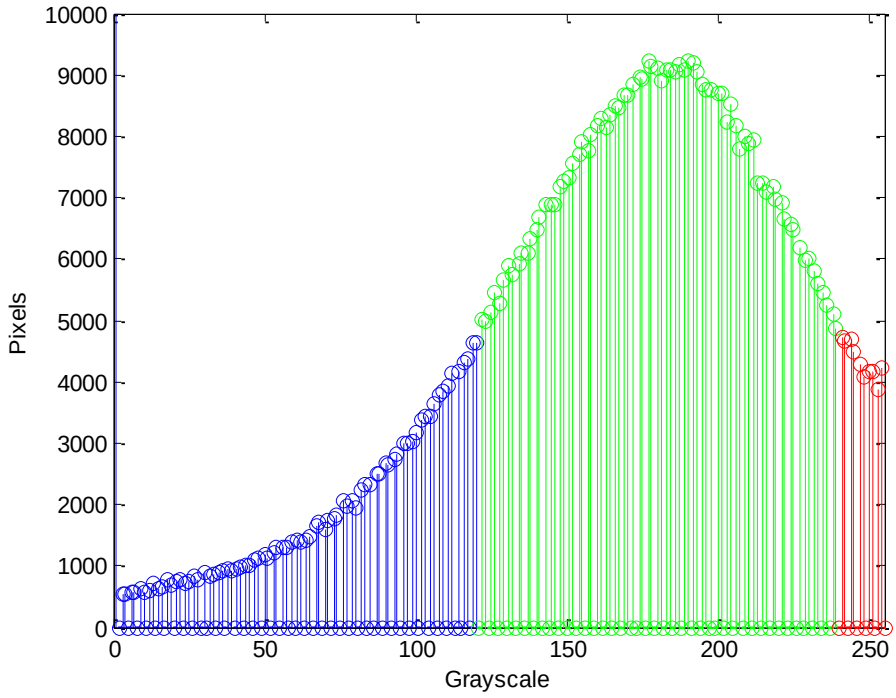

Porosity is 20%

CSH is 74%

CH is 6%

10% Silica Fume Water Cured at 7 Days

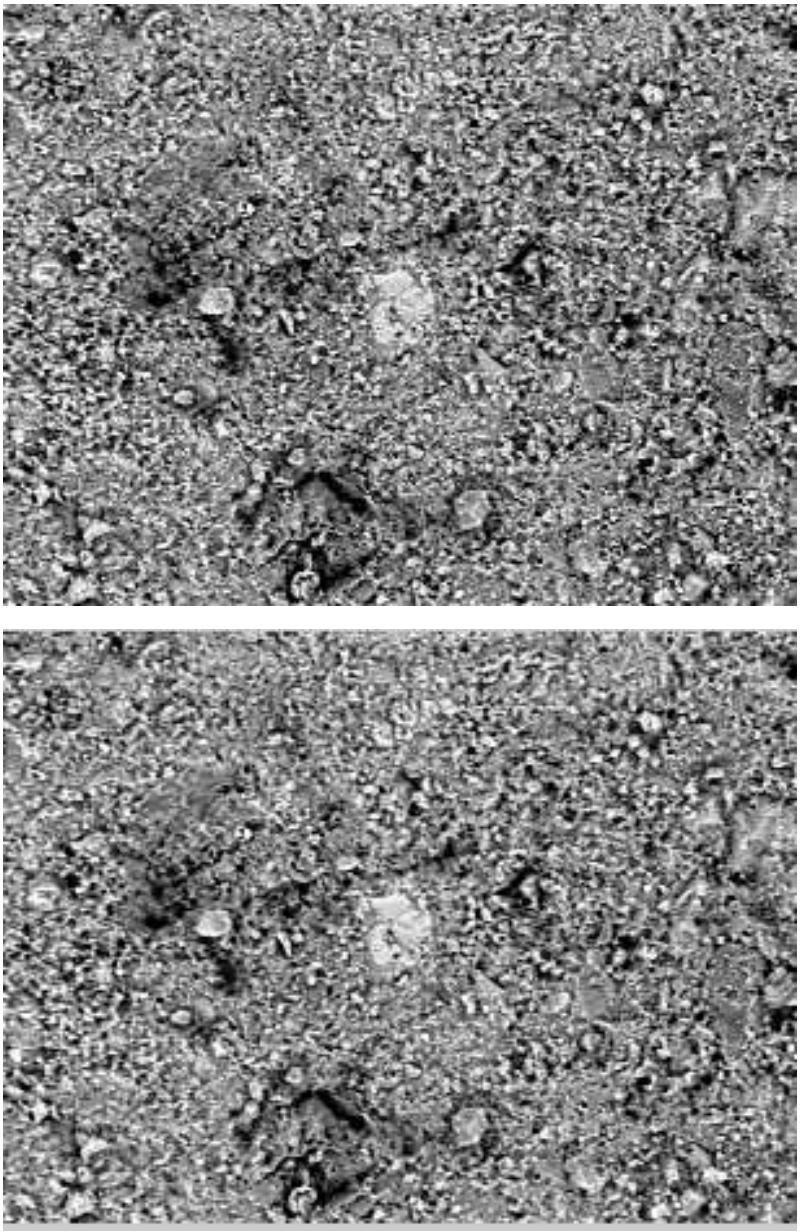

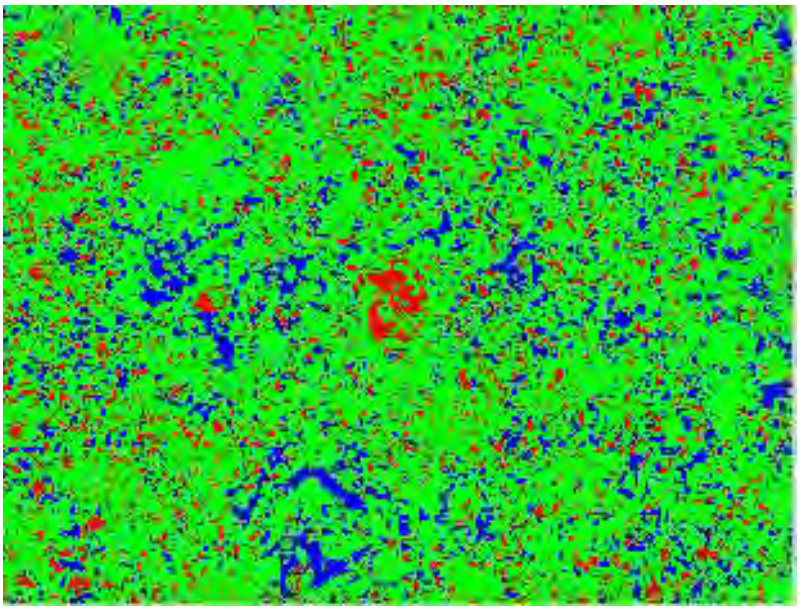

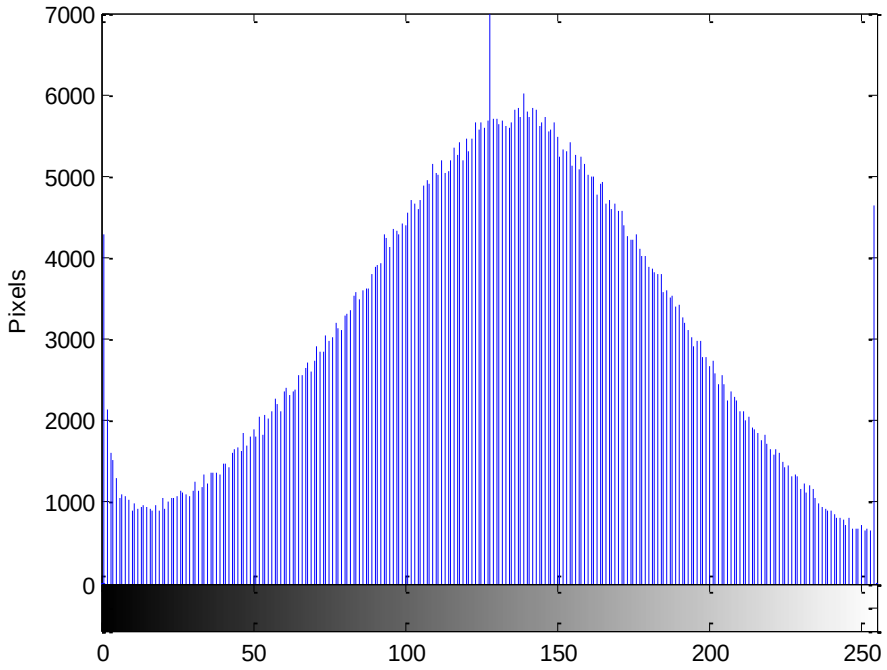
Pixels
7000
6000
5000
4000
3000
2000
1000
0
0
50
100
150
200
250

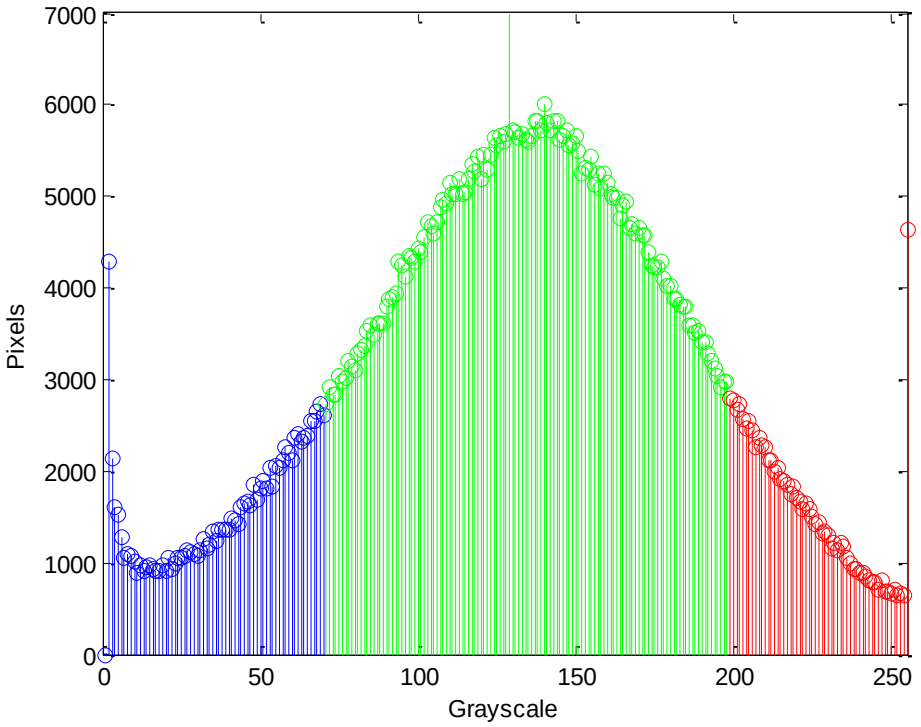

Porosity is 14%

CSH is 75%

CH is 11%

10% Silica Fume Water Cured at 14 Days

OUT

10% Silica Fume Water Cured at 28 Days

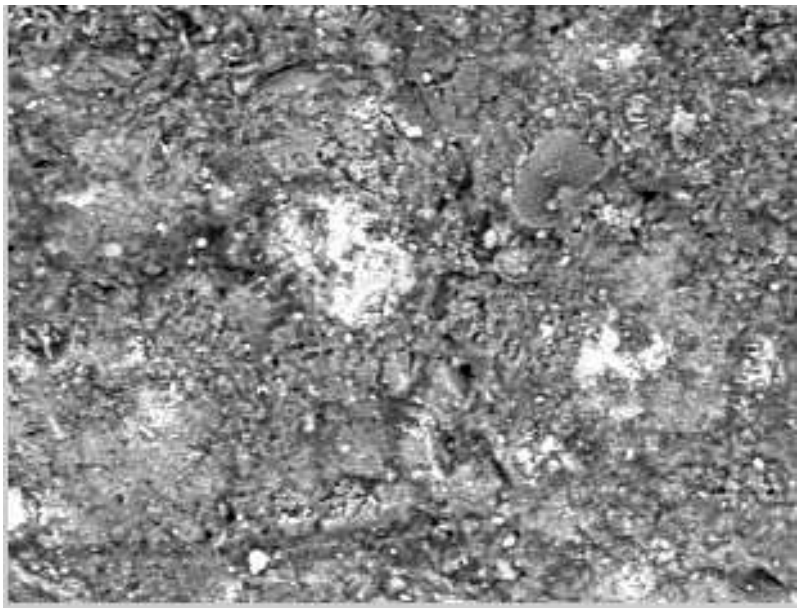

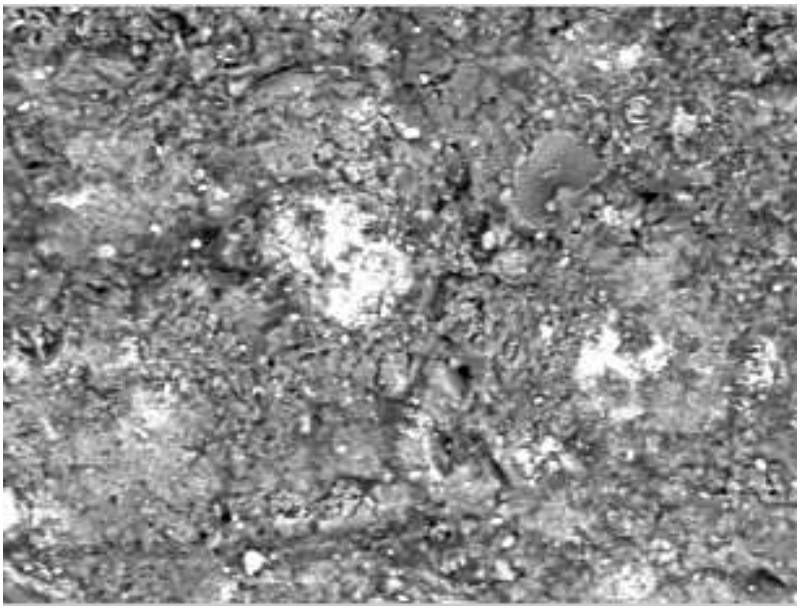

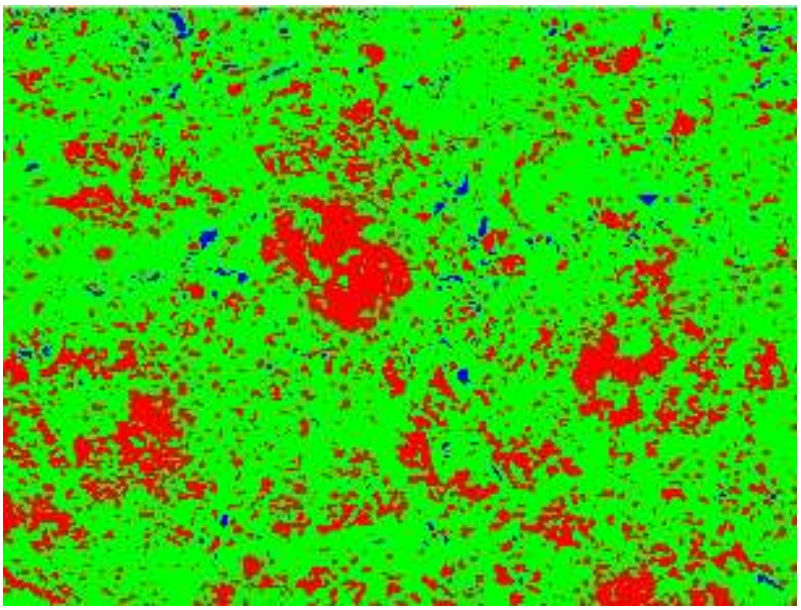

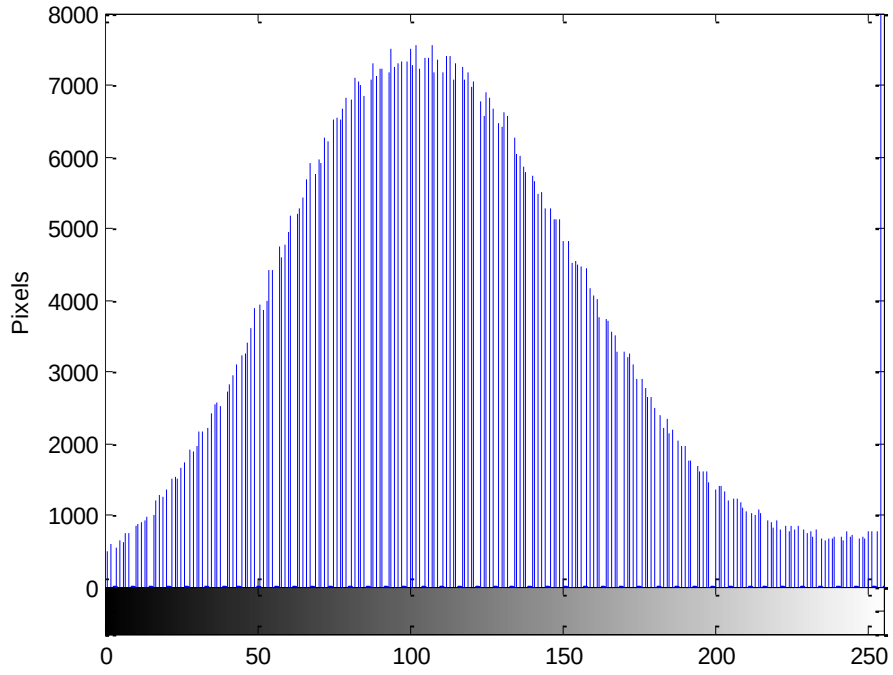
Pixels
8000
7000
6000
5000
4000
3000
2000
1000
0
0
50
100
150
200
250

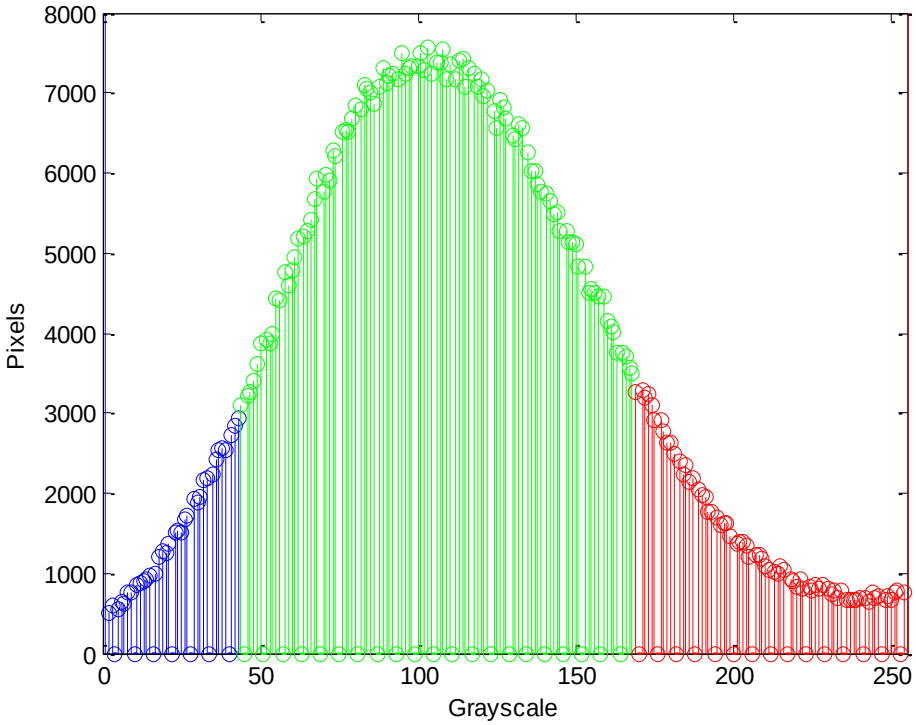

Porosity is 8%

CSH is 78%

CH is 14%

10% Silica Fume Water Cured at 56 Days

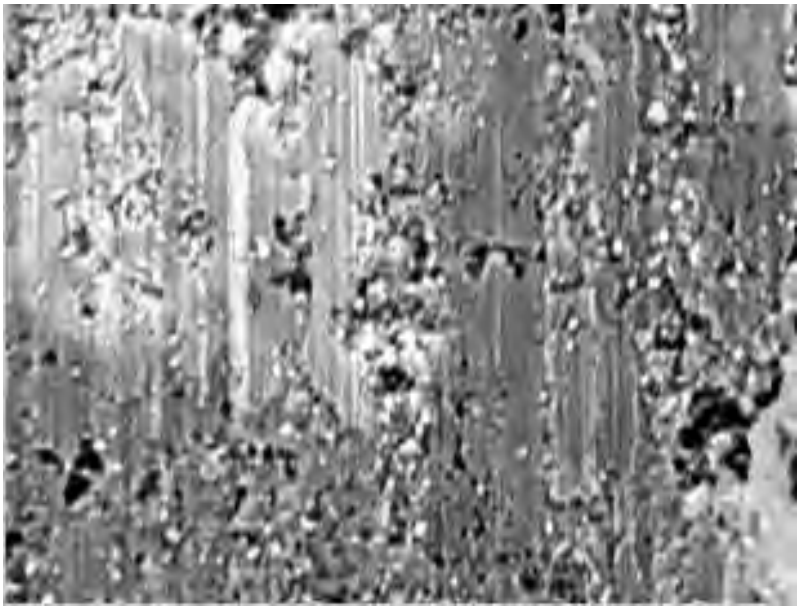

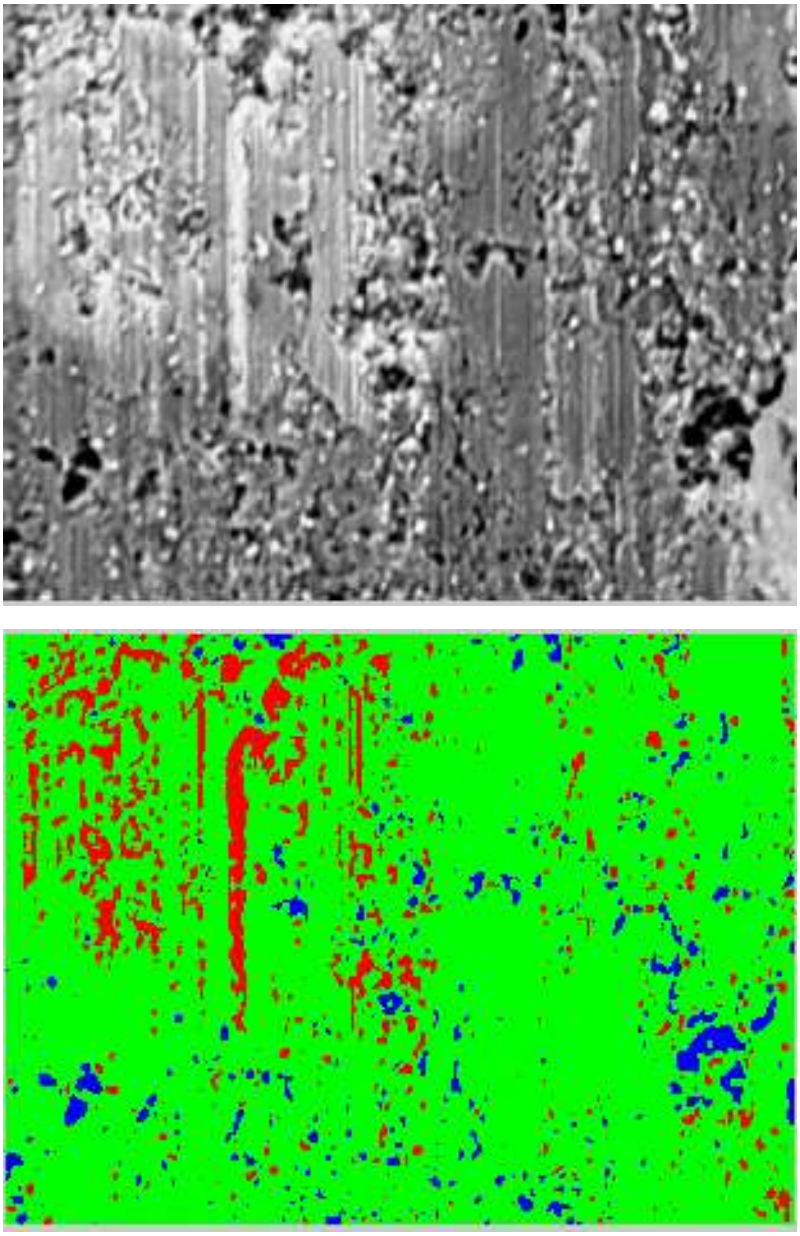

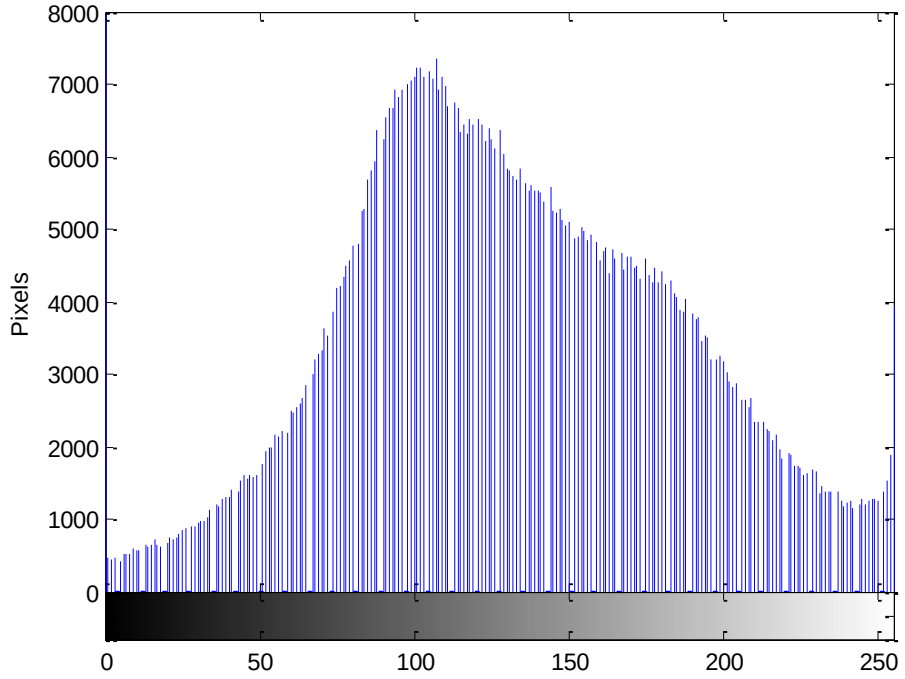

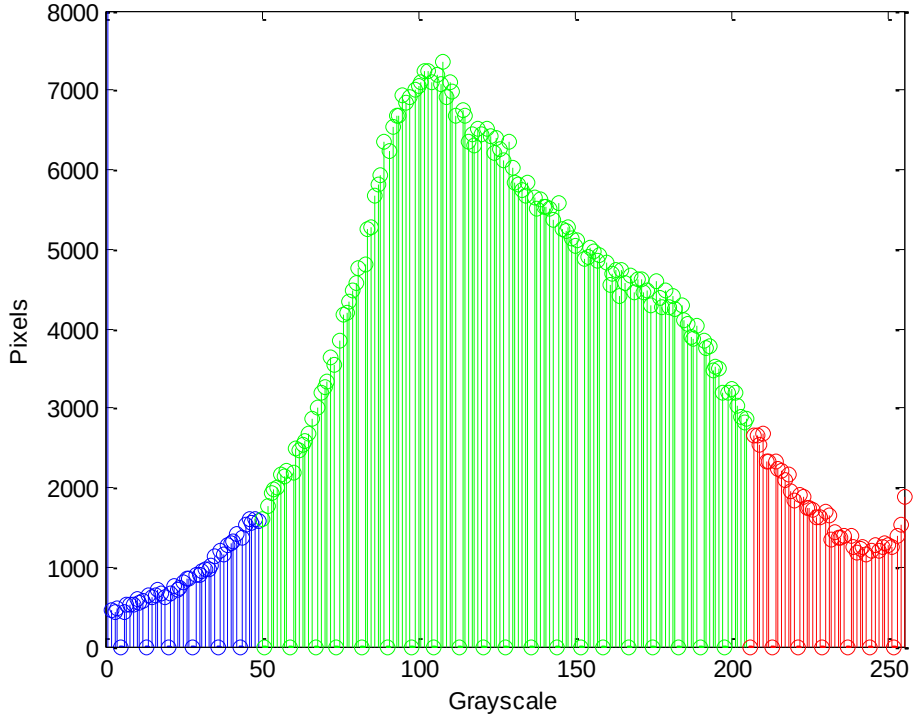

Porosity is 7%

CSH is 84%

CH is 10%

Appendix C: FTIR Spectra

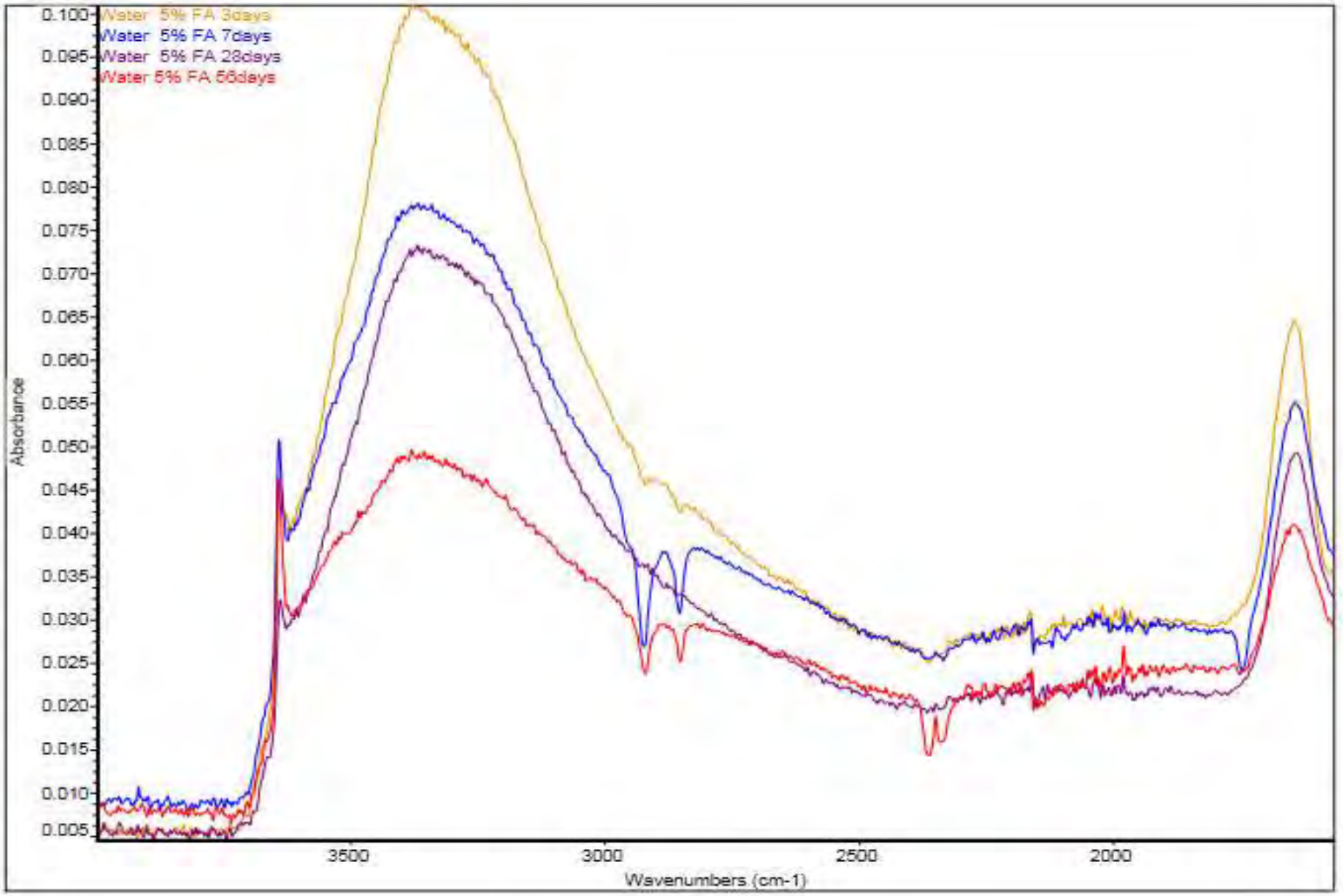

Spectra of 5% fly ash cement replacement for 3, 7, 28 and 56 days after water curing. The spectra are shown offset for clarity.

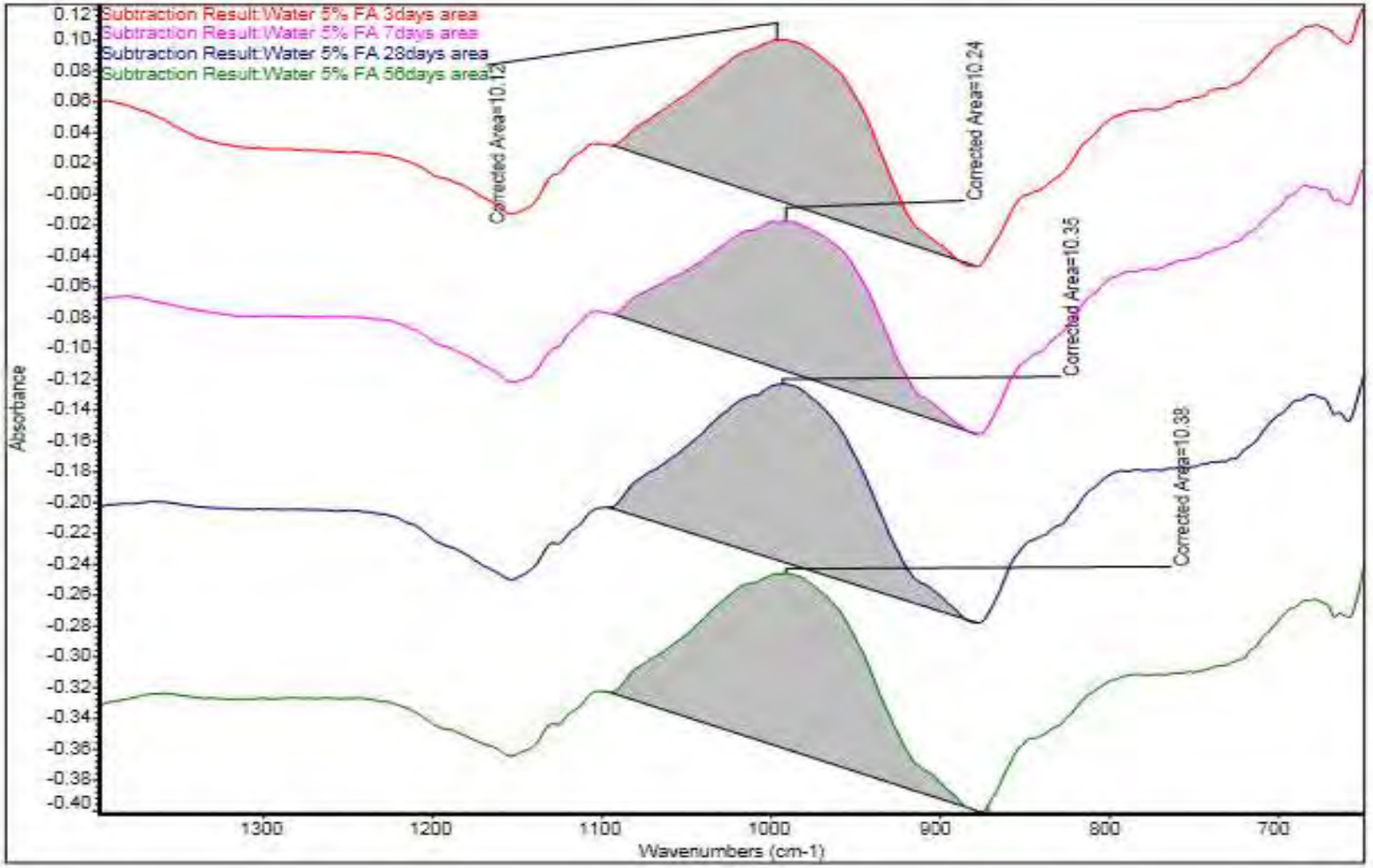

Difference spectra where the absorbance spectrum of as received dry cement has been subtracted from the absorbance spectra of 5% fly ash of cement replacement hydrated for 3, 7, 28 and 56 days after water curing. Reference samples zoomed to range of 700 - 1400 cm^{-1}; with area of possible CSH highlighted. The spectra are shown offset for clarity.

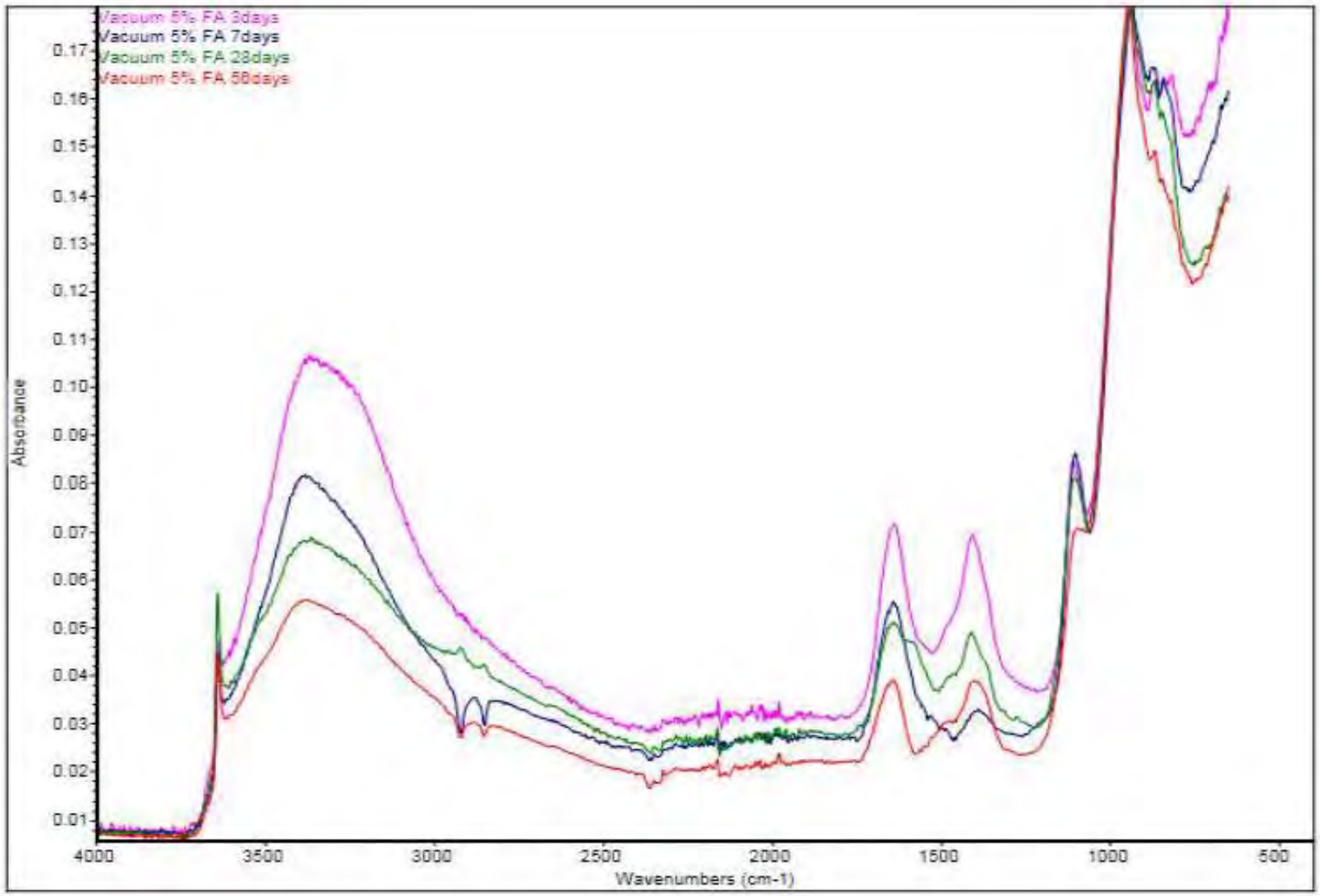

Spectra of 5% fly ash cement replacement for 3, 7, 28 and 56 days after vacuum curing. The spectra are shown offset for clarity.

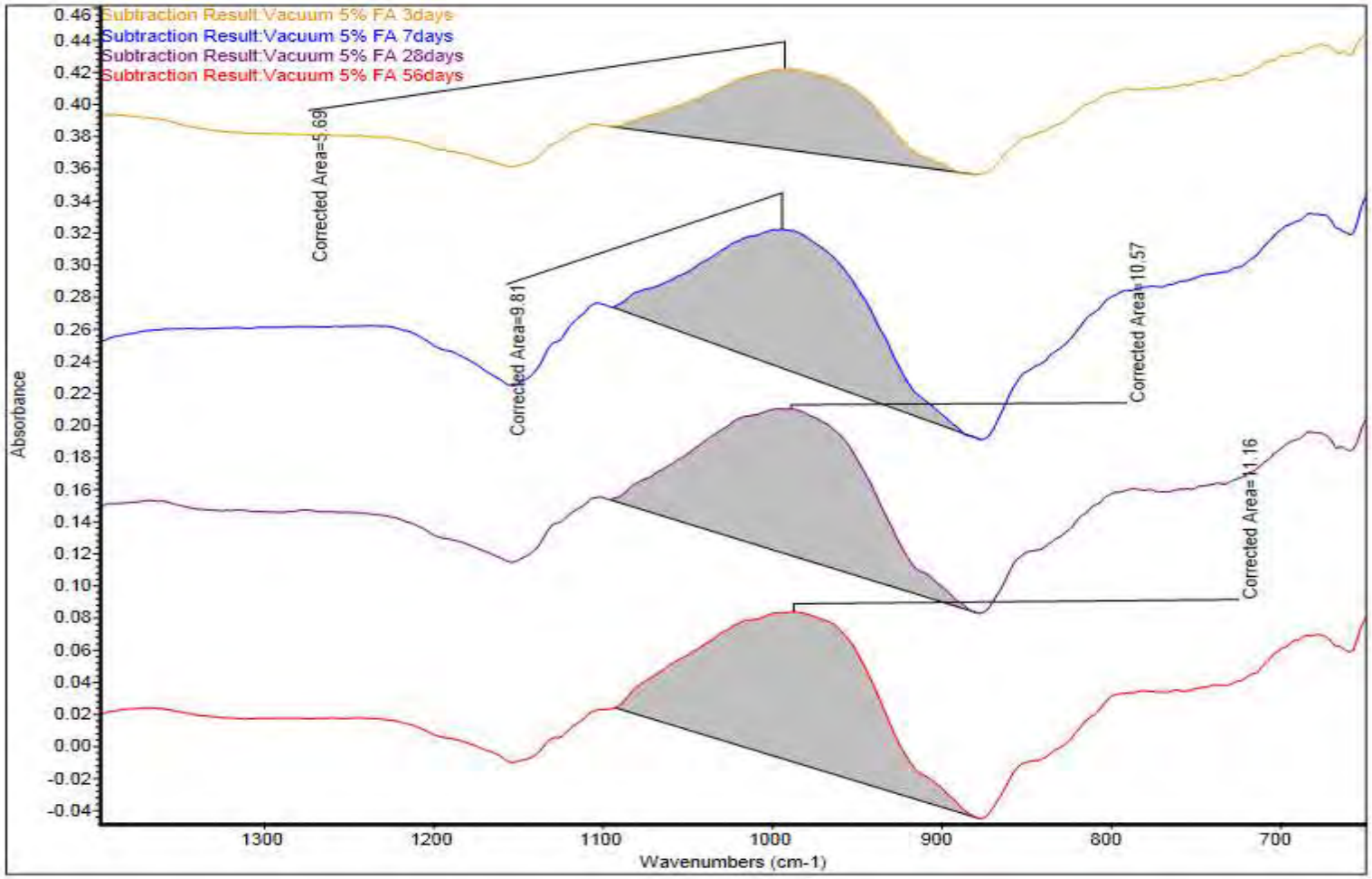

Difference spectra where the absorbance spectrum of as received dry cement has been subtracted from the absorbance spectra of 5% fly ash of cement replacement hydrated for 3, 7, 28 and 56 days after vacuum curing. Reference samples zoomed to range of 700 - 1400 cm^{-1}; with area of possible CSH highlighted. The spectra are shown offset for clarity.

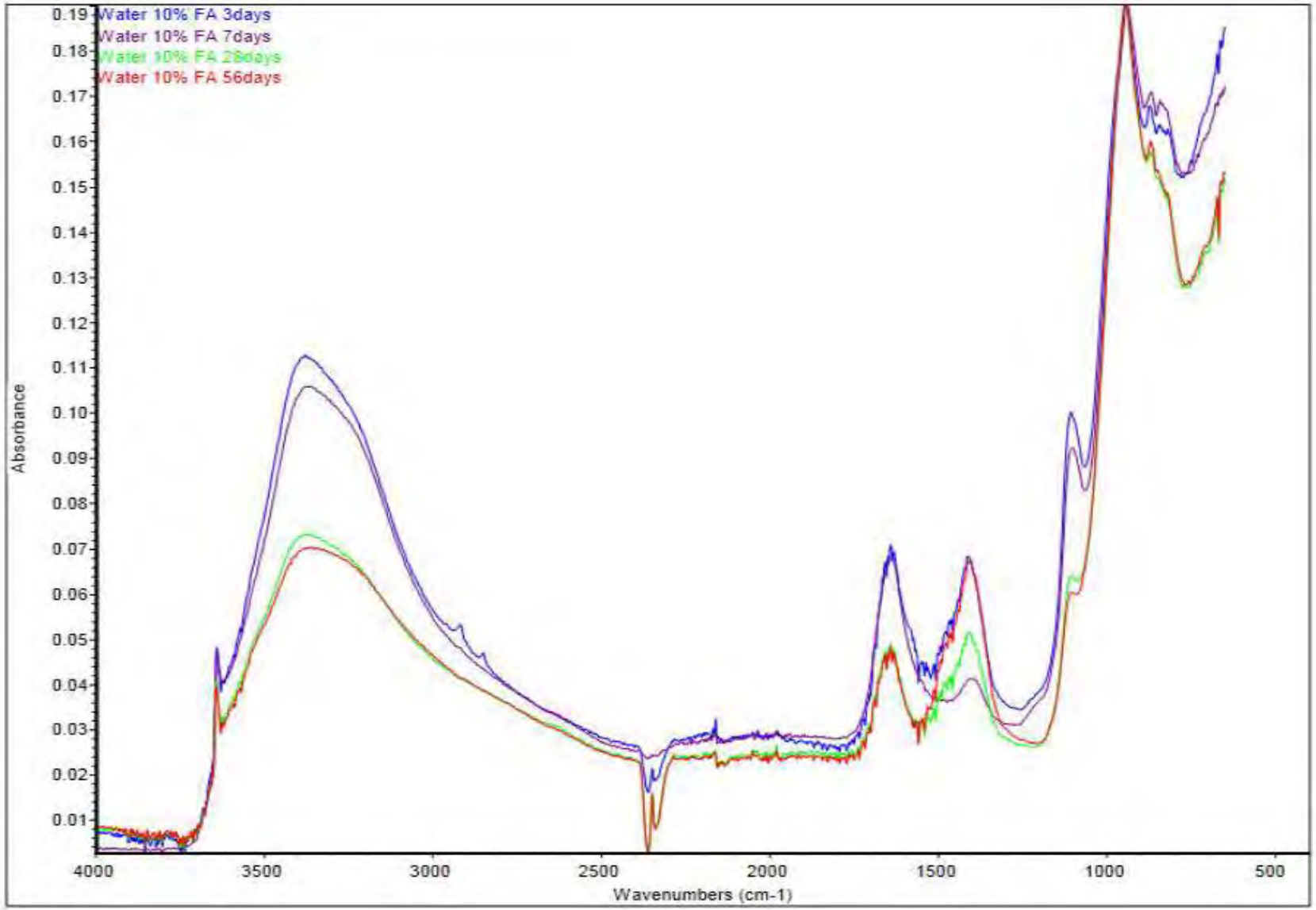

Spectra of 10% fly ash cement replacement for 3, 7, 28 and 56 days after water curing. The spectra are shown offset for clarity.

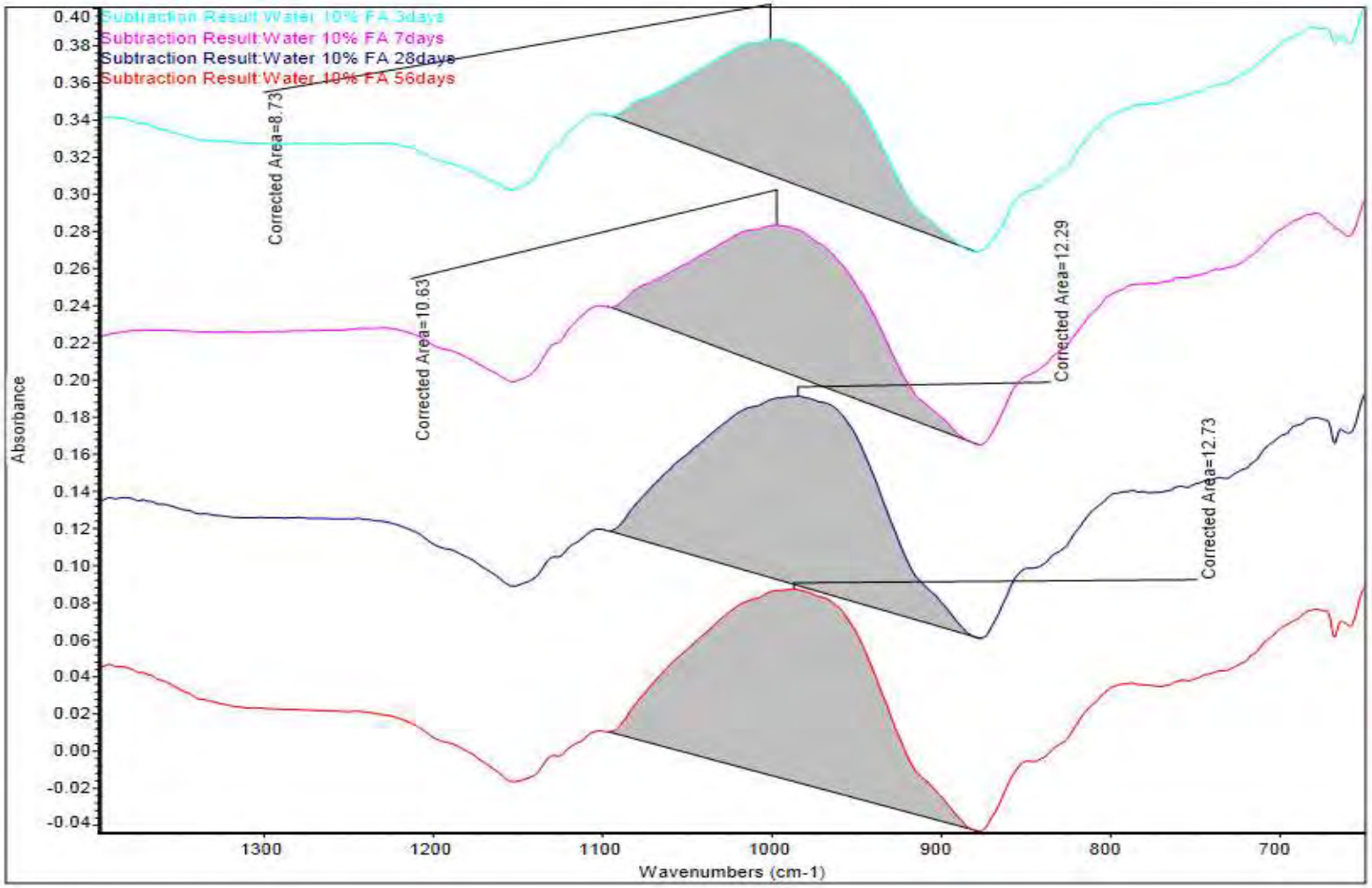

Difference spectra where the absorbance spectrum of as received dry cement has been subtracted from the absorbance spectra of 10% fly ash of cement replacement hydrated for 3, 7, 28 and 56 days after water curing. Reference samples zoomed to range of 700 - 1400 cm^{-1}; with area of possible CSH highlighted. The spectra are shown offset for clarity.

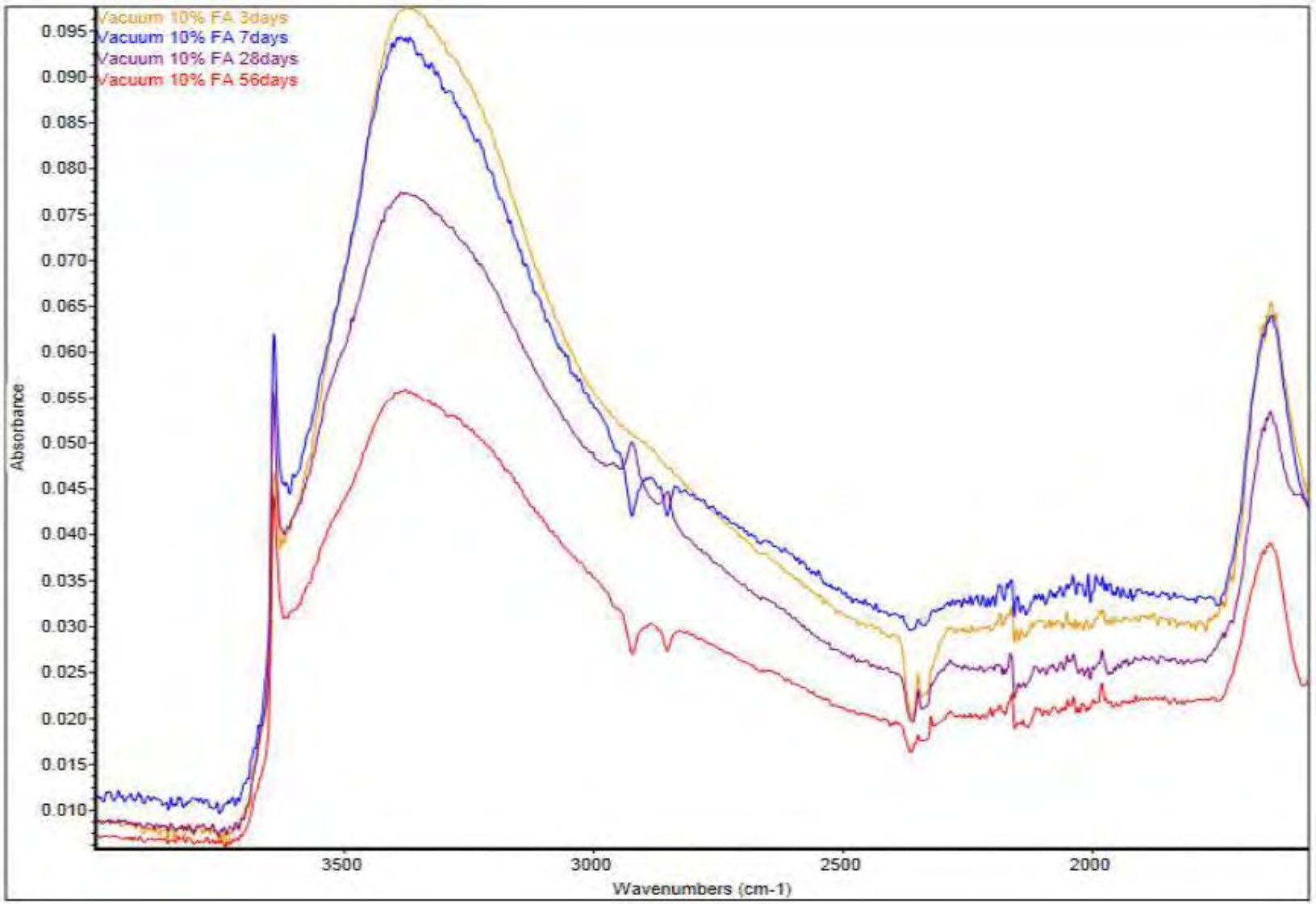

Spectra of 10% fly ash cement replacement for 3, 7, 28 and 56 days after vacuum curing. The spectra are shown offset for clarity.

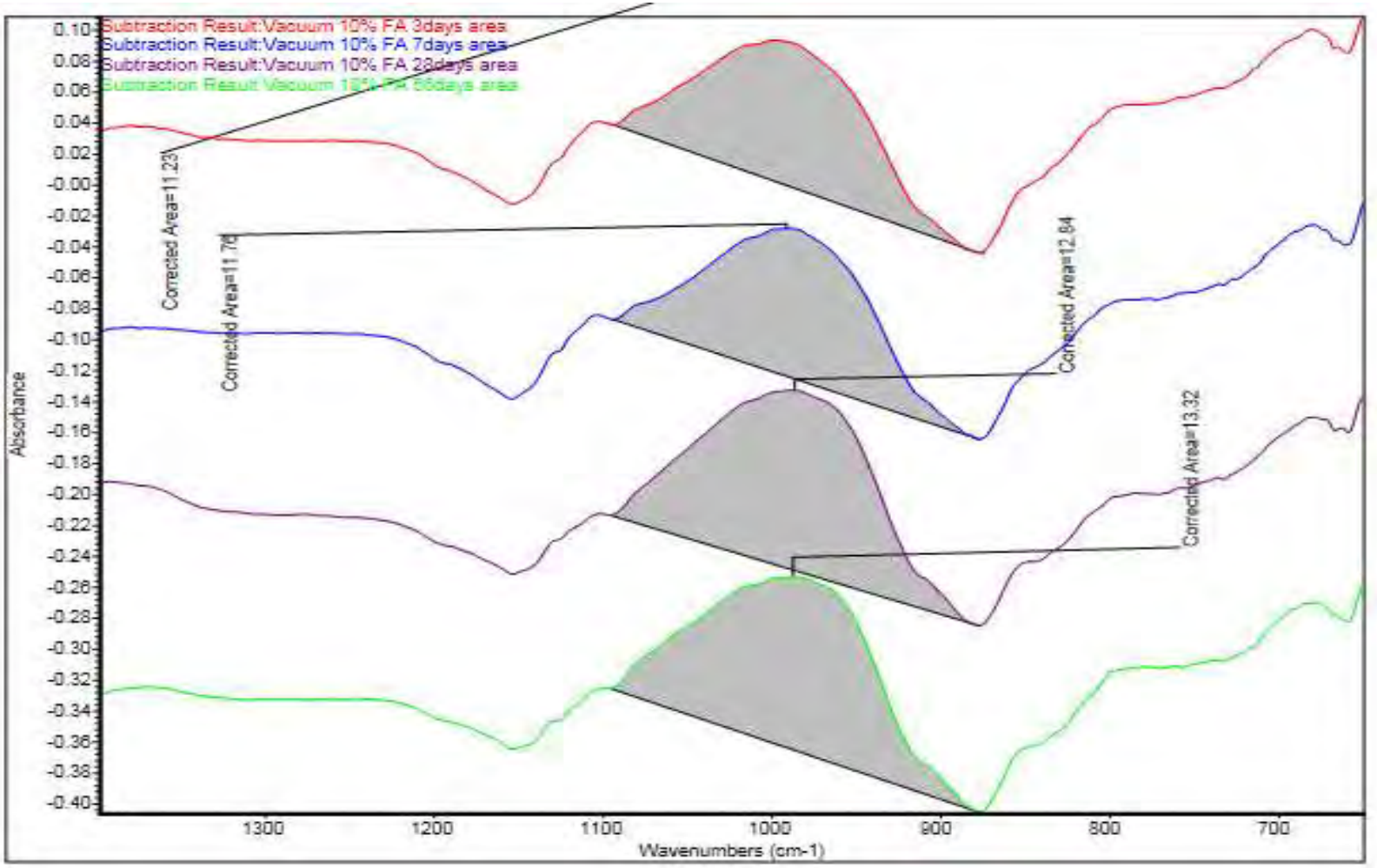

Difference spectra where the absorbance spectrum of as received dry cement has been subtracted from the absorbance spectra of 10% fly ash of cement replacement hydrated for 3, 7, 28 and 56 days after vacuum curing. Reference samples zoomed to range of 700 - 1400 cm^{-1}; with area of possible CSH highlighted. The spectra are shown offset for clarity.

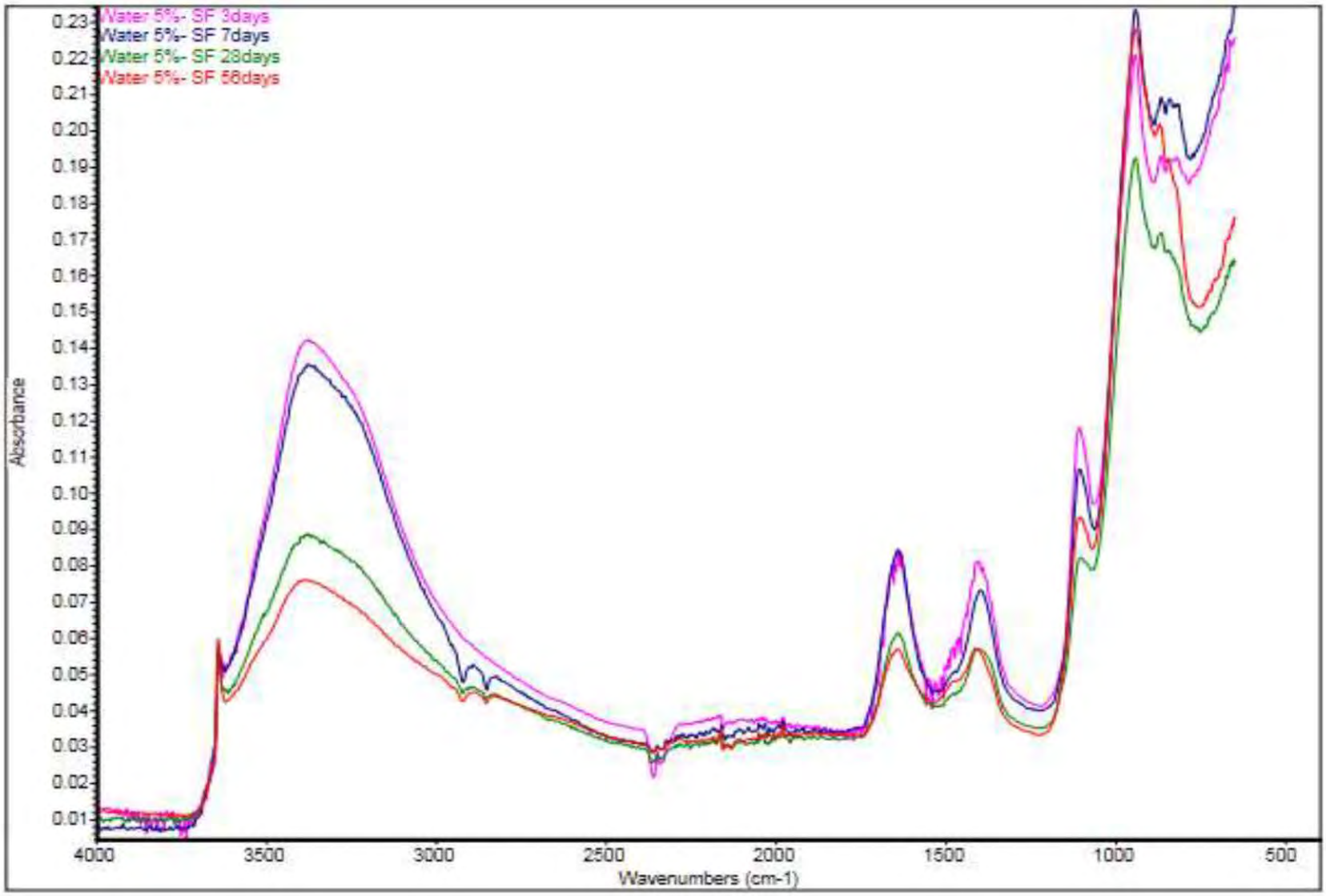

Spectra of 5% silica fume cement replacement for 3, 7, 28 and 56 days after water curing. The spectra are shown offset for clarity.

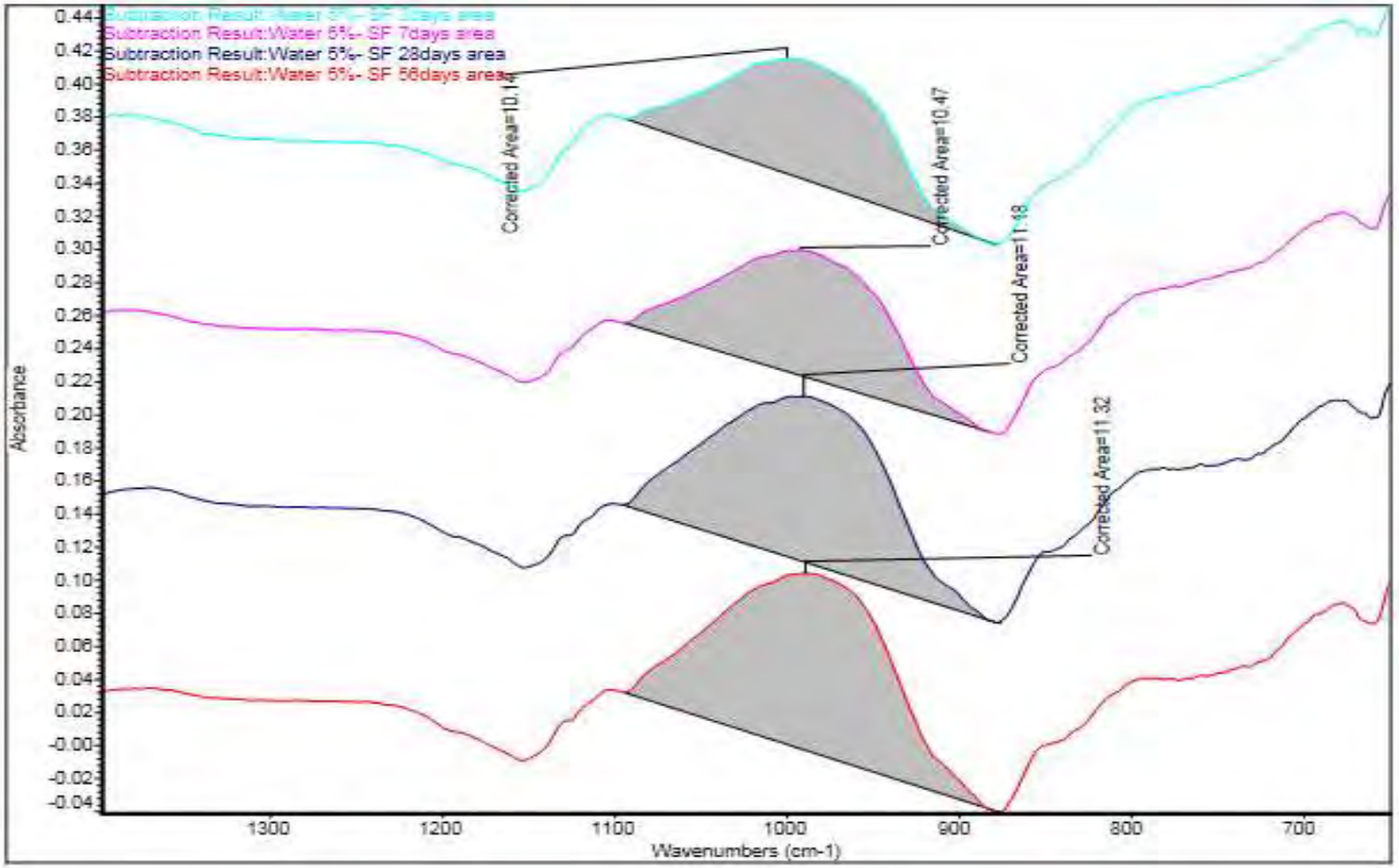

Difference spectra where the absorbance spectrum of as received dry cement has been subtracted from the absorbance spectra of 5% silica fume of cement replacement hydrated for 3, 7, 28 and 56 days after water curing. Reference samples zoomed to range of 700 - 1400 cm^{-1}; with area of possible CSH highlighted. The spectra are shown offset for clarity.

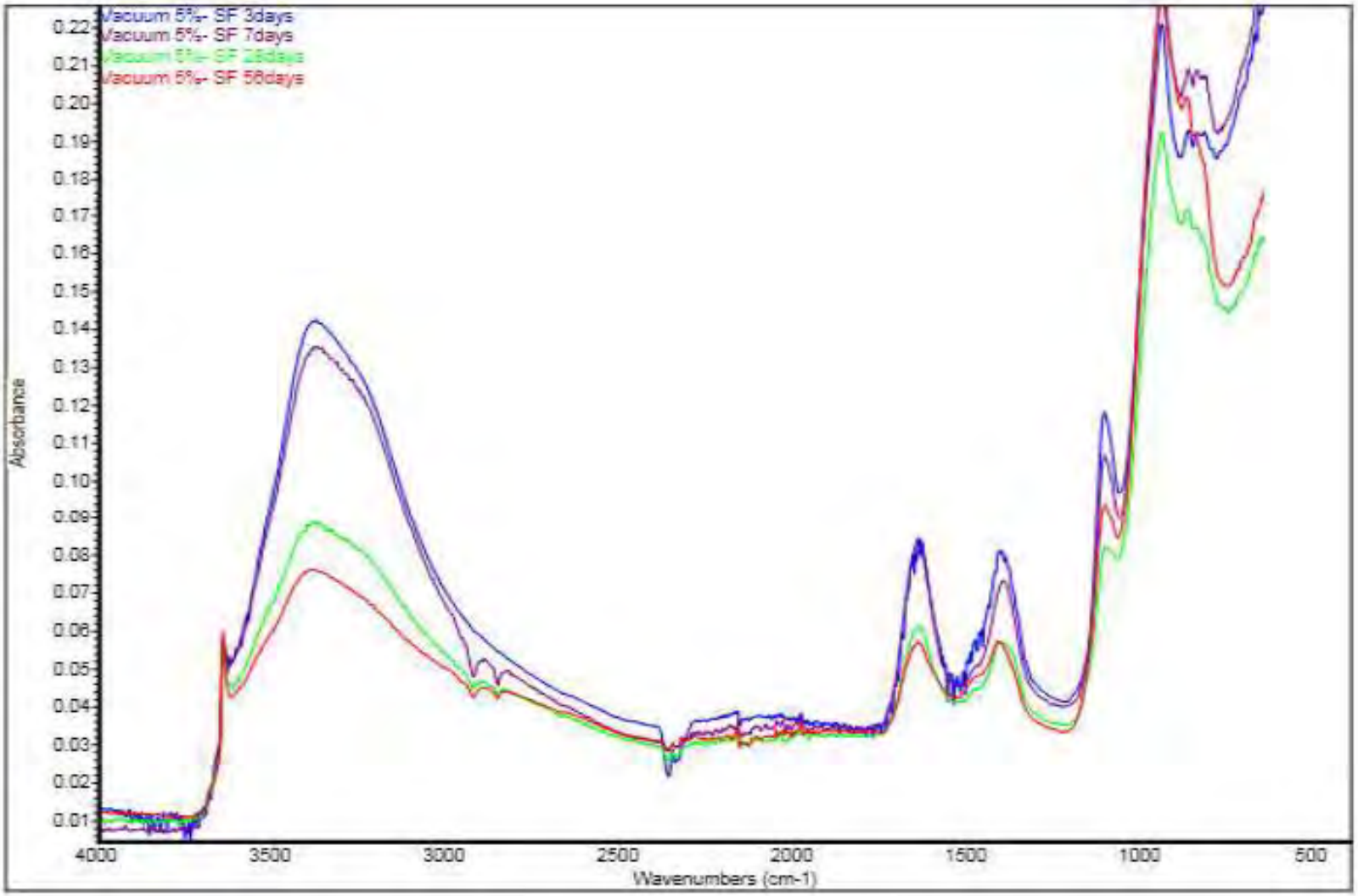

Spectra of 5% silica fume cement replacement for 3, 7, 28 and 56 days after vacuum curing. The spectra are shown offset for clarity.

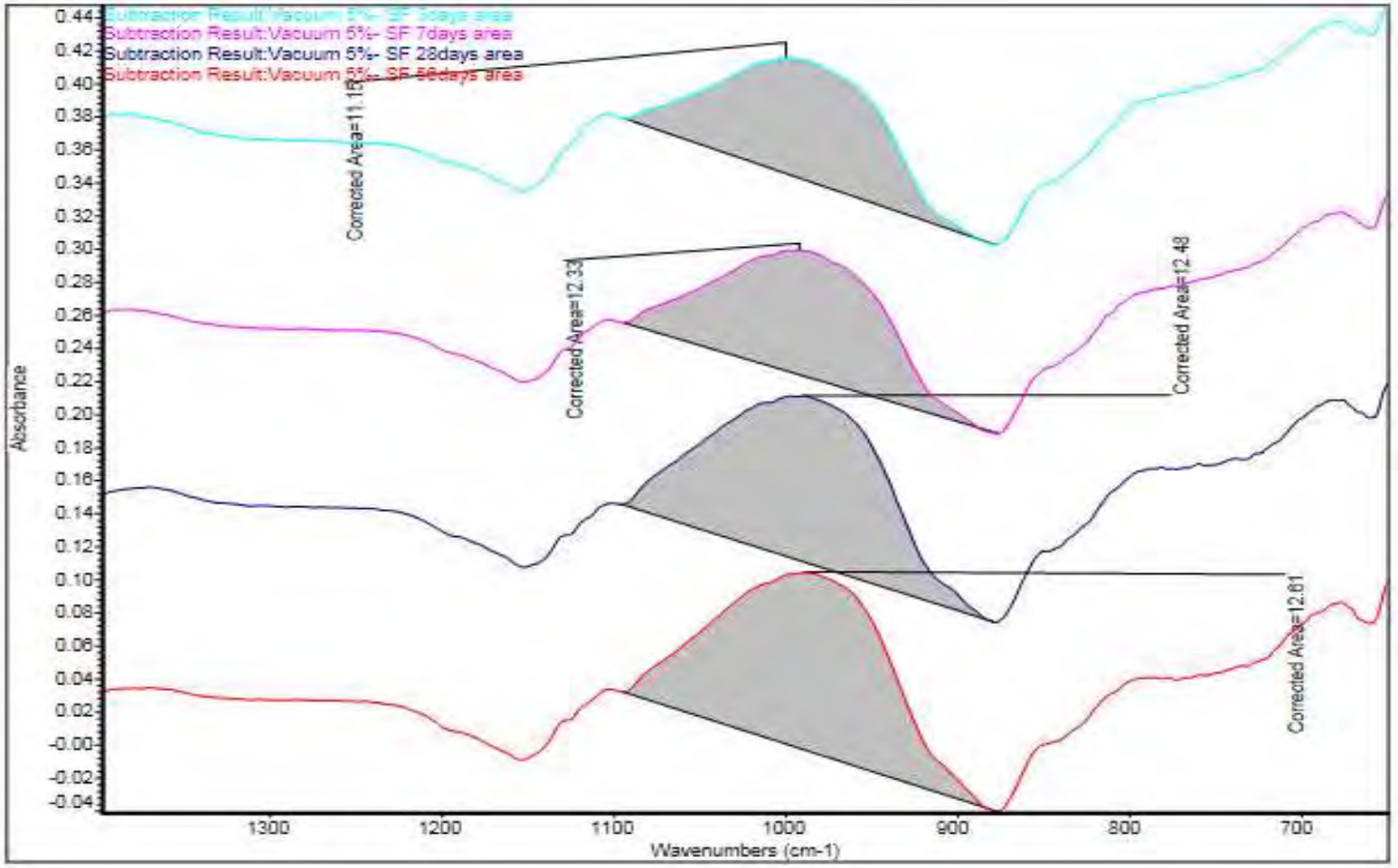

Difference spectra where the absorbance spectrum of as received dry cement has been subtracted from the absorbance spectra of 5% silica fume of cement replacement hydrated for 3, 7, 28 and 56 days after vacuum curing. Reference samples zoomed to range of 700 - 1400 cm^{-1}; with area of possible CSH highlighted. The spectra are shown offset for clarity.

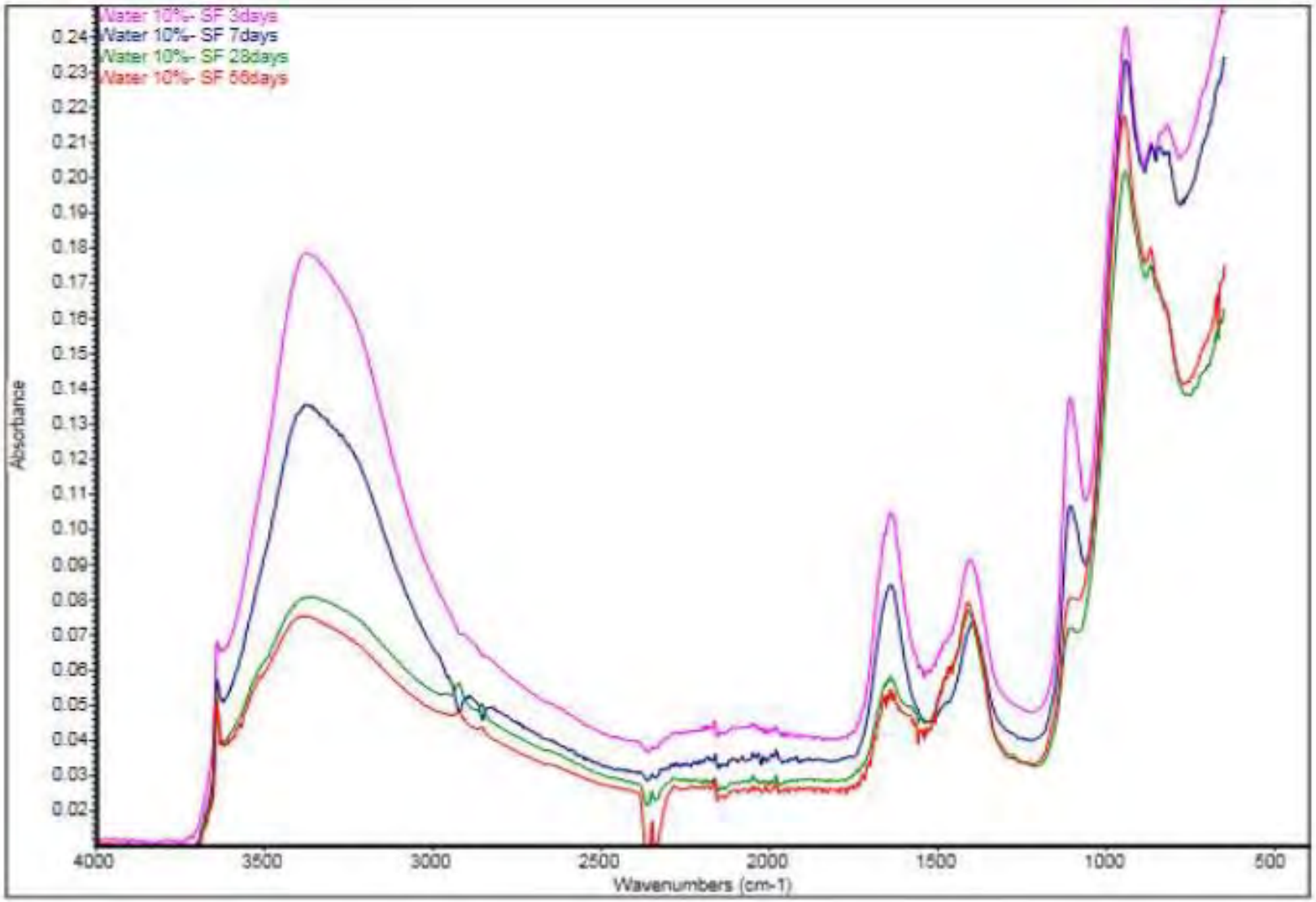

Spectra of 10% silica fume cement replacement for 3, 7, 28 and 56 days after water curing. The spectra are shown offset for clarity.

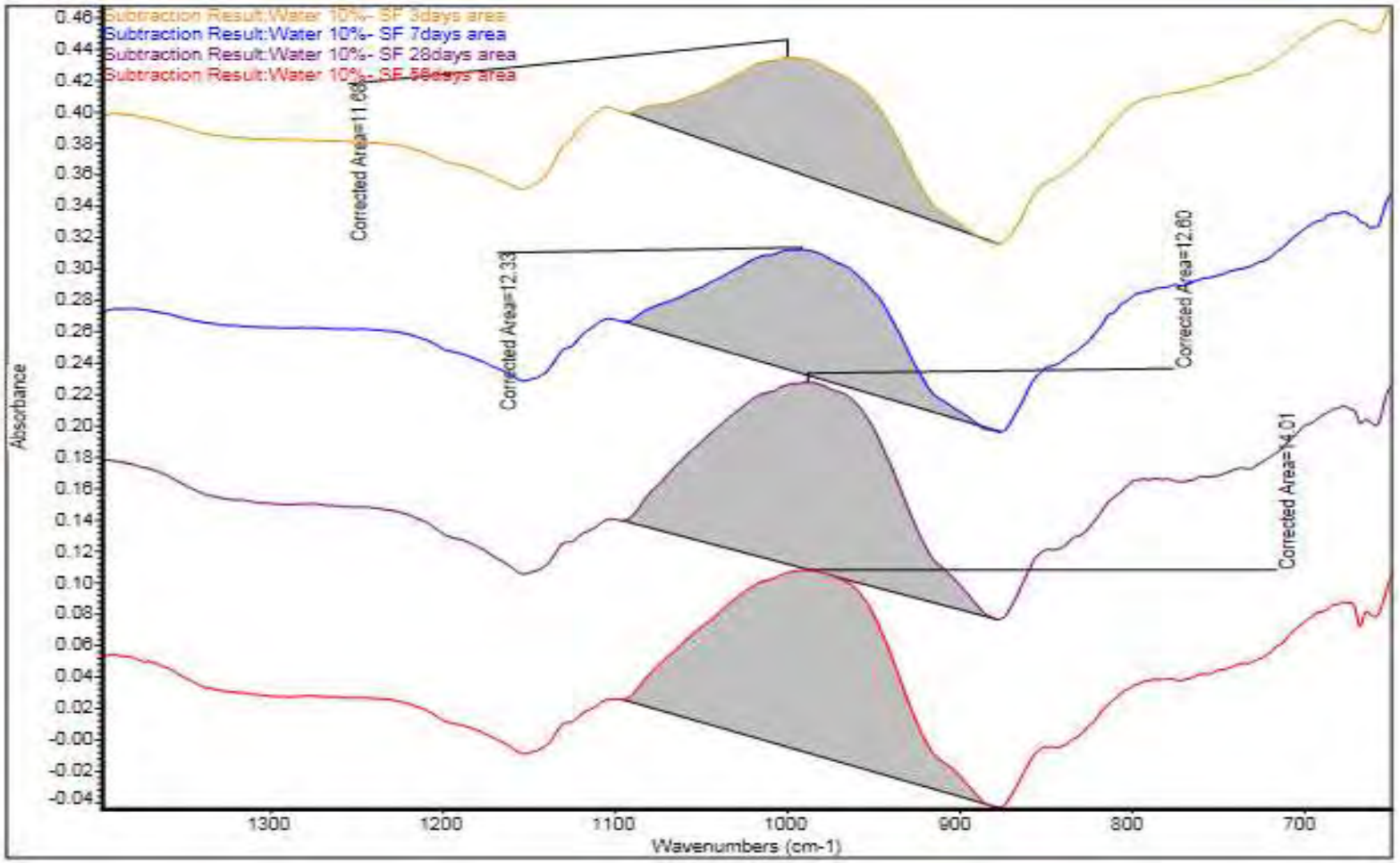

Difference spectra where the absorbance spectrum of as received dry cement has been subtracted from the absorbance spectra of 10% silica fume of cement replacement hydrated for 3, 7, 28 and 56 days after water curing. Reference samples zoomed to range of 700 - 1400 cm^{-1}; with area of possible CSH highlighted. The spectra are shown offset for clarity.

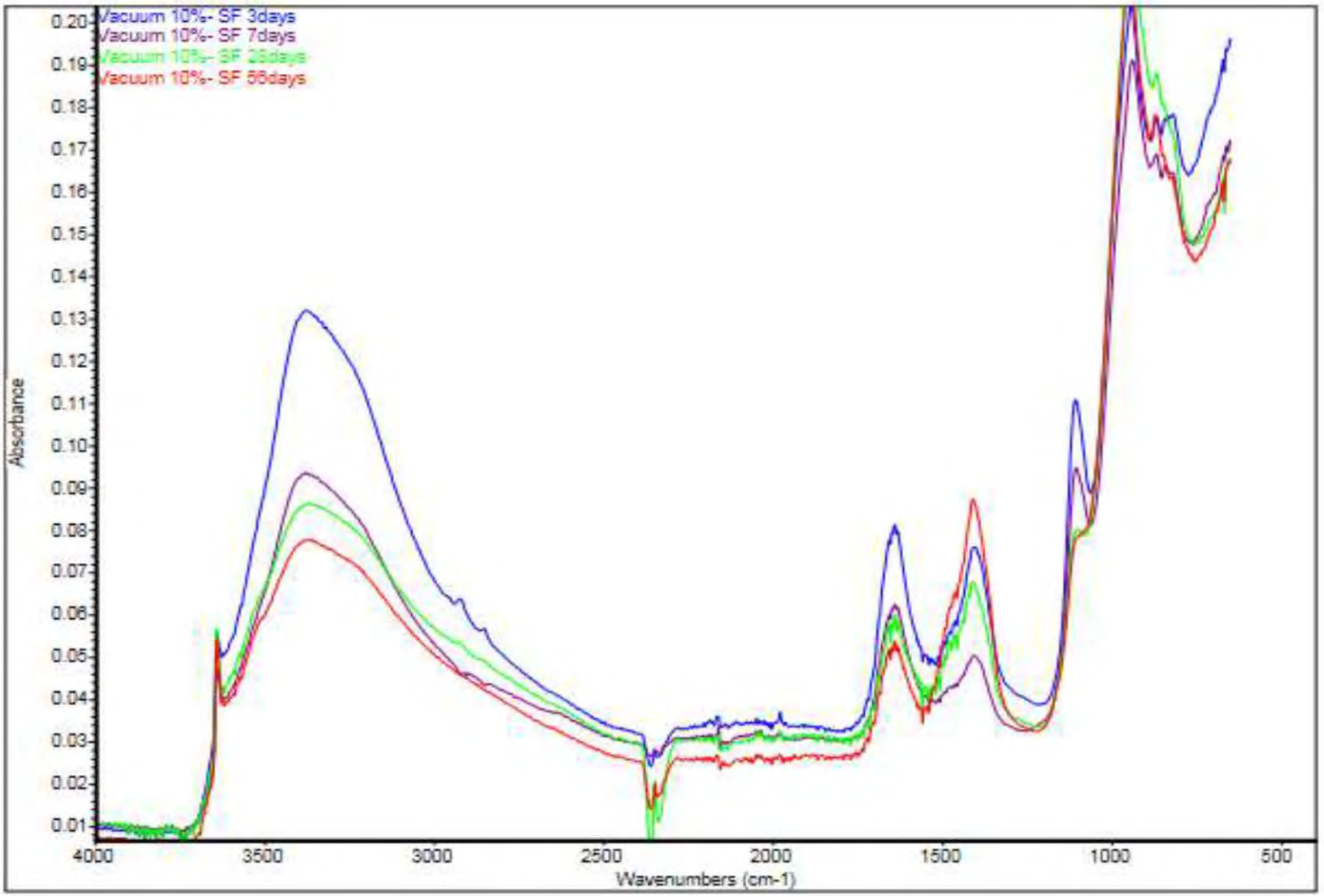

Spectra of 10% silica fume cement replacement for 3, 7, 28 and 56 days after vacuum curing. The spectra are shown offset for clarity.

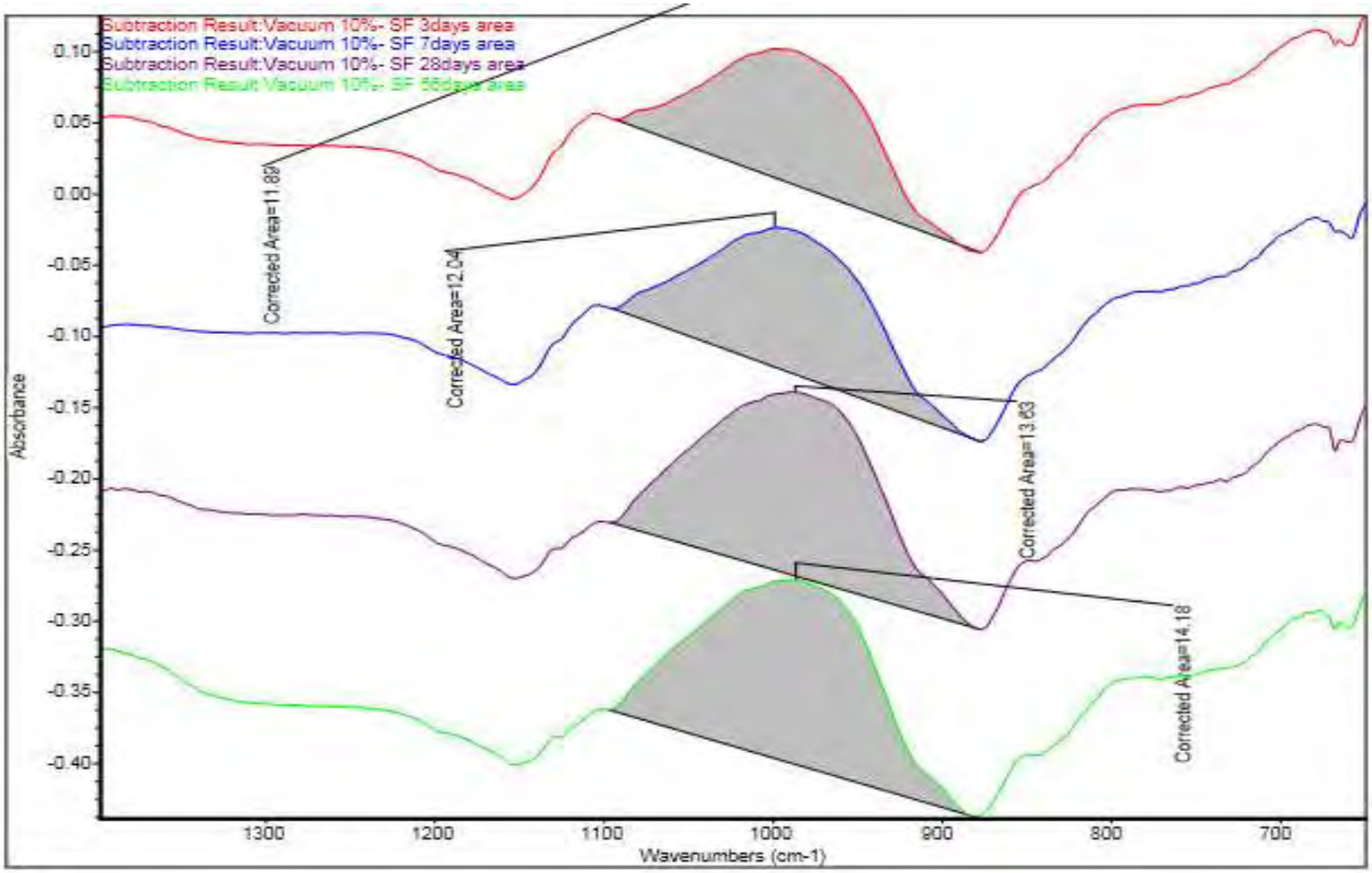

Difference spectra where the absorbance spectrum of as received dry cement has been subtracted from the absorbance spectra of 10% silica fume of cement replacement hydrated for 3, 7, 28 and 56 days after vacuum curing. Reference samples zoomed to range of 700 - 1400 cm^{-1}; with area of possible CSH highlighted. The spectra are shown offset for clarity.

Appendix D: MTS Stress-Strain Curves

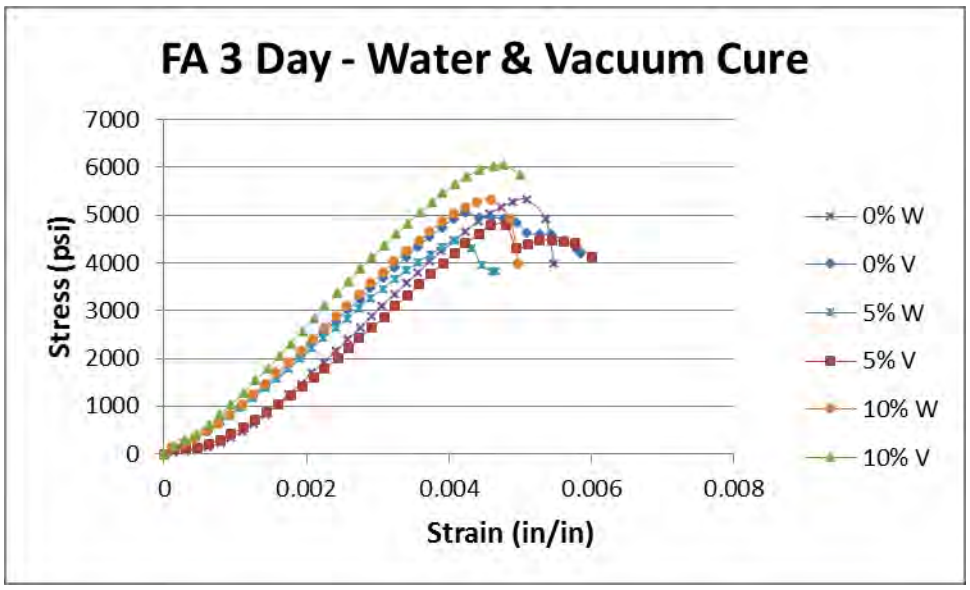

3-day stress-strain curves of controlled cement paste, 5%, and 10% fly ash

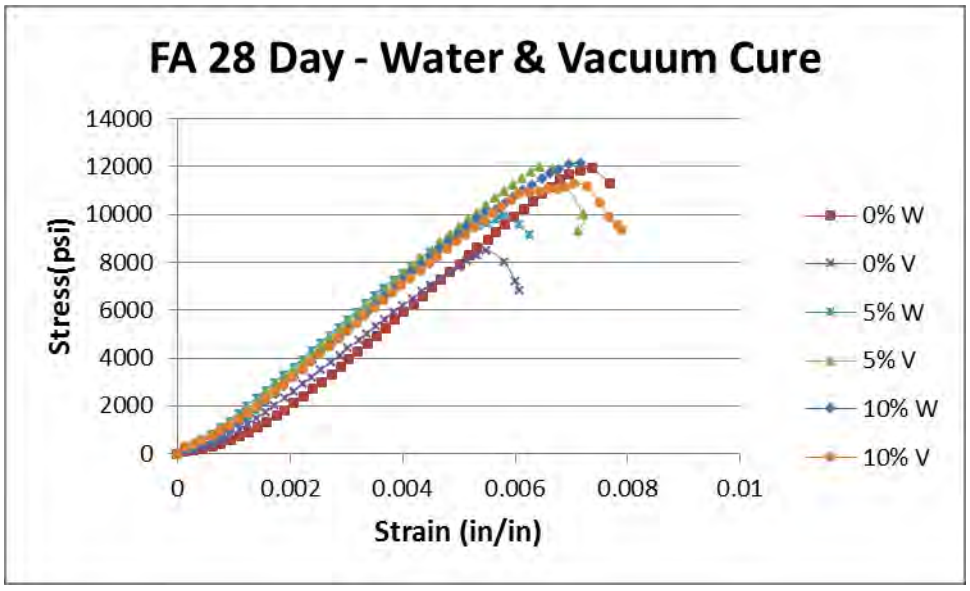

28-day stress-strain curves of controlled cement paste, 5%, and 10% fly ash

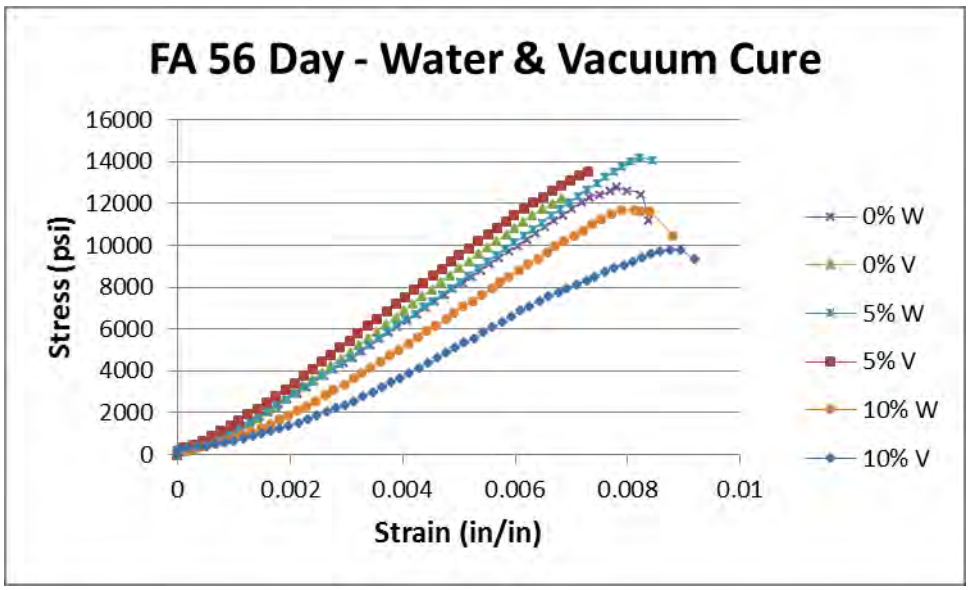

56-day stress-strain curves of controlled cement paste, 5%, and 10% fly ash

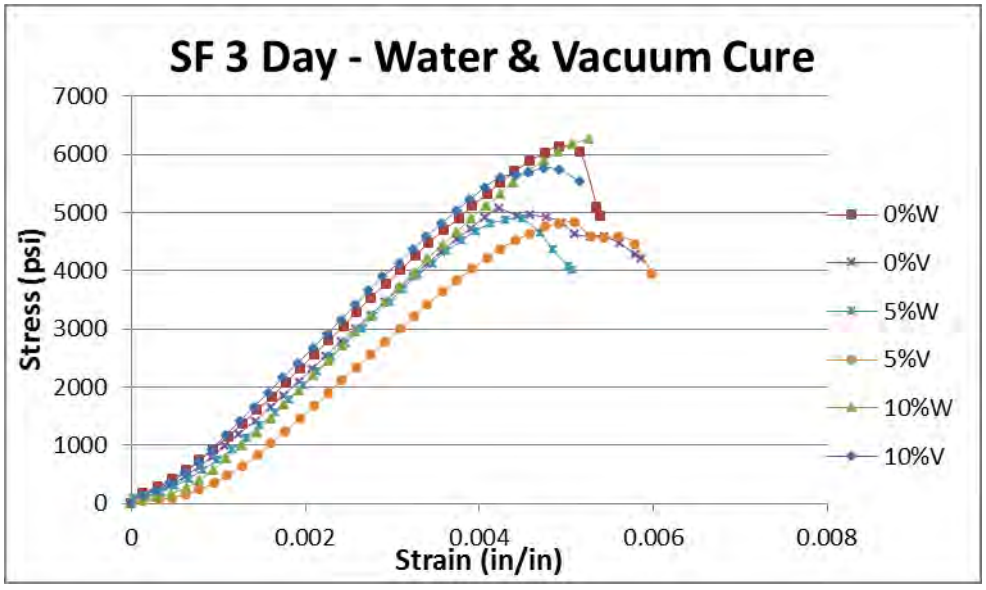

3-day stress-strain curves of controlled cement paste, 5%, and 10% silica fume

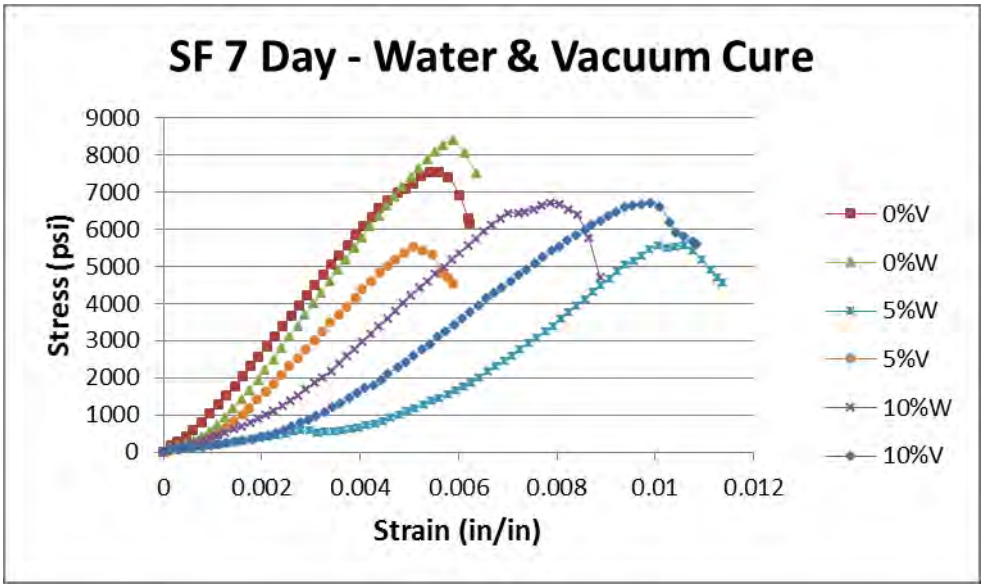

7-day stress-strain curves of controlled cement paste, 5%, and 10% silica fume

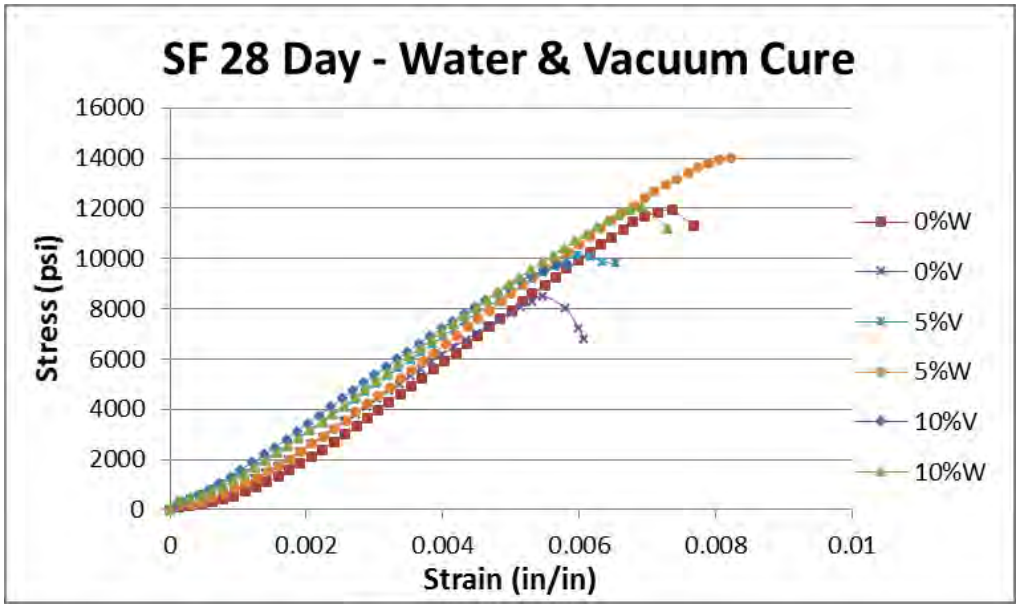

28-day stress-strain curves of controlled cement paste, 5%, and 10% silica fume

Appendix E: Unit Weight Table

Unit Weights (pcf):		Days				
Material	**Cure**	**3**	**7**	**14**	**28**	**56**
0%	**Water**	123.525	121.489	122.468	118.872	122.060
	Vacuum	121.940	120.744	119.386	122.169	121.690
	Avg.	122.732	121.116	120.927	120.520	121.875
5% FA	**Water**	121.415	121.801	121.954	122.165	120.979
	Vacuum	122.492	120.102	120.272	120.946	121.201
	Avg.	121.954	120.951	121.113	121.555	121.090
10% FA	**Water**	121.470	121.015	119.522	126.286	120.487
	Vacuum	121.193	120.596	120.403	121.201	119.964
	Avg.	121.331	120.806	119.962	123.743	120.225
5% SF	**Water**	120.361	121.574	120.796	122.131	120.880
	Vacuum	121.285	120.347	113.386	122.233	121.923
	Avg.	120.823	120.960	117.091	122.182	121.401
10% SF	**Water**	121.941	121.163	119.897	121.405	116.773
	Vacuum	121.420	120.685	121.746	121.361	116.389
	Avg.	121.680	120.924	120.821	121.383	116.581